Anorganische Chemie

Oxygen activation and transfer mediated by copper(I) complexes with polyfunctional bisguanidine ligands

Von der Fakultät für Naturwissenschaften

Department Chemie

der Universität Paderborn

zur Erlangung des akademischen Grades eines

Doktors der Naturwissenschaften

- Dr. rer. nat.-

genehmigte Dissertation

von

Sonja Herres-Pawlis

aus Schwelm

Paderborn 2005

Datum der Einreichung: 9.9.2005

Datum der mündlichen Prüfung: 20.10.2005

Erster Gutachter: Prof. Dr. Gerald Henkel

Zweiter Gutachter: Prof. Dr. Stephan Schulz

Die experimentellen Untersuchungen zu dieser Arbeit wurden im Zeitraum von November 2002 bis August 2005 unter Anleitung von Prof. Dr. G. Henkel im Department Chemie der Universität Paderborn durchgeführt.

To $\mathfrak{B}$

To my family

To my dear Alex

Tudo está bem quando termina bem.

Brasilian proverb

Abstract

In this thesis in the field of Bioinorganic Chemistry, biological relevant copper complexes were synthesised which are capable to activate and transfer molecular oxygen.
As ligand systems, substituted guanidines were used because the N donor functions of these ligands resemble the basic δ imin donor functions of the histidine residues which contribute to copper coordination in almost all copper enzymes.
In order to approach the functionality of tyrosinase and catechol oxidase, a synthetic protocol was developed which allows the unrestricted modification of the spacer as well as of the guanidine unit. By using this modular principle, a library of bisguanidine ligands was built up. This ligand library contains members with total flexibility of the guanidine-connecting spacers as well as of the substitution pattern of the guanidine moieties. Via modification of the spacer, it is possible to change the denticity, the "bite" angle and the coordination geometry, whereas via modification of the guanidine moities, the σ donating and π accepting properties of the N_{imine} atom can directly be influenced. The reaction of the obtained bisguanidines with copper(I) salts yielded copper(I) bisguanidine complexes which were investigated towards their ability to activate molecular oxygen. As result, the observed ability to bind oxygen under formation of Cu_2O_2 adduct complexes was correlated with the degree of conjugation within the guanidine units.
The ligand matrix was screened regarding the oxidation capability of its Cu(II)/Cu(III)O_2 complexes. The possibility of controlling the oxidation selectivity of these Cu(II)/Cu(III)O_2 species by peripheric modifications is a particularly attractive feature of this ligand design.

The studies presented in the following may contribute to a better understanding of oxygen transport and activation in biological systems. Furthermore, this information can support the directed oxygenation of organic substrates.

Abstract

Im Rahmen dieser Doktorarbeit auf dem Gebiet der Bioanorganischen Chemie wurden biologisch relevante Kupferkomplexe synthetisiert, die in der Lage sind, Sauerstoff zu aktivieren und eine Oxidationsaktivität zu entfalten.

Als Ligandensysteme werden substituierte Guanidine verwendet. Die N-Donorfunktionen dieser Liganden ähneln den basischen δ-Imin-Donorfunktionen der Histidinreste, die in biologischen Systemen an der Koordination des Kupfers in den meisten kupferhaltigen Enzymen beteiligt sind. Um der Funktionalität der Tyrosinase und der Catechol-Oxidase möglichst nahe zu kommen, wurde ein Syntheseprotokoll entwickelt, das es ermöglicht, sowohl die Spacer als auch die Guanidineinheit frei zu wählen. Mit Hilfe dieses modularen Prinzips wurde eine Bibliothek aus Bisguanidinliganden aufgebaut. Diese Ligandenbibliothek enthält Vertreter mit vollständiger Flexibilität sowohl der die Guanidineinheit verbindenden Spacer als auch der Substitutionsmuster dieser Guanidineinheiten. Durch geeignete Wahl der Spacer ist es möglich, die Zähnigkeit, den "Ligandenbiß" und die Koordinationsgeometrie zu variieren, während durch die Modifikation der Guanidineinheiten direkt die σ-Donor- und π-Akzeptoreigenschaften am N_{imin}-Atom beeinflußt werden können. Die erhaltenen Bisguanidine wurden mit Kupfer(I)salzen zu Kupfer(I)bisguanidinkomplexen umgesetzt, welche auf ihre Fähigkeit zur Aktivierung von molekularem Sauerstoff hin untersucht wurden. Als Ergebnis konnte die Fähigkeit dieser Komplexe, Sauerstoff unter Bildung von Cu_2O_2-Adduktkomplexen zu binden, mit dem Ausmaß der Konjugation innerhalb der Guanidineinheiten korreliert werden.

Die Ligandenmatrix wurde hinsichtlich der Oxidationseigenschaften ihrer Cu(II)/Cu(III)O_2-Komplexe untersucht. Die Kontrolle über die Oxidationsselektivität der Cu(II)/Cu(III)O_2-Komplexe durch periphere Modifikationen ist eine besonders attraktive Eigenschaft dieses Ligandendesigns.

Die im folgenden geschilderten Untersuchungen sollen zu einem tieferen Verständnis von Sauerstofftransport und -aktivierung in biologischen Systemen führen und diese Information für die gezielte Oxygenierung organischer Substrate nutzbar machen.

Acknowledgement

First of all, I would like to thank all the persons who have supported me and this thesis.
I thank my mentor Prof. Dr. G. Henkel very cordially for the challenging subject, the great freedom in research and our long and fruitful discussions.
My gratitude goes also to Prof. Dr. S. Schulz for the friendly adoption of the correferate of this work.
Furthermore, I would like to thank Dr. U. Flörke for carrying out the crystal structure analyses and the expert advice in questions concerning X-ray crystallography.
For the numerous and sometimes very difficult NMR measurements, my gratitude goes to K. Stolte and PD Dr. H. Egold who always gave advice, not only in NMR matters. For the very numerous mass spectrometric and gaschromatographic measurements, I thank Dr. H. Weber, K. Stolte and M. Zukowski. In addition, my gratitude for the elemental analyses goes to M. Busse and H. Mulka. Furthermore, my gratitude goes to Dr. T. Seshadri for teaching me "organic synthesis". I would like to thank also Prof. Dr. H. Marsmann for the ^{19}F NMR experiments and helpful advice.

Special thanks go to Prof. Dr. F. Tuczek, F. Studt and O. Sander for the Raman measurements at the University of Kiel.

I would like to thank all members of the AK Henkel for the lively time in the lab and the good atmosphere in our bureau, but especially Dr. O. Seewald and A. Neuba for many helpful discussions and the correction of this manuscript.

I gratefully acknowledge the financial support of the Fonds der Chemischen Industrie in form of a Fonds fellowship and of the University of Paderborn in form of a Promotionsabschlußstipendium.

Last, but not least, I would like to thank very cordially my parents Dr. G. Herres and H. Platberg-Herres as well as my grandmother H. Platberg for all the love and encouragement.
Finally, my thanks go to my dearest husband Dr. A. Pawlis who did not have an easy time with me, but gave me all his love, encouragement, printing ink and "Schnittchen".

Contents

List of Figures

List of Tables

List of Abbreviations

Bu	butyl
Bn	benzyl
btmmo	bis(trimethylmethoxyguanidino)propane
^{t}Bu	tert-Butyl
Cys	cysteine
δ	chemical shift (NMR), deformational vibration (IR)
d	dublett (NMR)
dd	double dublett (NMR)
ϵ	extinction coefficient
en	ethylenediamine
EI	electron impact ionisation (MS)
Et	ethyl
Hex	hexyl
His	histidin
J	coupling constant (NMR)
k	reaction constant
kDa	kilodalton
LMCT	Ligand to Metal Charge Transfer
m	multiplett (NMR), medium (IR)
M	molar
Me	methyl
MeCN	acetonitrile
Met	methionine
MMoEG$_2$p	bis(methylmethoxyethyleneguanidino)propane
$\tilde{\nu}$	valence vibration (IR)
NHE	normal hydrogen electrode
Ph	phenyl
Pr	propyl
R	alkyl rest
s	singulett (NMR), strong (IR)
t	triplett (NMR)
THF	tetrahydrofuran
TMMoG$_2$ch	bis(trimethylmethoxyguanidino)cyclohexane
TMMoG$_2$MePA	bis(trimethylmethoxyguanidino)-*N*-methyl-diphenyleneamine
vs	very strong (IR)
vw	very weak (IR)
w	weak (IR)

List of Compounds

L1-2	TMG_2doo
L1-3	TMG_2ch
L1-4	TMG_2PA
L1-5	TMG_2MePA
L1-6	TMG_2mX
L1-7	TMG_2py
L2-1	TEG_2p
L2-6	TEG_2mX
L2-7	TEG_2py
L3-1	$TiPG_2p$
L4-1	$DMEG_2p$
L4-2	$DMEG_2doo$
L4-3	$DMEG_2ch$
L4-6	$DMEG_2mX$
L4-7	$DMEG_2py$
L5-1	$DMPG_2p$
L5-2	$DMPG_2doo$
L5-5	$DMPG_2MePA$
L5-6	$DMPG_2mX$
L5-7	$DMPG_2py$
L6-1	$DPPG_2p$
L7-1	$DPipG_2p$
L8-1	$B(DMPip)G_2p$
L9-1	$B(TMPip)G_2p$
L10-1	$DImG_2p$
L11-1	$DMorphG_2p$
L11-2	$DMorphG_2doo$
L12-1	$DSMorphG_2p$
L13-1	$MorphDMG_2p$
L14-1	$(DMPip)DMG_2p$
	B^FPPG_2p

C1	$[Cu(TMG_2PA^*)I]$
C2	$[Cu(DMorphG_2p)I]$
C3	$[Cu_2(btmgp)_2][PF_6]_2$
C4	$[Cu_2(TMG_2ch)_2][I]_2$
C5	$[Cu_2(DMEG_2p)_2][PF_6]_2$
C6	$[Cu_2(DMEG_2ch)_2][Cu_2I_4]$
C7	$[Cu_2(DMEG_2ch)_2][Cu_4I_6]$
C8	$[Cu_2(DMPG_2p)_2][PF_6]_2$
C9	$[Cu_2(DPipG_2p)_2][PF_6]_2$
C10	$[Cu(DMEG_2p)]_n[PF_6]_n$
C11	$[Cu(DMEG_2p)]_n[I]_n$
C12	$[Cu(TMG_2mX)]_n[I]_n$
C13	$[Cu(DPPG_2p)]_n[CuI_2]_n$
C14	$[Cu_2(TMGbenzPA)_2][PF_6]_2$
C15	$[Cu_2(btmmO)_2][PF_6]_2$
C16	$[Cu_2(TMMoG_2MePA)_2][PF_6]_2$
C17	$[Cu_2(TMMoG_2MePA)_2][ClO_4]_2$
C18	$[Cu_2(TMMoG_2MePA)_2][BF_4]_2$
C19	$[Cu_2(TMG_2MePA)_2(\mu\text{-}OH)_2][Cu_2I_4]$
C20	$[Cu_2(TMG_2MePA)_2(\mu\text{-}OH)_2][I_3]_2$
C21	$[Cu_2(MMoEG_2p)_2][PF_6]_2$
C22	$[Cu(DPipG_2p)_2(\mu\text{-}OH)_2][PF_6]_2$
C23	$[Cu_2(TMMoG_2ch)_2][I]_2$
C24	$[Cu_2(TMMoG_2ch)_2][PF_6]_2$
C25	$[Cu_2(TMMoG_2ch)_2][ClO_4]_2$
C26	$[Cu_2(MorphDMG_2p)_2(\mu\text{-}F)_2][PF_6]_2$

1 Introduction

1.1 Bioinorganic chemistry

Bioinorganic Chemistry is an interdisciplinary research field between Inorganic Chemistry and Biochemistry. On the one hand, knowledge about inorganic reaction mechanisms can be applied on biochemical processes. On the other hand, the elegant and efficient solutions which have been developed by nature supply with indications for new applications of inorganic chemistry.[1] Thus, the most important tasks of bioinorganic chemistry lie in structural elucidation of metallo-biomolecules and the investigation of the complex functions of metal active sites in biologic systems.[2, 3] Living organisms have to maintain a steady state far from the thermodynamic equilibration in a permanently changing environment by continuous supply with nutrients and energy. Equilibrium means death for an organism. The biologic role of inorganic substances is the control of the nutrient flux and the production of dynamic three-dimensional structures.[1]

The structural characterisation of metallo-biomolecules and also the investigation of corresponding model systems contribute to the clarification and the comprehension of biological processes. As these biomolecules have molecular masses sometimes of more than 10^6 g/mol, their crystallisation is difficult and the application of X-ray diffraction is limited. Hence the concept of model compounds, which has been developed by Wieghardt,[4] Holm and Ibers,[5] came to great importance. It can be distinguished between replicative and speculative models.[3] Replicative models reproduce as exact as possible the coordinational surrounding of the metal of a structural characterised metalloprotein. The absence of the protein matrix in these small-molecular compounds facilitates the characterisation considerably. Without exact structural information, the structural proposals are made as speculative models. At the same time, newly gained insights regarding the model or the enzyme must be transferable to each other. A particularly significant example for the importance of these models is the reinterpretation of the coordination of molecular oxygen (end-on → side-on)

in the transport protein hemocyanin. The structural suggestion could be confirmed by an X-ray structure analysis of oxy-hemocyanin after the synthesis of the corresponding model complex.[2]

1.2 The bioinorganic chemistry of copper

Copper is a so-called coinage metal with a natural abundance in the earth shell of 0.007 % and belongs to the 11th group of the periodic system. However, it differs in its special properties clearly from its group homologues silver and gold. Copper is for many organisms an essential trace element although even small doses of copper(II)salts are extremely poisonous for algae, fungi and bacteria. The total quantity of this element in the body of a human adult amounts up to 150 mg. In higher organisms like humans, genetically caused diseases of the copper metabolism lead to illnesses like the Wilson disease (pathologic accumulation of copper in liver and brain), the Menke kinky hair syndrome (disruption of the intracellular copper transport, severe disfunction of the mental and physical development of babies accompagnied by frizzly hair) and the amytrophic lateralsclerosis (ALS, neurodegenerative illness caused by genetic defect of the [CuZn] dismutase).[2]
Furthermore, regarding its complex chemical properties, copper differs from its heavier homologues as well as from its neighbours of the 3d row (Ni, Zn) which generally have even numbered electron configurations in their complex compounds by its relatively high stability of the d^9 configuration (Cu(II)). Copper(I) ions are very flexibel with regard to their coordination number due to their d^{10} configuration and the resulting lack of ligand field stabilisation. In addition, very short Cu...Cu distances in polynuclear complexes indicate possible attractive d^{10}-d^{10} interactions.[6, 7] One origin of the high reactivity of Cu(I) compounds towards triplet oxygen is the orbital mixing (3d/4s or 3d/4p). In aqueous solutions, the smaller Cu(II) ions are more stable then the Cu(I) ions as they possess a higher hydration enthalpy. Hence, Cu(I) ions disproportinate easily in aqueous solutions. The Cu(II)-d^9 system is a classical example for the Jahn-Teller effect. In this system, the square-planar environment is favorised, in some cases complemented by weaker coordination of an axial ligand.

1.3 Copper proteins in biological systems

1.3.1 Overview of the biological processes under participation of copper enzymes

Regarding their function, copper proteins can be divided into two main groups: pure electron transferring proteins and systems which interact with molecular oxygen or its metabolites. Besides these groups, some huge proteins have several functions like the ceruloplasmin in the regulation of the iron metabolism. Copper proteins divide up after their structural, functional and analytical characteristics into the "classic" types (Figure 1.1) and the recent "non-classic" types (Figure 1.2).[8]

	Coordinational geometry	Function, abundance, spectroscopic characteristics
Type 1	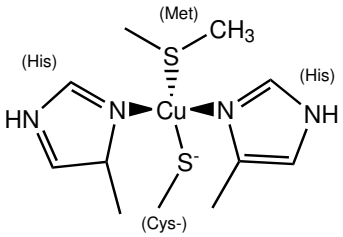	electron transfer; blue copper proteins, e.g. plastocyanin, azurin; strongly distorted polyhedron; intensive LMCT (Cys-Cu^{II}); weak $^{63,65}Cu$ hyper fine coupling and g-anisotropy
Type 2	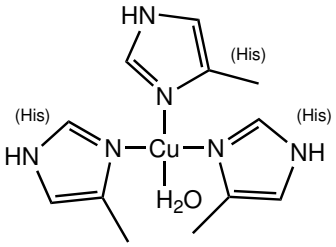	catalysis, redox activity; amine oxidases, galactose oxidase, (CuZn)-superoxide dismutase, cytochrome-c-oxidase; largely planar; no intensive absorptions, only forbidden ligand field transitions, normal Cu^{II} epr parameter
Type 3	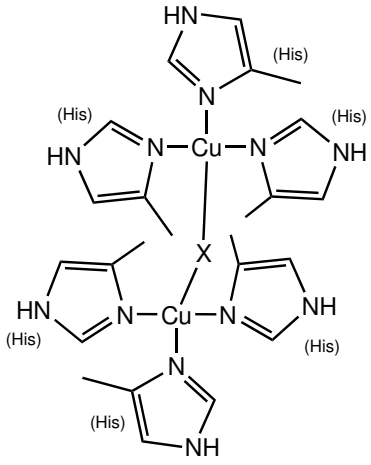	O_2 transport and activation; hemocyanin, tyrosinase; bridged dimer, Cu-Cu distance 360 pm; after O_2 uptake intensive absorptions at 350 and 600 nm, LMCT transitions O_2^{2-} to Cu^{II}; store and transport form; epr inactive due to antiferromagnetic coupled d^9 centres

Figure 1.1: "Classic" copper centers in biologic systems [2]

	Coordinational geometry	Function, abundance, spectroscopic characteristics
Type (2+3)-Trimer	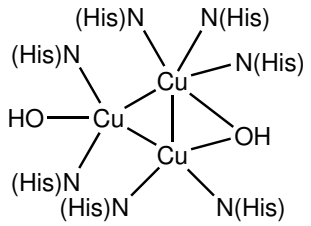	O_2 activation for oxidase function; ascorbat oxidase, laccase; intensive LMCT (Cys-Cu^{II}); normal Cu^{II} epr parameter
Cu_A	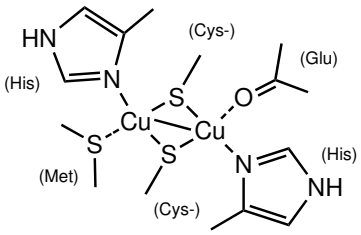	electron transfer; N_2O reductase, cytochrome-c-oxidase; absorption in the near IR (MMCT), very weak Cu hyper fine splitting due to two equivalent Cu; small g-factor
MT-Cu	diverse centres	regulation, store and transport form; CUP2; metallothioneins, Cu transport ATPase, no oxidised form

Figure 1.2: "Non-classic" copper centers in biologic systems [8]

1.3.2 Copper enzyme-mediated oxygen activation and transfer

Copper containing enzymes that activate O_2 act as dioxygenases, monooxygenases and oxidases (Figure 1.3).[8, 10, 11, 12] The nuclearity of the active site does not correlate directly with the type of reactivity, e.g. mononuclear Cu enzymes perform all three types of reactions. Copper-containing oxidases constitute one of the major classes of biocatalysts that participate in dioxygen processing.[10] They possess mononuclear, dinuclear or trinuclear copper-active sites, many of which involve histidine imidazoles as supporting ligands.[13]
Typical examples of the mononuclear active site are found in dopamine β-monooxygenase, peptidylglycine α-amidating monooxygenase and quercetin 2,3-dioxygenase which catalyse the oxygenation of various organic substrates by molecular oxygen.[11, 14] A series of copper-containing amine oxydases, lysyl oxydase and galactose oxidase also contain a mononuclear copper active site.
The most important dinuclear copper-active sites are found in hemocyanin, tyrosinase and catechol oxidase.[10, 15, 16, 17, 18, 19, 20] Tyrosinases are widely distributed throughout bacteria, fungi, plants and animals, catalysing the *ortho*-hydroxylation of phenols to catechols (phenolase activity, equation 1 in Figure 1.4) and the oxidation of catechols to *o*-quinones (catecholase activity, equation 2 in Figure 1.4).

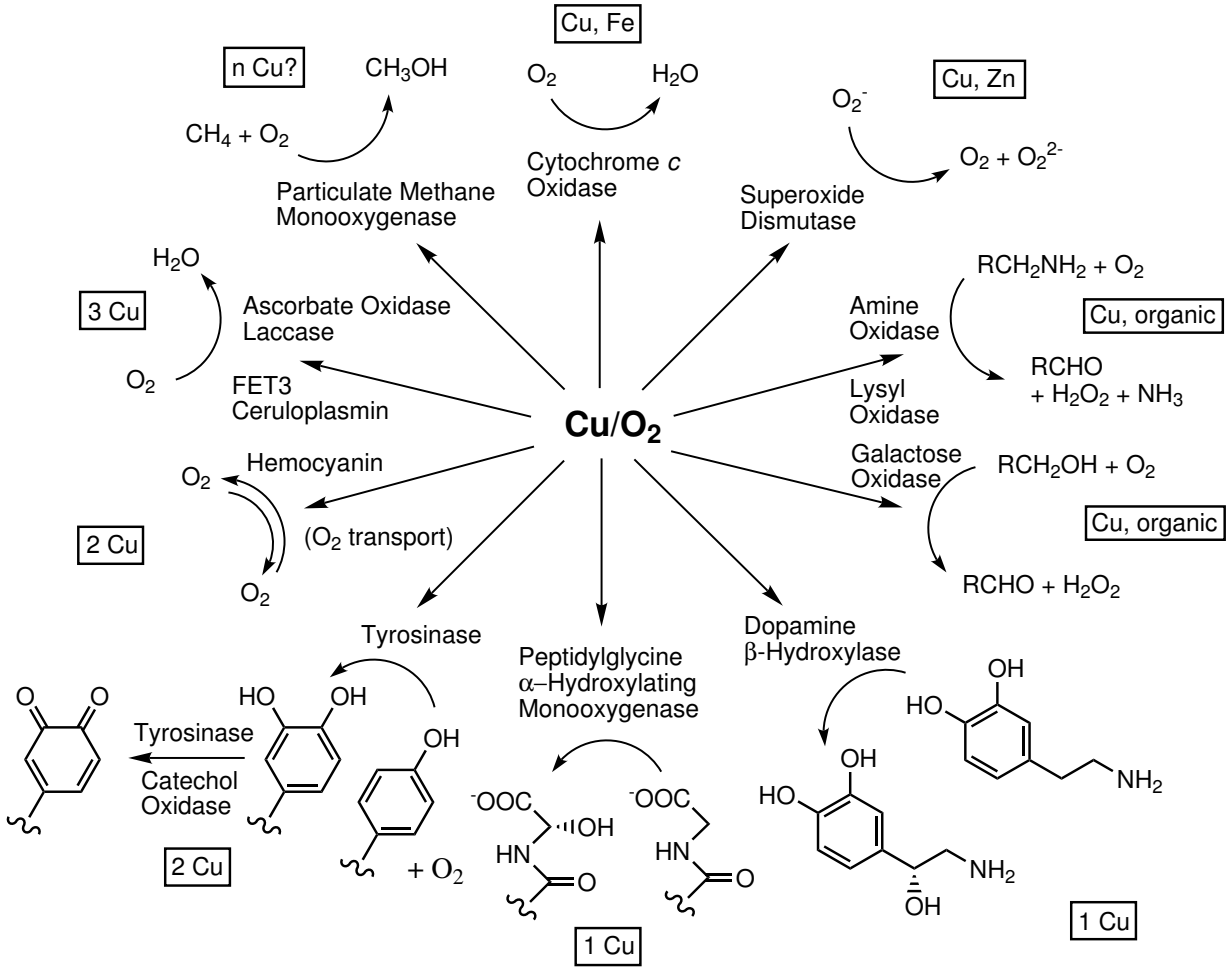

Figure 1.3: Selected Cu enzymes und proteins that activate O_2 [8]

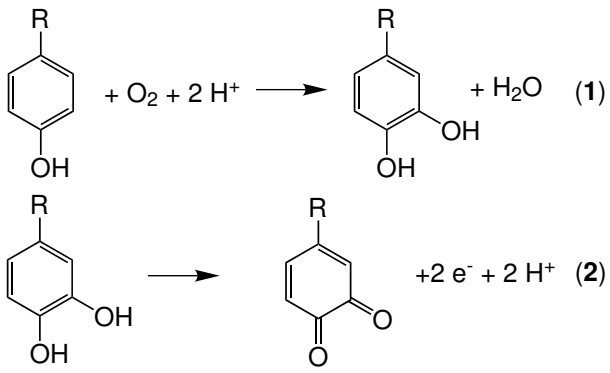

Figure 1.4: Phenolase activity (1), catecholase activity (2)

These two processes are also referred as "cresolase activity" or "monophenolase activity" and "diphenolase activity", respectively. Such reactions represent the initial steps of vertebrate pigmentation (melanin biosynthesis) and the browning of fruits and vegetables.[10, 15] Catechol oxidases are ubiquitous plant enzymes which also catalyse the oxidation of a broad range of catechols to the corresponding o-quinones (catecholase activity), but lack the phenolase activity. The most plausible function proposed for plant catechol oxidases is a role in the disease resistance of higher plants. The enzyme is cytosolic or membrane-bound, whereas possible substrates are kept separated in the vacuole. After disruption of the cell by wounding or infection, the membrane is lysed, and these two com-

ponents can come in contact. This causes the formation of quinones which spontaneously polymerise to melanins. Some parasites have been found to use inhibitors of the catechol oxidases, indicating that the catechol oxidase/diphenol system is an obstacle against the colonisation of the host.[21] As further functions of catechol oxidases, a role located in the thylakoid membrane during the photosynthesis has been discussed. Regarding the function of tyrosinase in mammals and insects, there is no controversy. In mammals, tyrosinase initiates the formation of pigmentation. The absence or inactivation of the enzyme leads to forms of albinism (tyrosinase-negative albinism and occultaneous albinism). In insects, tyrosinases are involved in sclerotisation, i.e., the hardening of the chitinous cuticle and defense.[21] Although the crystal structure of tyrosinase has yet to be solved, chemical and spectroscopic investigations have unambigously demonstrated that the structure of the dinuclear copper-active site in tyrosinase is very similar to those of catechol oxidase and the dioxygen carrier protein, hemocyanin, whose structures have been determined by X-ray crystallographic analysis.[9, 22, 23, 24, 25, 26, 27] In addition to these copper enzymes, there are some other copper-containing monooxygenases such as particulate methane monooxygenase (pMMO) and ammonia monooxygenase (AMO), in which the active site is believed to constitute a multi-copper reaction center.[10]

1.3.3 Oxygen transport by hemocyanin

Hemocyanin (Hc) is a protein with a type-3-copper site, initially studied in the early 70´s,[28] and the crystal structure of its active form was first reported in 1993 by Magnus and coworkers.[24, 25] Hcs are copper-containing respiratory proteins, freely dissolved in the hemolymph of many arthropod and mollusc species.[29] This function is related to the capacity of Hc to bind molecular oxygen reversibly at the active site that is a dinuclear copper centre. The protein is thus found in two different forms, i.e. deoxy-Hc, containing a [Cu(I)Cu(I)] pair with a Cu-Cu distance of 4.6 Å, and oxy-Hc. In the latter form, dioxygen was found to bridge between both copper(II)ions separated by a distance of 3.6 Å, reflecting an electron transfer process from Cu(I) to dioxygen, where the peroxide dianion is coordinated as a bidentate ligand in a $\mu - \eta^2 : \eta^2$ fashion (Figure 1.5).

Hcs can be divided into two classes depending on their biological source: the arthropodan (e.g., lobsters and spiders) and the molluscan (e.g., octopus and snails) hemocyanins. These have different subunit organisations and only a weak evolutionary relationship.[26] Molluscan Hcs are hollow cylindrical molecules with molecular masses of 3.4 MDa to 9 MDa or greater.

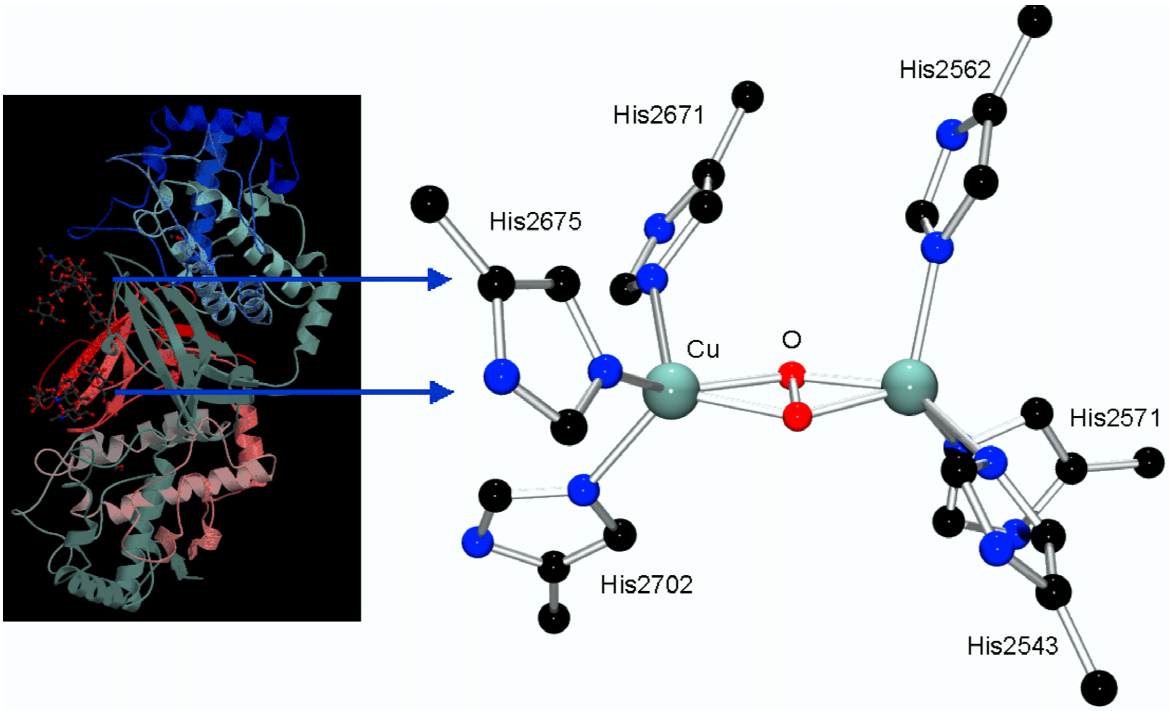

Figure 1.5: Dinuclear $\mu - \eta^2 : \eta^2$ peroxo copper active site of oxyhemocyanin from *Octopus dofleini* [27]

Each subunit has a molecular mass on the order of 400 kDa. These associate as decamers, di-decamers, or sometimes larger assemblies. The decamer is the smallest cooperative unit, and this is the structure found in cephalopods and chitons, whereas most gastropods have tail-to-tail dimers of such decamers. Each subunit contains 7 or 8 beads 50 to 60 Å in diameter, and each of these is a "functional unit" containing one binuclear copper site and about 400 amino acid residues. Functional units are more protease resistant than the intervening or "linker" regions, allowing their isolation.[27] *Octopus dofleini* hemocyanin is formed by ten nearly identical polypeptides (the subunits) arranged in an antiparallel fashion around a molecular 5-fold axis of symmetry. Magnesium or other cations are necessary for a stable decamer, without which it dissociates into subunits. The Hc oxygen binding-site consists of six histidine residues which coordinate two copper atoms and it is not exposed to the solvent exterior. Each copper atom is coordinated by the $N_{\epsilon 2}$ of three histidine side-chains. When viewed down the copper-copper axis, the ligands emanate nearly trigonally from each copper atom and the two sets are partially staggered with respect to each other. The peroxide bonding can be regarded as bifurcated Cu to O_2^{2-} bonding, each Cu atom is thus coordinated as a tetrahedron flattened with respect to the Cu-Cu axis.

1.3.4 Activation of molecular oxygen by type 3-centers

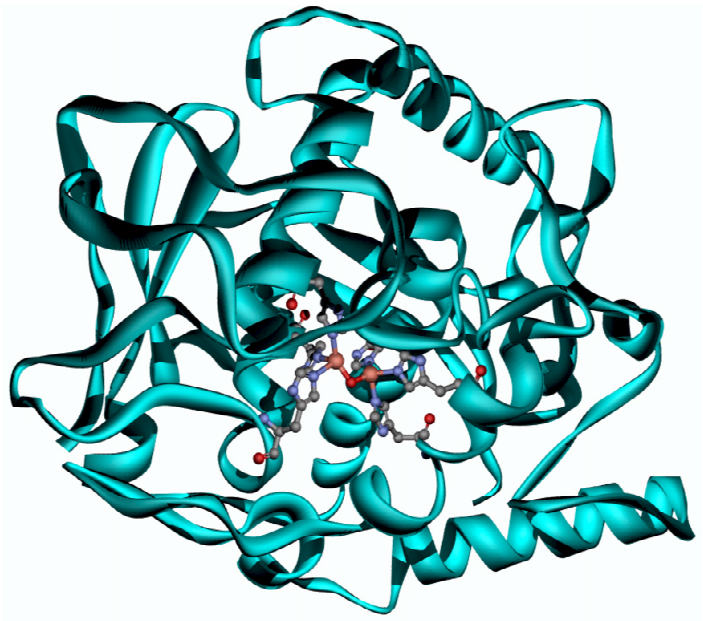

Figure 1.6: Overall structure of catechol oxidase from sweet potatoes [17]

Catechol oxidases are found in plant tissues and in some insects and crustaceans,[30] whereas tyrosinases can be isolated from a broader variety of plants, fungi, bacteria, mammalians, crustaceans and insects.[10, 30] The structure of the catechol oxidase from the sweet potatoe *Ipomoea batatas* could be elucidated by means of X-ray crystallography in its met state as well in the deoxy state by Krebs et al. (Figure 1.6). [17] Indeed, the active site of the catechol oxidase exhibits great similarities to the active site in hemocyanin. The catechol oxidase from *Ipomoea batatas* (ibCO) has an ellipsoidal shape with axes of about 55, 45 and 45 Å. The secondary structure is dominated by α-helical regions. Both copper atoms forming the metal centre are coordinated by three histidine N atoms. An unusual covalent thioether bond joins Cys92 to the coordinating His109 (Figure 1.7). An analogous thioether bridge has been reported to occur in tyrosinase from *Neurospora crassa*, in hemocyanin from *Helix pomatia*[31, 32] and from *Octopus dofleini*.[27] The involvement of the Cys-His bridge in the catalytic pathway is possible, but a structural function is also under discussion.

The active site is situated in a hydrophobic pocket. In the met state with both copper atoms in the oxidation state +II, the two cupric ions are at a distance of 2.9 Å. They are bridged by a hydroxide ion at a distance of 1.8 Å. The coordination sphere of each copper atom can be described as a trigonal pyramid with His109 and His240 in the apical position, respectively. In the deoxy or reduced state, both copper atoms are reduced to the oxidation state +I with a Cu-Cu distance of 4.4 Å. The coordination numbers are 4 for CuA (three His ligands and a coordinating water molecule) and 3 for CuB (three His ligands). The coordination sphere is distorted trigonal pyramidal for CuA and square-planar for CuB with one vacant coordination site. [17]

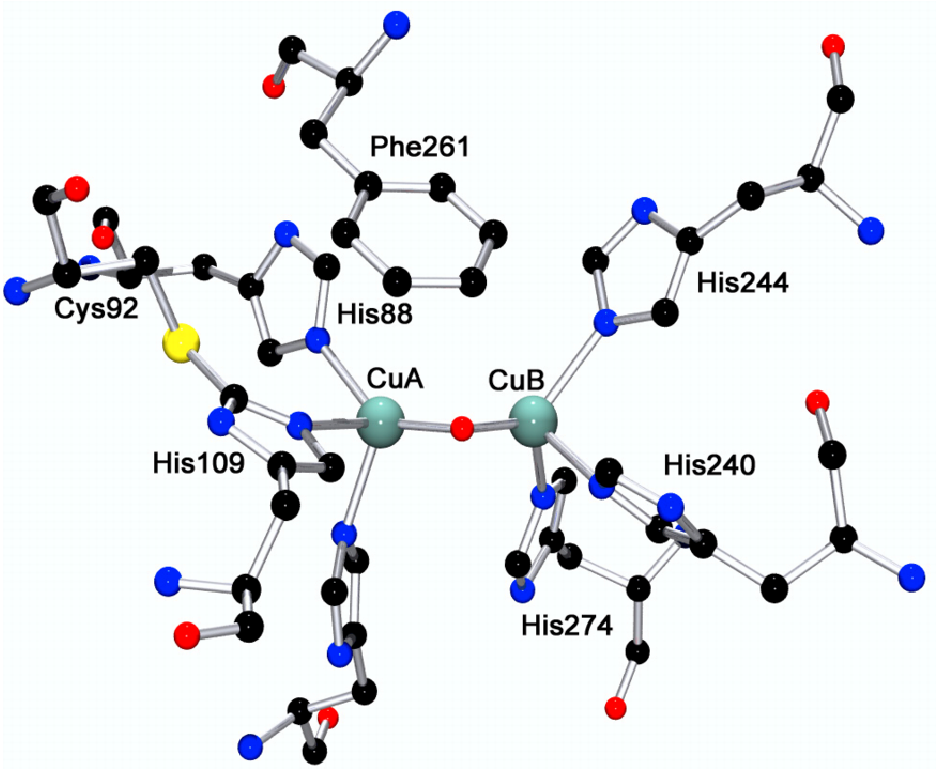

Figure 1.7: Coordination sphere of the dinuclear copper centre in the met state [17]

The inhibitor complex with phenylthiourea has with 4.2 Å a large Cu-Cu distance compared with the met state.[17] The sulfur atom of the inhibitor substitutes the bridge of the met state. The coordination sphere are identical with those of the met state, but a conformational change of the amino acid residues takes place under rotation of the aromatic ring of Phe261. The small changes of the spatial structure lead to the conclusion that the pocket of the active site is rigid; the observed differences can be merely attributed to movements of the copper atoms in this pocket. By means of the inhibitor complex, it has been proven that the Phe261 is located above the active centre acting as gate which can rotate when the inhibitor is bound. Thus, access of the substrate to the catalytic site seems to be controlled by this "gate residue". With this gate, the enzyme is supposed to differentiate between phenolic and catecholic substrates. The metal centres in hemocyanin, tyrosinase and catechol oxidase have very similar coordination spheres, but the substrate differentiation is determined by the enzymatic pocket. Comparison of the ibCo structure with arthropodan hemocyanin structures reveals that the hemocyanins have an aditional N-terminal domain. The size and the position of this domain suggests that it acts a shield hindering the free access of phenolic substrates to the dicopper centre. The phenyl alanine residue Phe49 of the "shield region" reaches into the pocket of the oxygen-binding site. In the case of Limulus polyphemus hemocyanin, Phe49 was shown to superimpose exactly on the position of the

substrate in an ibCO-substrate complex, thus blocking substrate binding. This means that in hemocyanins, the gate is so narrow that only O_2 can pass it without the possibility of further reaction.[20] This hypothesis is supported by the observation that spider hemocyanin shows weak catecholase activity after proteolysis.

For the mechanism of the tyrosinase or catecholoxidase mediated phenol or catechol oxidations with molecular dioxygen, several proposals have been made. The mechanism primarily developed by Solomon et al.[10] and extented with recent results [15, 31] is presented in Figure 1.8.[17] This mechanism suggests the oxy state to be the starting point of cresolase activity (inner circle). This state is present in the resting form of tyrosinase in a proportion of about 15 % (85 % met state). A monophenol substrate binds to the oxy state and is monooxygenated to *o*-diphenol. This diphenol subsequently binds to the copper centre of met tyrosinase in a bidentate binding mode proposed on the basis of a model compound (see section 1.5.2).[33] Oxidation of the diphenol substrate leads to the reduced state of the dinuclear copper centre. Reoxidation of the reduced state to the oxy state occurs by attack of dioxygen and closes the catalytic cycle.

The mechanism of catecholase activity (outer circle) starts from the oxy and met states.

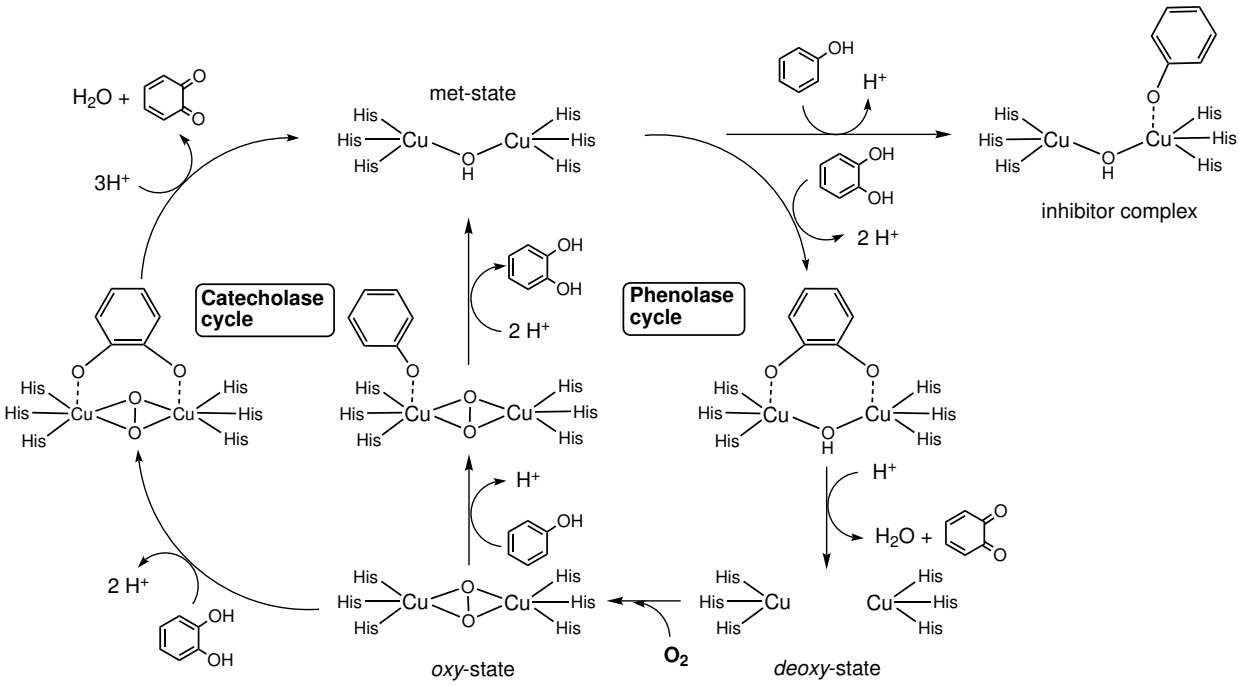

Figure 1.8: Mechanism of cresolase and catecholase activity of tyrosinase and/or catechol oxidase [17]

A diphenol substrate binds to the met state, followed by the oxidation of the substrate to the first quinone and the formation of the reduced state of the enzyme. Binding of dioxy-

gen leads to the oxy state which is subsequently attacked by the second diphenol molecule. Oxidation to the second quinone forms the met state again and closes the catalytic cycle.

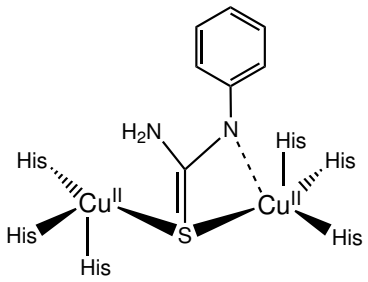

Figure 1.9: PTU inhibitor complex

Alternative reaction mechanisms include a radical mechanism proposed by Kitajima and Moro-oka [34] and a mechanism involving a Cu(III) intermediate based on measurements of model compounds.[35] Krebs et al. postulate on the basis of the crystal structure of the phenylthiourea (PTU) inhibitor complex only a monodentate attack of the catechol at one of the copper atoms.[17] Very recently, Stack et al. have reported that the electrophilic reaction observed for tyrosinase does not exclude the intermediacy of bis(μ-oxo)dicopper(III)-core components.[36] It is discussed that, during the coordination of the phenolate to the μ-η^2:η^2-peroxodicopper(II) core, the peroxo bond is cleaved reductively under formation of the Cu(III) species. The distinct difference between catechol oxidase and tyrosinase has yet not been explained. A lag phase in the monophenolase activity of tyrosinase has been found and studied and is proposed to be a result of temporary inhibition of the met state of tyrosinase by excess of the monophenol substrate (Figure 1.8).[15] Monophenolase activity increases when the diphenol product displaces the monophenol from met tyrosinase and allows the continuation of the catalytic cycle.

1.4 Technical application of copper compounds in catalytic oxidative transformations

Industrially,[37] copper has long been used as a catalyst in the Glaser process, which couples terminal acetylenes to give diacetylenes using cuprous chloride and molecular oxygen (process 1 in Figure 1.10). This is a historically important (but now obsolete) catalytic process for producing the precursor to chloroprene which is then used to produce neoprene rubber. Another important industrial process which utilises copper/dioxygen chemistry is the oxidative coupling of 2,6-xylenol to form a *para*-phenylene oxide polymer by coupling an oxygen of one phenol molecule to the para carbon of another to form an aromatic polyether by the trade name PPO (process 2 in Figure 1.10).[38] This polyether is a high melting plastic that is extremely resistant to heat and to water, and it is useful as an engineering thermoplastic. Another less common process also uses copper(I)chloride to catalyse the analogous oxidation

of 2,6-diphenylphenol to form an even more rigid and higher melting material than PPO. A further important copper-catalysed process is the oxidative decarbonylation of benzoic acid to phenol which was patented by Dow Chemical in 1955 (process 3 in Figure 1.10).[39] Behind the Cumol process it is the second most important process (200,000 t/a) in industrial phenol production.

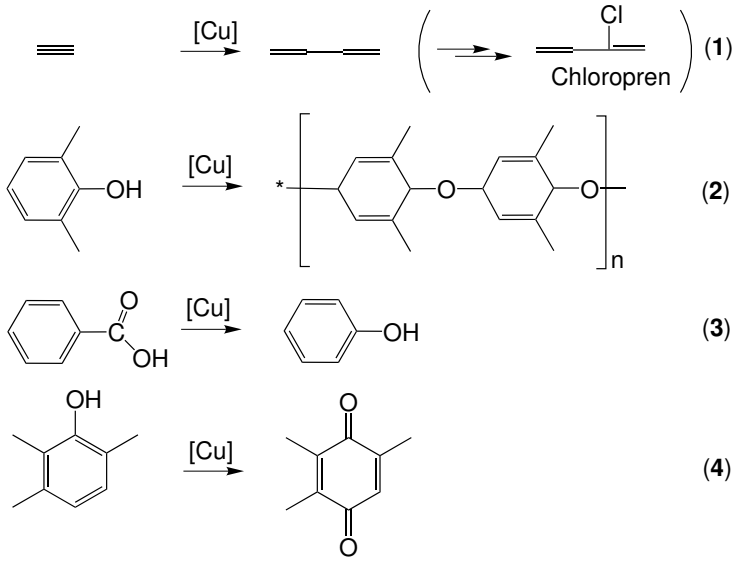

Figure 1.10: Copper-catalysed processes in industry

Also of technical interest is the oxidation of aromatic substrates such as phenols to quinones,[40] e.g. 2,3,6-trimethylphenol to trimethyl-p-benzoquinone, an important vitamin E precursor, that had been claimed by a patent of the Mitsubishi Gas Corp. in the mid 1980´s.[41] Aerobic oxidation of catechols to o-quinones and the hydroxylation of arenes are just two more copper induced catalytic processes that are currently studied.[35] The oxidative carbonylation of alcohols attracted particular attention in the past because a row of products (e.g. polyurethanes, polycarbonates) are based on the organic carbonates that are formed in that catalysis.[42] An important industrial process that indirectly utilises copper/dioxygen chemistry is the Wacker process which produces acetaldehyde from ethylene.[43] In this process, both palladium chloride and cupric chloride are used. Although the copper catalyst is not directly involved in the oxidation of the ethylene substrate, it is crucial for catalysing the re-oxidation of Pd(0) to Pd(II) to sustain the catalytic cycle. Synthetically, copper/dioxygen reactivity has been utilised in a similar fashion, in the osmium-catalysed hydroxylation of olefins. Cupric chloride/O_2 is used to catalyse the re-oxidation of osmium from a formal oxidation state of +6 to +8. Other synthetic uses of Cu/O_2 catalysts include the oxidation of various substrates such as aniline, aromatic diamines, alcohols and thiols.[44]

1.5 Biomimetic model systems for type 3-copper centres

1.5.1 Reactions of Cu(I) complexes with molecular oxygen under formation of Cu/O_2 adduct complexes

Reproducing complex biological reactivity within a simple synthetic molecule is a challenging endeavour with two goals. First, the sequence of examining biological reactivity, creating similar chemical architectures, and determining functional reaction conditions for model systems is a process that allows the biological code of reactivity to be deciphered. This process is greatly aided by X-ray structural data as the atomic arrangement at the active site fully encodes the observed reactivity. Second, the greater availability of such structural information now allows a shift in the role of synthetic modeling from structural and spectroscopic endeavours to development of functional and catalytic models. Functional models can provide an opportunity to examine a biological reactivity at a small-molecule level in detail through systematic and comparative studies. Although one goal of modeling is reproduction of reactivity, the extension of this reactivity towards catalytic applications in industry is an even more important objective as tailored ligand design can lead to effective and environmental friendly oxidation catalysts. There are many recent reviews describing different aspects of Cu/O_2 adduct formation, characterisation and subsequent reactivity toward substrates.[16, 45, 46, 47, 48, 49, 50, 51, 52, 53]

The expanded research efforts during the past two decades to stabilise and characterise Cu/O_2 species formed by the oxygenation of Cu(I) complexes can be attributed partly to a greater accessibility of appropriate spectroscopic tools and to a better appreciation of the appropriate reaction conditions. Low temperature, aprotic solvents and weakly coordinating anions are now standard conditions. This approach contrasts with earlier studies that relied on using ambient temperatures and coordinating anions; under these conditions, most Cu(I) complexes react with O_2 in a 4:1 stoichiometry without any measurable accumulation of intermediates. The ensuing products are Cu(II) complexes ligated by oxide-level ligands - oxide, hydroxide, or water - created by O_2 reduction.[45] Lower reaction temperatures enhance the lifetime of the initially formed Cu/O_2 species by reducing the entropic costs of formation and by attenuating subsequent reactions. This strategy has yielded well-characterised thermally sensitive species with $Cu:O_2$ reaction stoichiometries of 1:1, 2:1 and 3:1. An overview of this diverse array of Cu/O_2 species is given in Figure 1.11. Table 1.1 summarises the characteristic spectroscopic features of some Cu_nO_m adduct complexes.

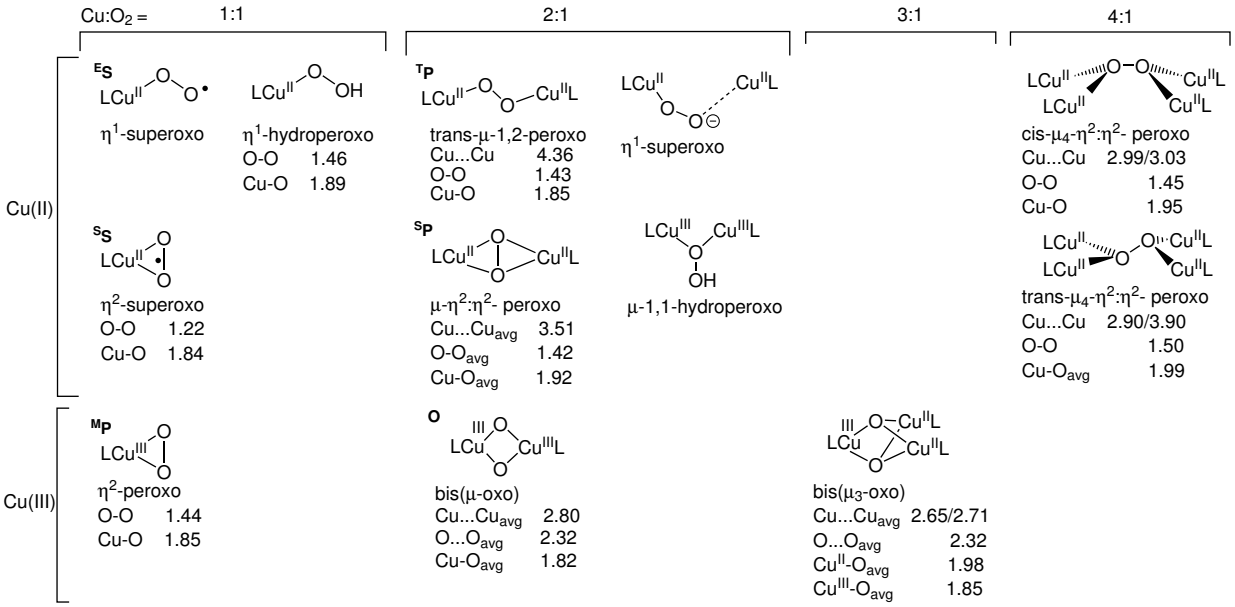

Figure 1.11: Cu_nO_m cores in characterised complexes (for crystallographically characterised species, significant metrical parameters (Å) are given) [45]

1.5.2 Ligand systems and their influence on the formation of Cu/O_2 adduct complexes

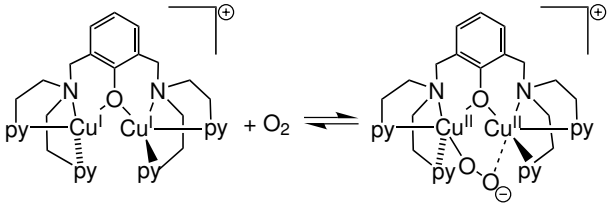

Figure 1.12: Reaction of $[Cu_2(XYL\text{-}O^-)]^+$ with O_2

In 1984, Karlin et al. [67] reported the first case of reversible dioxygen binding to copper, where the reaction product was also proven to possess an intact O-O bond. This involves a dicopper complex with a bridging phenoxide ligand. The dicopper(I) complex $[Cu_2(XYL\text{-}O^-)]^+$ reversibly reacts with one mole of O_2 at -80°C to form the adduct $[Cu_2(XYL\text{-}O^-)(O_2)]^+$ (Figure 1.12). This species is a peroxo-dicopper(II) complex as determined from resonance Raman (ν(O-O) 803 cm^{-1}) and X-ray absorption spectroscopic studies. Structural insights from EXAFS spectroscopy (Cu...Cu 3.31 Å) and a mixed isotope (^{16}O - ^{18}O) resonance Raman experiment suggest that the peroxo ligand is terminally bound, consistent with the presence of two peroxo-to-copper(II) charge transfer bands, assigned as π^*_σ (505 nm) and π^*_v (610 nm) transitions. In 1988, Karlin and coworkers [57, 58] characterised the first copper-dioxygen adduct X-ray crystallographically. The reversible oxygenation of the precursor complex $[(TMPA)Cu^I(RCN)]^+$ yielded the trans-μ-1,2-peroxo dicopper species $[(TMPA)Cu_2(O_2)]^{2+}$ (Figure 1.13).

Table 1.1: Characteristic spectral features of some Cu_nO_m adduct complexes

Coordination mode	UV/Vis: λ_{max}/nm[ϵ/$M^{-1}cm^{-1}$]	Raman: ν(O-O)/cm^{-1}	references
η^1-superoxo	400-430(4000-8000) 580-600(1000-1700)	O^{16}-O^{18}: 800-900 $\Delta[O^{18}]$: 50-60	Karlin et al.[51]
η^2-superoxo	450-510(200-300) 660-700(40-90)	O^{16}-O^{18}: 1050-1200 $\Delta[O^{18}]$: 50-60 (smaller ν(Cu-O) at 550 cm^{-1})	Solomon et al.[54]
η^2-peroxo	400-420(2300-2400) 600(broad, 220)	O^{16}-O^{18}: 960-970 $\Delta[O^{18}]$: 50	Tolman et al.[55, 56]
trans-μ1,2-peroxo	435(3000-2400) 520-550(9000-15000) 590-625(7000)(sh)	O^{16}-O^{18}: 830-845 $\Delta[O^{18}]$: 40-50(smaller ν(Cu-O) at 550 cm^{-1})	Karlin et al.[57, 58] Suzuki et al.[59]
μ-η^2:η^2-peroxo	330-365(20000) 530-600(850), further band at 420-490 for butterfly core[68]	O^{16}-O^{18}: 710-765 $\Delta[O^{18}]$: 40	Kitajima et al.[34, 60] Kodera et al.[62]
bis(μ-oxo)	290-330(10000-12000) 390-430(13000-15000)	O^{16}-O^{18}: 580-600 $\Delta[O^{18}]$: 20-25	Tolman et al.[63]
μ-1,1-hydroperoxo	350-395(3000-4200) 450(1600)(sh) 630(400) (very weak)	O^{16}-O^{18}: 850-890 $\Delta[O^{18}]$: 50	Itoh et al.[64]
bis(μ_3-oxo)	290(12500) 355(15000) 480(1400), 620(800)	O^{16}-O^{18}: - $\Delta[O^{18}]$:-	Stack et al.[65]
μ_4-peroxo	390(9500) 590(600)	O^{16}-O^{18}: 880-890 $\Delta[O^{18}]$: 40	Krebs et al.[66]

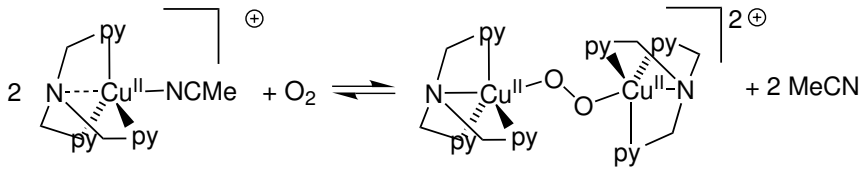

Figure 1.13: Reaction of $[(TMPA)Cu^I(RCN)]^+$ with O_2

In 1994, Kitajima and coworkers [34, 61] used a sterically hindered tridentate ligand in characterising $Cu^{II}[HB(3,5\text{-}i\mathrm{Pr}_2\mathrm{pz})_3]_2(O_2)$ ($HB(3,5\text{-}i\mathrm{Pr}_2\mathrm{pz})_3$ = hydrotris(3,5-diisopropyl-pyrazolyl)borate anion, see also Figure 1.14), which has a side-on ligated μ-η^2:η^2-peroxodicopper(II) structure with physical properties closely matching those of *Limulus polyphemus* oxy-hemocyanin. This important contribution to synthetic modelling of metalloproteins in fact preceded confirmation of the protein Cu_2O_2 side-on structure.

Since then, the research field of bioinorganic copper-dioxygen chemistry has flourished.[45, 48, 49] Central topic are the investigations on the influence of N donor ligands on the formation and structure of the Cu/O_2 adduct complexes as well as the mechanisms of the oxygen-uptake reactions. In Figure 1.14, the most prominent ligand families are depicted. Since the copper centres in biological systems like hemocyanin and catechol oxidase are coordinated by three terminal histidine functions, the use of multidentate N donor ligand systems has been successful in the synthesis of model complexes. Especially the use of bi- and tridentate N donor systems was fruitful for the stabilisation of the (4+1) square-planar coordination of the Cu atoms in the diverse oxo states. Besides the denticity, the hardness of the ligands can be tuned by the use of harder aminic or softer aromatic or iminic N donor functions. By using different alkyl substitution patterns, the electronic properties of the N donor function can be modified. The bite as well as the steric demands of the ligands are also essential parameters. This may be illustrated by the example of the $HB(3,5\text{-}i\mathrm{Pr}_2\mathrm{pz})_3$ system: Kitajima et al. were able to show that, by substitution of the ^{i}Pr groups against ^{t}Bu groups, no longer the μ-η^2:η^2-peroxodicopper(II) complex is formed upon oxygenation but the mononuclear η^2-peroxo complex.[68]

1.5.3 Reactions of d^{10} precursor complexes with triplet oxygen

The reaction of Cu(I) precursors with molecular oxygen is influenced by many factors and not yet fully understood. During the reaction of Cu(I) to Cu(II), the coordination spheres have to change drastically. The spheric symmetrical Cu(I) ion (d^{10}) is found in coordination numbers of 2 to 5 with domination of linear, trigonal planar and distorted tetrahedral arrangements. The Cu(II) ion (d^9) favourises coordinational environments with four strongly bound equatorial ligands and 1 or 2 weaker bound axial ligands (Jahn-Teller-effect). The change of the coordinational environment results in an energetic barrier which dictates kinetics as well as thermodynamics of this system.[84] By the coordinating ligand, the redox properties of the Cu(I)/Cu(II) systems are strongly influenced. Soft donor functions like S, P or unsaturated N systems stabilise Cu(I) compounds whereas N and O donor systems favourise Cu(II) compounds. Furthermore, the redox potentials can be influenced by the size of the chelate rings and the polarity of the solvent.

In spite of the strong O-O bond (118 kcal/mol) is oxygen known to be a strong oxidant. Although the oxidation products are thermodynamically favoured, the course of the reaction is kinetically inhibited. So, the educts are relatively inert under normal conditions. In

Bidentate ligands

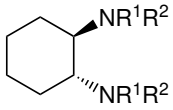

R1,R2cd, Stack [69]

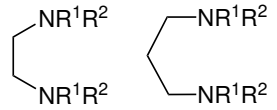

R1,R2ed and R1,R2pd, Stack [46, 70]

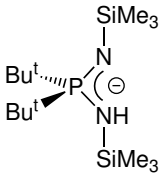

PN_2, Hofmann[71]

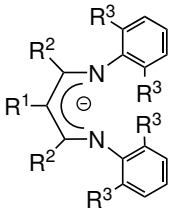

R1,R2DkR3, Tolman [72]

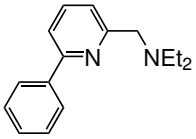

$PhPyNEt_2$, Tolman [73]

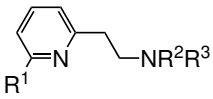

R1Py1R2,R3, Itoh [74]

Tridentate ligands

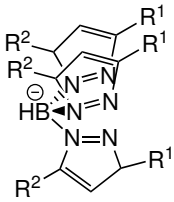

TpR1,R2, Kitajima [34]

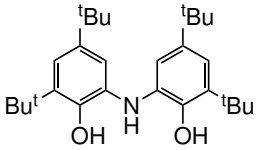

H_3bpa, Wieghardt [75]

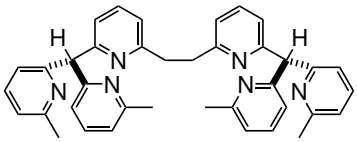

bitripy, Kodera [62]

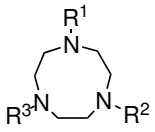

R1,R2,R3tacn, Tolman [48]
"Wieghardt´s ligand"

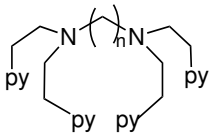

Py2-Nn, Karlin [76]

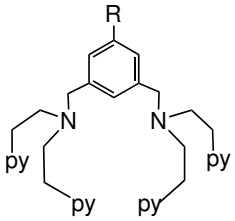

Py2-*m*-xylR, Karlin [77]

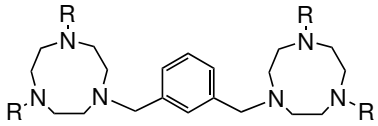

R_4dtn-*m*-xyl, Tolman [78]

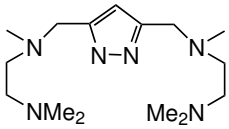

pzdien, Meyer [79]

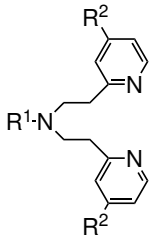

R1Py2R2, Karlin [80]

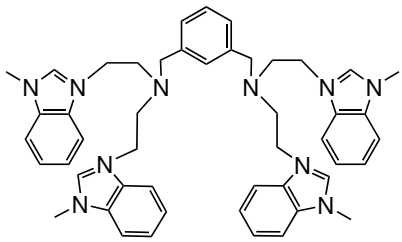

L66, Casella [81]

Tetradentate ligands

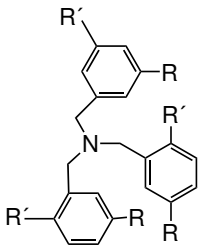

R,R´-tpa, Karlin [58]

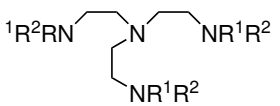

$R^1{}_3R^2{}_3$tren, Schindler [82]

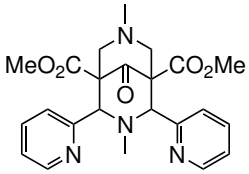

bisp, Comba [83]

Figure 1.14: Overview of ligand families

fact, the redox reactions with the transfer of 4 e^- to O_2 under formation of water (E^0 = + 1.23 V) or of 2 e^- to hydrogen peroxide (E^0 = + 0.69 V) are thermodynamically favoured, whereas processes under stepwise electron transfer (formation of O_2^-: E^0 = - 0.16 V) are unfavourable. One reason for this behaviour is the triplet state of oxygen. The $^3O_2$ molecule is a diradical with the orbital occupation of $[KK](\sigma_z)^2(\Pi_x,\Pi_y)^4(\Pi_x^*)^1(\Pi_y^*)^1$. Therefore, the $^3O_2$ molecule can react in spin-permitted processes with a molecule that has unpaired electrons or the reaction has to lead to a product with triplet ground state. Nevertheless, even at low temperatures (-80°C), a very fast reaction of $^3O_2$ with Cu(I) complexes can be observed. This result is somehow surprising as Cu(I) possesses with its d^{10} configuration a closed 3d electron shell and thus is diamagnetic. However, the greater spin-orbital coupling in metal ions leads to a decrease of the kinetic barrier for a spin reverse and the spin restriction is no langer in force. During the binding of the oxygen to the metal centre, it comes to a classical σ donor and π acceptor binding mode. The O-O bond is weakened and, formally seen, electrons are transferred to the oxygen which is reduced under oxidation of the metal. In the last years, the reaction kinetics of the formation of Cu/O_2 adduct complexes were investigated by means of stopped-flow methodes by Zuberbühler and Schindler.[85, 50] The connections are complex and strongly related to the corresponding systems. In Figure 1.15, the reaction of a monomeric precusor complex **A** with oxygen is shown. First, a fast, reversible side-on-binding of an oxygen molecule under formation of the mononuclear complex **B** takes place. Then, this complex reacts with a second precusor molecule in an irreversible, rate-determining step to the dinuclear complex **C**. Itoh et al. observed a second-order kinetic for this step.[86] By temperature-depending measurements the activation enthalpy ($\Delta H^\ddagger$) and

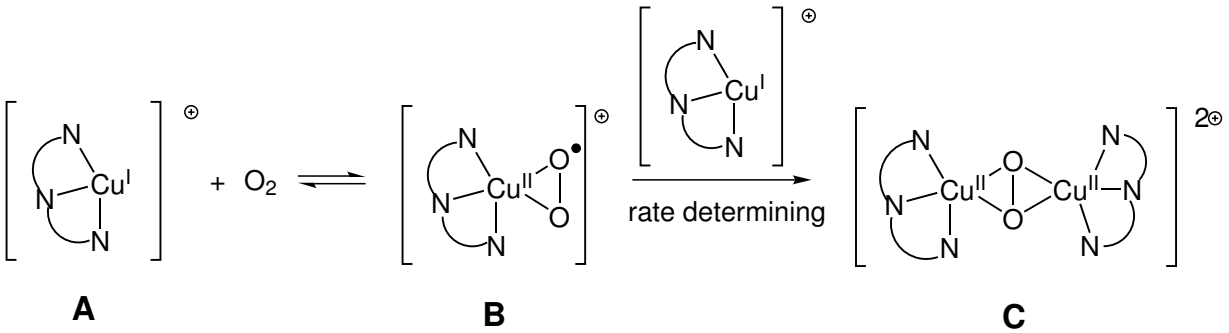

Figure 1.15: Reaction of mononuclear Cu(I) precursor complexes with molecular oxygen

the activation entropy ($\Delta S^\ddagger$) can be determined. Generally, the values of $\Delta H^\ddagger$ are in the range of 10-50 kJ/mol which is quite small. Contrastingly, the values for $\Delta S^\ddagger$ are strongly negative in the range of -100 to -300 kJ/mol. Thus, the stability of the oxygen binding is

controlled by favourable enthalpies and unfavourable entropies such that Cu_2O_2 compounds should not be observed at room temperature.[85] However, in the meantime, Kodera at al. synthesised a μ-η^2:η^2-peroxo dicopper system which is stable at 25°C in CH_2Cl_2 for one day.[62] Gorun and coworkers also reported on the synthesis of a room temperature stable μ-η^2:η^2-peroxodicopper complex, by replacing C-H bonds in the vicinity of the Cu_2O_2 core with C-F bonds.[87]

1.5.4 Complexes with μ-η^2:η^2-peroxo and bis(μ-oxo) dicopper cores

The reactions of the Cu(I) precursors with molecular oxygen can be observed very well by means of UV/Vis and resonance Raman spectroscopy. The crystallisation is possible only under special conditions. Fortunately, the distinction between the μ-η^2:η^2-peroxo and bis(μ-oxo) dicopper cores (P- and O-cores, respectively) can be made with these spectroscopic methods.[48] Figure 1.16 depicts some structural features of these two cores. In the UV/Vis

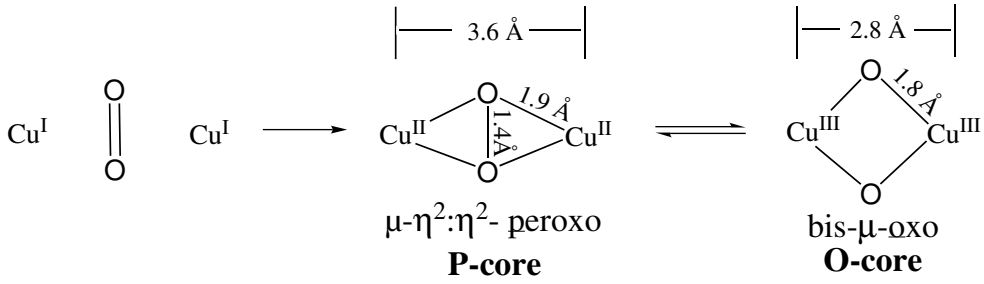

Figure 1.16: Equilibrium between μ-η^2:η^2-peroxo and bis(μ-oxo) dicopper cores

spectra, the P-core shows characteristic absorptions at 350 nm ($\epsilon \approx 20000$ $M^{-1}cm^{-1}$, assigned to the peroxo-Cu(II) charge transfer) and at 550 nm ($\epsilon \approx 1000$ $M^{-1}cm^{-1}$), whereas the O-core has a pair of characteristic absorptions at 300 nm and 400 nm with an extinction coefficient of approximately 14000 $M^{-1}cm^{-1}$. These bands can be assigned to O^{2-}-Cu(III) charge transfers. The P-core is antiferromagnetically coupled, both cores are EPR-silent. In the resonance Raman spectrum, the O-O bond of the P-core can be detected at 750 cm^{-1}, whereas the O-core exhibits a Cu_2O_2 breathing mode at 600^{-1}. A closer discussion of the MO situation of these two cores can be found in section 5.1. Tolman et al. reported that the equilibrium between these two species can be shifted by the solvents and the counterions. [63] Coordinating solvents favour the formation of a bis(μ-oxo) species whereas non-coordinating solvents stabilise the μ-η^2:η^2-peroxo species. Furthermore, a change in the substitution pattern of a ligand system (e.g. diamines, tacn) can switch the P/O equilibrium totally to one side. [45, 49] Generally, tridentate ligand systems favour merely the P-core and bidentate

systems the O-core, but there are numerous counter-examples for this trend. [48] In spite of great efforts in this field, not all types of influence have been fully understood.

1.6 Guanidines - model systems for the enzymatic environment

The synthesis and characterisation of novel ligand systems plays an important role for coordination chemistry as the coordinating ligands determine the formed complexes regarding their thermodynamic and kinetic stability, their solubility and their redox properties. The purpose of this thesis is the synthesis of biomimetic oxygen activating copper complexes. Therefore, the ligand design has to be orientated by efficient solutions of Nature. Suited ligand systems are ligands with N donor functions which are similar to the basic δ imin function of histidine, one of the most versatile and successful systems found in biologic coordination chemistry. The essential amino acid histidine coordinates several metals in high oxidation states, e.g. copper in all type 3-centres, iron in hemerythrin, manganese in manganese catalase and manganese superoxid dismutase. In the CuZn superoxid dismutase, histidine acts as well as bridging ligand between the two metals.[2] Furthermore, the desired bio-inspired ligand system should be multidentate, chelating and neutral. The stabilisation of higher oxidation states like Cu(III) succeeds better with a strongly basic molecule. The demanded basicity and biomimetic coordination properties are combined by guanidine systems.
Peralkylated guanidines belong to the strongest organic neutral bases known. They are several magnitudes superior in basicity than tertiary amines due to the excellent stabilisation of the positive charge in their protonated form (Figure 1.17).[88]

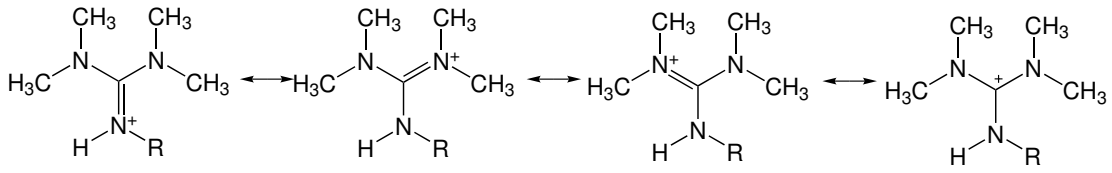

Figure 1.17: Delocalisation of the positive charge in a guanidinium cation

The type and number of substituents influence considerably the basicity of the guanidine function as it is shown in Table 1.2.[88, 89] This possibility of variation is important for the complexation properties and the stabilisation of higher metal oxidation states. Via introduction of a methyl group (no. 2), the basicity decreases compared with the unsubstituted parent compound guanidine (no. 1) as the symmetry in the equivalence of the resonance

structures of the conjugated guanidinium cation is disturbed. This effect can not be fully compensated by a single methyl group by hyperconjugation, whereas in the case of multiple methyl substitution (nos. 5 and 6), this effect is overcompensated. The torsion of the substituent planes can also be decisive: the full substitution with sterically demanding alkyl groups (no. 7) leads to a slight diminuishing of the basicity in comparison to pentamethylguanidine (no. 6). By the twisting of the substituent planes, the efficiency of the conjugation as well as the hyperconjugative effect is reduced. Such a distortion can be hindered by the integration of the guanidine groups into a cycle (no. 8) resulting in a slightly higher basicity. However, the introduction of acceptor and aryl substituents generally leads to a decrease of the basicity (nos. 3 and 4) which can be traced back to the good donor qualities of the substituents.

Table 1.2: pK_S-values of the conjugated acids of guanidines in water and MeCN [88, 89]

No.	R^1	R^2	R^3	R^4	R^5	$pK_S(H_2O)$	pK_S(MeCN)
1	H	H	H	H	H	13.6	
2	Me	H	H	H	H	13.4	
3	Ph	H	H	H	H	10.77	
4	Ac	H	H	H	H	8.20	
5	H	Me	Me	Me	Me	13.6	23.3
6	Me	Me	Me	Me	Me	15.6	25.0
7	*i*Pr	*i*Pr	*i*Pr	*i*Pr	*i*Pr	13.8	
8	R	R	R	R	Me		25.43
							R = -$(CH_2)_3$-

Guanidines are ubiqitous in Nature, e.g. in the essential amino acid arginin which is present in almost all proteins. In organic synthesis, guanidines are used as phase transfer catalysts,[90] as non-nucleophile bases and as solvents in form of ionic liquids.[91] In technical systems, guanidines are found as components or intermediates in the production of pharmazeutics and pesticids like chloronicotinylguanidine. Some guanidinium salts have come to importance as impregnants or flameproofing agents as well as emulsifiers or antistatic agents in textile industry.

1.6.1 Peralkylated Bisguanidine Ligands

In 1965, guanidines were investigated as neutral ligands for the first time by Longhi and Drago who supposed good donor properties by the high basicity of tetramethylguanidine

(TMG).[92] In 1970, Snaith, Wade and Wyatt synthesised extremely hydrolysis sensible adducts of TMG and aluminium alkyls.[93] Later, Pruszynski et al. designed the first chelating guanidine ligands.[94]

Today, guanidines are emerging as a potentially useful ligand class due to their versatile coordination chemistry. Neutral guanidines $[(R_2N)_2C{=}NR]$, guanidinates(1-) $[(RN)_2CNR_2]^-$ and guanidinates(2-) $[(RN)_2C{=}NR]^{2-}$ are capable of exhibiting a variety of coordination modes and a range of donor properties leading to compatibility with a remarkably wide range of metal ion requirements from all parts of the periodic table. [95, 96, 97, 98, 99] Furthermore, numerous complexes are reported in which guanidinium cations are present, but these are not located within the coordination sphere of the metal ion and consequently merely represent counterions.[100, 101] Whilst application of the negatively charged guanidinates has become more widespread in coordination chemistry, the use of the neutral guanidines has not received similar attention to date.[95] Bailey and coworkers investigated the behaviour of monodentate guanidine ligands [102] whereas Coles et al. introduced bicyclic guanidine systems into coordination chemistry.[96, 97, 98] Mostly, these systems are not peralkylated, but meanwhile, peralkylated phosphorus [103] or silicon [104] bridged systems have been developed. Pruszynski et al.,[94] Pohl et al.[105, 106] and Sundermeyer et al.[107, 108, 109, 110] investigated peralkylated guanidine systems with organic bridges. Furthermore, Kuhn et al.[111] developed imidazolin-based systems which belong to the bisguanidine class of ligands. In guanidine complexes, coordination occurs almost exclusively via donation of the lone-pair of the N_{imine} atom into appropriate acceptor orbitals of the metal.

In search of bifunctional nitrogen donor ligands able to stabilise unusually high metal oxidation states, our interests were attracted by peralkylated guanidyl-type systems. Following this approach, bis-tetramethylguanidinopropylene (btmgp) was synthesised as the first member of a series of bifunctional peralkylated guanidine ligands designed for use in biomimetic coordination chemistry.[105, 106, 112] A great advantage of guanidine ligands lies in their stability towards fragmentation reactions. We could show that btmgp-containing copper-dioxygen complexes react only with the peripheric substituents under conservation of the guanidine scaffold [113] in contrast to other systems where dealkylation reactions are observed.[49]

1.6.2 Synthesis methods for guanidines

Alkylation of tetrasubstituted guanidines

The simpliest method for the synthesis of chelating guanidine systems is the reaction of guanidine derivatives with dihalogenoalkanes (Figure 1.18).[105] Unfortunately, this method requires a great excess of the guanidine, long reaction times and only btmgp can be synthesised in sufficient yields. The reason for these difficulties lies in the occuring side reactions such as polyalkylation or elimination reactions.

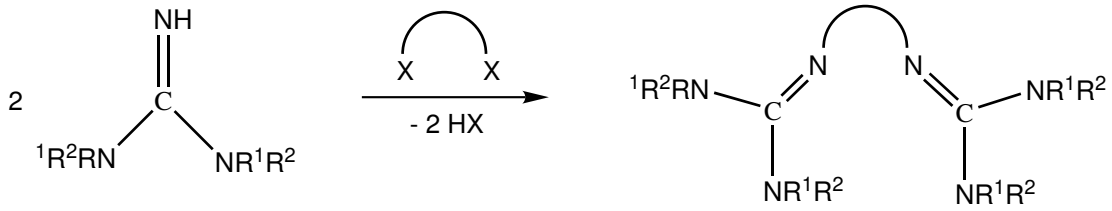

Figure 1.18: Reaction of guanidine derivatives with a halogenealkane

The Bredereck method

In the so-called Bredereck method,[114] several pentaalkyl- and aryltetraalkylguanidines can be accessed by combining peralkylated ureas with phosphoroxychloride. This method is based on the activation of the urea by the phosphoroxychloride for the following reaction with the amine (Figure 1.19). Although an equimolar reaction of urea, $POCl_3$ and amine seems possible, the use of amines and $POCl_3$ in excess is advantageous. In addition, thioureas are more reactive than ureas due to the higher nucleophilicity of the sulfur atom facilitating the primary attack of $POCl_3$. Disadvantageous in this method are the generally long reaction times of 8 h.

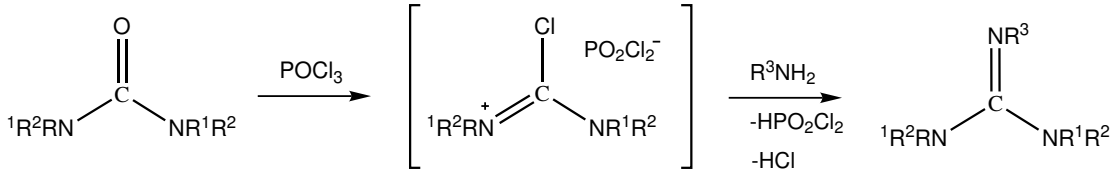

Figure 1.19: Synthesis of guanidines after Bredereck

Reaction of isocyaniddichlorides with amines

A further possibility for the preparation of pentasubstituted guanidines is the reaction of isocyaniddichlorides with secondary amines (Figure 1.20).[115] This synthetic strategy is useful

for the synthesis of unsymmetrically substituted guanidines due to the principal possibility of isolating the intermediately obtained chloroformamidines.

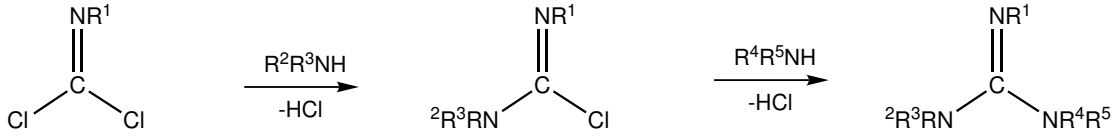

Figure 1.20: Guanidines via reaction of isocyaniddichlorides with amines

Condensation of amines with Vilsmeier salts

The most efficient method to synthesise peralkylated guanidine systems is the strategy analogue to the Vilsmeier synthesis.[116] In classic organic synthesis, activated aryls like phenols and dialkylanilines are formylated via the Vilsmeier synthesis. By reaction of a equimolar mixture of a N,N-disubstituted formamid and phosphoroxychloride with an activated aromat and subsequent hydrolysis, the formylation product can be obtained in good yields (Figure 1.21). In the primary reaction of the formamid with the phosphoroxychlorid via a Vilsmeier complex, a chloromethaniminium salt is formed as reactive intermediate which attacks the aromatic core electrophilicly.

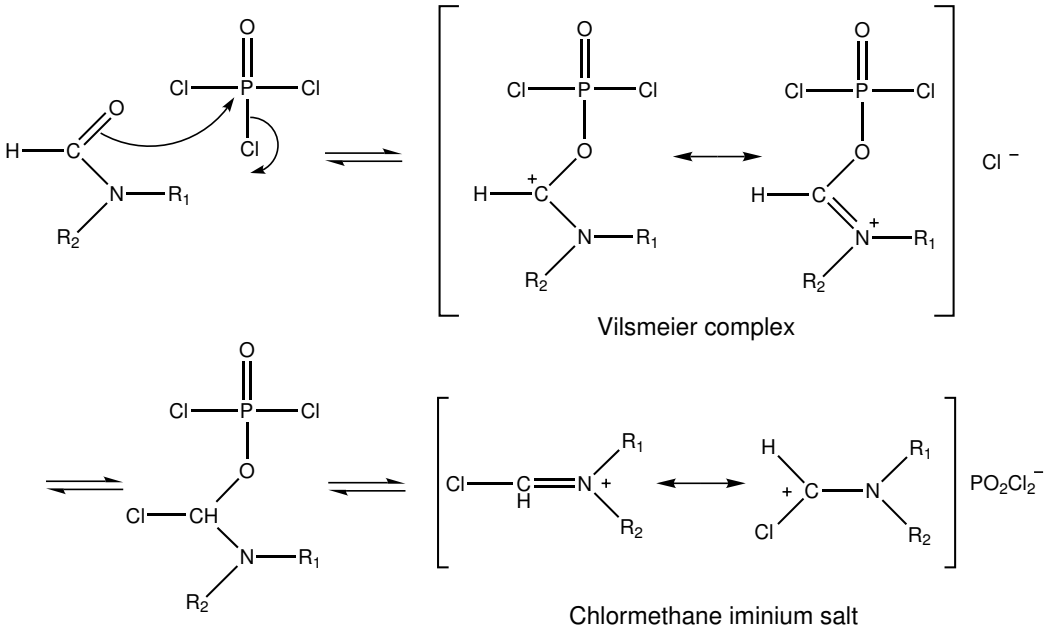

Figure 1.21: Formation of the reactive iminium salt species in the Vilsmeier synthesis

For the synthesis of guanidines, one can take advantage of the strong activation of the ureas in form of iminium salts. Therefore, peralkylated ureas are transformed into the corresponding chloroformamidinium chlorides (sometimes called Vilsmeier salts) by use of

phosphoroxychloride or thionylchloride. Phosgene is a clean alternative to these both as the accompanying by-product CO_2 leaves the reaction mixture.

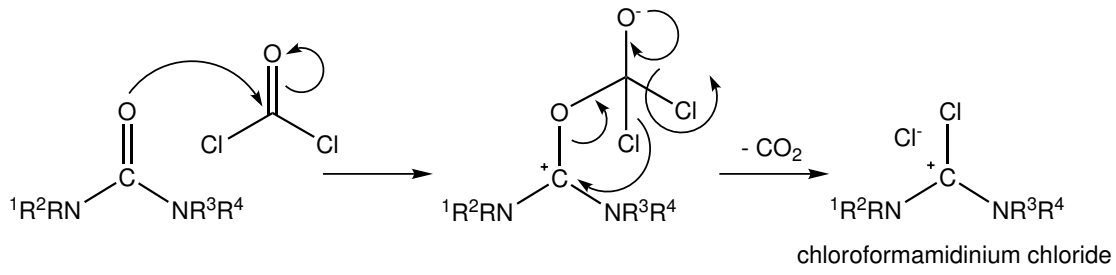

Figure 1.22: Mechanism of the reaction of a peralkylated urea with phosgen

In the second step, the reaction of the Vilsmeier salt with an amine in the presence of an auxiliary base like triethylamine is following to give the protonated form of the peralkylated guanidine. This guanidinium chloride can be deprotonated with 50% aqueous KOH solution to yield the free guanidine base. Guanidines can be obtained crystalline, but they are mostly of oily or waxy consistence. This synthetic strategy was developed by Kantlehner et al.[117] who added an auxiliary base in equimolar amounts to the reaction mixture. This auxiliary base removes the formed HCl and facilitates considerably the progress of the reaction to the intermediate guanidinium chloride (a similar consideration might explain the more efficient course of the Bredereck method by using an excess of amine). By Kantlehner´s method, pentasubstituted guanidines are obtained in good yields.

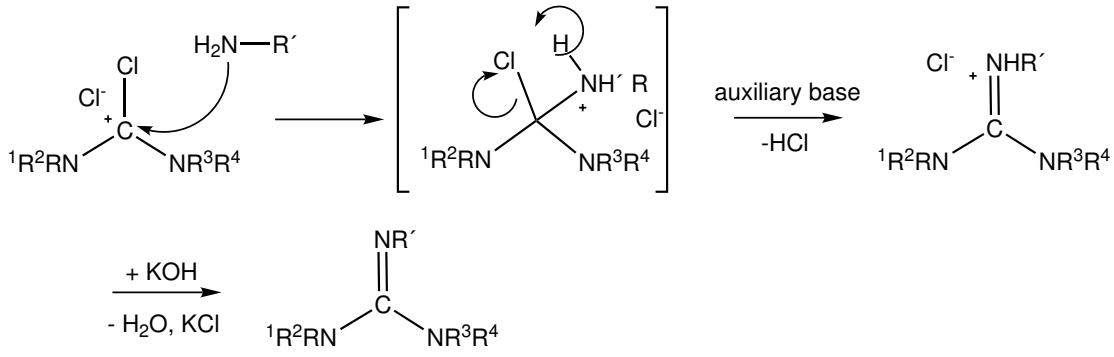

Figure 1.23: Mechanism of the condensation of chloroformamidinium chlorides with amines under use of an auxiliary base

2 Objective and outline

2.1 Objective of the present work

The modelling of the active sites of metalloproteins is one of the most challenging tasks in bioinorganic chemistry. Copper proteins form part of the stimulating field of research as copper enzymes are mainly involved in oxidation bio-reactions. Thus, the understanding of the structure-function-relationship of their active sites will allow the design of effective and environmental friendly oxidation catalysts.

A key research objective of this work is to understand how supporting ligand structural features influence the relative stabilities and interconversions of copper-oxygen adduct species, and especially the effects which control the equilibrium between μ-η^2:η^2-peroxo and bis(μ-oxo) dicopper cores that are relevant to proposed metalloprotein active site intermediates. A systematic investigation provides with new insights into this field which is still controversely discussed.

Hence, an important topic of this work is the design and the synthesis of biomimetic ligands with the subsequent synthesis of the corresponding copper(I) complexes. In search of bifunctional nitrogen donor ligands able to stabilise unusually high metal oxidation states, peralkylated guanidyl-type systems appear to be suited for use in biomimetic coordination chemistry. Great significance is attached to the structural characterisation of copper(I) bisguanidine complexes in order to analyse correlations between structure and function. The main focus lies on the activation of molecular oxygen mediated by the synthesised copper(I) bisguanidine complexes. The mechanisms of dioxygen activation are still under discussion and, even more, the mechanisms of the following reactions are far from clear. The subsequent reactions of the generated Cu_2O_2 species have to be studied because they give information about the degree of the oxidation potentials. At this stage, efficient use of this potential is restricted due to a lack of accessible ligands demonstrating that a synthetic protocol has to be developed which supports the designing of oxidation catalysts.

By suitable modification of the guanidine substitution patterns in such complexes, their hydroxylation potential shall be redirected from the ligand to external substrates. As the ligands are bidentate, the reaction centre should easily be accessible for external substrates and well suited for substrate pre-coordination. A further important focus which is based on the development of efficient copper containing oxidation catalysts is their screening in suited test reactions and the investigation of their reaction mechanisms.

2.2 Outline of the present work

The present thesis deals with the above-descibed topics in a systematic order in the chapters 3 to 7. These chapters are based on each other, but they can be read independently.
In Chapter 3, a modular approach and an efficient synthetic protocol for the synthesis of bisguanidine ligands are presented. Furthermore, this chapter sheds light on characteristic features of these biomimetic ligands like typical structural properties and their coalescence behaviour in NMR spectroscopy. The synthesis of copper(I) complexes containing these ligands and their structural and electrochemical properties are treated in Chapter 4. These copper(I) bisguanidine complexes serve as precursors for the highly reactive Cu_2O_2 species which are discussed in Chapter 5. Additionally, Chapter 5 provides with a correlation of the structure of these precursors and their reactivity in the activation of dioxygen. This correlation is completed with an intensive discussion of the theoretical foundations and a study of the kinetics of the Cu_2O_2 adduct formation. In Chapter 6, the products of the hydroxylation reactions of selected ligands by subsequent reactions of the Cu_2O_2 adducts are presented and their structural features are set in comparison. A possible hydroxylation mechanism has to be discussed as well. Finally, in Chapter 7, the oxidation potential of the reactive Cu_2O_2 species is directed towards external substrates, namely 2,4-di^{tert}butylphenol, 2,6-di^{tert}butylphenol and 3,5-di^{tert}butylcatechol. These substrates have been chosen as test substrates for the investigation of oxidation and oxygenation reactions mediated by the copper(I) bisguanidine catalysts. Chapter 8 contains the experimental part of this thesis.
New insights obtained from the investigations of this work and the resulting possibilities for future studies are summarised in Chapter 9.

3 Bisguanidine ligands

3.1 Synthesis of the ligands

3.1.1 Motivation

By suitable modification of the guanidine substitution patterns in bisguanidine complexes, it is intended to redirect their hydroxylation potential from the ligand to external substrates. As the ligands are bidentate, the reaction centre should easily be accessible for external substrates and well suited for substrate pre-coordination. In addition, the oxygen is shielded against too fast reaction with these substrates by the spatially demanding guanidine moieties resulting in enhanced oxidation selectivities. At this stage, efficient use of this potential is restricted due to a lack of accessible ligands demonstrating that a synthetic protocol has to be developed which supports these objectives.

For this purpose, a modular approach for bisguanidine compounds had to be developed which provides a library of biomimetic ligands (Figure 3.5). This library contains members with complete flexibilities in the spacers connecting the guanidine functionalities as well as in the substitution patterns of the guanidine moieties. Via modification of the spacer, it is possible to vary the denticity, the bite angle and the coordination geometry, whereas via modification of the guanidine moities, the σ-donating and π-accepting properties of the N_{imine} atom might be influenced. In order to increase the steric demand of the guanidine moieties and thus the oxygen-shielding effect in their complexes, a series of chloroformamidinium chlorides from secondary amines containing the required bulky substituents had to be prepared. By this method, the transformation of almost every aliphatic secondary amine into the corresponding chloroformamidinium chloride should be possible.

3.1.2 Realisation of a modular approach

The synthesis of the ligands was accomplished following a general procedure that allows the condensation of almost every aliphatic urea with almost every primary amine to form a

guanidine compound. This condensation proceeds via the transformation of the urea component into its corresponding chloroformamidinium chloride which is sometimes referred to as Vilsmeier salt.[117] Conventional chloroformamidinium chlorides are obtained in good yields by reaction of the specific peralkylated ureas with phosgene in toluene or acetonitrile.[117] The biomimetic approach requires spatially demanding substituents at the guanidine moieties because sterically hindered systems are expected to control the access of substrates to the oxygen in the corresponding copper-dioxygen complexes. Therefore, a straightforward synthetic protocol starting with bulky secondary amines has been developed (Schemes 3.1 and 3.2). This one-pot synthesis consists of the combination of two equivalents of the corresponding secondary amine with two equivalents of phosgene in acetonitrile. In the first reaction step, the alkyl substituted urea is formed and triethylamine acts as auxiliary base by capturing the released HCl (Scheme 3.1, Reaction (1)). In the second step, a further equivalent of phosgene transforms this urea into the chloroformamidinium chloride. A possibility for the synthesis of non-symmetric chloroformamidinium chlorides and the subsequent formation of non-symmetric substituted bisguanidine ligands is the reaction of carbamoyl chlorides with secondary amines in the presence of one equivalent of NEt_3 (Scheme 3.1, Reaction (2)). In the second step, one equivalent of phosgene transforms this non-symmetric urea into the chloroformamidinium chloride.

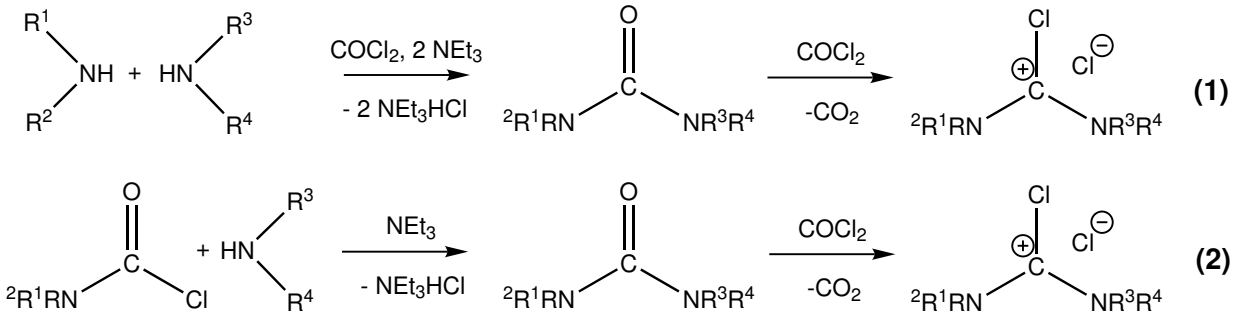

Figure 3.1: Generation of the chloroformamidinium chlorides

Reaction of the mixture containing the chloroformamidinium chloride in the presence of triethylamine as an auxiliary base with a bisamine leads to the bis-hydrochloride of the ligand. Separation from the by-product NEt_3HCl is accomplished by adding 1 equiv. of NaOH per guanidine functionality und removing the resulting NEt_3 and the solvent under reduced pressure. The hydrochloride is not isolated but deprotonated by using a two-phase system of MeCN/50 % aqueous KOH in order to obtain the pure free base which needs no further purification (Scheme 3.2).

Table 3.1 gives an overview of the prepared chloroformamidinium chlorides. Using these chlo-

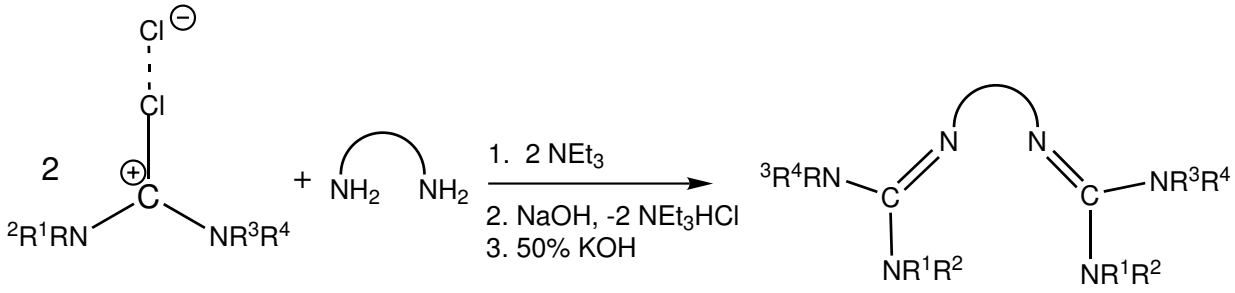

Figure 3.2: Reaction between the chloroformamidinium chloride and the bisamine

roformamidinium chlorides, the guanidine moieties shown in Figure 3.3 could be synthesised. Within this figure, Gx assigns the guanidine moiety associated to the chloroformamidinium chloride Vx, R_S assigns the connection with the spacer.

Table 3.1: Overview of the chloroformamidinium chlorides (reactions starting from the urea are marked with an asterisk)

Substituents R^1 - R^4	**Chloroformamidinium chloride**
R^1, R^2, R^3, R^4: -Me	Tetramethylchloroformamidinium Chloride* (V1)
R^1, R^2, R^3, R^4: -Et	Tetraethylchloroformamidinium Chloride* (V2)
R^1, R^2, R^3, R^4: -iPr	Tetraisopropylchloroformamidinium Chloride (V3)
R^1, R^4: -Me, R^2-R^3:-$(CH_2)_2$-	Dimethylethylenechloroformamidinium Chloride* (V4)
R^1, R^4: -Me, R^2-R^3:-$(CH_2)_3$-	Dimethylpropylenechloroformamidinium Chloride* (V5)
R^1, R^4: -nPr, R^2-R^3:-$(CH_2)_3$-	Dipropylpropylenechloroformamidinium Chloride* (V6)
R^1-R^2, R^3-R^4: -$(CH_2)_5$-	Dipiperidylchloroformamidinium Chloride* (V7)
R^1-R^2, R^3-R^4: -CH(Me)$(CH_2)_3$CH(Me)-	Bis(dimethylpiperidyl)chloroformamidinium Chloride (V8)
R^1-R^2, R^3-R^4: -C(Me)$_2(CH_2)_3$C(Me)$_2$-	Bis(tetramethylpiperidyl)chloroformamidinium Chloride (V9)
R^1-R^2, R^3-R^4: -CHNCHCH-	Diimidazolylchloroformamidinium Chloride* (V10)
R^1-R^2, R^3-R^4:-$(CH_2)_2O(CH_2)_2$-	Dimorpholinochloroformamidinium Chloride (V11)
R^1-R^2, R^3-R^4:-$(CH_2)_2S(CH_2)_2$-	Dithiomorpholinochloroformamidinium Chloride (V12)
R^1, R^2: -Me, R^3-R^4:-$(CH_2)_2O(CH_2)_2$-	Morpholinodimethylchloroformamidinium Chloride (V13)
R^1, R^2: -Me, R^3-R^4:-CHMe$(CH_2)_3$CHMe-	Dimethylpiperidinodimethylchloroformamidinium Chloride (V14)

The spacers shown in Figure 3.4 are used as constituents of bisguanidine ligands for several reasons: the propan-1,3-yl (p) spacer is a typical aliphatic spacer with a suitable "bite" for 3d-metal coordination, [11,14,16,20] the flexible (3,6-di-oxa)octan-1,8-yl (doo) spacer offers more donor functions for metal coordination whereas the cyclohexan-1,3-yl (ch) system is more rigid. The aromatic systems diphenyleneamine (PA), N-Methyl-diphenyleneamine (MePA) and pyridin-2,6-yl (py) offer a further N donor function whilst the m-xylol-α,α'-yl (mX) unit has a great "bite" and more flexibility than the other spacers.

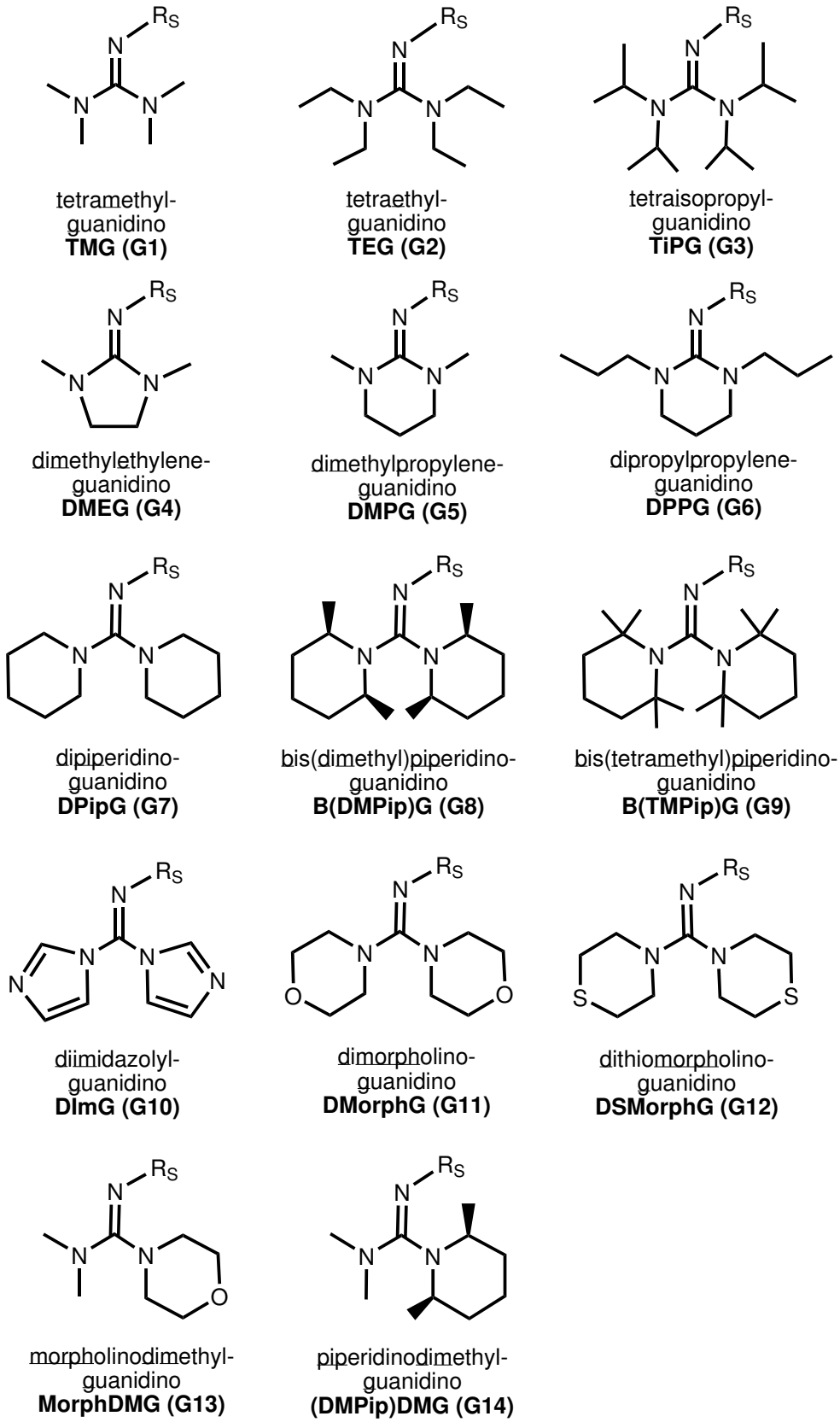

Figure 3.3: Guanidine portions

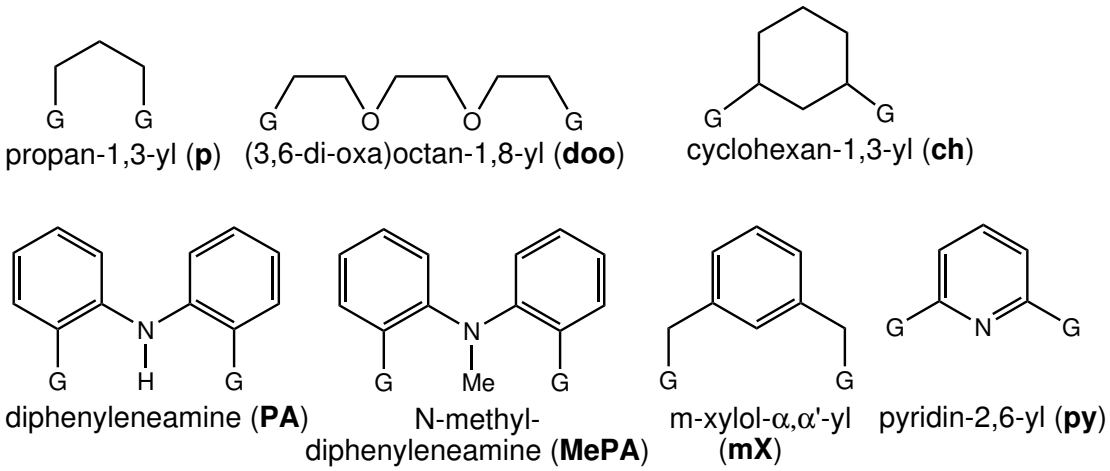

Figure 3.4: Spacer units (G assigns the position of the attached guanidine moiety)

The modular approach which is illustrated in Figure 3.5 allows a systematic tuning of the properties of polyguanidine ligands. By combining the varieties of the spacer and the guanidine moiety, a library of bisguanidine ligands could be built up (Tables 3.3 and 3.2).

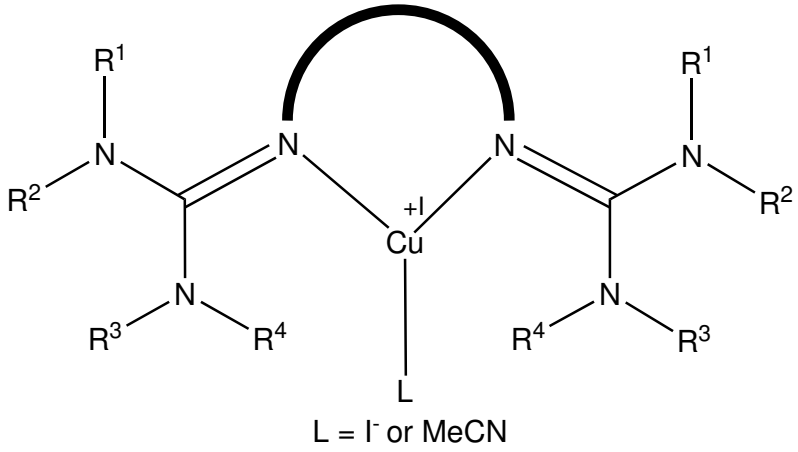

Figure 3.5: Schematic representation of the variable moduls within bisguanidine ligands

Table 3.2: Overview of the synthesised ligands with aromatic spacers

Guanidine moities	**PA**	**MePA**	**mX**	**py**
TMG (G1)	TMG_2PA (**L1-4**)	TMG_2MePA (**L1-5**)	TMG_2mX (**L1-6**)	TMG_2py (**L1-7**)
TEG (G2)			TEG_2mX (**L2-6**)	TEG_2py (**L2-7**)
DMEG (G4)			$DMEG_2mX$ (**L4-6**)	$DMEG_2py$ (**L4-7**)
DMPG (G5)		$DMPG_2MePA$ (**L5-5**)	$DMPG_2mX$ (**L5-6**)	$DMPG_2py$ (**L5-7**)

Table 3.3: Overview of the synthesised ligands with aliphatic spacers

Guanidine moities	**p**	**doo**	**ch**
TMG (G1)	TMG_2p (**L1-1**)	TMG_2doo (**L1-2**)	TMG_2ch (**L1-3**)
TEG (G2)	TEG_2p (**L2-1**)		
TiPG (G3)	$TiPG_2p$ (**L3-1**)		
DMEG (G4)	$DMEG_2p$ (**L4-1**)	$DMEG_2doo$ (**L4-2**)	$DMEG_2ch$ (**L4-3**)
DMPG (G5)	$DMPG_2p$ (**L5-1**)	$DMPG_2doo$ (**L5-2**)	
DPPG (G6)	$DPPG_2p$ (**L6-1**)		
DPipG (G7)	$DPipG_2p$ (**L7-1**)		
B(DMPip)G (G8)	$B(DMPip)G_2p$ (**L8-1**)		
B(TMPip)G (G9)	$B(TMPip)G_2p$ (**L9-1**)		
DImG (G10)	$DImG_2p$ (**L10-1**)		
DMorphG (G11)	$DMorphG_2p$ (**L11-1**)	$DMorphG_2doo$ (**L11-2**)	
DSMorphG (G12)	$DSMorphG_2p$ (**L12-1**)		
MorphDMG (G13)	$MorphDMG_2p$ (**L13-1**)		
(DMPip)DMG (G14)	$(DMPip)DMG_2p$ (**L14-1**)		

3.2 Crystal structures

3.2.1 Crystal structure of N,N,N´,N´-tetraethylchloroformamidinium chloride

Deprotonation of chloroformamidinium salts is the most popular way to generate diaminocarbenes,[118, 119] but the chlorformamidinium chlorides themselves represent adducts between the corresponding carbenes and molecules of chlorine. The synthesis of **V2** is accomplished by a standard method for Vilsmeier salts,[117] but to our knowledge no structure has been reported. Kuhn et al.[120] and Arduengo et al. [121] reported the structure of the dichlor-adducts of carbenes containg the cyclic imidazolyl fragment. Acyclic carbenes have been synthesised by Alder al. [122] and Bertrand et al. [123], but to this point of knowledge chlorformamidium chlorides have been regarded as salt-like precursors of carbenes.

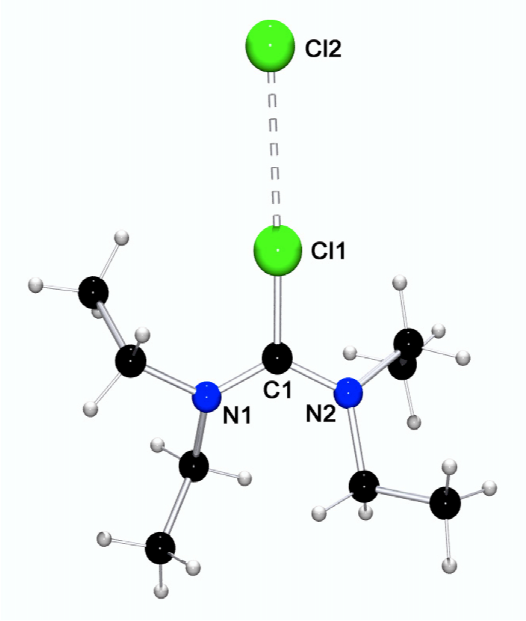

Figure 3.6: Molecular structure of **V2**

The crystal structure of **V2** shows that a linear C-Cl-Cl fragment and not an isolated chloride ion is existing in the solid state. The synthesis of **V2** is accomplished in good yields by combining tetraethylurea with phosgene in toluene as it is shown in Figure 3.1. Following the literature procedure,[117] the Vilsmeier salt N,N,N´,N´-tetraethylchloroformamidinium chloride can be obtained from the toluene solution by filtration as honey-like yellowish oil which crystallises in the triclinic space group $P\bar{1}$ upon standing after several months . The structure (Figure 3.6) shows a planar arrangement of N1, N2, C1 and Cl1, deviations from the best plane range from -0.003(1) to 0.008(1) Å. Angles at C1 are N-C-N 125.9(1)°, N-C-Cl 117.0° (average) and the C-Cl distance measures 1.736(1) Å as expected for a C(sp^2)-Cl bond. Cl1 has an almost linear coordination of C-Cl-Cl amounting to 175.7(1)° and the Cl-Cl distance is 3.1523(5) Å long which is clearly shorter than a van der Waals contact. This Cl coordination is similar to that from the related imidazol compound [120] with Cl-Cl 3.159(3) Å and C-Cl-Cl 166.1(1)°. Compared with other chloroformamidinium salts, the C-Cl distance is slightly elongated. Several imidazolium systems reported in the literature

[120, 121, 124, 125] exhibit a C-Cl distance of 1.68 Å which is not dependent from the accompanying anion (Cl^-,[120, 121] $PO_2Cl_2^-$, [124] SO_2Cl^- [125]). The single acyclic system $[(NMe_2)_2CCl]_2[PtCl_6]$ shows a C-Cl distance of 1.724 Å.[126] Thus, the C-Cl distance is not determined by the anion but by the type of formamidinium system. This relation is not fully understood and requires more structural data of related acyclic systems.

Regarding from the synthetic side, **V2** can be seen as Vilsmeier salt, whereas the structural analysis shows that it is as well a dichloro-carbene adduct. The reactivity of **V2** as chloroformamidinium salt is strongly electrophilic. Hence, we use it in the synthesis of bisguanidine ligands as Vilsmeier salt. In the reaction with suited reagents like $Hg(SiMe_3)_2$, the carbene can be generated.[123]

Therefore, compound **V2** can be regarded both as a Vilsmeier salt and as a charge-transfer adduct of a carbene with dichlorine. Chloroformamidinium chlorides seem to prefer the adduct-structure to the ionic salt-like structure.

3.2.2 Crystal structures of selected bisguanidine ligands

Single crystals of **L5-1** and **L7-1** could be obtained by slow evaporation of the acetonitrile solution under glove-box conditions. **L5-1** crystallises triclinic in the space group $P\bar{1}$ with two molecules per unit cell, whereas **L7-1** crystallises monoclinic in the space group P $2_1/n$ with four molecules per unit cell. The results of the structure analyses are shown in the Figures 3.7 and 3.8, while selected bond lengths and angles are collected in Table 3.4, and parameters relating to the data collection and refinement are listed in the Tables A1 and A2.

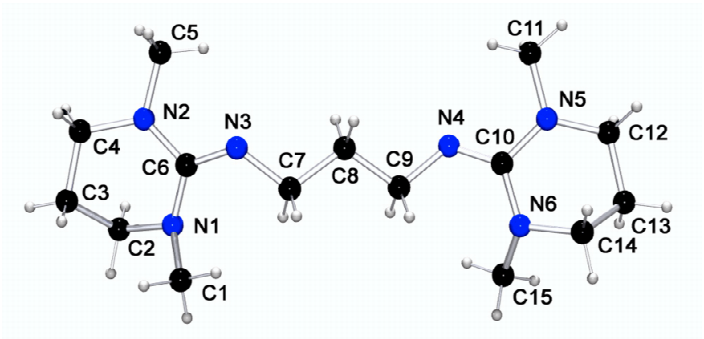

Figure 3.7: Molecular structure of **L5-1**

In **L5-1**, the C-N single-bond lengths range from 1.375 (3) to 1.407 (3) Å, and the mean of the C6=N3 and C10=N4 double bonds is 1.284 Å. The mean of the N1-C6-N2 and N5-C10-N6 angles is 114.8°, and the mean of the C6-N3-C7 and C9-N4-C10 angles 119.5°. Thus, the guanidyl double bonds in **L5-1** are clearly localised. The same is valid for the related compound **L7-1**.

Table 3.4: Selected distances and angles of the molecules in crystals of **L5-1** and **L7-1** (average values)

Distances (Å)	**L5-1**	**L7-1**
N=C	1.276	1.284
C_{imine}-N_{amine}	1.398	1.391
Angles (°)		
N_{amine}-C-N_{amine}	113.9	114.8

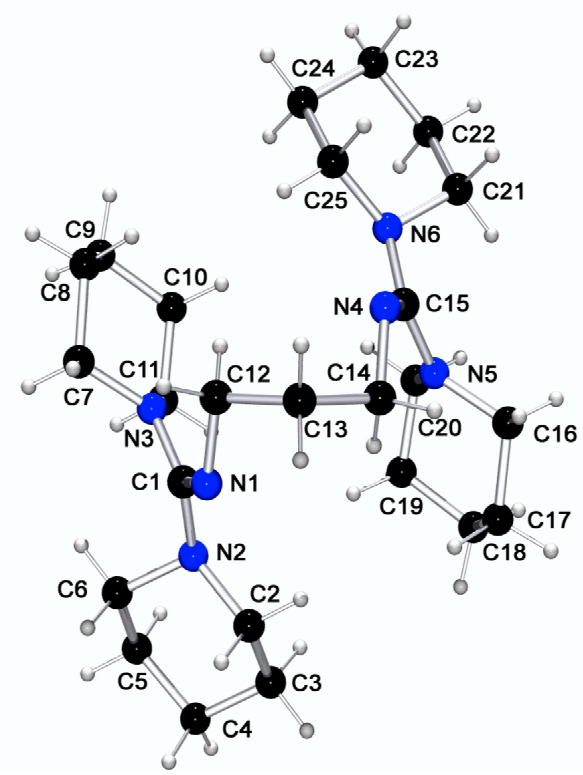

Figure 3.8: Molecular structure of **L7-1**

The molecule **L7-1** lies roughly on a non-crystallographic twofold axis running through C13, with a trans arrangement of the guanidyl groups relative to the C12-C13-C14 centre. The resulting torsion angles are N1-C12-C13-C14 = 70.3 (1)° and N4-C14-C13-C12 = 68.8 (1)°. The C-N single bonds range from 1.392 (1) to 1.404 (1) Å, while the C=N double bonds, C1=N1 and C14=N4, have similar values, with a mean of 1.276 Å. The mean of the N2-C1-N3 and N5-C15-N6 angles is 113.9°, and that one of the C1-N1-C12 and C15-N4-C14 angles is 119.9°. Thus, the guanidyl double bonds in **L7-1** are clearly localised as well. Similar double-bond localisation is observed in bis(tetramethylguanidino) naphthalene,[109] with equally unprotonated imine N and NR_2 amino groups having a mean C=N bond length of 1.282 (3) Å and a mean C-N bond length of 1.384 (1) Å. In bis(tetramethylguanidino)biphenyl,[94] with a protonated imine N atom, strong delocalization is observed among the three C-N bonds, which are in the range 1.31 (1) - 1.34 (1) Å. 2-Cyanoguanidine, with C-N bonds in the range 1.3327 (3) - 1.3441 (3) Å,[127] and, to a lesser extent, tetrabenzylcyanoguanidine, with C=N = 1.315 Å and C=N = 1.370 Å,[128] also show delocalisation, but this is due to the cyano groups attached to the imine N atom. Substitution of the NH_2 groups in cyanoguanidine with NBz_2 leads to the observed increase in localisation.

In order to discuss structural features of the diverse kinds of ligands, three crystal structures have been chosen for a nearer look: the structure of **L1-4** denotes typical properties of aromatic bisguanidine ligands, whereas **L11-1** represents a typical aliphatic bisguanidine ligand. Compound [H_2**L1-2**]I_2·Et_2O contains a typical bisprotonated bisguanidine system. Single crystals of [H_2**L1-2**]I_2·Et_2O were grown by slow diffusion of diethyl ether into acetonitrile solutions. Single crystals of **L1-4** are obtained by crystallisation at -25°C whereas **L11-1** crystallised by slow evaporation of the acetonitrile solution. **L1-4** and [H_2**L1-2**]I_2·Et_2O crystallise monoclinic in the space group $P2_1n$ with eight and two molecules per unit cell, respectively. **L11-1** crystallises monoclinic with the space group C2/c and four molecules per unit cell. The results of the structure analyses are shown in Figures 3.9 - 3.10, while selected bond lengths and angles are collected in Table 3.5, and parameters relating to the data collection and refinement are listed in the Tables A2 and A3.

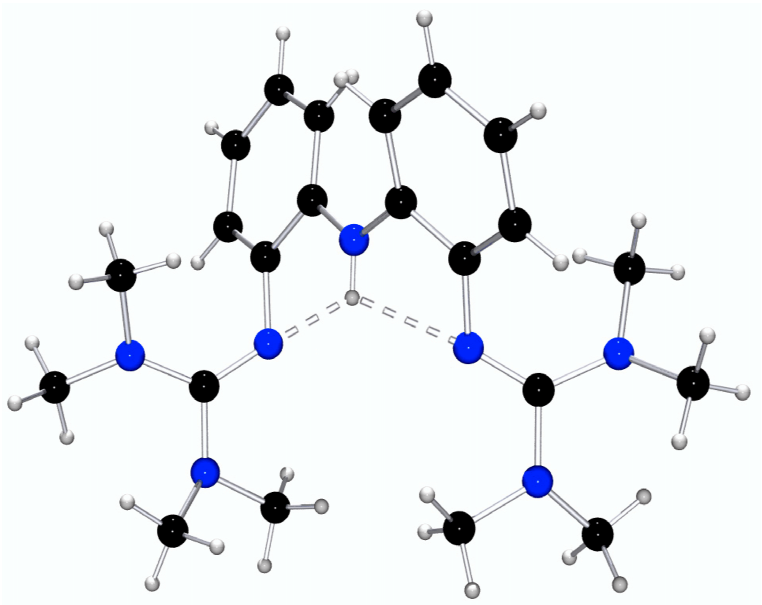

Figure 3.9: Molecular structure of **L1-4**

Crystals of **L1-4** contain two crystallographically independent but otherwise identical molecules. One of them (A) is shown in Figure 3.9. The structural features of this aromatic guanidine ligand (N=C 1.281, C_{imine}-N_{amine} 1.365, N_{imine}-C_{arom} 1.402 Å) are comparable with those reported for TMGN (N=C 1.282, C_{imine}-N_{amine} 1.384, N_{imine}-C_{arom} 1.399 Å).[109] Remarkable is the trigonal-planar environment of the N atom which connects both phenyl rings. The corresponding N-C bonds are drastically shortened to 1.400 Å which indicates a delocalisation of the free amine electron pair into the phenyl π-system. The phenyl rings are twisted against each other by an angle of 36.7°. The dihedral angles between the CN_3-

guanidine plane and the C_{imine}-N_{amine}-$(C_{alkyl})_2$-planes within the guanidine moieties have a mean value of 31.9° (individual values from 22.2 to 38.6). Furthermore, the N-H group forms a bifurcated hydrogen bridge to the imine N atoms (av. 2.235 Å, corrected for N-H 1.080 Å).

The molecular structure of **L11-1** is depicted in Figure 3.10. The molecule lies on a crystallo-

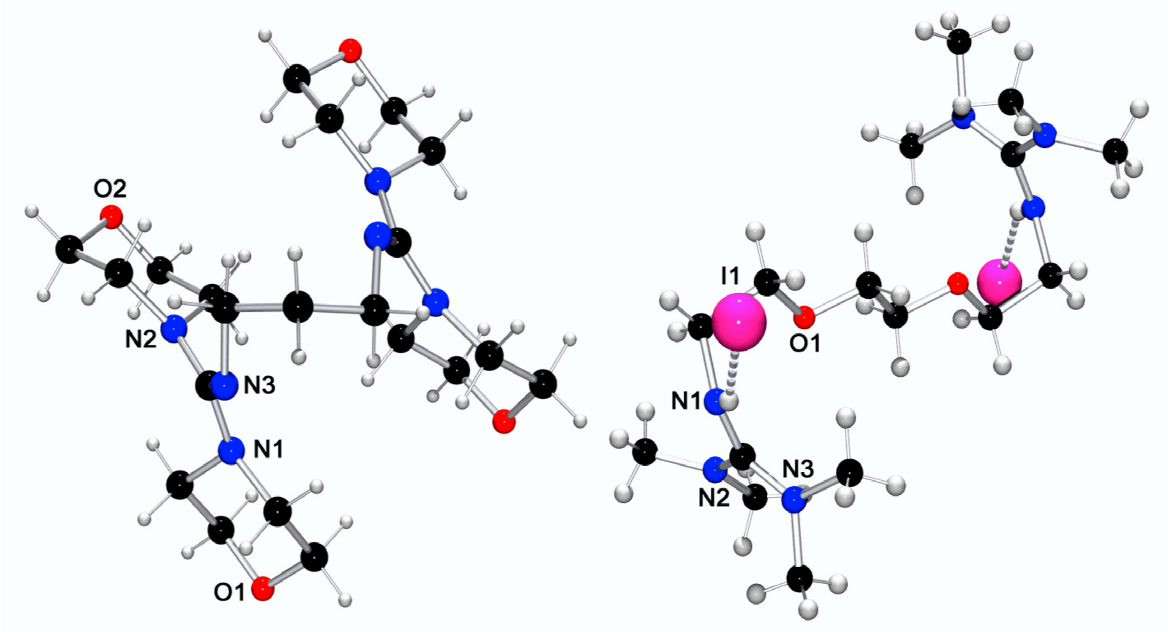

Figure 3.10: Molecular structure of **L11-1** (left) and of $[\mathbf{H_2L1\text{-}2}]\mathbf{I_2}\cdot\mathbf{Et_2O}$(right)

graphic two-fold axis which runs through the center of the spacer. The geometric parameters of this ligand are in good agreement with those of the aliphatic guanidine ligand $DPipG_2p$ (**L7-1**): N=C 1.272, C_{imine}-N_{amine} 1.402 Å compared with $DPipG_2p$: N=C 1.276, C_{imine}-N_{amine} 1.399 Å. The guanidine moieties are planar as expected. The dihedral angles between the CN_3-guanidine plane and the C_{imine}-N_{amine}-$(C_{alkyl})_2$-planes are larger (on average 36.0°; individual values from 29.0 to 42.9°) than those of **L1-4** as the steric hindrance forces the NR_2 units to twist around the C_{imine}-N_{amine} axis. The N=C double bonds are clearly localised in contrast to the bisprotonated form of **L1-2** where the double bond is delocalised over the guanidine centre. Compound $[\mathbf{H_2L1\text{-}2}]\mathbf{I_2}\cdot\mathbf{Et_2O}$ comprises the bis-protonated form of TMG_2doo, two iodine anions and a diethylether molecule. The centroid of the cation lies on a crystallographic inversion centre. The bond lengths are typical for a protonated guanidine: $C{=}NH^+$ 1.349(3), C_{imine}-N_{amine} av. 1.336 Å compared with $[H_2btmgp]^{2+}$: $C{=}NH^+$ 1.334, C_{imine}-N_{amine} 1.341 Å.[106] The bonds in the guanidine centre are of equal length. Therefore, the conjugation is enhanced although the dihedral angles are diminished only to a small extent (on average 30.8°; individual values from 29.8 to 31.8°). The iodide ions are stabilised by N-H...I hydrogen bonds with H...I distances of 2.768 Å.

Table 3.5: Selected distances and angles of the molecules in crystals of **L1-4**, **L11-1** and of the ligand cation in crystals of **[H_2L1-2]I_2·Et_2O** (average values)

Distances (Å)	**L1-4**	**L11-1**	**[H_2L1-2]I_2·Et_2O**
N=C	1.282	1.273	1.349
C_{imine}-N_{amine}	1.365	1.402	1.336
Angles (°)			
N_{amine}-C-N_{amine}	113.6	112.0	120.1

As a structural parameter that allows estimation of charge delocalisation within the guanidine moiety by comparing the shortest C=N bond distance **a** to the average of the other two C-NR_2 distances **b** and **c**, the value $\rho = 2a/(b+c)$ was established.[107] Table 3.6 summarises the ρ values for the above discussed ligands.

Table 3.6: Quotient ρ for **L5-1**, **L7-1**, **L1-4**, **L11-1** and of the ligand cation in crystals of **[H_2L1-2]I_2·Et_2O** (average values)

	ρ
L5-1	0.924
L7-1	0.912
L1-4	0.936
L11-1	0.909
[H_2L1-2]I_2·Et_2O	1.009

In the free guanidines **L5-1**, **L7-1**, **L1-4** and **L11-1**, ρ has values of 0.90 to 0.94 assigning a clear localisation of the guanidine double bond. The greater value for **L1-4** can be explained by the fact that the aromatic spacer contributes to the delocalisation in the system.[109] The guanidinium cation **[H_2L1-2]I_2·Et_2O** shows a perfect charge delocalisation with $\rho = 1.009$.

3.3 NMR spectroscopy of selected bisguanidine ligands

The chemical shifts of the dimethylamino groups of the ligands containing the tetramethylguanidine moiety are listed in Table 3.7 for comparison purposes. The ^{1}H and ^{13}C NMR spectra of the guanidine ligands with aliphatic spacers exhibit two seperate signals for the methyl groups. On heating, these two signals approach each other and

coincide on reaching the coalescence temperature. Compared with the aliphatic situation described above, the aromatic systems exhibit only one signal for the methyl groups at room temperature. This signal splits into two resonances of equal intensity if the temperature is lowered (Figure 3.12). This behaviour is caused by a syn-anti exchange typical for guanidines which has been discussed for selected TMG systems by Kessler and Leibfritz.[129] In the case of pentasubstituted guanidines, a rotation around the C-NR_2 single bonds as well as a syn-anti isomerisation can take place (Figure 3.3). The rotation around a C-NR_2 single bond is too rapid with respect to the NMR timescale to result in individual resonances even at low temperatures. This is not the case for the syn-anti exchange which can principally be caused by rotation around the C=N bond or by inversion.[129] The coalescence behaviour of selected guanidine ligands was investigated by EXSY ^{1}H NMR spectroscopy. The kinetic data were determined from the resulting Eyring plots (Figs. 3.13 - 3.15 and Table 3.8).

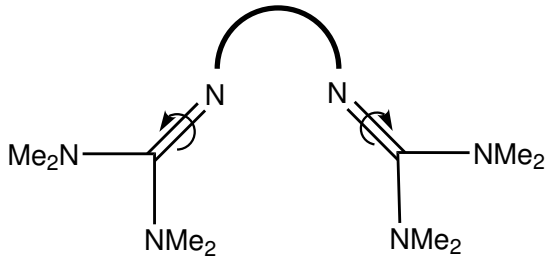

Figure 3.11: Rotation around the C=N double bond

Table 3.7: Comparison of NMR spectroscopic shifts of the NMe_2 groups at 298 K (*:Ref. [109])

	^{1}H		^{13}C	
btmgp (L1-1)	2.56	2.65	38.6	39.4a)
H_2btmgpCl_2 (H_2L1-1Cl_2)	2.94	3.02	40.1	40.5a)
TMG_2doo (L1-2)	2.51	2.60	38.6	39.5
$H_2TMG_2dooI_2$ (H_2L1-2I_2)	2.95	3.09	40.0	40.4
TMG_2ch (L1-3)	2.42	2.49	39.1	39.6
TMG_2PA (L1-4)	2.68		38.6	
TMG_2MePA (L1-5)	2.58		39.9	
TMG_2mX (L1-6)	2.65		38.7	
TMG_2py (L1-7)	2.73		39.9	
TMGN	2.65*		39.4*	
H_2TMGN$(PF_6)_2$	2.95*		41.6*	

Table 3.8 clearly shows that aromatic tetramethyl guanidines have lower activation barriers for the syn-anti exchange than aliphatic ones. Our findings thus are in accordance with data

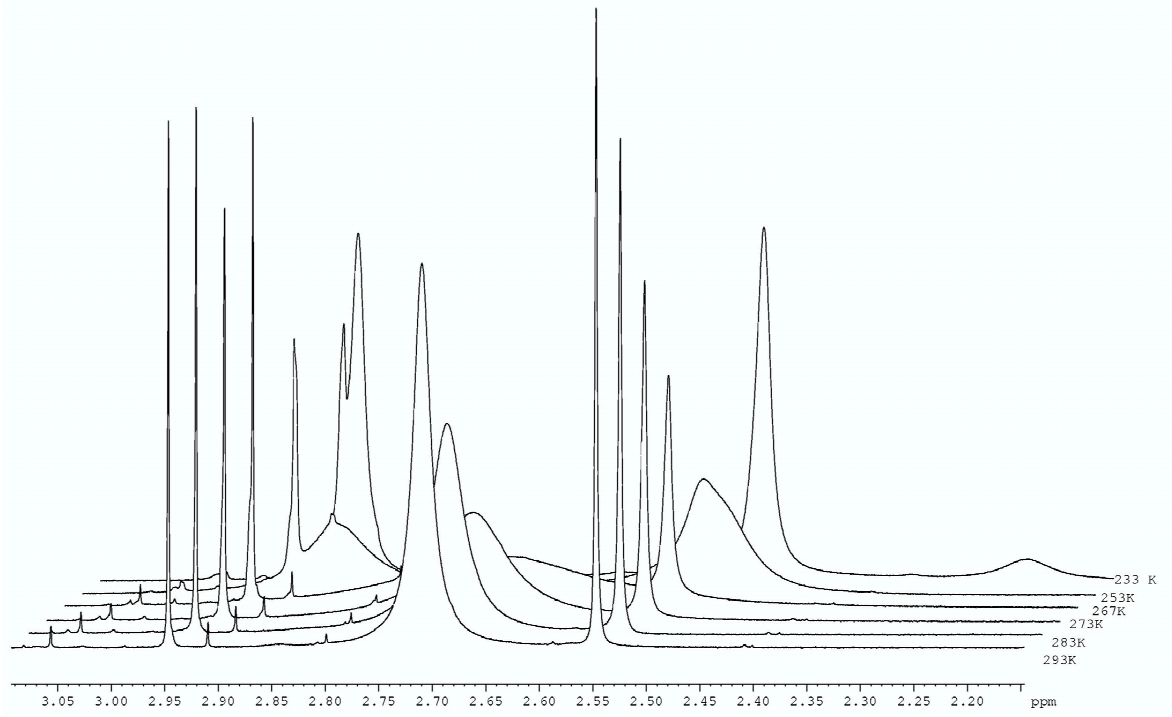

Figure 3.12: Coalescence behaviour of TMG_2PA (L1-4) between 293 and 233 K

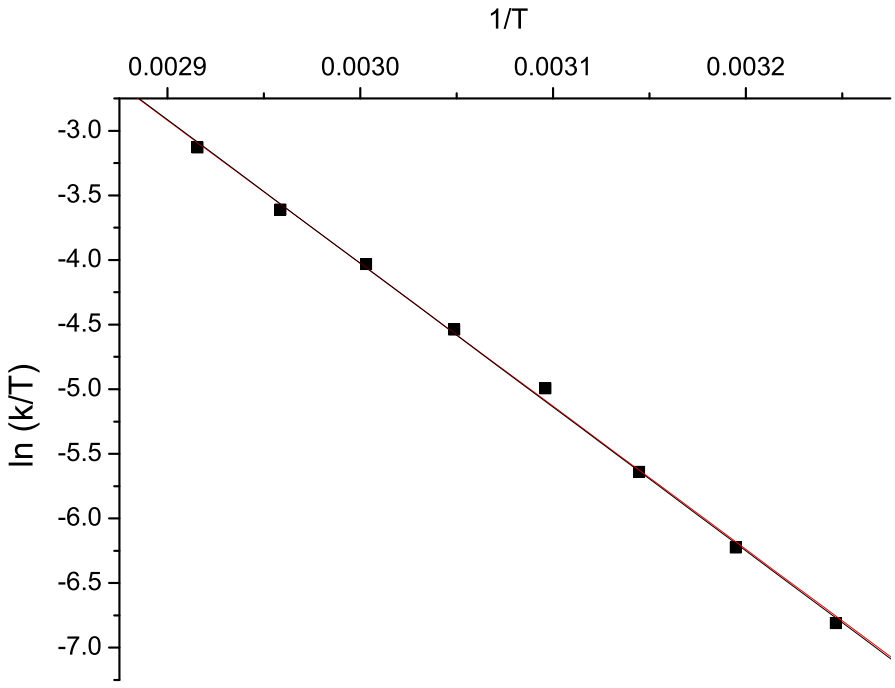

Figure 3.13: Eyring plot (308 - 343 K) for the syn-anti exchange in btmgp (**L1-1**)

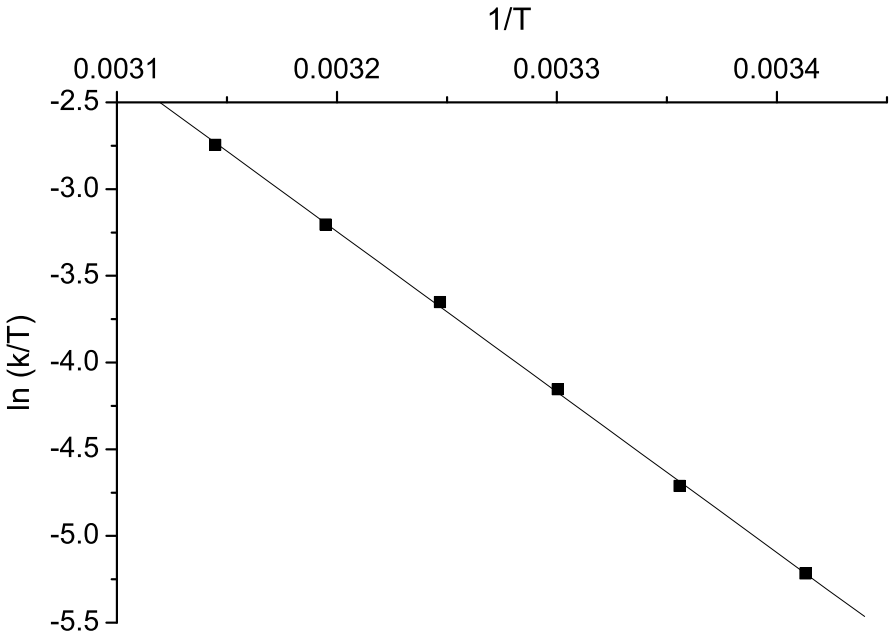

Figure 3.14: Eyring plot (293 - 318 K) for the syn-anti exchange in TMG_2doo (**L1-2**)

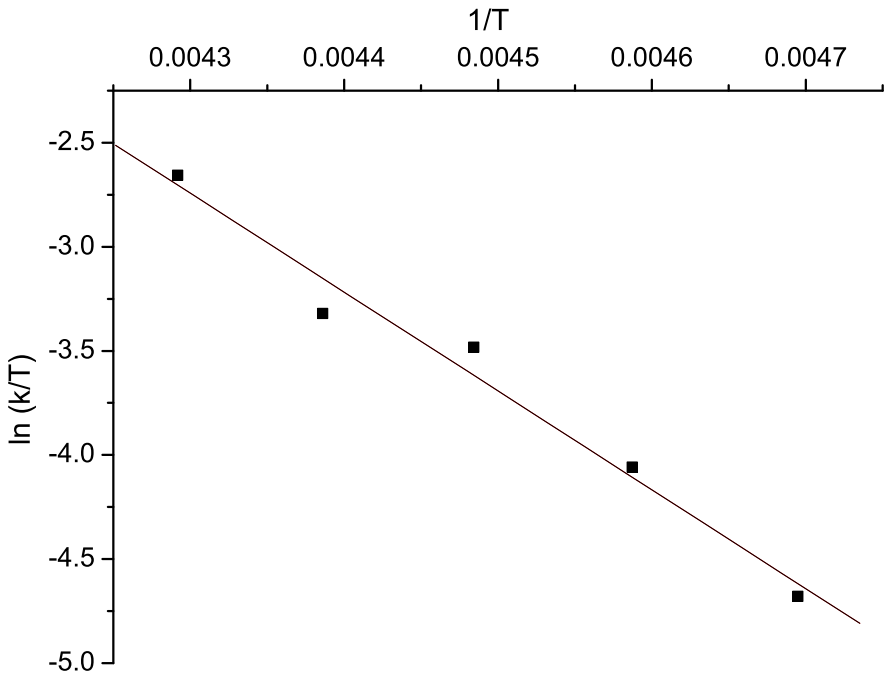

Figure 3.15: Eyring plot (213 - 233 K) for the syn-anti exchange in TMG_2PA (**L1-4**)

for related systems reported in the literature.[109, 129] In aromatic systems like TMG_2PA and TMGN, the C=N bond is weakened by conjugation with the adjacent aromatic system resulting in lower energy barriers whereas in aliphatic systems like btmgp, TMG_2doo or $[Bz_2TMG]^+$ which lack these effects, the free energies of activation have to be considerably higher. The data for the free energy of btmgp and TMG_2doo are in good agreement with the values reported for simple alkyl substituted guanidines like pentamethylguanidine (TMG-CH3) and tetramethyl-ethyl- or tetramethyl-propyl-guanidine (TMG-C_2H_5 and TMG-C_3H_7, resp.).

Table 3.8: Comparison of coalescence parameters of the syn-anti isomerisation; a) temperature range limited by solvent (T_{min} 183 K);b) Ref. [109]; c) Ref. [129]; d) Ref. [130]

	Solvent	T_c[K]	$\Delta H^{\ddagger}$[kJ/mol]	$\Delta S^{\ddagger}$[J/(mol·K)]	$\Delta G_0^{\ddagger}$[kJ/mol]
btmgp (L1-1)	d^6-DMSO	375	92.4±1.5	46.2±0.8	78.6±1.7
TMG_2doo (L1-2)	d^6-DMSO	348	77.0±0.8	21.8±0.3	70.5±0.9
TMG_2PA (L1-4)	CD_2Cl_2	267	41.5±2.3	-40.9±2.7	53.7±3.0
TMG_2MePA (L1-5)	CD_2Cl_2	242			- [a]
TMG_2py (L1-7)	CD_2Cl_2	229			- [a]
TMGN	CD_2Cl_2	253[b]	53.4[b]		48.3[b]
TMGPh	$CDCl_3/CS_2$	238[c]			50.7[c]
$TMGBz_2^+$	$CDCl_3$	276[d]			61.1[d]
TMG-CH_3	$CDCl_3$	346[c]			78.2[c]
TMG-C_2H_5	$CDCl_3$	338[c]			76.2[c]
TMG-C_3H_7	$CDCl_3$	326[c]			73.2[c]

In the case of btmgp and TMG_2doo, an inversion mechanism appears to be unlikely due to the restrictions introduced by the second guanidyl function attached to the same linker. This means that a rotation takes place which is facilitated if we go from smaller to larger alkyl chains. Having this in mind and taking the data for comparable monoguanidine molecules into account which are nearly identical,[129] a unique rotational mechanism for all these systems can be postulated. The inductive effect of homoaromatic neighbourhoods can be enhanced by using a more electron rich system like pyridin as has been observed for TMG_2py (Tc = 229 K). The aromatic ligand TMG_2MePA exhibits coalescence of the methyl singlets at 242 K. A similiar value was found for TMGPh (TC = 238 K),[129] whereas the methyl signal of the TMG_2PA molecule splits into two components below 267 K. This temperature is remarkably high in comparison with those reported for other aromatic systems like TMGN (253 K).[109] Additionally, TMG_2PA has a negative activation entropy for the ro-

tation around the C=N bond indicating that hydrogen bonds participate in the exchange mechanism (Figure 4). It is assumed that the bifurcated hydrogen bond between the amino-hydrogen and the two guanidine nitrogen atoms stabilises the conformation observed in the crystal resulting in a raised activation barrier of rotation and thus in a higher coalescence temperature.

3.4 Electrochemistry of selected bisguanidine ligands

Selected guanidine ligands have been investigated on their redox properties by means of cyclovoltammetry. The cyclovoltammogram of **L1-4** (0.1 mol/L $[NBu_4][PF_6]$; 50 mV/s; Au/Pt/Ag-AgCl) exhibits a quasireversible electron transfer at 94 mV/NHE (Figure 3.16) which can be indicative for the reduction of the aminic hydrogen atom to molecular hydrogen. The cyclovoltammogram of **L1-5** (0.1 mol/L $[NBu_4][PF_6]$; 50 mV/s; Au/Pt/Ag-AgCl) shows two electron transfers (Figure 3.17). The first redox transition at 105 mV/NHE is irreversible. The second redox wave at 496 mV/NHE can be classified as quasireversible. Both redox transitions belong to redox processes which are delocalised in the aromatic system. Thus, they can not assign exactly special redox processes.

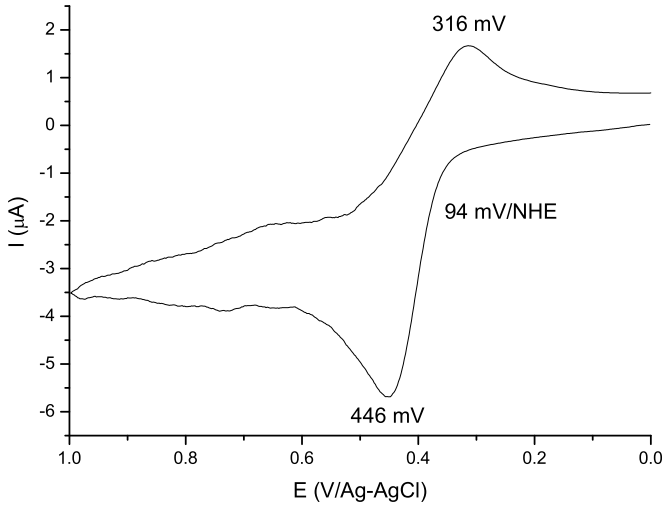

Figure 3.16: Cyclovoltammogram of **L1-4** in CH_2Cl_2

The cyclovoltammograms of the aliphatic ligands **L4-1**, **L5-1**, **L7-1** and **L11-1** do not show any significant electron transfers in the range of -2 and +2 V in CH_2Cl_2 and in MeCN as solvent. btmgp has been reported to be oxidised at potentials between 1 and 1.4 V/SCE.[112] Appearently, ligands with differently substituted guanidine moieties are more redox stable than btmgp. Probably, they are oxidised at potentials of more than 2 V/NHE which is outside the window given by the solvent.

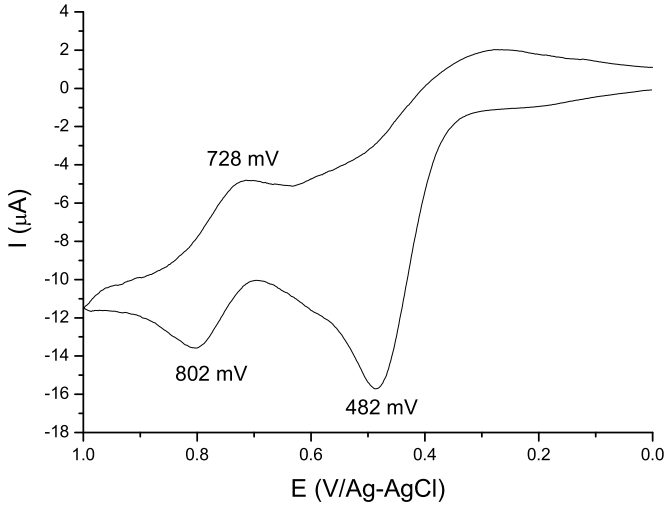

Figure 3.17: Cyclovoltammogram of **L1-5** in CH_2Cl_2

3.5 Synthesis of a fluorinated bisguanidine ligand

In order to direct the oxidation potential of the copper complexes towards external substrates, the ligand has to be shielded against self-oxidation. This approach has proven to be successful as Gorun and coworkers have shown with their fluorinated hydro(trispyrazolyl)borate system which supports a room-temperature stable μ-η^2:η^2-peroxo dicopper core.[87]
All attempts to fluorinate suited ligand precursors by electrofluorination resulted in extremely small yields, and the subsequent reaction to the desired ligand failed due to HF evolution. Another pathway to a fluorinated ligand was the substitution of an urea with perfluorinated side-chains and the subsequent transformation into the corresponding chloroformamidinium chloride (Figure 3.18, (**1**)) which reacts in the following reaction with 1,3-diaminopropane to the desired ligand (Figure 3.18, (**2**)). Going this path-

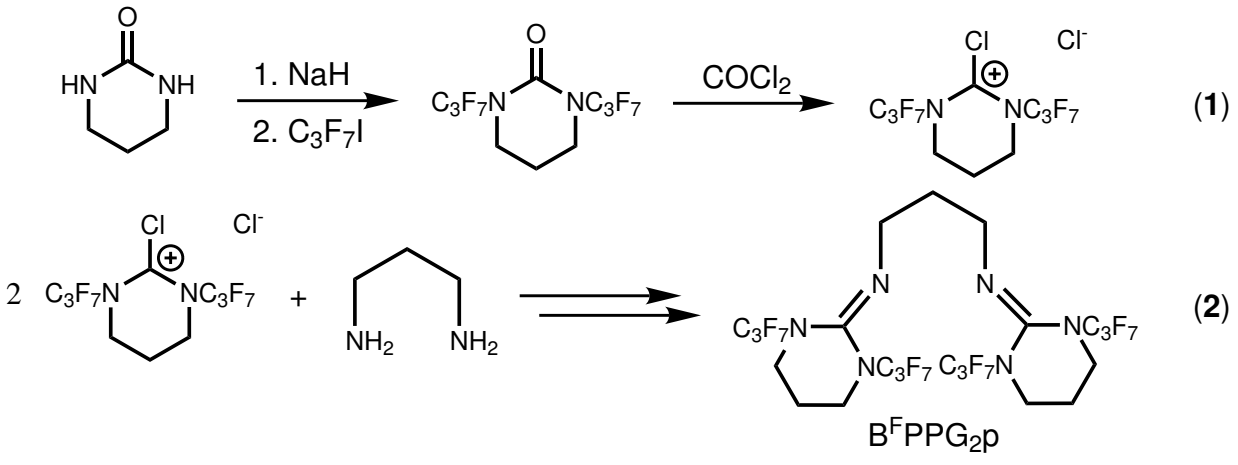

Figure 3.18: Synthesis of the fluorinated bisguanidine ligand B^FPPG_2p

way, trimethyleneurea was deprotonated twice by NaH in THF, and heptafluoropropyliodide was added. The reaction occurs immediately, but the by-product NaI can not be removed efficiently. It turned out that NaI reacts with phosgene in the subsequent reaction to iodophosgene which is unstable and decomposes into iodine and carbon monoxide. The iodine could be proven with the iodine-starch-test of the dark violet solution. The generation of iodine disturbs the formation of the desired fluorinated chloroformamidiniumchloride. Therefore, the NaI has to be totally separated from the solution. Literature reported synthesis [131] of subsituted ureas were carried out in dioxane because of the small solubility of NaI in dioxane, but even this small solubility turned out to be too great for the subsequent reaction with phosgene. Different methods of deprotonation were tested, e.g. deprotonation with lithium-*n*-butylate or lithium-*t*-butylate in hexane or dichloromethane at -80°C, but the reaction with trimethyleneurea yielded no results. Deprotonation with LiH (as attempt to obtain LiI instead of NaI) did not work either. The most effective deprotonation method is that one using NaH in THF (16 h at reflux). Hence, after the deprotonation step, the solvent was evaporated and another solvent added which is not able to dissolve NaI, e.g. dichloromethane. This method failed as the generated and only partly redissolved bis-deprotonated trimethyleneurea did not react with the heptafluoropropyliodide. Refluxing of this reaction mixture is difficult as well because of the low boiling point of heptafluoroiodine (34.5°C). A more effective method appeared to be the precipitation and subsequent filtration of NaI from the starting solution. The volumes of precipitation solvents like diethylether were very great, such that the concentration of the compounds got very low. Reconcentration of the filtrated solutions failed because of the volatility of the fluorinated urea.
Finally, the deprotonation was carried out in diethylether with NaH. Taking into account that the reflux temperature of diethylether is smaller, the reaction mixture has to be refluxed during 36 h, followed by the addition of heptafluoropropyliodide to the ice-cooled solution and further 36 h of mild reflux. By filtration over chromatographic silica, the extremely fine precipitate of NaI could be removed. The obtained diethylether solution containing the bis(heptafluoropropyl)trimethyleneurea was purged with phosgene at 0°C for 5 min. The reaction mixture was warmed up to room temperature and stirred for 30 min. The colour of the red solution changed to greenish-brown due to decomposition reactions of the generated fluorinated chloroformamidinium chloride. So, this chloroformamidinium solution was instanteneously added to a MeCN solution of 1,3-diaminopropane. The resulting reaction mixture was not heated as usually due to thermal decomposition but only stirred 48 h at room temperature. The workup was carried out as described for the other ligands. Due

to the thermal instability of several reaction intermediates, the yield was mostly very small (10-15 %). An optimisation of this reaction sequence is under investigation.

3.6 Conclusion: Bisguanidine ligands

The assembly of bisguanidine molecules starting from secondary amines and phosgene for use in biomimetic coordination chemistry, especially in the field of copper-controlled oxygen activation, has provided a set of bifunctional N-donor ligands. Each member of this set is expected to influence the redox capabilities of its corresponding Cu(I) complexes towards molecular oxygen in a specific fashion depending on the spatial demands of the guanidine functionalities as well as on the conformational freedom possible within the steric limits allowed by the spacer fragments connecting these units. In contrast to established literature procedures, the described method to arrive at bisguanidine molecules is not dependent from predefined peralkylated urea precursors as we start from secondary amines as simple building blocks and thus define the urea intermediates by simply choosing suitably substituted educts. The synthetic protocol has been optimised to obtain overall yields in the range from 65 to 95 %. The modular approach allows the universal modification of the aliphatic guanidine substitution as well as of the spacers with respect to rigidity, extension of the backbone and additional donor functions.

In general, such a matrix of bisguanidine ligands can also be screened regarding their ability to stabilise complexes of other transition metals in unusually high oxidation states.

4 Copper(I) bisguanidine complexes

4.1 General topologies of copper(I) bisguanidine complexes

The neutral bisguanidine ligands can be synthesised in gram scale and they are capable of coordinating metal centres in a chelating and as well a bridging mode to form mononuclear and dinuclear complexes or even polynuclear chains. In both coordination modes, the ligands show great flexibility ranging from linear via trigonal-planar to square-planar coordination of the metal centre. The topologies of copper(I) bisguanidine complexes are summarised in Figure 4.1. The square-planar coordination is often found in bis(μ-alkoxo)- and bis(μ-hydroxo) bridged dinuclear copper complexes. This type of complexes is discussed in section 6.1.

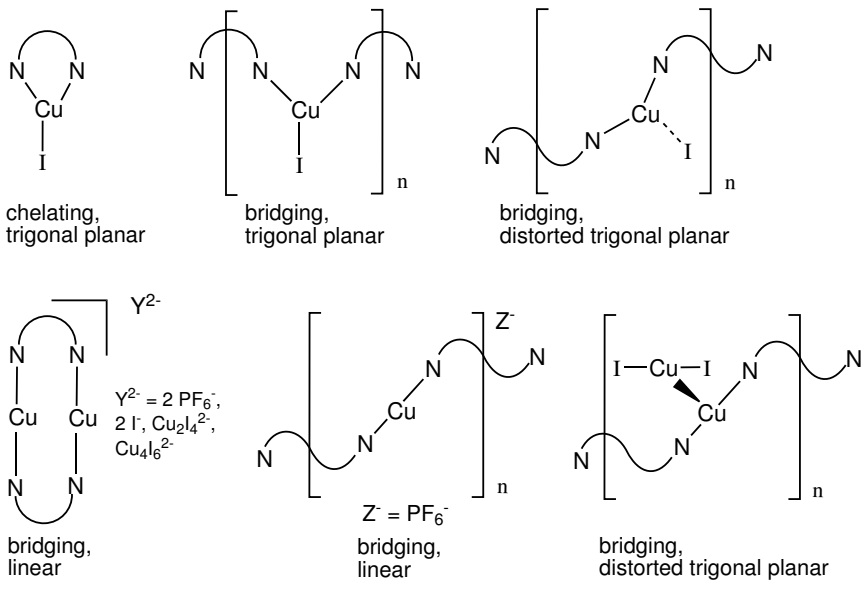

Figure 4.1: Topologies of copper(I) bisguanidine complexes

4.2 Synthesis of mononuclear copper(I)bisguanidine complexes

In general, mononuclear copper(I) bisguanidine complexes were synthesised in good yields by combining CuI with 1.05 equiv. of the bisguanidine ligand in dry acetonitrile and stirring for 30 min (Scheme 4.2).

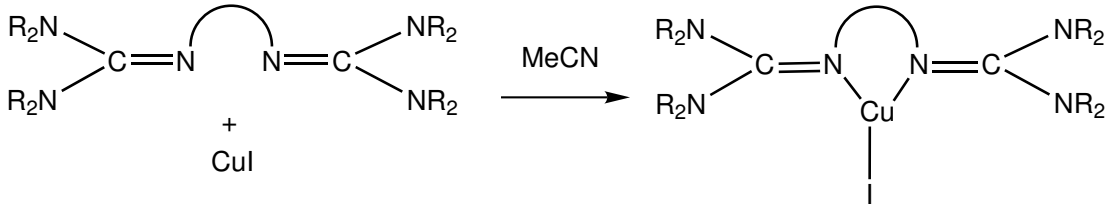

Figure 4.2: Complexation of CuI with bisguanidine ligands

4.2.1 Crystal structures of mononuclear copper bisguanidine complexes

By using TMG_2PA in the reaction with CuI (Figure 4.3), the copper is oxidised to Cu(II) and the proton from the acidic N_{amine} function is reduced to hydrogen. The hydrogen combines to dihydrogen which purges off the solution. Probably, the relieve of the hydrogen atom is facilitated by agostic interactions between the N-H bond and the Cu(I) ion. During this reaction, a dark green solid is formed which can be recrystallised as green needles from MeCN/diethylether. **C1** crystallises orthorhombic in the space group Pbca. Crystals of **C1** contain eight isolated molecules per unit cell. The results of the structure analyses are shown in Figure 4.4, while selected bond lengths and angles are collected in Table 4.1, and parameters relating to the data collection and refinement are listed in Table A4.

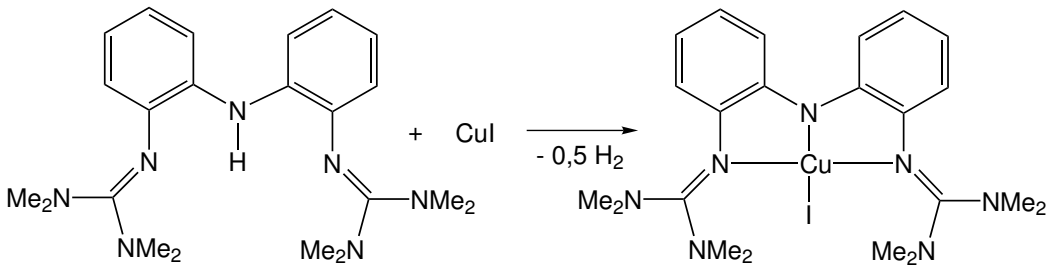

Figure 4.3: Complexation of CuI with TMG_2PA under oxidation of the copper

The copper(II) ion is coordinated in a distorted butterfly (C_{2v}) geometry. The distance of the Cu to the N1N2N3 plane measures 0.484 Å, the iodine atom lies 2.487 Å below this

Table 4.1: Selected distances and angles of **C1**

Distances (Å)		**Angles (°)**	
Cu-I	2.5941(8)	$\mathbf{N}_{amide}$-**Cu**-$\mathbf{N}_{imine}$	84.2
Cu-N$_{amide}$	1.903(4)	$\mathbf{N}_{amide}$-**Cu-I**	144.2(2)
Cu-N$_{imine}$	1.961	$\mathbf{N}_{imine}$-**Cu**-$\mathbf{N}_{imine}$	151.1(2)
$\mathbf{N}_{amide}$-$\mathbf{C}_{arom}$	1.394	$\mathbf{C}_{arom}$-$\mathbf{N}_{amide}$-$\mathbf{C}_{arom}$	124.2(5)
$\mathbf{N}_{imine}$-$\mathbf{C}_{arom}$	1.418		
$\mathbf{N}_{imine}$-$\mathbf{C}_{imine}$	1.348		

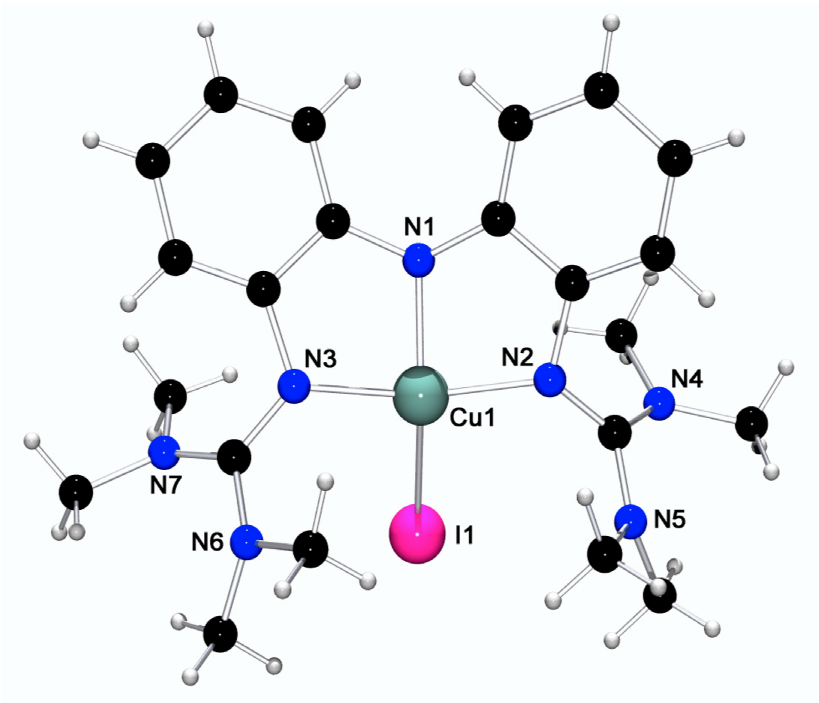

Figure 4.4: Molecular structure of **C1**

plane. The three N donor functions of the ligand surround the copper centre not planar as the N_{imine}-Cu-N_{imine} angle of 151.1(2)° shows. The sum of the six angles at the copper centre is 668.6°, thus, the coordination can be described as a distorted tetrahedron (ideal tetrahedron: 656°, square-planar geometry: 720°). The bite angle (N_{amide}-Cu-N_{imine}) of the ligand is 84.2° indicating the degree of distortion of the tetrahedral geometry. The phenyl rings are twisted about 36.8° out of the plane, the corresponding torsion angle in the ligand is 36.7°. The Cu-I distance is relatively long with 2.5941(8) Å, but shorter than the sum of the van-der-Waals-radii with ≈ 2.77 Å. The N_{amide} atom is surrounded distorted trigonal planar (angle sum: 352°). The ligand is deprotonated at this position because the redox potential is lowered by coordination under the redox potential for hydrogen evolution. The

negative charge is delocalised from one guanidine group via the aromatic rings to the other guanidine group. This delocalisation is indicated by several points: the N_{amide}-C_{arom} bonds are with 1.394 Å relatively short (standard N-C_{arom} bond: 1.42 Å) and the N_{imine}-C_{imine} bonds are with 1.348 Å longer than those in other guanidine complexes which assigns a weakened double bond character. The angle between the two CN_3-guanidine planes is 72.5°. The structural parameter ρ is calculated to be 1.002 assigning perfect delocalisation within the guanidine moiety. This is due to the aromatic spacer and the deprotonation of the aminic N atom. By using $DMorphG_2p$ in the reaction with CuI, the mononuclear complex [Cu($DMorphG_2p$)I] (**C2**) can be synthesised. Colourless single crystals are obtained in good yields by vapour diffusion of diethylether into the MeCN containing reaction mixture. **C2** crystallises orthorhombic in the space group Pnma. Crystals of **C2** contain four isolated molecules **C2** per unit cell. The results of the structure analyses are shown in Figure 4.5, while selected bond lengths and angles are collected in Table 4.2, and parameters relating to the data collection and refinement are listed in Table A4.

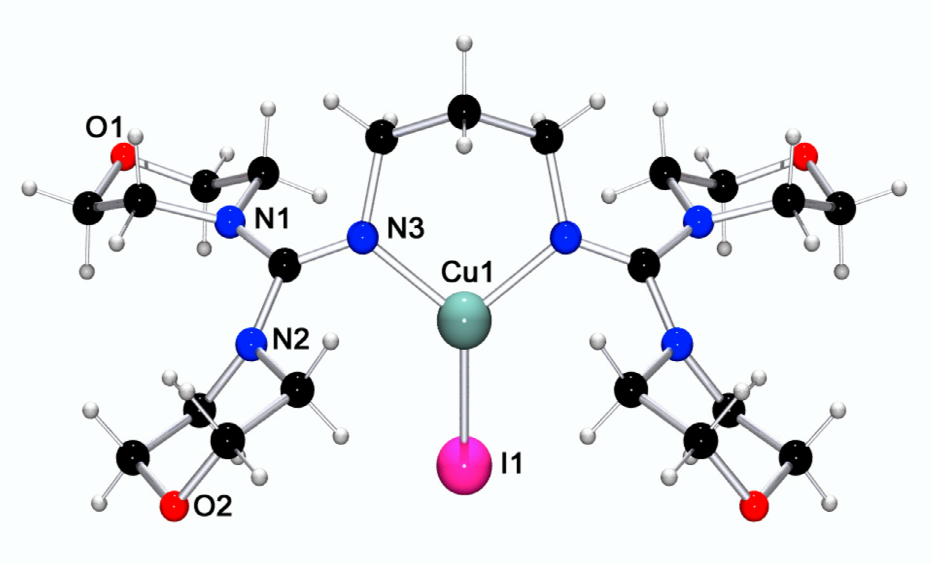

Figure 4.5: Molecular structure of **C2**

The copper centre is coordinated almost ideal trigonal-planar with a sum of the angles of 358°. The Cu-N_{imine} and Cu-I distances are in the range observed for [Cu(btmgp)I].[105, 112] Regarding the other structural details, the similarities are obvious. With regard to the dihedral angles between the CN_3-guanidine plane and the C_{imin}-N_{amin}-$(C_{alkyl})_2$-planes within the guanidine moieties, there are as well only small differences: in [Cu(btmgp)I] the torsion within the guanidine moiety amounts to 37.4°[35.9 - 38.9°] whereas in **C2** the torsion is 33.3°[26.4 - 40.2°].[112] The structural parameter ρ is calculated to be 0.942, a typical value for Cu(I) guanidine systems.[108]

Table 4.2: Selected distances and angles of **C2**

Distances (Å)	**C2**	**[Cu(btmgp)I]**
Cu-I	2.4815(4)	2.491
Cu-N$_{imine}$	1.997(2)	2.006
N=C(av)	1.298(2)	1.295
Angles (°)		
N$_{imine}$**-Cu-N**$_{imine}$	102.6(1)	103.3
N$_{imine}$**-Cu-I**	127.51(4)	128.3
N$_{amine}$**-C-N**$_{amine}$**(av)**	114.9(2)	155.1

4.2.2 Electrochemistry of mononuclear copper bisguanidine complexes

The cyclovoltammogram of complex **C1** (0.1 mol/L [NBu_4][PF_6]; 100 mV/s; Au/Pt/Ag-AgCl) exhibits two electron transfers (Figure 4.6). The redox transition at -115 mV/NHE is reversible and can be assigned to the Cu(II)/Cu(I) redox pair. The reversible redox transition at 756 mV/NHE can be attributed to the iodine ion ($E°(I_2/2I^-)$ = +535 mV/NHE).

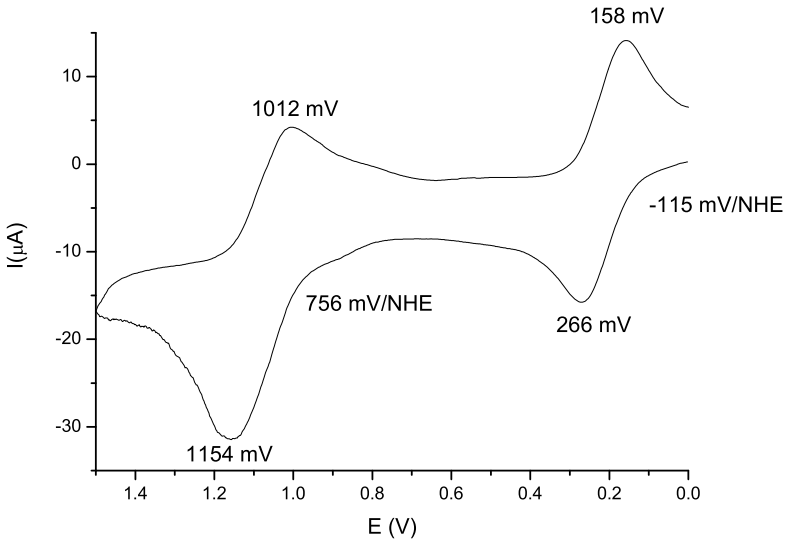

Figure 4.6: Cyclovoltammogram of **C1** in CH_2Cl_2

In Figure 4.7, the cyclovoltammograms of **C2** (0.1 mol/L [NBu_4][PF_6]; Au/Pt/Ag-AgCl) are depicted. The oxidation wave is clearly irreversible and shifts strongly with the scan velocity to higher potentials. Normalised to the NHE, the average oxidation potential of **C2** can be calculated to be -0.05 V/NHE.

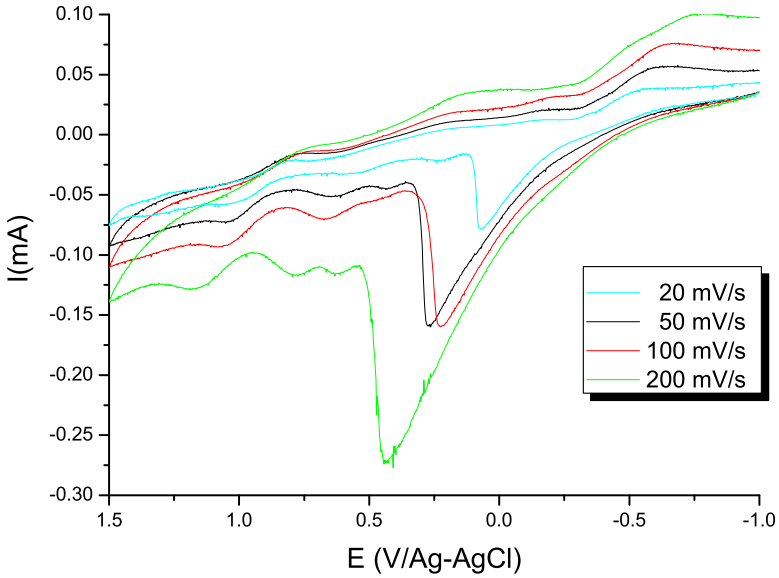

Figure 4.7: Cyclovoltammograms of **C2** in MeCN (20 mV/s - 200 mV/s)

4.3 Synthesis of dinuclear copper(I)bisguanidine complexes with linear copper coordination

The complexes containing propylene-briged bisguanidine ligands were synthesised in good yields by combining $[Cu(MeCN)_4][PF_6]$ with 1.05 equiv. of the bisguanidine ligand in dry acetonitrile and stirring for 30 min (Scheme 4.8). The kinetic data (see Section 5.4) are indicative for the dinuclear nature of these complexes in solution as well.

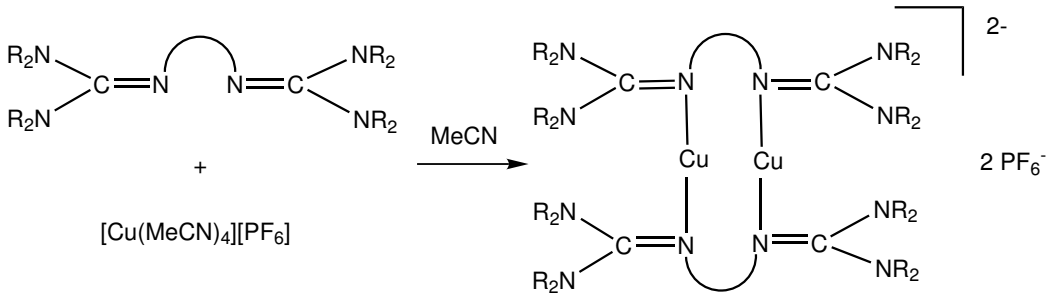

Figure 4.8: Complexation of $[Cu(MeCN)_4][PF_6]$ with propylene-briged bisguanidine ligands

The complexes containing cyclohexyl-briged bisguanidine ligands were synthesised analogously by combining CuI with 1.05 equiv. of the bisguanidine ligand in dry acetonitrile and stirring for 30 min (Scheme 4.9). As the ligands TMG_2ch and $DMEG_2ch$ are given as racemic mixture of the cis and trans compound, two types of complexes were expected. Nevertheless, only the complexes of the cis isomers with a bis-equatorial arrangement of the substituents at the cyclohexyl ring crystallised. For both ligands, the corresponding cis isomer is bet-

ter suited to coordinate the copper in this bridging mode which is shown in Figure 4.12. Possibly, the trans isomers are under these conditions subject to further reactions (e.g. cyclisation) preventing them from coordinating the copper. When an excess of CuI is present in the reaction mixture, the trans complex did not form anyway. The excess of CuI was added to the counterion iodine instead, in order to form the polynuclear counterions $Cu_2I_4^{2-}$ and $Cu_4I_6^{2-}$. The resulting complex salts **C3** - **C9** are soluble in polar aprotic media such as MeCN, CH_2Cl_2 and THF, but insoluble in diethylether and hydrocarbons. All compounds are extremely sensitive to air and moisture due to the high proton affinity of guanidines which is caused by delocalisation of the positive charge in the guanidine moiety.

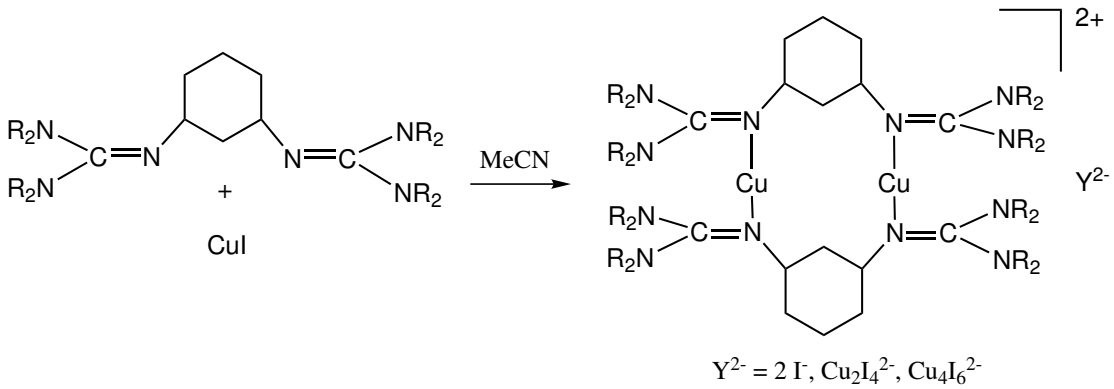

Figure 4.9: Complexation of CuI with cyclohexyl-bridged bisguanidine ligands

4.3.1 Crystal structures of dinuclear copper(I) bisguanidine complexes

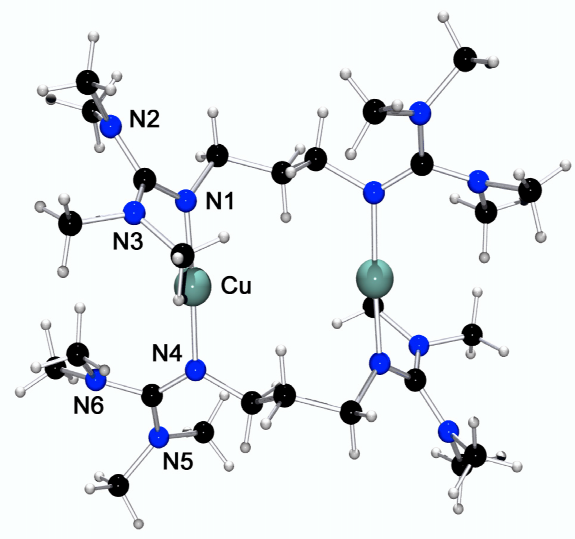

Figure 4.10: Structure of $[Cu_2(btmgp)_2]^{2+}$ in crystals of **C3**

Single crystals of the compounds **C3** - **C9** suitable for X-ray crystallography were grown by slow diffusion of diisopropyl ether into acetonitrile solutions. All compounds are obtained as colourless needles expect **C7** which forms bright yellow needles. The complex salts **C3**, **C4** and **C9** crystallise monoclinic (**C3**: $P2_1/n$, **C4**: $P2_1/c$, **C9**: C2/c) whereas the complex salts **C5** - **C8** crystallise triclinic in the space group $P\bar{1}$. The unit cell in crystals of **C3** and **C4** contains two molecules, in crystals of **C5**, **C6**, **C7** and **C8** only one molecule and in crystals of **C9** four molecules. Additionally, in

crystals of **C4** 0.37 MeCN per sum formula and in **C5** one molecule of MeCN per asymmetric unit is present. The results of the structure analyses are shown in Figures 4.10 - 4.13, while selected bond lengths and angles are collected in Table 4.3 (* shortest H...H contact between parallel propylene spacer groups; the H-H vector passes through the centroid of the corresponding complex cation), and parameters relating to the data collection and refinement are listed in the Tables A5 - A8.

Table 4.3: Selected distances and angles of the copper(I) complexes **C3** - **C9**

Distances (Å)	**C3**	**C4**	**C5**	**C6**	**C7**	**C8**	**C9**
Cu...Cu	4.121(1)	5.034(1)	4.488(1)	5.054(1)	4.974(1)	4.358(1)	4.723(1)
Cu-N$_{imine}$	1.876(2)	1.859(6)	1.878(2)	1.878(2)	1.877(2)	1.872(1)	1.876(3)
	1.878(2)	1.865(5)	1.873(2)	1.882(2)	1.888(2)	1.867(1)	1.856(3)
N=C	1.323(3)	1.295(8)	1.310(3)	1.313(2)	1.309(4)	1.323(2)	1.310(3)
	1.315(3)	1.312(8)	1.318(3)	1.308(2)	1.317(3)	1.325(2)	1.297(4)
Angles (°)							
N$_{imine}$**-Cu-N**$_{imine}$	176.7(1)	174.7(3)	175.3(1)	174.9(1)	176.3(1)	177.2(1)	176.8(1)
N$_{amine}$**-C-N**$_{amine}$	116.0(2)	114.0(6)	110.0(2)	109.9(2)	108.8(2)	117.5(1)	114.7(4)
	116.8(2)	115.1(6)	110.9(2)	109.4(2)	109.7(2)	117.6(1)	116.0(4)
H...H*	3.37	2.19	3.00	2.08	2.28	3.26	2.30
ρ	0.971	0.959	0.967	0.956	0.966	0.976	0.959

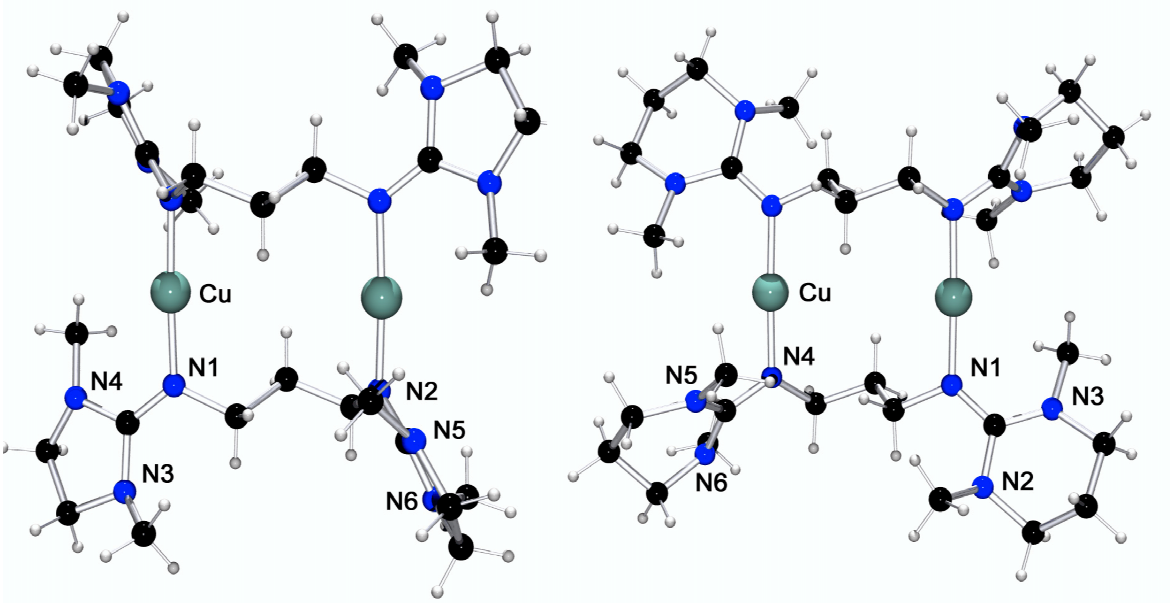

Figure 4.11: Molecular structures of $[Cu_2(DMEG_2p)_2]^{2+}$ in crystals of **C5** (left) and of $[Cu_2(DMPG_2p)_2]^{2+}$ in crystals of **C8** (right)

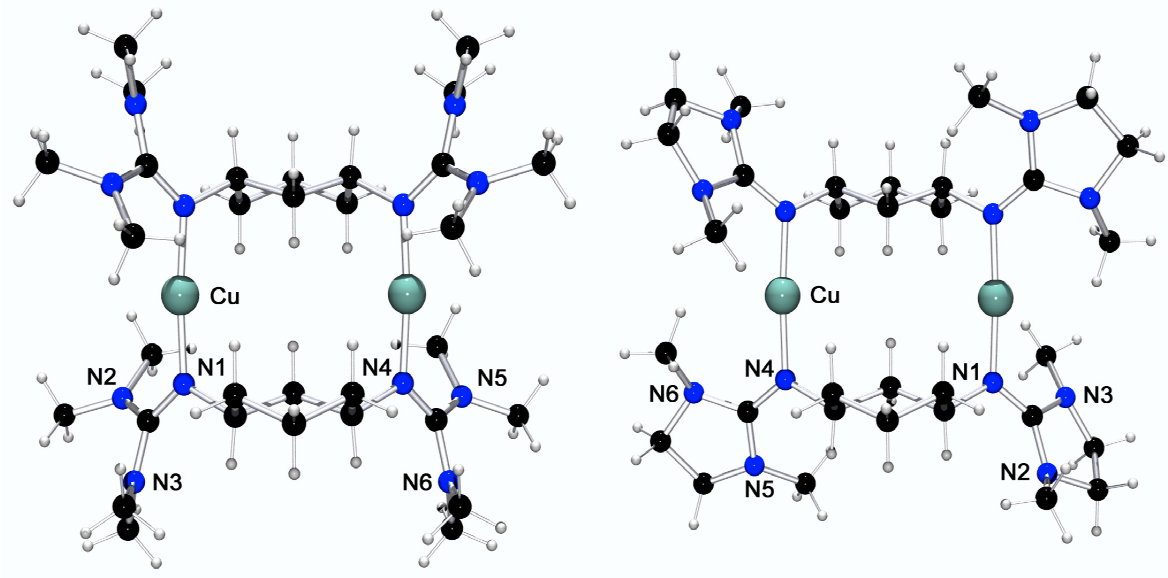

Figure 4.12: Molecular structures of $[Cu_2(TMG_2ch)_2]^{2+}$ in **C4** (left) and of $[Cu_2(DMEG_2ch)_2]^{2+}$ in **C6** and **C7** (right)

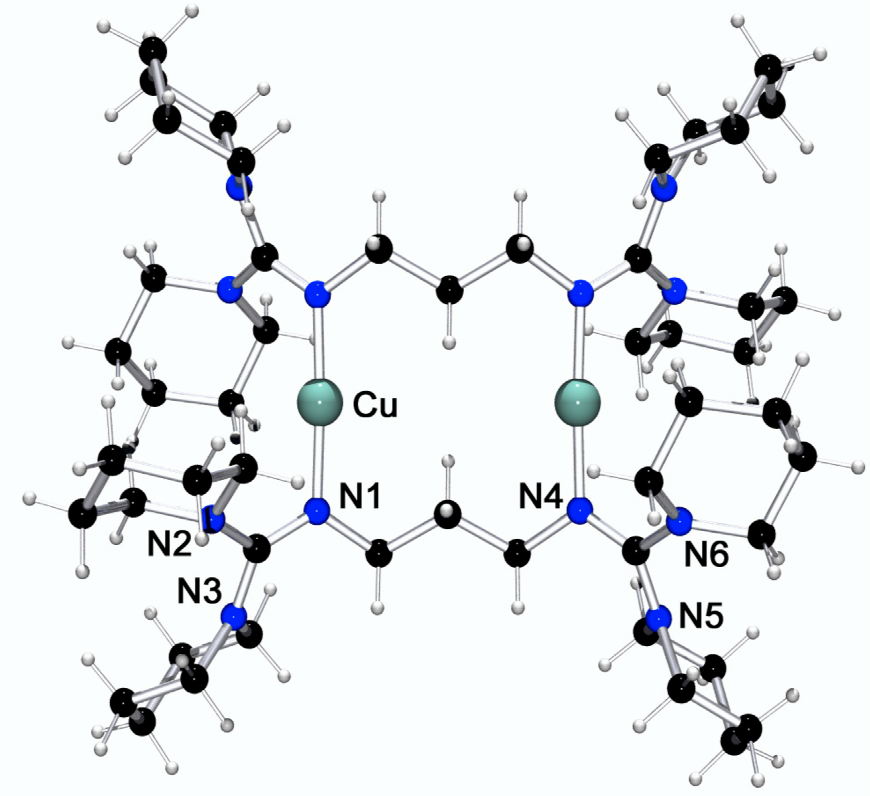

Figure 4.13: Molecular structure of **C9**

The dinuclear complex cations present in all seven compounds exhibit molecular ring structures (Figures 4.10 - 4.13) with significant differences in the folding of their propylene chains and in their corresponding interligand H...H separations passing through the centroids of the molecules. The copper centres show almost linear twofold coordination from two nitrogen

donor atoms of different ligands with N-Cu-N angles of 176.7(1), 174.7(3), 175.3(1), 174.9(1), 176.3(1), 177.2(1) and 176.8(1)° for **C3** to **C9**, respectively. The centroids of the molecules lie on crystallographic inversion centres resulting in perfectly planar Cu_2N_4 moieties. Corresponding Cu-N, N=C, N-C and propyl-bridge C-C distances vary only very slightly from **C3** to **C9** (averaged values in the order **C3** - **C9**): Cu-N 1.877, 1.862, 1.875, 1.880, 1.883, 1.869, 1.866 Å, N=C 1.319, 1.305, 1.314, 1.311, 1.313, 1.324, 1.309 Å, C-N_{amine} 1.358, 1.348, 1.359, 1.371, 1.360, 1.357, 1.364 Å and N-C(spacer) 1.474, 1.502, 1.474, 1.484, 1.483, 1.474, 1.471 Å. The Cu-N-C and N-C-C ring angles vary slightly in a non-systematic manner, the C-C-C angles are 111.6(2), 114.3(5), 112.7(2), 113.3(2), 114.3(2), 112.4(1) and 115.6(3)° for **C3** to **C9**. These differences may be traced back to variations in the Cu...Cu separations (4.121(1), 5.034(1), 4.488(1), 5.054(1), 4.974(1), 4.358(1), 4.723(1) Å). The variation in the Cu...Cu separations can be correlated with the non-bonding H...H separations as it is shown in Figure 4.14. This correlation is nearly linear: when the spacer is stretched, the hydrogen atoms at the center of the spacer are approaching each other and the copper centres are reaching for a longer distance. Only **C9** does not lie on this correlation line because the sterically demanding piperidine subsituents have other secondary interactions than the TMG, DMEG or DMPG systems. The structural parameter ρ for these complexes lies in the range of 0.96 to 0.98.

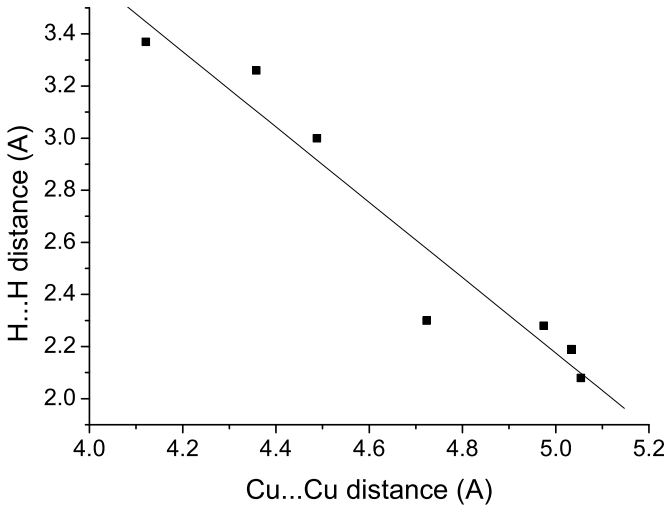

Figure 4.14: Correlation between the Cu...Cu separations and the H...H distances

In **C3**, the N=C(N)$_2$ planes of the guanidine moieties are nearly perpendicular to each other with a dihedral angle of 86.3°. For **C4**, **C7**, and **C8**, these angles are similar with 82.4, 83.6 and 80.0°, respectively. For **C5**, **C6** and **C9**, they are diminuished to 68.4, 70.6 and 71.5°, respectively. There is no clear tendency, therefore these differencies can only be traced back to crystal packing. Compared with the free ligands DMPG_2p and

Table 4.4: Dihedral angles [°] between the CN_3-guanidine plane and the C_{imin}-N_{amin}-$(C_{alkyl})_2$-planes (mean values and ranges of individuals)

Compound	**Angles**	**Compound**	**Angles**
btmgp	n/a	$[Cu_2(btmgp)_2][PF_6]_2$ (**C3**)	34.1 [32.3 - 35.9]
TMG_2ch	n/a	$[Cu_2(TMG_2ch)_2]I_2$ (**C4**)	35.9 [31.1 - 39.3]
$DMEG_2p$	n/a	$[Cu_2(DMEG_2p)_2][PF_6]_2$ (**C5**)	17.4 [12.7 - 23.1]
$DMEG_2ch$	n/a	$[Cu_2(DMEG_2ch)_2][Cu_2I_4]$ (**C6**)	15.9 [14.2 - 17.3]
		$[Cu_2(DMEG_2ch)_2][Cu_2I_4]$ (**C7**)	13.1 [11.5 - 13.4]
$DMPG_2p$	25.9 [19.7 - 31.8]	$[Cu_2(DMPG_2p)_2][PF_6]_2$ (**C8**)	24.8 [16.7 - 33.5]
$DPipG_2p$	40.7 [39.2 - 42.7]	$[Cu_2(DPipG_2p)_2][PF_6]_2$ (**C9**)	37.6 [32.2 - 43.2]

$DPipG_2p$, the C=N bonds in **C8** and **C9** are clearly elongated by about 0.04 Å whereas the remaining geometric ring parameters show no relevant influence from copper complexation. The $N{=}C(N)_2$ planes in these ligands show dihedral angles of 23.1° and 31.5°. Compared with the complexes **C3**, **C4**, **C8** and **C9** (116.4, 114.6, 117.6, 115.4°), the N_{amine}-C-N_{amine} angles in **C5**, **C6** and **C7** are diminished to 110.5, 109.7 and 109.3°, as the short ethylene linker in the DMEG guanidine moietiy introduces steric strain as it is illustrated in Figure 4.15. Table 4.4 summarises the dihedral angles between the CN_3-guanidine plane and the C_{imin}-N_{amin}-$(C_{alkyl})_2$-planes within the guanidine moieties in the crystalline free bases and in the solid complex salts. It is assumed that the deviation of an individual angle from the mean value reflects mainly packing forces of the crystals. In solution, however, these angles are not subjected to anisotropic interactions with the solvent. For that reason, the following discussion is based on the assumption that the mean angle found in the crystalline state comes close to the situation in solution.

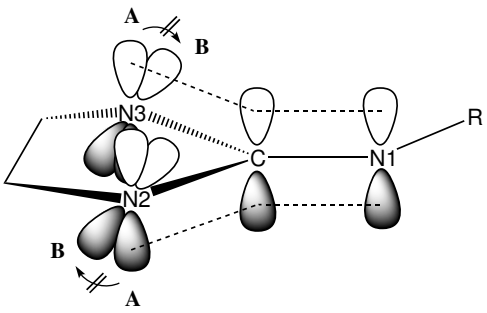

Figure 4.15: Schematic representation of the almost orthogonal p_z orbitals in DMEG groups

The tetramethylguanidino groups present in btmgp and TMG_2ch show a torsional effect in the dihedral angles between the CN_3-guanidine plane and the C_{imin}-N_{amin}-$(C_{alkyl})_2$-planes of around 35° whereas in dimethylethyleneguanidine containing systems like $DMEG_2p$ and $DMEG_2ch$, the ethylene linker imposes geometric strain on the guanidine centres resulting in a very small averaged dihedral angle of around 15° (Figure

4.15). By choosing a propylene linker, the averaged dihedral angle increases to about 25° as the system gains more constitutional flexibility. Without any linker, the p_z orbitals twist like in TMG and dipiperidylguanidines to avoid the steric hindrance. Thus, the dihedral angles in dipiperidylguanidines reach their maximum value of around 39°.

4.3.2 Electrochemistry of dinuclear copper(I) bisguanidine complexes

The copper(I) complexes **C3**, **C5**, **C8** and **C9** were also investigated cyclovoltammetrically to determine their redox activities. In Figure 4.16, the cyclovoltammogram of **C8** (0.1 mol/L $[NBu_4][PF_6]$; 100 mV/s, C/Pt/Ag-AgCl) is depicted as exemplified. The oxidation wave at -0.23 V/NHE is clearly irreversible. In the course of these measurements, irreversible oxidation waves at ca. -0.2 V attributable to the oxidation of Cu(I) to Cu(II) are observed for all the complexes (Table 4.5). This behaviour is not surprising as the initially linear coordination of Cu(I) requires subsequent rearrangement processes on changing the oxidation state of copper. Interestingly, no correlation between the oxidation potentials of the copper(I) complexes **C3**, **C5**, **C8** and **C9** and their abilities to stabilise P- or O-core complexes could be found (see section 5.1).

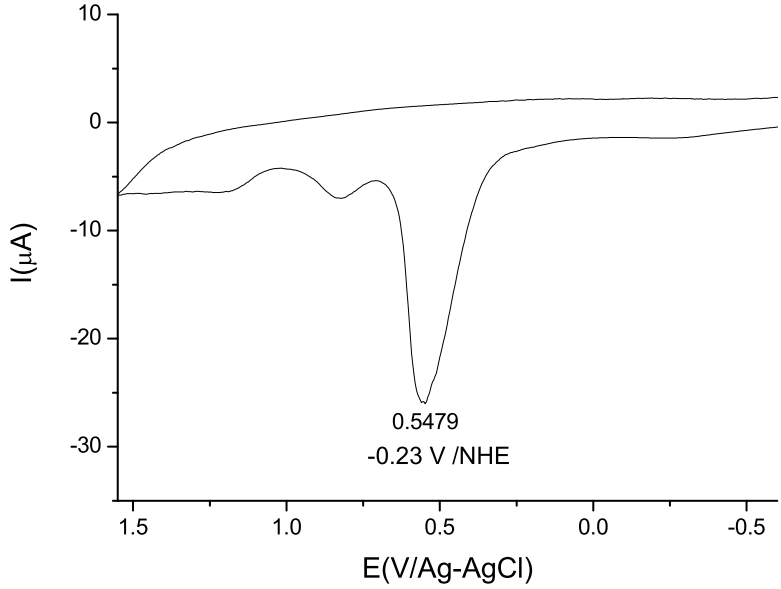

Figure 4.16: Cyclovoltammograms of **C8** in MeCN

Table 4.5: Cyclovoltammetric data for **C3**, **C5**, **C8** and **C9** (MeCN, v = 100 mV/s, 25°C)

Copper complex (+1/+2)	$\mathbf{E}_{ox}$ **[V/NHE]**
$[Cu_2(btmgp)_2][PF_6]_2$ (**C3**)	-0.18
$[Cu_2(DMEG_2p)_2][PF_6]_2$ (**C5**)	-0.23
$[Cu_2(DMPG_2p)_2][PF_6]_2$ (**C8**)	-0.21
$[Cu_2(DPipG_2p)_2][PF_6]_2$ (**C9**)	-0.29

4.4 Synthesis of polynuclear copper(I)bisguanidine chains

4.4.1 Synthesis of polynuclear Cu($DMEG_2p$) chains

The ligand $DMEG_2p$ is not only capable of stabilising dinuclear copper complexes with linear coordination but also of polynuclear chains with linear as well as trigonal-planar copper coordination modes. The decision between dinuclear complex and polynuclear chain is made by the choice of the solvent: if the complex is formed by reaction of $[Cu(MeCN)]_4[PF_6]$ and $DMEG_2p$ in acetonitrile, the dinuclear compound **C5** crystallises upon addition of ether. By using THF instead, the copper bisguandine chain of **C10** with linear copper coordination (Figures 4.17 and 4.18) can be obtained. The reaction of CuI and $DMEG_2p$ in THF yields the copper bisguanidine chain of **C11** exhibiting a trigonal-planar copper coordination which is illustrated in the Figures 4.19 and 4.20. Both copper bisguanidine chains crystallise upon additin of apolar solvents like diethyl or diisopropyl ether monoclinic in the space group $P2_1/n$. The unit cells contain four molecules, but in crystals of **C10** two additional molecules of acetonitrile per asymmetric unit are present originating from the educt compound $[Cu(MeCN)]_4[PF_6]$. Selected bond lengths and angles are collected in Table 4.6, and parameters relating to the data collection and refinement are listed in the Tables A8 and A9, respectively.

The chain structures exhibit several interesting features: in crystals of **C10**, the copper centres are coordinated almost linearly (N-Cu-N 178.7°) whereas in crystals of **C11**, one copper centre is coordinated T-shaped with an N-Cu1-N angle of 163.5° and N-Cu-I angles of 98.0° and the other one trigonal-planar with an N-Cu2-N angle of 115.5° and N-Cu2-I angles of 122.2°. This coordinational difference is further denoted in the different Cu-N bonds which measure around the T-shaped Cu1 centre about 1.918 Å and around the trigonal-planar Cu2 centre about 2.013 Å. At the same time, the Cu1-I1 distance is as long as 2.9291(5) Å whereas the Cu2-I2 distance in the trigonal situation has been determined

Table 4.6: Selected distances and angles of the copper(I) chains **C10** and **C11**

Distances (Å)	**C10**	**C11**
Cu-N$_{imine}$	Cu1-N1 1.877(2)	Cu1- N4 1.915(3)
	Cu1-N4 1.872(2)	Cu1 -N3 1.920(3)
	Cu2-N7 1.873(2)	Cu2 -N10 2.002(3)
	Cu2-N10 1.878(2)	Cu1 -N7 2.024(3)
Cu-I		Cu1- I1 2.9291(5)
		Cu2- I2 2.5413(5)
N=C(av)	1.308	1.291
Angles (°)		
N$_{imine}$**-Cu-N**$_{imine}$	N4-Cu1-N1 177.9(1)	N4-Cu1-N3 163.5(1)
	N7-Cu2-N10 179.5(1)	N10-Cu2-N7 115.5(1)
N$_{imine}$**-Cu-X**		N4-Cu1-I1 97.1(1)
		N3-Cu1-I1 98.9(1)
		N10-Cu2-I2 124.2(1)
		N7-Cu2-I2 120.2(1)
N$_{amine}$**-C-N**$_{amine}$**(av)**	109.7	109.0
ρ	0.951	0.933

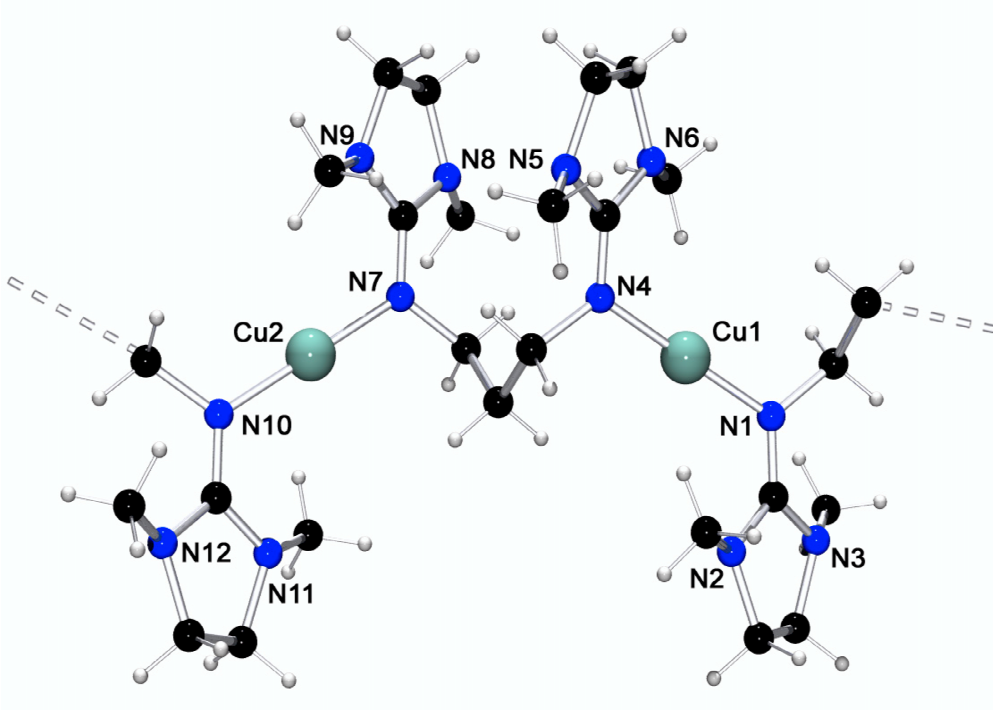

Figure 4.17: Section of the molecular structure of **C10**

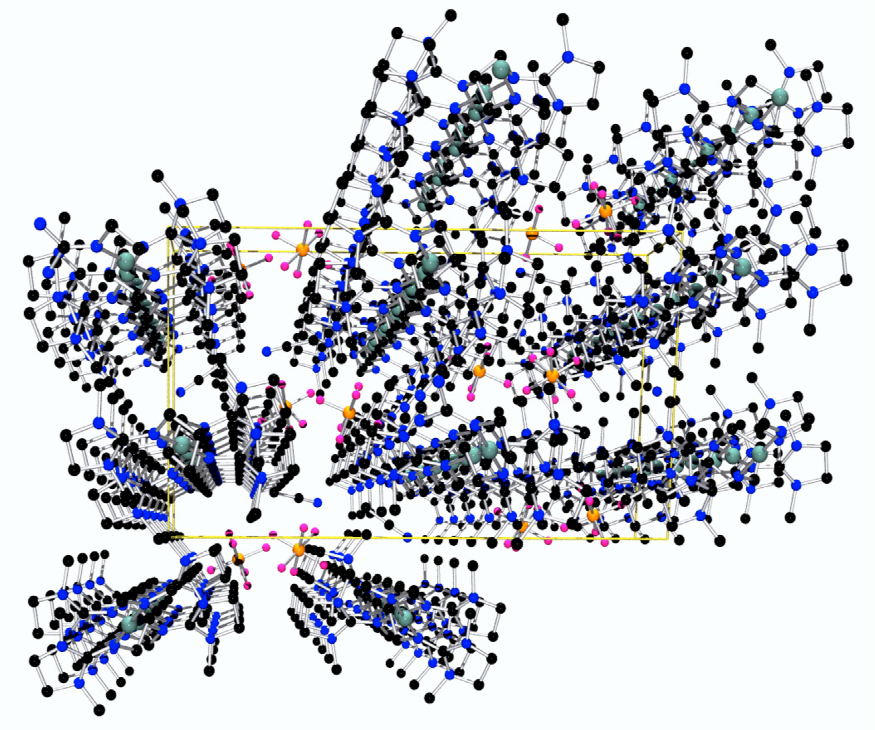

Figure 4.18: A view normal to the 001-plane in crystals of **C10**

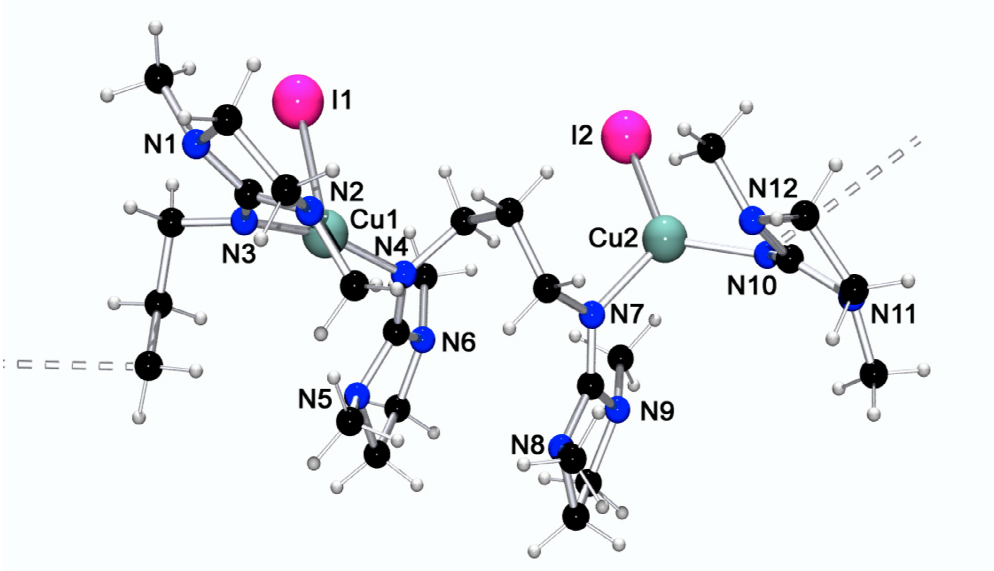

Figure 4.19: Section of the molecular structure of **C11**

to 2.5413(5) Å. Compared to **C10** with strictly twofold coordination, the averaged Cu-N distances in **C11** are elongated by about 0.09 Å to 1.965 Å due to the higher coordination number. The N_{amine}-C-N_{amine} angles in **C10** and **C11** have the characteristic value for $DMEG_2p$ containing systems in which the ethylene linker tights the N_{amine} atoms together. In Figures 4.18 and 4.20, a view normal to the 001-plane is given in order to illustrate the crystal packing. In both structures, the stacking of the almost planar DMEG moieties is clearly recognisable. In the packing of **C11**, one can distinguish the two different Cu-I units which are alligned by turns.

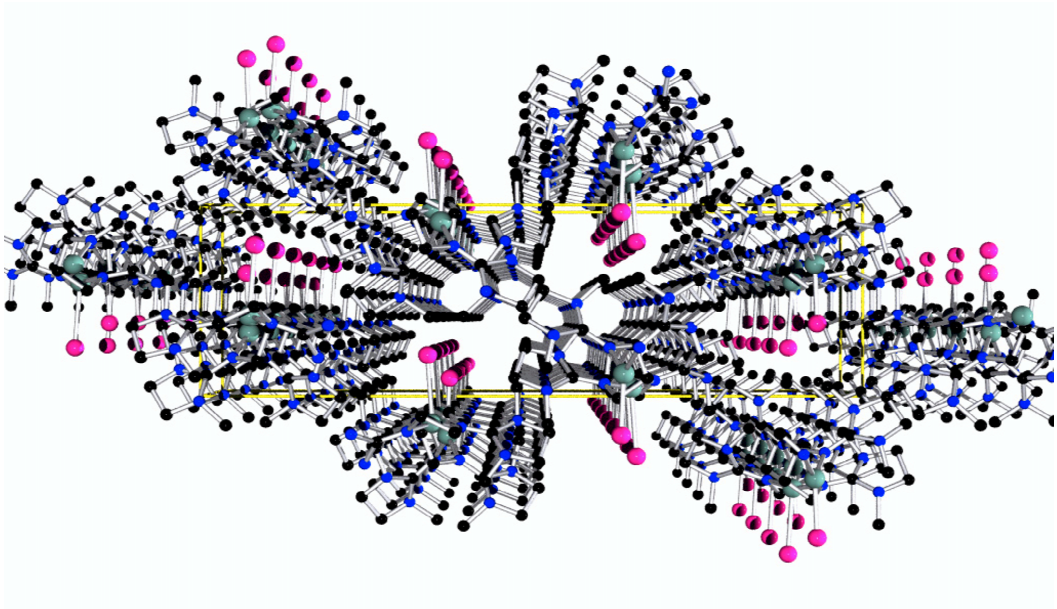

Figure 4.20: A view normal to the 001-plane in crystals of **C11**

4.4.2 Synthesis of further polynuclear copper(I)bisguanidine chains

By using TMG_2mX as coordinating ligand, a copper bisguanidine chain molecule with an intermediate between trigonal-planar and linear coordination of the copper centres can be synthesised. The reaction of CuI and TMG_2mX in MeCN yields the copper bisguanidine chain of **C12** exhibiting a very distorted trigonal-planar copper coordination which is illustrated in the Figures 4.21 and 4.23. Crystals of **C12** could be obtained by vapour diffusion of diethylether into the reaction mixture. **C12** crystallises in the monclinic space group $P2_1/n$ with four molecules per unit cell. By using $DPPG_2p$ as coordinating ligand, a copper bisguanidine chain molecule with T-shaped coordination of the copper centres and a strong Cu...Cu interaction can be synthesised. The reaction of CuI and $DPPG_2p$ in MeCN yields the copper bisguanidine chain $[Cu(DPPG_2p)]_n[CuI_2]_n$ (**C13**) which is depicted in the Figures 4.22 and 4.24. Crystals of **C13** could be obtained by evaporation of a acetonitrile/dichloromethane solution in the glove-box. **C13** crystallises in the orthorhombic space group $P2_12_12_1$ with four molecules per unit cell. In the $[CuX_2]$ unit, the halide positions are occupied by iodine (85 %) and by chlorine (15 %). As possible source for chlorine, the dichloromethane and the synthesis process of the ligand have to be considered (chloroformamidinium chlorides). The presence of chlorine was confirmed by microanalysis, too. Selected bond lengths and angles of **C12** and **C13** are collected in Table 4.7, and parameters relating to the data collection and refinement are listed in the Tables A9 and A10, respectively.

In crystals of **C12**, the copper centres are coordinated in a distorted (2+1) trigonal-planar

Table 4.7: Selected distances and angles of the copper(I) chains in crystals of **C12** and **C13**

Distances (Å)	**C12**	**C13**
Cu-N$_{imine}$	Cu1 -N1 1.911(2)	Cu1 -N1 1.903(3)
	Cu1-N4 1.905(2)	Cu1 -N4 1.906(2)
Cu-I	3.1423(5)	Cu2-I1 2.3935(7)
		Cu2-I2 2.3898(6)
N=C(av)	1.314	1.313
Angles (°)		
N$_{imine}$**-Cu-N**$_{imine}$	N4-Cu1-N1 169.8(1)	N1-Cu1-N4 178.9(1)
N$_{imine}$**-Cu-X**	N1-Cu1-I1 94.5(1)	N1-Cu1-Cu2 91.2(1)
	N4-Cu1-I1 95.6(1)	N4-Cu1-Cu2 88.1(1)
N$_{amine}$**-C-N**$_{amine}$**(av)**	116.0	115.7
ρ	0.960	0.959

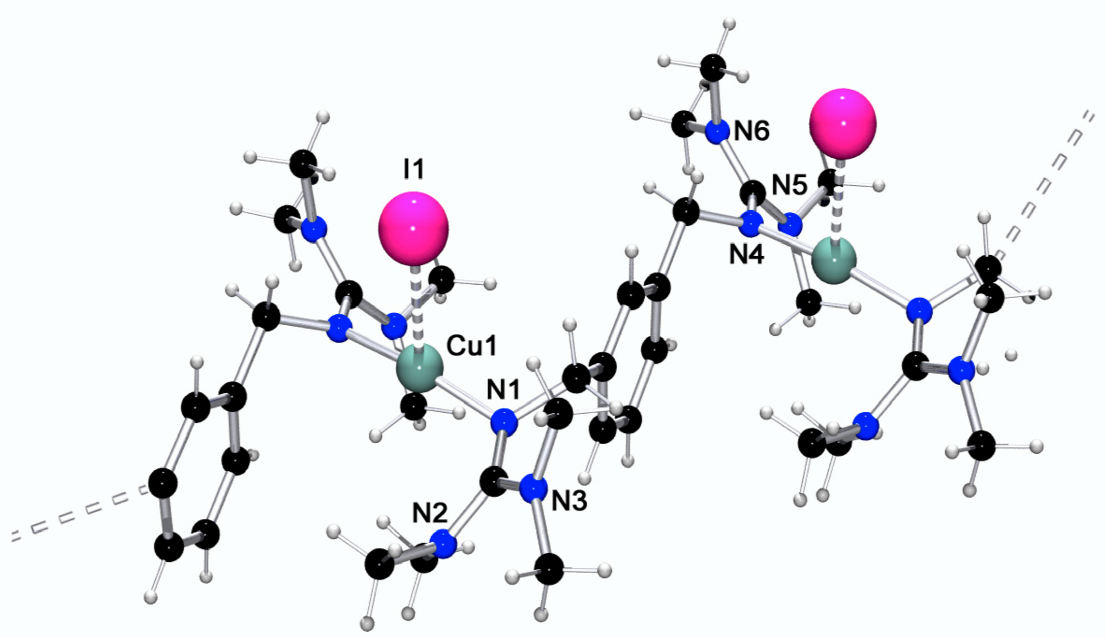

Figure 4.21: Section of the molecular structure of **C12**

geometry (N-Cu-N 169.8(1)°). The copper lies only 0.008(1) Å above the N1N4I1A plane. The Cu-I distance is relatively long with 3.1423(5) Å, thus, it can be regarded as contact due to the clear distortion of the N-Cu-N angle which measures in a linear coordinational environment like in **C10** up to 178° (averaged). Compared to **C10** with strictly twofold coordination, the averaged Cu-N distances in **C13** are slightly elongated by about 0.03 Å to 1.908 Å due to the higher coordination number. This mode of coordination represents an intermediate between linear coordination with non-coordinating anion and a trigonal-planar

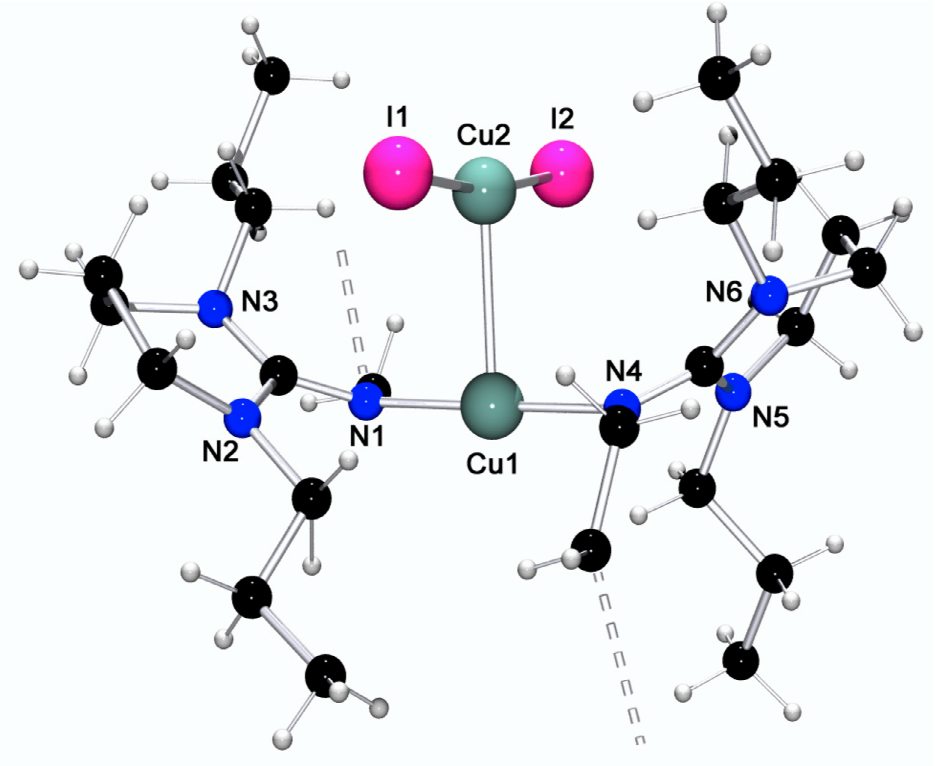

Figure 4.22: Section of the molecular structure of **C13**

coordination where the iodine acts as third donor. The N_{amine}-C-N_{amine} angles are in the range of other tetramethyl guanidines.

In crystals of **C13**, the Cu1 centre is coordinated T-shaped with an N-Cu1-N angle of 178.9(1) and averaged N-Cu1-Cu2 angles of 89.7°. The Cu...Cu distance measures 2.6732(6)Å and the Cu-I distances average to 2.392 Å. The Cu2 centre is as well coordinated T-shaped with an I1-Cu2-I2 angle of 169.63(2)° and averaged I-Cu2-Cu1 angles of 95.2°. The coordination axes of the CuN_2 and the CuI_2 unit are approximately perpendicular to each other as the torsion angles indicate (N1-Cu1-Cu2-I1 91.1°, N4-Cu1-Cu2-I2 90.3°). It is instructive to compare the structure of **C13** with similar systems with Cu...Cu interactions: Siemeling et al. characterised a similar perpendicular $N_{py,2}$Cu...$CuCl_2$ constellation with a Cu...Cu separation of 2.810(2) Å [132] whereas Köhn was able to crystallise the $[Cl_2Cu...CuCl_2]^{2-}$ dianion stabilised in a complex salt exhibiting a Cu...Cu separation of 2.92 Å.[133] Very recently, Köhn found a cuprophilic interaction of only 2.54 Å in a dinuclear structure stabilised by triazacyclohexanes.[134] Shorter contacts have only been observed by Strähle et al.[135] Thus, complex **C13** represents a rare example of this structural class with a remarkably short Cu...Cu distance of 2.6732(6)Å. Upon closer consideration, it has to be mentioned that this close Cu...Cu contact in **C13** is not stabilised by a ligand bridging the copper centres like in Strähles system. Such close contacts may be interpreted in terms of weak

bonding interactions between the two d^{10} metal centres. Attractive interactions between formally closed-shell metal centres are documented for several metals.[136] In the case of gold, the term aurophilicity has been coined to describe this special kind of metal-metal bonding interaction,[137] but the question of whether a similar metallophilicity [138] exist in the case of the other two coinage metals, copper and silver, is still a matter of controversy. An interesting case is the trinuclear copper complex $[Cu(CH_3C_6H_4\text{-}N_5C_6H_4CH_3)_3]$, where the metal centres have an average distance of only 2.35 Å.[135] This existence of cuprophilic interaction has both been supported [139] and refuted [140] at various levels of theory. Generally, weak metallophilic effects are easily blurred or even overruled by other secondary interactions. Therefore, crystal packing forces may very well overrule weak cuprophilic interactions explaining the greater distances in Siemelings system under account of all similarities.[141] However, compared to **C12** with distorted trigonal-planar coordination, the averaged Cu-N distances in **C13** are in good accordance which shows that the CuI_2 moiety acts as weak donor.

In Figures 4.23 and 4.24, the best view is given in order to illustrate the crystal packing. In both structures, the stacking of the guanidine moieties supports the crystallisation in spite of the flexible propylene chains in **C13**. Furthermore, the $N_2Cu...CuI_2$ unit in **C13** seems to stabilise the packing.

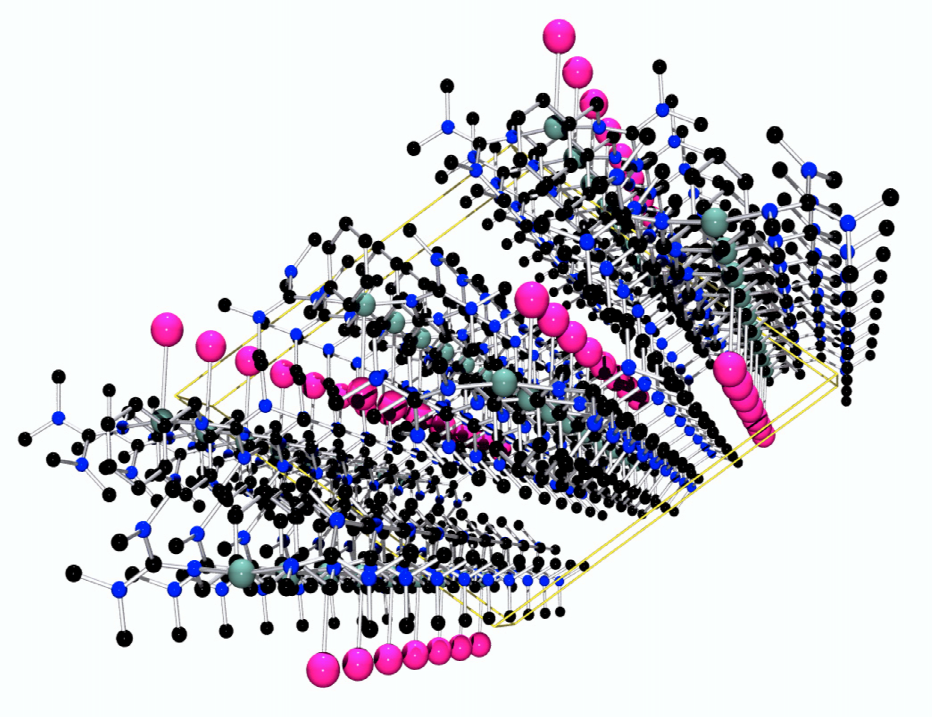

Figure 4.23: View on the crystal packing in **C12**

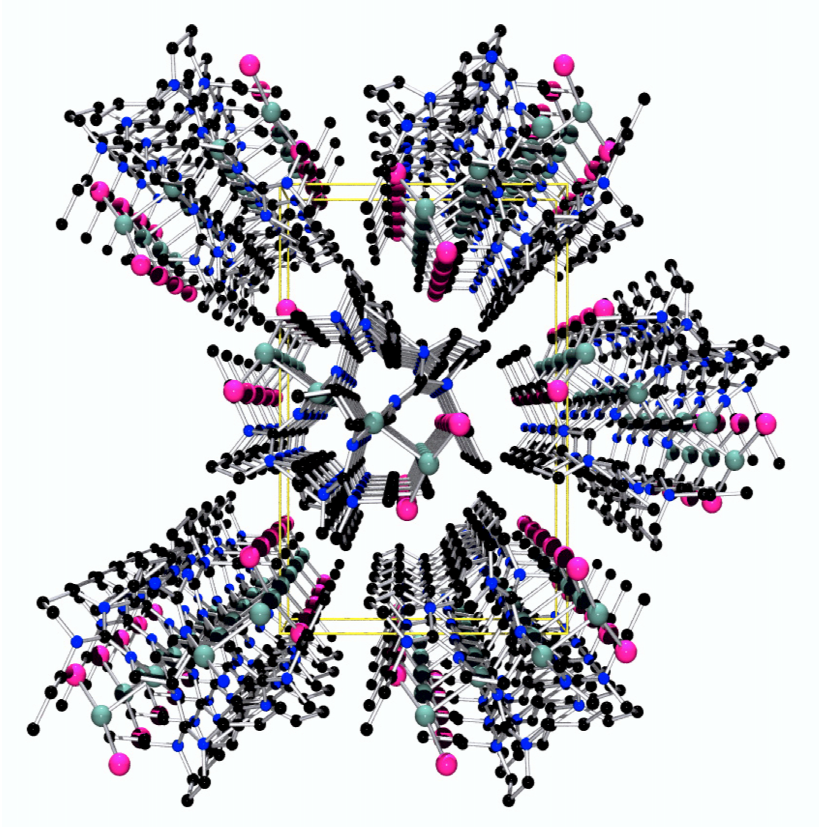

Figure 4.24: View on the crystal packing in **C13**

Table 4.8 summarises the dihedral angles between the CN_3-guanidine plane and the C_{imin}-N_{amin}-$(C_{alkyl})_2$-planes within the guanidine moieties in the complexes **C10** - **C13**. The ligand $DMEG_2p$ shows in these two complexes dihedral angles of around 16.7°, the tetramethyl system TMG_2mX of 35.5° and the dipropylpropylene system $DPPG_2p$ of 28.5°.

Table 4.8: Dihedral angles [°] between the CN_3-guanidine plane and the C_{imin}-N_{amin}-$(C_{alkyl})_2$-planes (mean values and ranges of individuals)

Compound	**Angles**
$[Cu(DMEG_2p)PF_6]_x$ (**C10**)	15.7 [12.2 - 19.0]
$[Cu(DMEG_2p)I]_x$ (**C11**)	17.8 [14.5 - 21.6]
$[Cu(TMG_2mX)I]_x$ (**C12**)	35.5 [29.4 - 40.1]
$[Cu(DPPG_2p)..CuI_2]_x$ (**C13**)	28.5 [22.5 - 34.3]

4.5 Synthesis of a dinuclear copper(I)benzimidazolyle-guanidine complex with linear copper coordination

By using TMG_2PA in the reaction with $[Cu(MeCN)]_4[PF_6]$, the copper is not oxidised to Cu(II), but a cyclisation of the bisguanidine ligand to a benzimidazole-monoguanidine system occurs and the dinuclear complex compound Bis2-(2-(2-(dimethylamino)-1H-benzo[d]imidazol-1-yl)phenyl)-1,1,3,3-tetramethylguanidine copper(I)hexafluorophosphate ($[Cu_2(TMGbenzPA)_2][PF_6]_2$, (**C14**) is formed. A proposed mechanism is illustrated in reaction scheme 4.25. Firstly, the copper is coordinated by the TMG_2PA ligand, then the acidic proton is abstracted under nucleophilic attack of the amide on one of the basic guanidine groups. It might be possible that these steps are occurring simultaneously resulting in a abstraction of $HNMe_2$. In this cyclisation reaction, the driving force is the formation of a aromatic benzimidazole compound. The former guanidine N=C bond is now part of the heterocyclic benzimidazole system. During all these steps, the copper is stabilised by the coordinating solvent acetonitrile. Finally, the mononuclear complex cation dimerises to yield complex **C14** because the coordinational environment with two strong ligand N donors is better than only one N donor from the ligand and one from MeCN. Appearently, in this case, this reaction is preferred to an oxidation of the copper and proton reduction to hydrogen (see section 4.2).

4.5.1 Crystal structure of $[Cu_2(TMGbenzPA)_2][PF_6]_2$ (C14)

Colourless single crystals could be obtained by vapour diffusion of diethylether into MeCN solution. **C14** crystallises monoclinic in the space group $P2_1/n$. Crystals of **C14** consist of isolated molecules, the unit cell contains two molecules of **C14**. The results of the structure analysis are shown in Figure 4.26, while selected bond lengths and angles are collected in Table 4.9, and parameters relating to the data collection and refinement are listed in Table A10.

The dinuclear complex cation **C14** exhibits a molecular ring structure (Figure 4.26) similar to those of the complexes **C3** - **C9**. In **C3** - **C9**, the ligand has a propylene spacer resulting in a twelve-membered heterocycle whereas in **C14**, the cyclisated ligand has a benzimidazol-phenylene spacer resulting in a fourteen-membered heterocycle. Hence, the Cu...Cu separation is with 4.704(1) Å longer than in the comparable **C3** (4.121(1) Å) . The copper centre

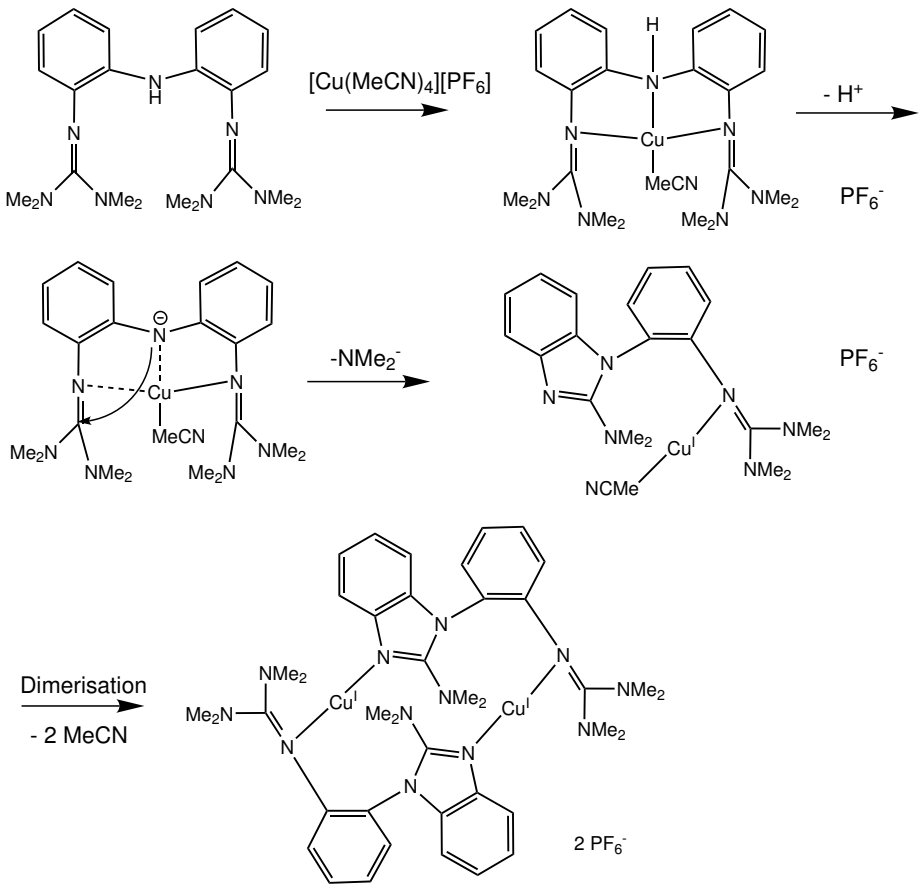

Figure 4.25: Reaction of TMG_2PA with $[Cu(MeCN)_4][PF_6]$

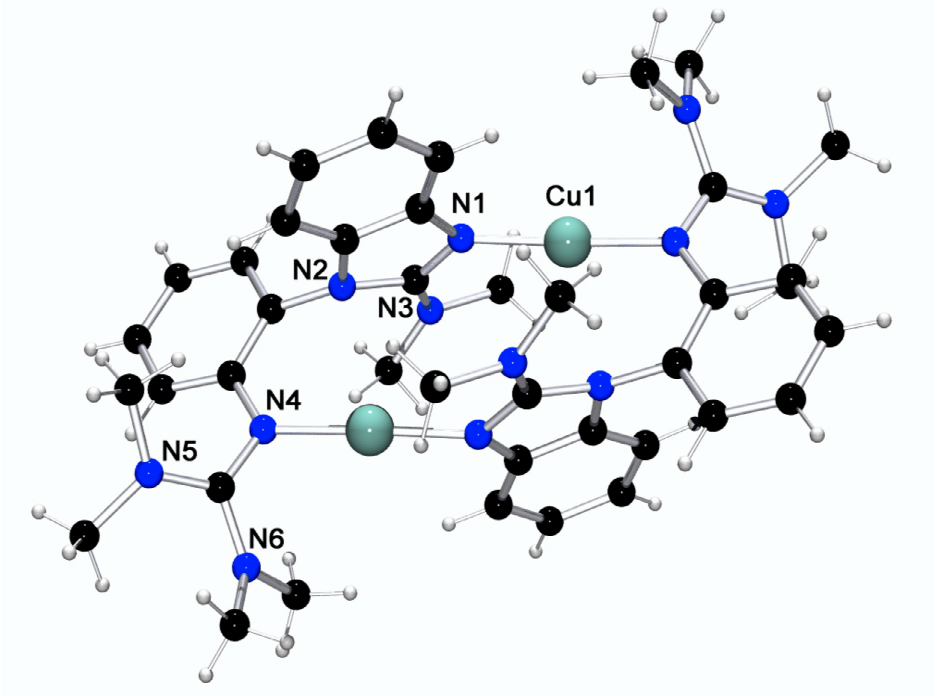

Figure 4.26: Molecular structure of **C14**

shows almost linear twofold coordination from two nitrogen donor atoms of different ligands with N-Cu-N angles of 173.8(3)°. The centroid of this molecule lies on the crystallographic

Table 4.9: Selected distances and angles of **C14**

Distances (Å)	**C14**	**C3**
Cu...Cu	4.704(1)	4.121(1)
Cu-N$_{imine}$	1.879(5)	1.876(2)
	1.895(6)	1.878(2)
N=C(gua)	1.324(9)	1.319
N=C(benz)	1.307(8)	
Angles (°)		
N$_{imine}$**-Cu-N**$_{imine}$	173.8(3)	176.7(1)

inversion centre resulting in a perfectly planar Cu_2N_4 moiety. The Cu-N_{imine} distances are in good agreement with those found in **C3** - **C9**. The N=C bond of the benzimidazole part of the TMGbenzPA ligand is not significantly shorter than the N=$C_{guanidine}$ bond. However, the calculation of the structural parameter ρ shows that the "real" guanidine moiety has a ρ value of 0.974 with good delocalisation, whereas the cyclisated guanidine moiety has a ρ value of 0.947 with stronger localisation of the C=N double bond.

4.5.2 Electrochemistry of $[Cu_2(TMGbenzPA)_2][PF_6]_2$ (C14)

The cyclovoltammogram of **C14** (0.1 mol/L $[NBu_4][PF_6]$; 50 mV/s; Au/Pt/Ag-AgCl) shows three irreversible electron transfers (Figure 4.27). The first oxidation wave at 442 mV/NHE

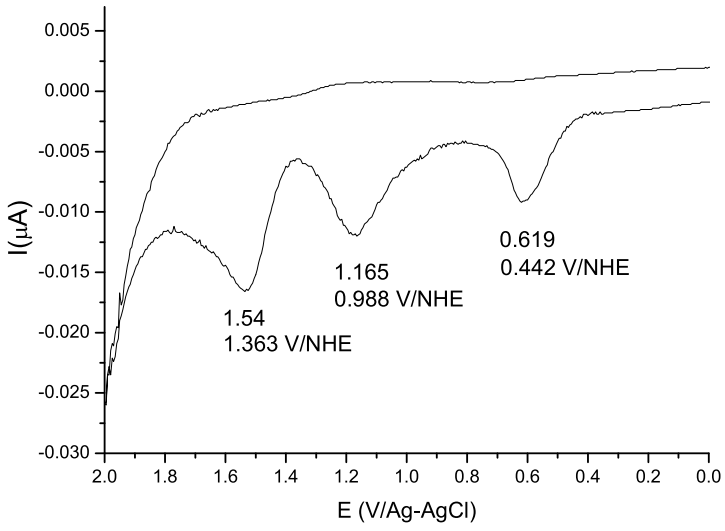

Figure 4.27: Cyclovoltammogram of **C14** in CH_2Cl_2

might be indicative for the oxidation of Cu(I) to Cu(II) whereas the oxidation waves at 988

and 1363 mV/NHE belong to redox processes which are delocalised in the aromatic system. Thus, they can not be assigned exactly to special redox processes.

4.6 Conclusion of the Syntheses of Copper(I)Bisguanidine complexes

It could be shown that bisguanidine complexes are able to stabilise copper(I) complexes in several coordination modes. The different topologies are summarised in the first section of this chapter. The presented ligands support the formation of mono-, bi- and polynuclear complexes, sometimes with solvent-depending equilibria between two coordination modes. Especially the ligand $DMEG_2p$ has shown to be very flexible: in crystals of **C15**, the coordination is bridging linear, whereas in the isomer **C10**, the ligand stabilises by linear coordination a polynuclear chain. By introducing further donor atoms like iodine in **C11**, the coordination changes to a trigonal-planar mode. Finally, in Chapter 6, the chelating coordination with this ligand in the copper(II) complex **C21** will be described.

5 Oxygen activation with Cu(I) bisguanidine complexes

5.1 Cu_2O_2 Bisguanidine species

As mentioned in Section 1.5.4, the supporting ligands can tune the equilibrium between μ-η^2:η^2-peroxo and bis(μ-oxo) dicopper cores (Figure 5.1). There are multiple influences which are imposed on this sensitive equilibrium, e.g. the denticity, the ligand bite, electronic factors dictating the σ donor strength and steric factors imposing steric strain.[48] In the following section, the influences of bisguanidine ligands on Cu_2O_2 species will be discussed.

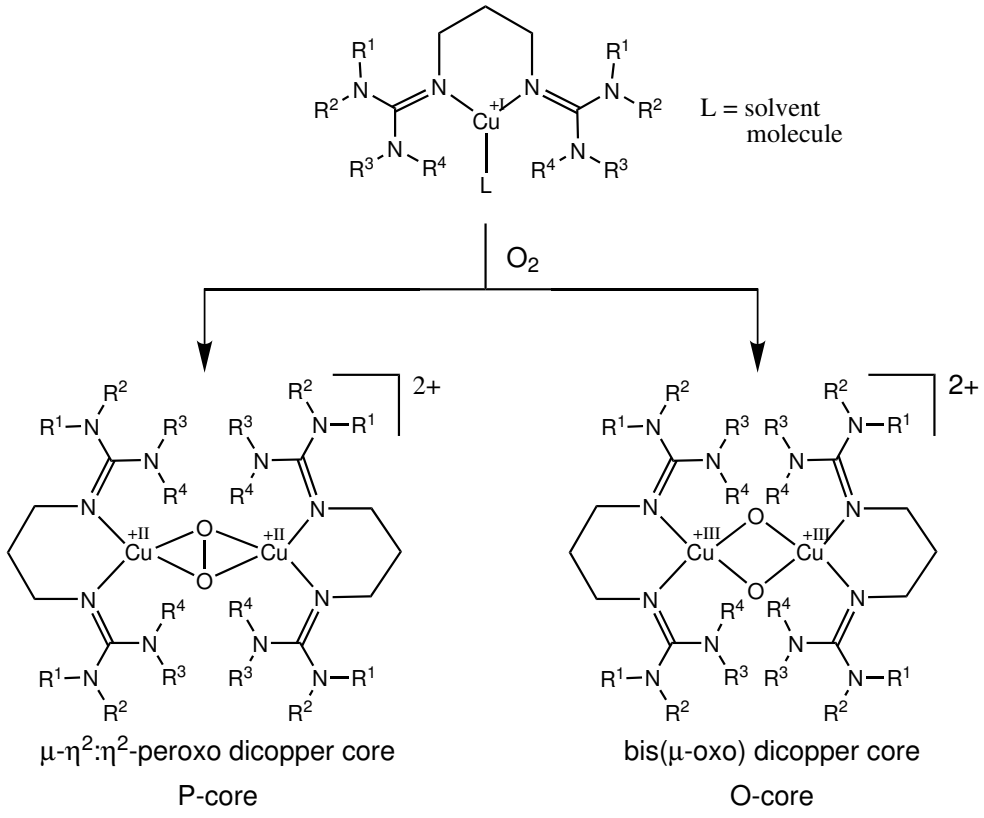

Figure 5.1: Equilibrium between μ-η^2:η^2-peroxo and bis(μ-oxo) dicopper bisguanidine complexes

5.2 UV/Vis-Spectroscopy of Cu_2O_2 Bisguanidine species

5.2.1 UV/Vis-Spectroscopy of Cu_2O_2 species with aliphatic bisguanidine ligands

Upon reaction of [Cu(DMorphG_2p)I] (**C2**), [Cu_2(btmgp)$_2$][PF_6]$_2$ (**C3**) and [Cu_2(DPipG_2p)$_2$][PF_6]$_2$ (**C9**) with O_2, intensive LMCT absorption bands at 300 ($\epsilon \approx$ 16000 mol/(Lcm)) and 390 nm ($\epsilon \approx$ 17000 mol/(Lcm)) are observed which are characteristic for all O-core complexes known so far (Figure 5.2). These species are unstable even at -80°C in dichloromethane. The initial red solutions change their colours to bluish-green upon warming up to room temperature within 1 - 2 h.[142]

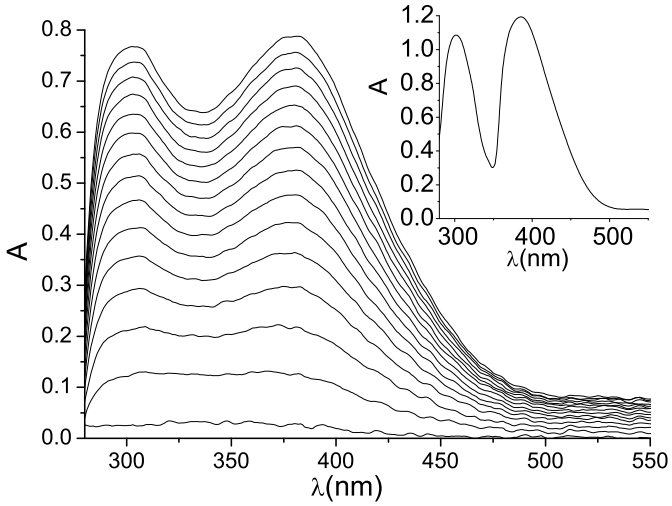

Figure 5.2: Time-dependent UV/Vis absorption spectra (every 2 min) observed upon introduction of O_2 gas into CH_2Cl_2 solution of **C9** (0.25 mM, -80°C) during 30 min; inset: spectrum after 2 h (0.33 mM)

Treatment of a 0.2 mM solution of [Cu_2(DMEG_2p)$_2$][PF_6]$_2$ (**C5**) in CH_2Cl_2 with dioxygen at -80°C resulted in a green colour of the solution. At higher concentrations, the solution turns dark brown. The UV/Vis spectrum observed 1 h after introduction of molecular oxygen is shown in Figure 5.3. The spectrum is dominated by a strong absorption band at 355 nm (ϵ = 17000 mol/(Lcm)) indicative of the predominant formation of the P-core complex. The shoulder at 320 nm (ϵ = 9500 mol/(Lcm)) is assigned to the formation of O-core contributors. [Cu_2(DMPG_2p)$_2$][PF_6]$_2$ (**C8**) reacts with O_2 in dichloromethane under predominant formation of a P-core complex which can be identified by LMCT absorptions at 350 nm (ϵ = 21200 mol/(Lcm))and at 550 nm (ϵ = 900 mol/(Lcm)). The band at ca. 300 nm (ϵ = 13500 mol/(Lcm)) originates from O-core components which are formed concomitantly with the P-core (Figure 5.4a). The O-core absorption at 390 nm is not resolved.

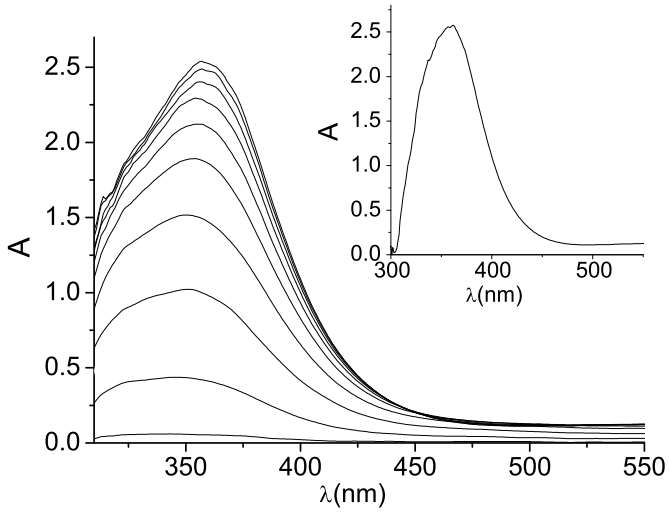

Figure 5.3: UV/Vis absorption spectrum observed upon introduction of O_2 gas into a solution of **C5** in MeCN/CH_2Cl_2 (1:10) (0.5 mM, -80°C) after 30 min, inset: spectrum after 1 h (0.25 mM)

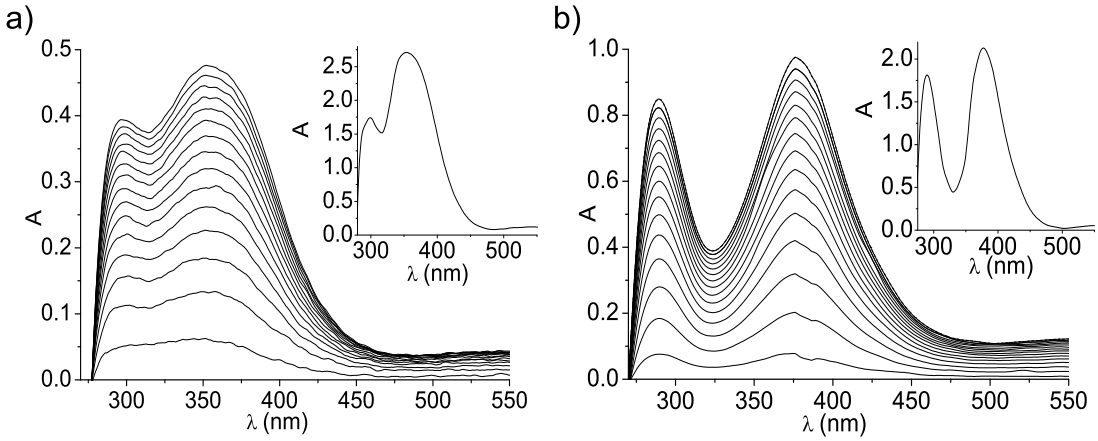

Figure 5.4: a)Time-dependent UV/Vis absorption spectra (every 2 min) observed upon introduction of O_2 gas into CH_2Cl_2 solution of **C8** (0.2 mM, -80°C) during 30 min; inset: spectrum after 2 h (0.5 mM); b)Time-dependent UV/Vis absorption spectra (every 30 s) observed upon introduction of O_2 gas into MeCN solution of **C8** (0.25 mM, -40°C) during 8 min; inset: spectrum after 1 h (0.5 mM)

In contrast, reaction of **C8** with O_2 in acetonitrile at -40°C results in the immediate formation of an O-core complex shown by the UV/Vis absorption bands at 290 (ϵ = 13000 mol/(Lcm)) and 390 nm (ϵ = 15800 mol/(Lcm)) (Figure 5.4b). By using MeCN as solvent, the equilibrium between P- and O-core is shifted almost completely to the O-core side. These results show that coordinating solvents are better suited to stabilise the O-core than non-coordinating ones and thus confirm reports of other groups published in the literature.[45, 49, 48]

Compound $[Cu_2(TMG_2ch)_2][I]_2$ (**C4**) reacts with O_2 in dichloromethane under formation of an O-core complex which can be identified by LMCT absorptions at 295 nm (ϵ = 16500

mol/(Lcm))and at 370 nm (ϵ = 11300 mol/(Lcm)) (Figure 5.5). The band at 370 nm is blue-shifted in comparison with other O-core complexes. Possibly, there are small amounts of P-core components which might shift the band from 400 nm to 370 nm. Interestingly, the red solution of this O-core species decays relatively fast within 20 min, hence the measurement had to be carried out using higher concentrations of the precursor complex. Treatment of a

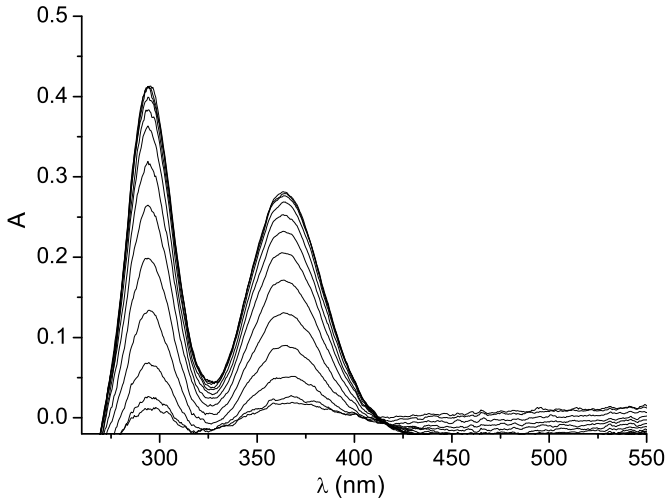

Figure 5.5: Time-dependent UV/Vis absorption spectra (every 1 min) observed upon introduction of O_2 gas into CH_2Cl_2 solution of **C4** (1 mM, -80°C) during 10 min

0.4 mM solution of $[Cu_2(DMEG_2ch)_2][Cu_2I_4]$ (**C6**) in CH_2Cl_2 with dioxygen at -80°C resulted in a greenish-blue colour of the solution. At higher concentrations, the solution turns dark brown. The UV/Vis spectra measured every 50 s are depicted in Figure 5.6. The spectrum is dominated by a strong absorption band at 360 nm (ϵ = 18500 mol/(Lcm)) indicative of the formation of the P-core complex.

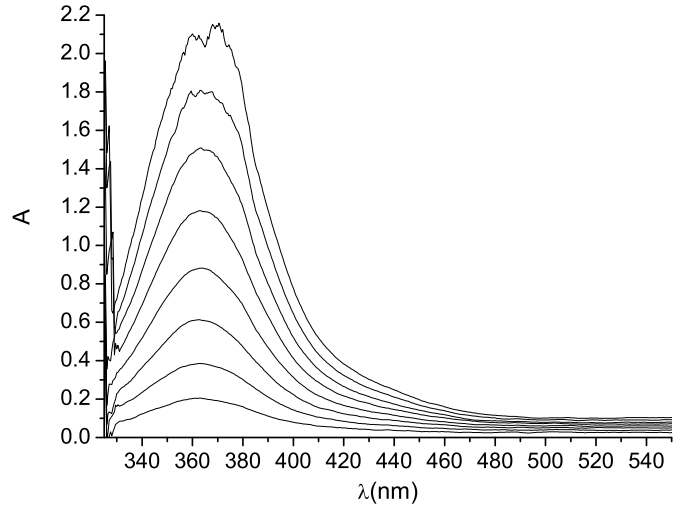

Figure 5.6: Time-dependent UV/Vis absorption spectra (every 50 s) observed upon introduction of O_2 gas into CH_2Cl_2 solution of **C6** (0.2 mM, -80°C) during 400 s

The reaction of $[Cu(DPPG_2p)I]$ with dioxygen in dichloromethane at -80°C yields a red

solution with an intensive absorption at 355 nm (ϵ = 19700 mol/(Lcm))(Figure 5.7). This species is stable for about 3 hours at -80°C. It has to be mentioned that there is no distinct side band of O-core components which is developed using the similar ligand $DMPG_2p$ (Figure 5.4).

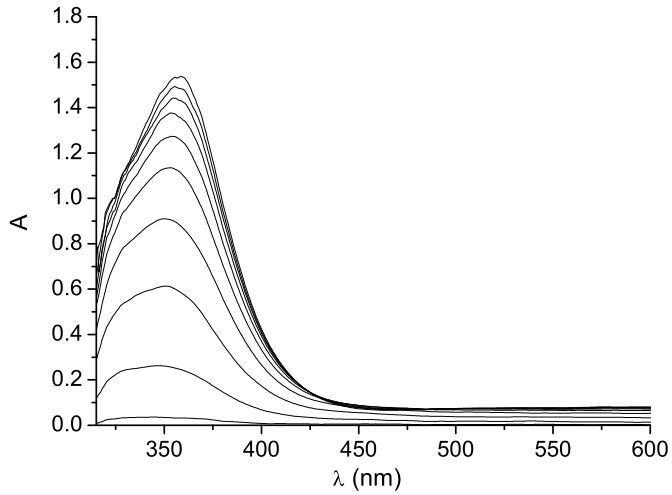

Figure 5.7: Time-dependent UV/Vis absorption spectra (every 2 min) observed upon introduction of O_2 gas into CH_2Cl_2 solution of [Cu($DPPG_2p$)]I (0.35 mM, -80°C) during 24 min

5.2.2 UV/Vis-Spectroscopy of Cu_2O_2 species with aromatic bisguanidine ligands

All TMG_2MePA containing complexes, e.g. [Cu(TMG_2MePA][X] (X = PF_6^-, ClO_4^-, BF_4^- and I^-), exhibit upon reaction with O_2 a dominant absorption at 395 nm ($\epsilon \approx$ 21000 mol/(Lcm)) which is not influenced by the counteranion (Figure 5.8). This characteristic O-core absorption is accompanied by a broad absorption at 550 nm ($\epsilon \approx$ 2800 mol/(Lcm)) which might be caused by aromatic side-products (not P-core). The solution is dark brown and turns upon warming up black.

Upon reaction of [Cu_2($DMPG_2$mX)$_2$]I_2 with O_2, an intensive LMCT absorption band at 350 (ϵ = 16500 mol/(Lcm)) assigning the development of a P-core species and a characteristic isosbestic point at 425 nm are observed (Figure 5.9). These species are unstable even at -80°C in dichloromethane. The initial red solution changes its colour to brownish-green upon warming up to room temperature within 1 - 2 h.

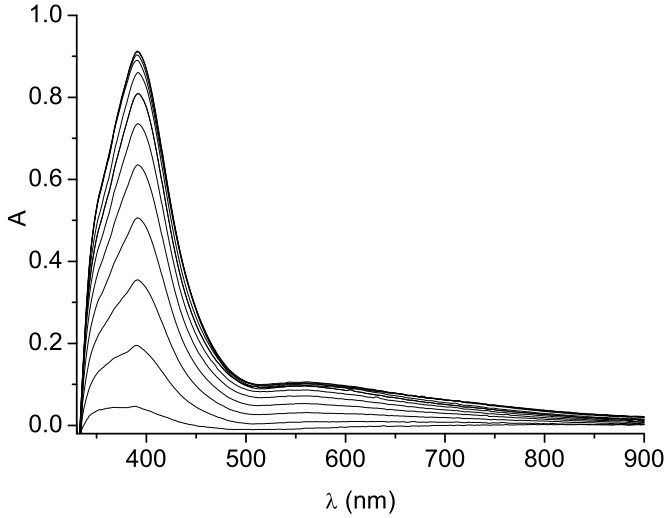

Figure 5.8: Time-dependent UV/Vis absorption spectra (every 2 min) observed upon introduction of O_2 gas into CH_2Cl_2 solution of $[Cu(TMG_2MePA)][PF_6]$ (0.1 mM, -80°C) during 22 min

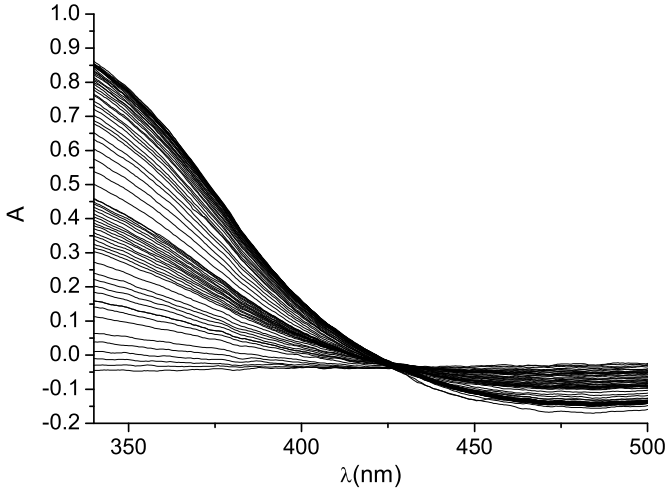

Figure 5.9: Time-dependent UV/Vis absorption spectra (every 1 min during 30 min, then every 5 min during further 150 min) observed upon introduction of O_2 gas into CH_2Cl_2 solution of $[Cu_2(DMPG_2mX)_2]I_2$ (0.1 mM, -80°C)

5.2.3 UV/Vis-Spectroscopy of Cu_2O_2 species with sterically demanding bisguanidine ligands

The reaction of $[Cu(B(TMPip)G_2p)]I$ containing a highly sterically demanding ligand with dioxygen proceeds very slowly at low temperatures. Thus, the reaction was observed at room temperature (Figure 5.10). As the strong absorption bands at 295 nm ($\epsilon = 18100$ mol/(Lcm)) and 370 nm (ϵ =9700 mol/(Lcm)) indicate, an O-core species is formed which is stable for two weeks at room temperature. This behaviour can be explained by the extreme shielding effect of the tetramethylpiperidino groups. The O-core can only hydroxylate N-CH_3 groups (see section 6.1) but not this environment, so, the course of subsequent reactions is hindered.

Resonance Raman measurements have been carried out in order to prove the existence of this room-temperature stable O-core. The resulting resonance Raman spectrum is depicted in Figure 5.11. The peak at 583 cm^{-1} belongs to the Cu_2O_2 breathing mode; this vibration is characteristic and diagnostic for an O-core.[48] At the same time, this resonance Raman spectrum shows that there are no detectable P-core components present which could shift the second absorption band to 370 nm. This blue-shifted band appears to be characteristic for some bisguandine Cu_2O_2 species.

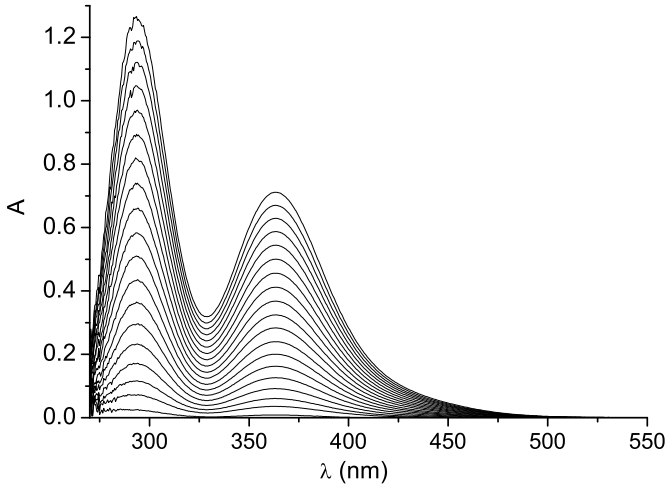

Figure 5.10: Time-dependent UV/Vis absorption spectra (every 30 min) observed upon introduction of O_2 gas into CH_2Cl_2 solution of [Cu(B(TMPip)G_2p)]I (0.3 mM, 25°C) during 600 min

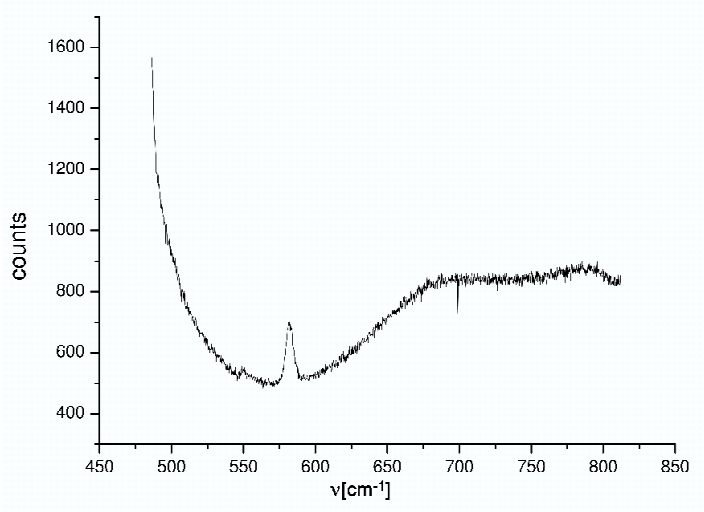

Figure 5.11: Resonance Raman spectrum of [Cu(B(TMPip)G_2p)]I (≈ 80 mM, 25°C, CH_2Cl_2), excitation wavelength: 350 nm

The UV/Vis absorption spectrum of [Cu((DMPip)DMG_2p)]I with dioxygen (Figure 5.12) exhibits the two characteristic absorption bands of an O-core species (290 nm (ϵ = 19500 mol/(Lcm)) and 370 nm (ϵ = 10400 mol/(Lcm))). This result shows that the guanidine moieties do not have to be such sterically demanding to stabilise a room-temperature stable

O-core species like it is the case in [Cu(B(TMPip)G_2p)]I. The ligand (DMPip)DMG_2p possesses only one dimethylpiperidino unit and one dimethylamino unit attached to the C_{imine} atom, but the sterical shielding seems to be great enough to support this O-core complex. The smaller guanidine moieties are reflected in an O-core formation which is more than five times faster than it would preceed with [Cu(B(TMPip)G_2p)]I, but nevertheless, this species is stable for one week.

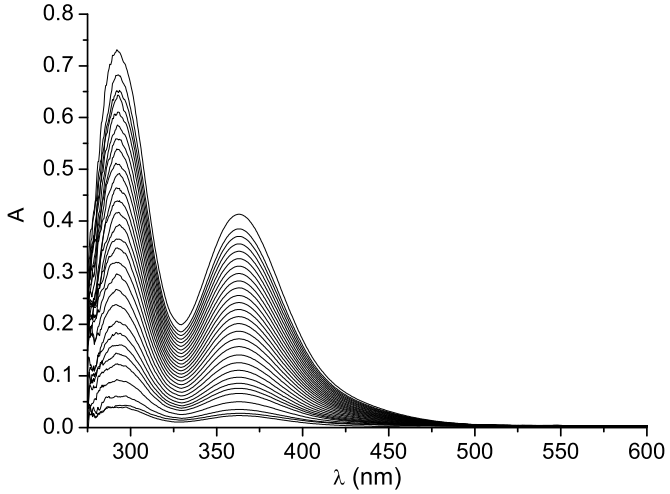

Figure 5.12: Time-dependent UV/Vis absorption spectra (every 2 min) observed upon introduction of O_2 gas into CH_2Cl_2 solution of [Cu((DMPip)DMG_2p)]I (0.15 mM, 25°C) during 60 min

5.2.4 UV/Vis-Spectroscopy of Cu_2O_2 species with the fluorinated bisguanidine ligand B^FPPG_2p

The shielding effect of relatively inert substituents at the guanidine centres can be combined with a smaller twist within the guanidine centre by using the fluorinated ligand B^FPPG_2p. The heptafluoropropyl chains are inert to hydroxylation and shield the Cu_2O_2 core against other decomposition reactions. The propylene backbone within the guanidine moiety tights the N_{amine} atoms together as can be seen in $DMPG_2$p and $DPPG_2$p. Both ligands support P-cores at low temperatures. By attaching long fluorinated groups to the guanidine moiety, the lifetime of the generated P-core species should be enhanced.

Figure 5.13 denotes the time-dependent absorption spectra observed during the reaction of [Cu(B^FPPG_2p)]I in dichloromethane with dioxygen at room temperature. The P-core is assigned by the characteristic absorption band at 358 nm ($\epsilon = 21400$ mol/(Lcm)), accompanied by a weak band at 600 nm($\epsilon = 540$ mol/(Lcm)). The inset shows that the band is relatively narrow and develops homogeneously. Figure 5.13 illustrates that the P-core species forms

very slowly in the time range of the O-core species of [Cu(B(TMPip)G_2p)]I. The brown-red solution of the generated P-core is stable for around four days. This stability is remarkable compared with the stabilities of complexes which have been reported in the literature by Kodera et al.[62] ($\tau_{1/2}$ = 25.5 h) and Gorun et al.[87]

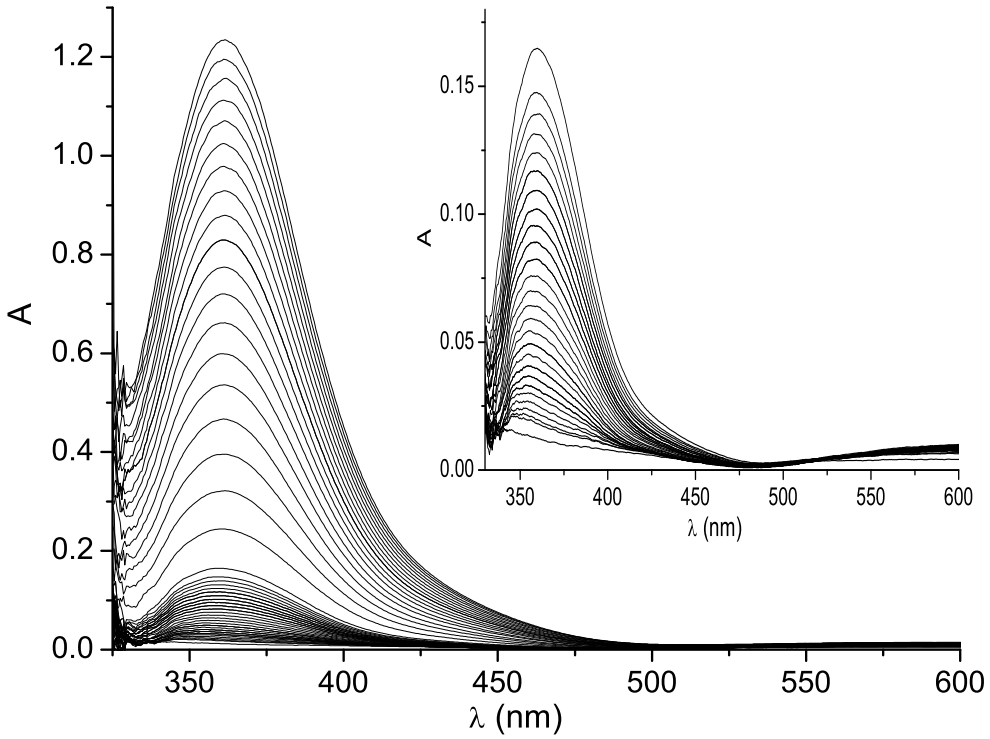

Figure 5.13: Time-dependent UV/Vis absorption spectra (every 20 min) observed upon introduction of O_2 gas into CH_2Cl_2 solution of [Cu(B^FPPG_2p)]I (0.35 mM, 25°C) during 400 min; inset: magnification of the first hour with spectra every 2 min during 60 min)

5.3 Interpretation of the results

5.3.1 Correlation of P/O-core development with structural properties

The above described results for the activation of dioxygen have to be correlated with structural properties of the investigated systems. Therefore, in Table 5.1, the dihedral angles between the CN_3-guanidine plane and the C_{imin}-N_{amin}-$(C_{alkyl})_2$-planes are set in connection with the capability of the Cu(I) compound of stabilising a P- or O-core complex.

Appearently, twisted systems like **C2**, **C3**, **C4** and **C9** with angles around 35° favour the stabilisation of an O-core complex, whereas "flat" systems with angles around 16° incorporated in **C5** and **C6** support P-core complexes. **C8** and **C13** have angles which are in the

Table 5.1: Correlation of the dihedral angles [°] between the CN_3-guanidine plane and the C_{imin}-N_{amin}-$(C_{alkyl})_2$-planes with the capability of stabilising a P or O-core

Complex	**Angle**	**P-core**	**O-core**
[Cu(DMorphG_2p)I] (**C2**)	33.3		x
[Cu_2(btmgp)$_2$][PF_6]$_2$ (**C3**)	34.1		x
[Cu_2(TMG_2ch)$_2$]I_2 (**C4**)	35.9		x
[Cu_2(DMEG$_2$p)$_2$][PF_6]$_2$ (**C5**)	17.4	x	
[Cu_2(DMEG$_2$ch)$_2$][Cu_2I_4] (**C6**)	15.9	x	
[Cu_2(DMPG$_2$p)$_2$][PF_6]$_2$ (**C8**)	24.8	x	x
[Cu_2(DPipG$_2$p$_2$)][PF_6]$_2$ (**C9**)	37.6		x
[Cu(DPPG$_2$p)]$_n$[CuI_2]$_n$ (**C13**)	28.5	x	

middle of this range with 24.8 and 28.5°, respectively. Hence, it can be understood why **C8** shows solvent-depending behaviour. The sensitive P/O-core equilibrium can be shifted at this point only by a change from a coordinating solvent to a non-coordinating one.

This correlation can be expanded by regarding the other systems for which no crystal data could be obtained. [Cu(TMG$_2$MePA)][X] (X = PF_6^-, ClO_4^-, BF_4^- and I^-) stabilises an O-core, perhaps because it incorporates a tetramethylguanidino unit. The TMG unit is generally twisted around 35° as further examples like [Mn(btmgp)Br_2] (34.2°)[143] and [Cu(btmgp)I] (35.7°)[112] show. [Cu_2(DMPG$_2$mX)$_2$]I_2 incorporating a DMPG unit which is twisted to a smaller degree stabilises a P-core. The sterically demanding systems [Cu(B(TMPip)G$_2$p)]I and [Cu((DMPip)DMG$_2$p)]I stabilise both an O-core. Since both systems contain substituents based on a twisted piperidino unit (vide supra, **C9**), this behaviour is in agreement with the other observations. The higher sterical demand results in an enhancement of the stability of the generated O-core. Even the fluorinated system [Cu(B^{F}PPG$_2$p)]I can be fitted into this correlation as the ligand B^{F}PPG$_2$p descends from its unfluorinated predecessor DPPG$_2$p (vide supra, **C13**). DPPG$_2$p supports a P-core at low temperatures, B^{F}PPG$_2$p does the same at room temperature. This may be due to a shielding effect of the inert fluorinated groups, but also to a sterical effect as these groups demand for more space than their unfluorinated analoga.

In summary, it can be recorded that the twist of the guanidine moiety determines the formation of P- or O-core and that the sterical demand tunes the stability of the generated core.

5.3.2 σ donor and π acceptor capabilities of the ligands

In order to explain the reaction behaviour of the copper(I) complexes with molecular oxygen, we have to look at the special coordination properties of the guanidine ligands described above. The dihedral angles within the guanidine moieties are decisive for the discussion of these coordination properties (vide supra). Depending on the residues attached to the guanidine systems, the resulting Cu_2O_2 species are either bis(μ-oxo)dicopper(III) or μ-η^2:η^2-peroxo dicopper(II) complexes or mixtures of both. The direction in which the equilibrium is driven depends on the degree of planarisation of the guanidine moieties. Within a guanidine residue, the observed structure is predominantly the result of an interplay of two major driving forces, one of them determined by electronic, the other one by steric interactions. Both types of interaction are competing against each other: as the π-orbitals of the peripheral $N_{amin}C_3$ portions search for reasonably good π interactions with the central CN_3 unit, this prerequisite demands for one common plane hosting all the involved C and N atoms. On the other hand, spatial demands of the substituents at the amin nitrogen atoms require propeller-like twists of the NC_3 portions around their N-C_{imine} bonds and thus prevent from a coplanar arrangement with the central CN_3 group. Furthermore, pyramidalisation tendencies of the peripheral $N_{amin}C_3$ portions can be observed which are amplified if both N atoms are part of a heterocyclic ring as realised in DMPG and in DMEG moieties. The degree of pyramidalisation depends on the steric strain in the heterocycle but has no influence on the coordination properties.

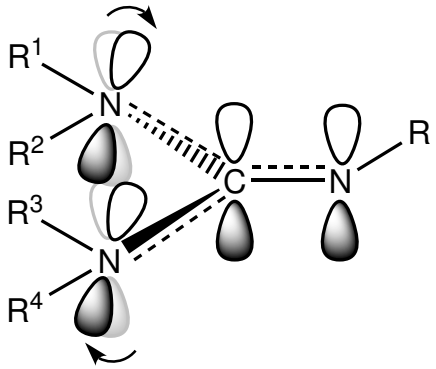

Figure 5.14: Competition of p-π conjugation and steric repulsion within the guanidine centre; arrows indicate twist from ideal conjugation (pale)

It turned out that the result of the interplay between electronic (p-π conjugation) and steric forces (repulsion of the substituents, Figure 5.14) is decisive for the equilibrium between the bis(μ-oxo)- and the μ-η^2:η^2-peroxo dicopper core. Small dihedral angles between adjacent $N_{amin}C_3$ and CN_3 units indicative for a good conjugation of the π orbitals in the guanidine moiety favour the μ-η^2:η^2-peroxo dicopper core whereas moderately larger ones induce a shift of the equilibrium towards the formation of the bis(μ-oxo)-dicopper state. The above reported dihedral angles are not a result of packing forces, but an inherent property of the

particular guanidine moiety as a large number of crystalline examples show: the TMG unit mostly exhibits dihedral angles of around 35° whereas the DMEG unit is almost "flat" with about 16°.[143] The DMPG unit has dihedral angles of 25°, the DPPG unit of 28° and the DPipG and DMorphG units of 37°. These values are averaged over crystal structures of the ligands and of the complexes with different coordination modes (linear, trigonal) as well as different counteranions which influence the packing.

A bonding description of the P-core was developed through a detailed correlation of spectral features, structural parameters and theoretical calculations by Solomon et al.[10, 144] Furthermore, it is reported that strictly σ-donating ligands should be better suited to stabilise O-core complexes whereas ligands with π-acceptor properties should favour the formation of their P-core counterparts.[45, 48] The key aspects of the theoretical description are reproduced in Figure 5.15. On the left hand side, the d^9 configuration of the two Cu(II) ions is

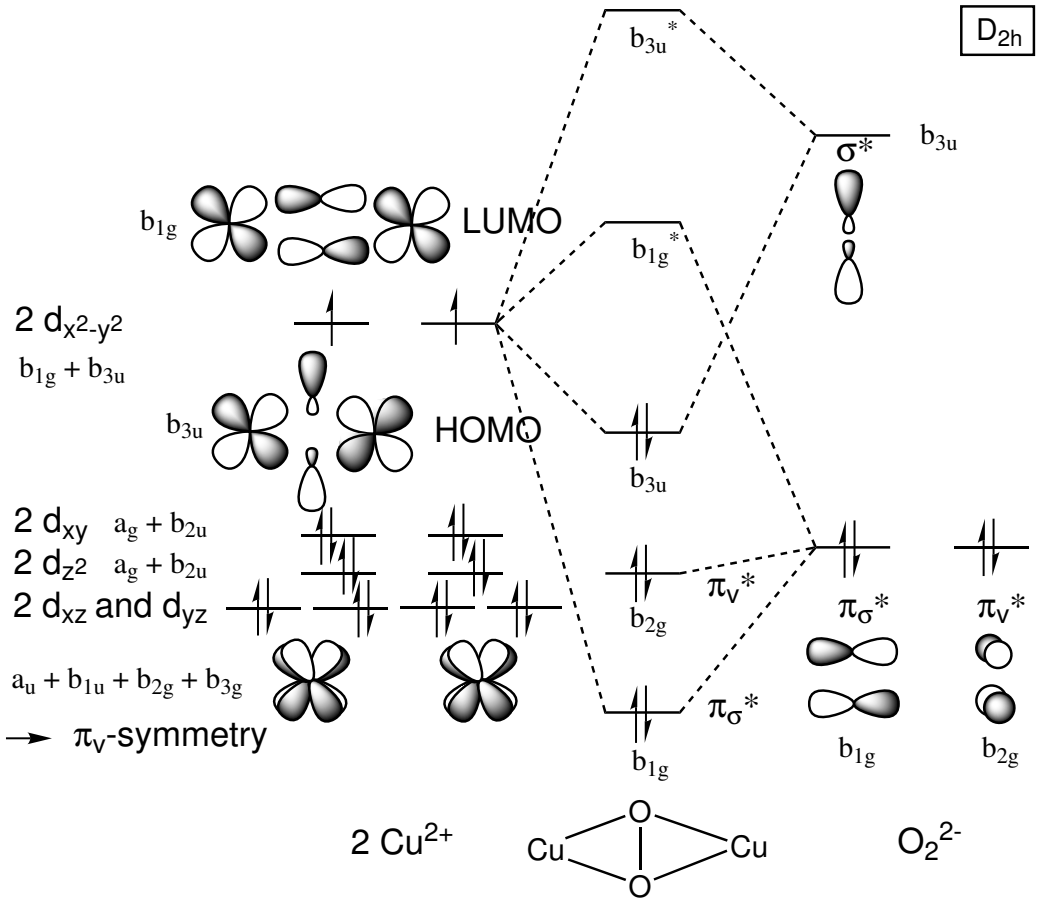

Figure 5.15: Partial molecular orbital diagram showing the frontier orbitals of the P-core, adapted from [35]

shown. The right hand side depicts the anti-bonding orbitals of the peroxide ion. Significantly, back-donation of electron density from the Cu(II) $d_{x^2-y^2}$ orbitals into the peroxide σ^* orbital in the HOMO rationalizes the weak O-O bond. Therefore, strong σ-donating ligands

transfer electron density via the Cu(II) $d_{x^2-y^2}$ orbitals into the peroxide σ^* orbital, so that the O-O-bond is disrupted reductively.

In Figure 5.16, the bonding situation comprising a bisguanidine ligand attached to the $Cu_2O_2^{2+}$ core portion is illustrated. In an attempt to elucidate the principal factors that

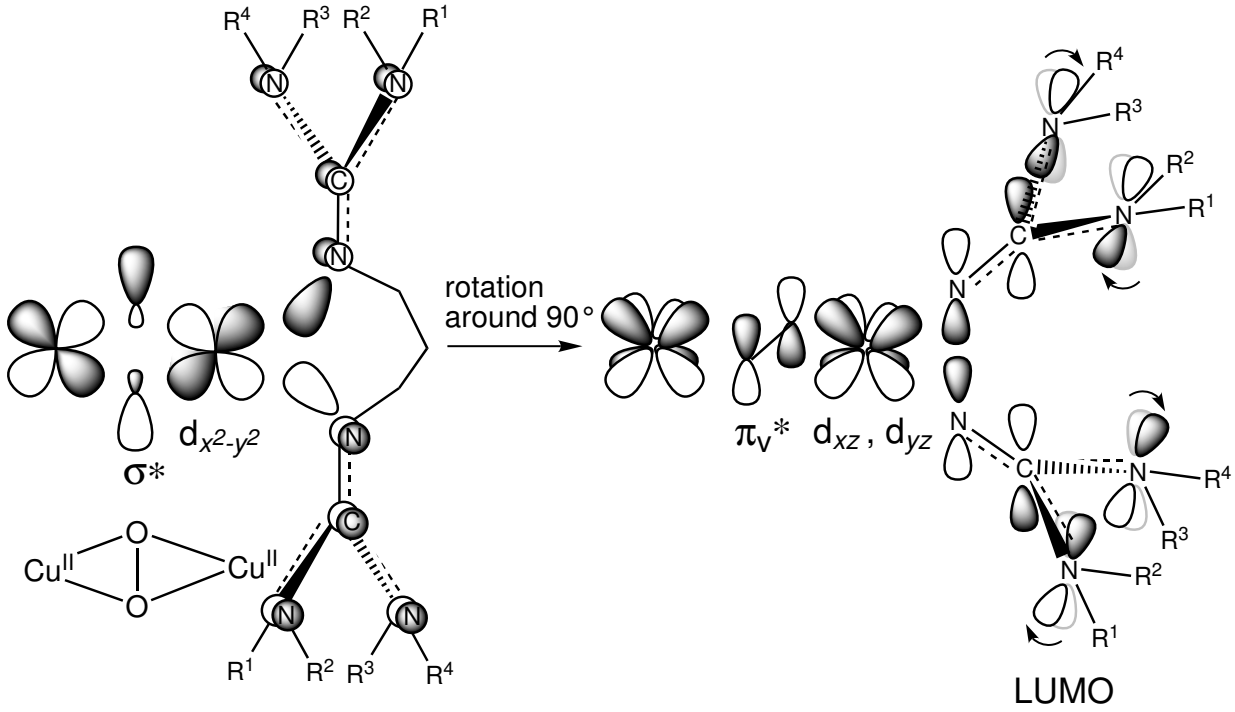

Figure 5.16: Bonding situation comprising a bisguanidine ligand attached to the $Cu_2O_2^{2+}$ core portion

control the P-core/O-core equilibrium, the degree of conjugation within the guanidine moiety is correlated with the reaction behaviour of the corresponding copper(I) complex towards oxygen. This correlation applies to bisguanidine ligands with propylene or cyclohexane backbones, respectively. In the σ-plane (Figure 5.16, left), the interaction of the σ-lobes of the coordinating imin nitrogen atoms with the Cu(II) $d_{x^2-y^2}$ orbital is denoted. Orthogonally to the σ-plane, the empty π^*-orbitals (Figure 5.16, right) of the guanidine moieties representing the LUMO possess the correct symmetry (b_{2g}) to accept electron density from the filled d_{xz} and d_{yz} orbitals of Cu(II). In the next step, electron density from the peroxide-π_v^*-orbital can now be transferred into the partially depleted d_{xz} and d_{yz} orbitals of Cu(II). In this stage, the degree of p-π conjugation within the guanidine system is of interest. Enhanced p-π overlap lowers the energy of the LUMO of the guanidine residue and makes it more accessible for π back-donation. In consequence, small modifications of the ligand geometries changing the guanidine conjugation are suited to influence the equilibrium between P- and O-core complex states. In the DMPG and DMEG moieties, the alkylene linkers tight the

amin nitrogen atoms together and the averaged guanidine dihedral angles are very small (vide supra). The guanidine conjugation is thus enhanced. Contrarily, in btmgp, DPipG$_2$p and DMorphG$_2$p the NR_2 moieties are twisted around their N_{amine}-C_{imine} bonds, and the guanidine conjugation is hindered. For that reason, the LUMO is raised in energy, and back-donation is diminished. Now, the σ^*-donating effect of the imin nitrogen atoms dominates the coordination and the O-core is stabilised.

5.4 Kinetics of the activation of dioxygen

5.4.1 Kinetics of copper/dioxygen chemistry

Kinetic measurements are of great importance for the understanding of the formation of Cu_2O_2 species. They provide information about kinetic-thermodynamic parameters, reaction mechanisms and reactive intermediates which might be observable on a faster time-scale (i.e., milliseconds, for stopped-flow experiments).

The kinetics of copper/dioxygen chemistry have been thoroughly investigated by Karlin and Zuberbühler.[85, 145] A suited method uses the time-dependent course of the absorbance of an characteristic absorption band to follow the reaction. Basis for closer examination is the well-known law of Lambert and Beer ($A = \epsilon \cdot c \cdot d$) with the absorption A, the extinction coefficient ϵ and the layer thickness d.

To facilitate the considerations, a first-order reaction is regarded as example. Indeed, Itoh et al. reported for the reaction of several copper systems with O_2 first-order rate laws because the primary uptake of O_2 under formation of a mononuclear copper/O_2 species can be rate-determining (Figure 5.17, process A).[86] According to this figure, dioxygen initially binds

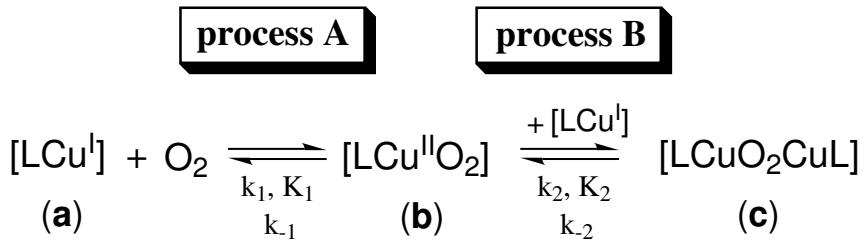

Figure 5.17: General mechanism of dioxygen-uptake by Cu(I) complexes

to a Cu(I) centre to form a 1:1 adduct (process A). This adduct usually, but not always, reacts with a second Cu(I) complex to form one or more dinuclear Cu_2O_2 species (process B). Further reaction with [LCu(I)] can occur to give tri- or tetranuclear adducts. While this

general picture encompasses the oxygenation pathways observed to date, differences in details are often significant, and reflect important influences of supporting ligand structure on the O_2 activation mechanism. For the assumption of a first-order rate law, the consideration has to start with a second order rate-law for the general case (eq. 5.1).

$$\frac{d\,[c_{Cu}]}{dt} = -k \cdot [c_{Cu}] \cdot [c_{O_2}] \tag{5.1}$$

$[c_{Cu}]$ = concentration of the copper(I) complex

$[c_{O_2}]$ = concentration of the oxygen

As oxygen is given in excess, $[c_{O_2}]$ is a constant which gives the following kinetic equation:

$$\frac{d\,[c_{Cu}]}{dt} = -k^* \cdot [c_{Cu}] \tag{5.2}$$

with $k^* = k \cdot [c_{O_2}]$.

This pseudo-first-order kinetic can be integrated as follows:

$$\int_{c_{Cu}}^{c} \frac{1}{[c_{Cu}]} \cdot d\,[c_{Cu}] = -k^* \cdot \int_0^t dt \tag{5.3}$$

$$\ln \frac{[c_{Cu}]}{[c_{Cu}]_0} = -k^* \cdot t \tag{5.4}$$

Regarding that $[c_{Cu}]_0 = [c_{Cu}]_t + [c_{Cu_2O_2}]_t = [c_{Cu_2O_2}]_\infty$ with $[c_{Cu_2O_2}]_t$ as concentration of the Cu_2O_2 species at the time t and $[c_{Cu_2O_2}]_\infty$ as concentration of the Cu_2O_2 species at $t \to \infty$, equation 5.5 can be derived:

$$\frac{[c_{Cu_2O_2}]}{[c_{Cu_2O_2}]_0} = \frac{[c_{Cu_2O_2}]_\infty - [c_{Cu_2O_2}]_t}{[c_{Cu_2O_2}]_\infty} \tag{5.5}$$

Applying Lambert-Beer´s law gives

$$A_0 = \epsilon_c \cdot [c_{Cu}]_0 \cdot d \tag{5.6}$$

$$A_\infty = \epsilon_{Cu_2O_2} \cdot [c_{Cu_2O_2}]_\infty \cdot d \tag{5.7}$$

$$A_t = \epsilon_c \cdot [c_{Cu}]_t \cdot d + \epsilon_{Cu_2O_2} \cdot [c_{Cu_2O_2}]_t \cdot d \tag{5.8}$$

With A_0 as absorbance for $t = 0$, A_∞ as absorbance for $t \to \infty$ and A_t as absorbance for the moment t, the algebraic combination of the equations 5.5 - 5.8 leads to equation 5.9.

$$\frac{[c_{Cu}]}{[c_{Cu}]_0} = \frac{[c_{Cu_2O_2}]_\infty - [c_{Cu_2O_2}]_t}{[c_{Cu_2O_2}]_\infty} = \frac{A_\infty - A_t}{A_\infty - A_0} \tag{5.9}$$

Combined with eq. 5.1, we obtain eq. 5.10:

$$\ln \frac{A_\infty - A_t}{A_\infty - A_0} = -k^* \cdot t \tag{5.10}$$

Eq. 5.10 corresponds a linear function:

$$\ln(A_\infty - A_t) = -k^* \cdot t + \ln(A_\infty - A_0) \tag{5.11}$$

with the abscissa $\ln(A_\infty - A_0)$. The plot of $\ln(A_\infty - A_t)$ versus the time t gives a linear plot which is also referred to as first-order plot.[146]

5.4.2 Kinetic results of the reaction of dinuclear copper complexes with O_2

The increase of the absorbance of the corresponding absorption bands during the reaction of **C3**, **C8** and **C9** with dioxygen in excess obeys first-order kinetics (Figure 5.18).

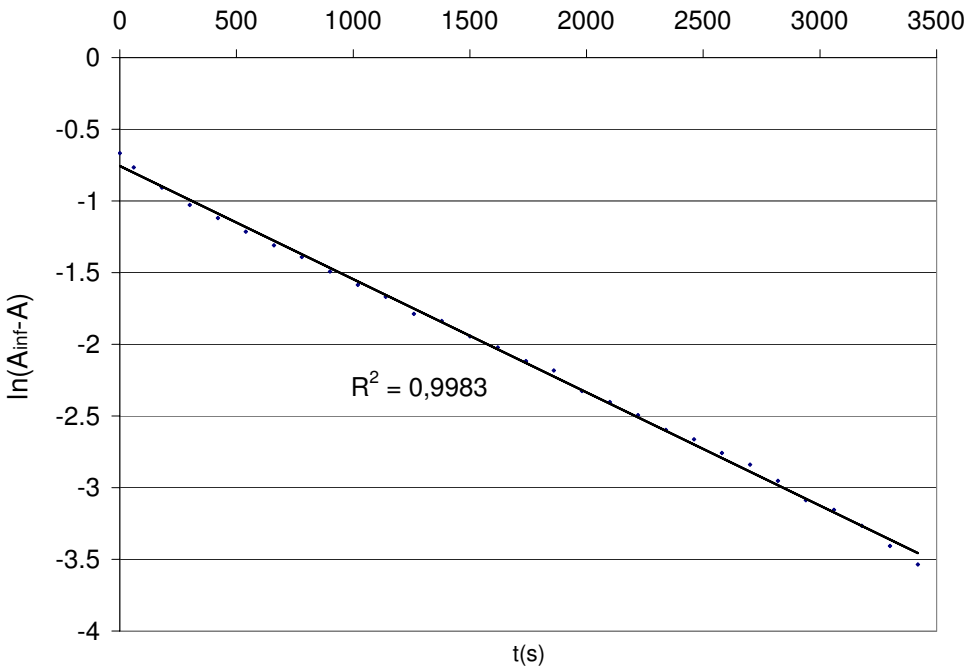

Figure 5.18: First-order plot based on the absorption change at 350 nm (P-core) for the reaction of **C8** at -80 °C with O_2

Moreover, the same first-order rate constants were obtained for reactions starting from different concentrations of **C8** in CH_2Cl_2. This observation indicates that the reaction of the copper(I) complexes with dioxygen is first-order with respect to the copper complex but of the order 0 with respect to O_2 if it is used in excess. The activation parameters ($\Delta H^\ddagger$ and $\Delta S^\ddagger$) for the formation of the O-core complexes of **C3** and **C9** and the P-core complex of **C8** have been determined from the temperature dependence of k (-40 to -80 °C). The Eyring plots for the reaction of **C3**, **C8** and **C9** with O_2 are depicted in the Figures 5.19 - 5.21.

The first-order rate constants (k) determined at -80 °C and the activation parameters for the formation of the copper-dioxygen species are summarised in Table 5.2. The kinetic data given below are in accordance with comparable systems reported in the literature which exhibit small activation enthalpies and very negative activation entropies.[86, 147] A small activation enthalpy is indicative for the high driving force for the reaction of a copper(I) complex with dioxgen whereas a negative activation entropy is the result of a reaction where two molecules are combined to form a new one.

Table 5.2: Kinetic data for the formation of copper-dioxygen species (first order kinetics)[28b]

Compound	$\mathbf{k_1[s^{-1}]}$	$\mathbf{\Delta H^{\ddagger}[kJ/mol]}$	$\mathbf{\Delta S^{\ddagger}[J/(mol*K)]}$
$[Cu_2(btmgp)_2][PF_6]_2$ (**C3**)	$1.6(1)*10^{-1}$	9(1)	-210(5)
$[Cu_2(DMPG_2p)_2][PF_6]_2$ (**C8**)	$7.9(3)*10^{-4}$	12(1)	-230(2)
$[Cu_2(DPipG_2p)_2][PF_6]_2$ (**C9**)	$6.3(3)*10^{-5}$	42(1)	-104(3)

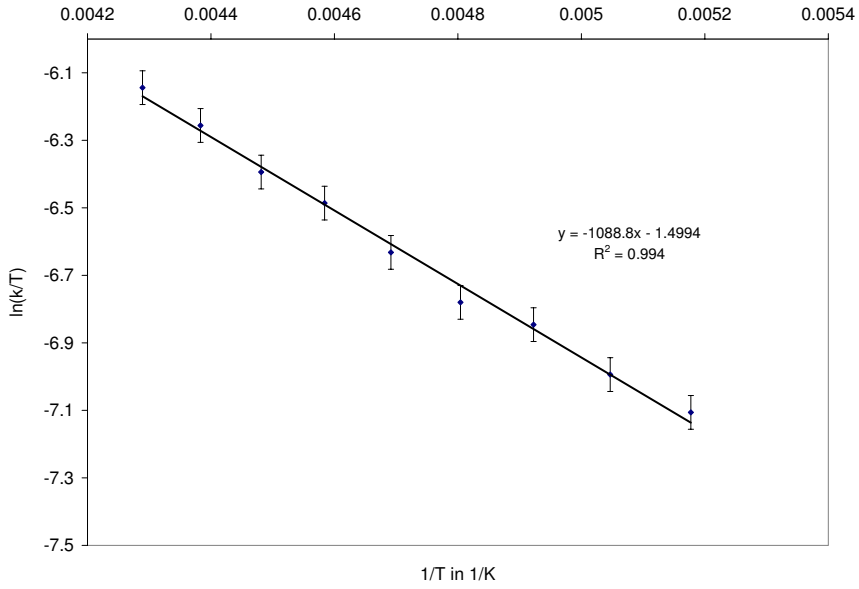

Figure 5.19: Eyring plot for **C3**

In comparison with **C3** and **C8**, complex **C9** shows a higher activation enthalpy and a smaller negative activation entropy which can be traced back to the steric demands of the piperidyl units.

The observed reaction with molecular oxygen has to be associated with a rearrangement of the bisguanidine ligands because the target area of this reaction is affected by significant H...H interactions between protons belonging to adjacent propylene spacers. This interaction has been discussed in section 4.3. The corresponding ligand conformation represents the maximum stretch of the propylene spacer which leads to a maximum intraligand N...N

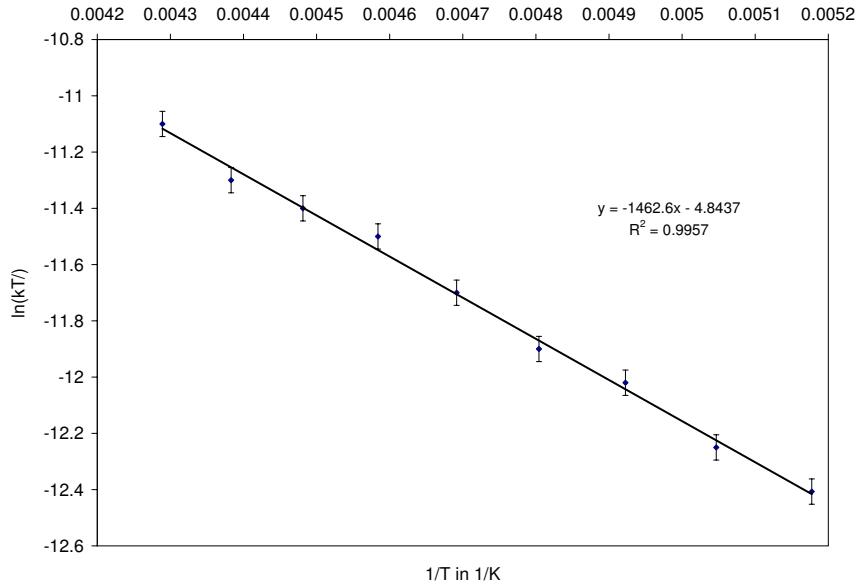

Figure 5.20: Eyring plot for **C8**

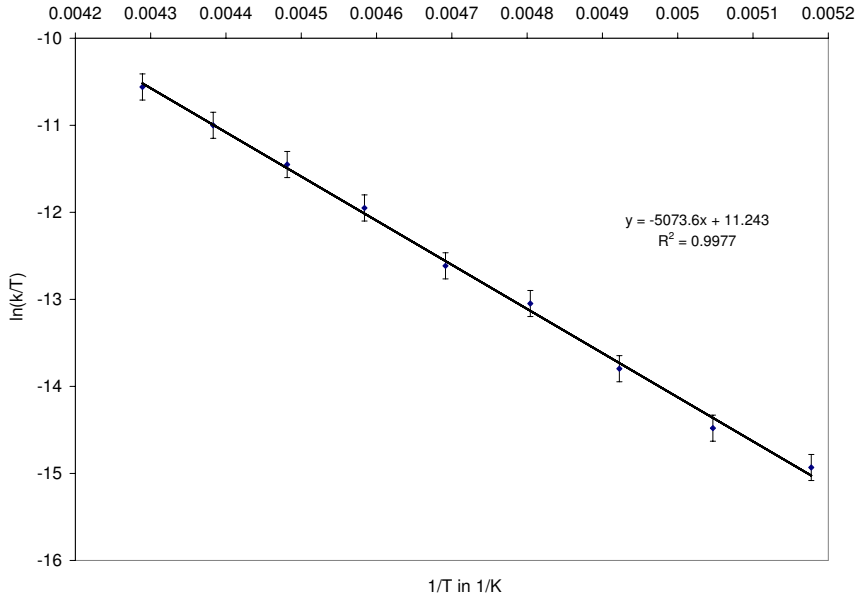

Figure 5.21: Eyring plot for **C9**

separation of 5.034(1) Å(**C6**). On going to shorter N...N separations as realized in the complex cations of **C3**, **C5**, **C7**, **C8** and **C9**, the propylene chain folds up allowing for longer H...H contacts as can be seen from Table 4.3 and Figures 4.10 - 4.13. This would principally facilitate potential oxygen insertion but is in contradiction with the requirements of a resulting $N_2Cu_2O_2N_2$ moiety demanding for intraligand N...N distances which are at least 5.5 Å in lengths. Thus, the situation under discussion does not allow any insertion of oxygen into this region without rearrangement of the ligands.

Based on the kinetic data, the following mechanism for the reaction with molecular oxygen can be proposed (Figure 5.22): the Cu(I) precursor complex **a** reacts in a sequence of first-order reactions with an excess of dioxygen to the P-core complex. The oxygen uptake within

step **A** is rate-determining. In the cases of **C3** and **C9**, the P-core complexes are less stable than their O-core counterparts, so that the reaction proceeds immediately via step **B**. In the case of **C8**, the P-core complex is more stable, and its formation was investigated kinetically. Reaction step **A** also includes the rearrangement of the bisguanidine moities from non-chelating ligands into chelating ones. The corresponding reaction path is currently under investigation.

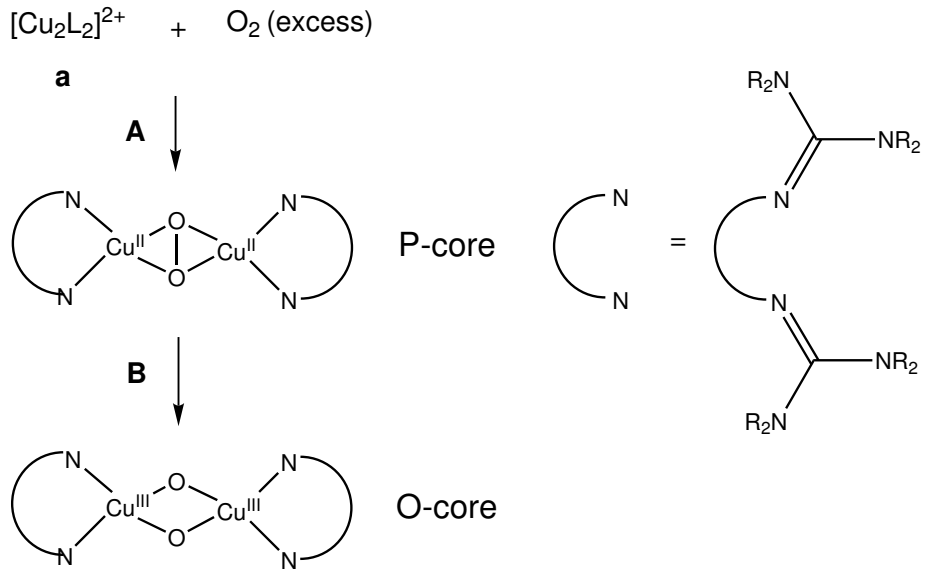

Figure 5.22: Proposed mechanism of the reaction of dinuclear copper complexes with O_2

5.4.3 Kinetic results of the reaction of the mononuclear copper complex [Cu(btmgp)I] with O_2

As described in the previous section, dinuclear copper(I) complexes are predefined for the uptake of O_2 in a first-order reaction because two copper centres are already close to each other. For a mononuclear copper(I) complex, the situation becomes more complicated as the different reaction rates for the oxygenation of the mononuclear precursor (process A) and the addition of a further precursor molecule (process B) have to be taken into account (see Figure 5.17). Both processes can be rate-determining. Additionally, in several cases, these processes were found to be reversible, a fact which complicates the rate equations considerably.

The increase of the absorbance of the corresponding absorption bands during the reaction of [Cu(btmgp)I] with O_2 in excess could not be fitted after a simple first- or second-order rate law. Hence, the fitting had to take all reaction steps into consideration. The fact that

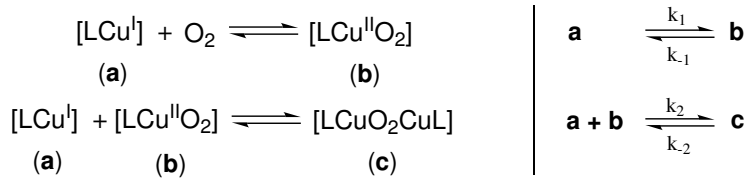

Figure 5.23: Schematic kinetics of dioxygen-uptake by Cu(I) complexes

oxygen is given in excess facilitates the equations to a lesser extent. Finally, the fitting had to be performed by numerical analysis of the equation system by MATLAB 6.5. In Figure 5.23, the reaction of a mononuclear Cu(I) complex with O_2 is schematically denoted. From this scheme, the rate equations for the reversible case are derived as listed in the following passage.

$$\frac{dc_a}{dt} = -k_1 \cdot c_a + k_{-1} \cdot c_b - k_2 \cdot c_a \cdot c_b + k_{-2} \cdot c_c \tag{5.12}$$

$$\frac{dc_b}{dt} = k_1 \cdot c_a - k_{-1} \cdot c_b - k_2 \cdot c_a \cdot c_b + k_{-2} \cdot c_c \tag{5.13}$$

$$\frac{dc_c}{dt} = k_2 \cdot c_a \cdot c_b - k_{-2} \cdot c_c \tag{5.14}$$

The numerical fitting by MATLAB 6.5 was not successful with this equation system. It appeared to exist a concurrence reaction which consumes species **b** to give more **c** than expected. Consequently, the mechanism had to be corrected in order to take these findings into account. The following hypothetical mechanism was proposed (Figure 5.24). The concurrence reaction is supposed to be the reaction of two intermediate Cu-O_2 adducts **b** forming the O-core species **c** as well, but under additional consumption of **b** and release of O_2. This release of O_2 has no consequences for the kinetic equations since oxygen is given in excess anyway. It turned out that the fitting with the following corrected rate equations (5.15 - 5.17) was better.

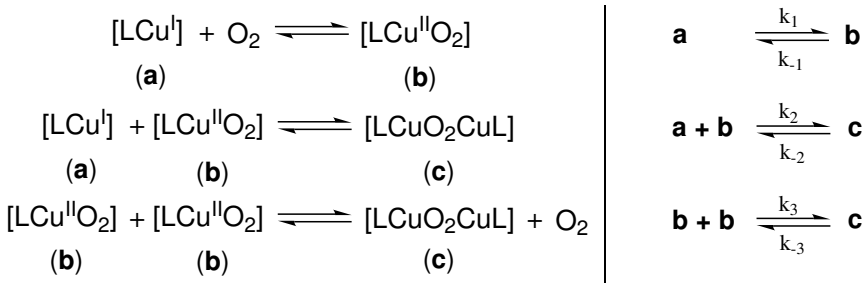

Figure 5.24: Hypothetical mechanism for the reaction of [Cu(btmgp)I] with O_2 as model for the numerical fit (left: chemical description, right: kinetical description)

$$\frac{dc_a}{dt} = -k_1 \cdot c_a + k_{-1} \cdot c_b - k_2 \cdot c_a \cdot c_b + k_{-2} \cdot c_c \quad (5.15)$$

$$\frac{dc_b}{dt} = k_1 \cdot c_a - k_{-1} \cdot c_b - k_2 \cdot c_a \cdot c_b + k_{-2} \cdot c_c - k_3 \cdot c_b^2 + k_{-3} \cdot c_c \quad (5.16)$$

$$\frac{dc_c}{dt} = k_2 \cdot c_a \cdot c_b - k_{-2} \cdot c_c + k_3 \cdot c_b^2 - k_{-3} \cdot c_c \quad (5.17)$$

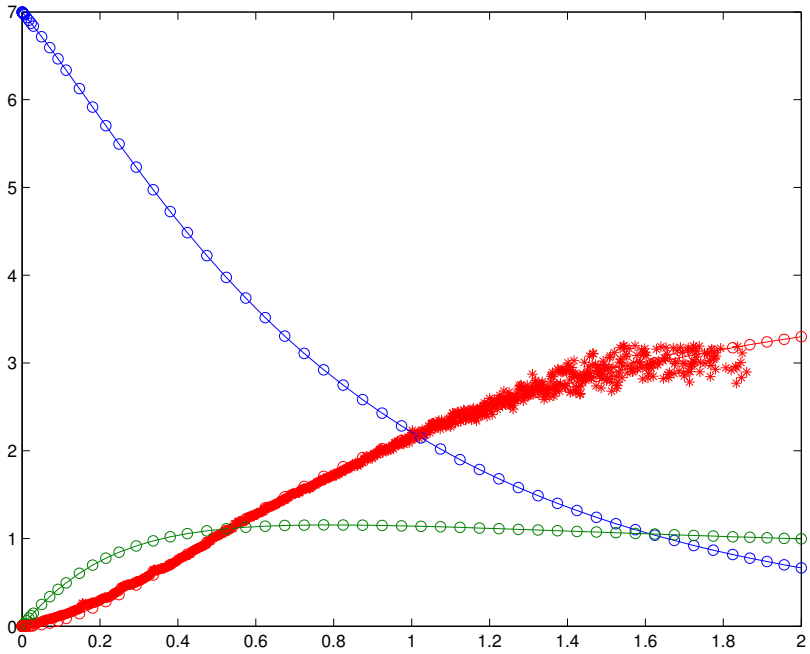

Figure 5.25: Fitting of the absorbance of the reaction of [Cu(btmgp)I] with O_2 by MATLAB 6.5 (blue: calc. concentration of the precursor **a**, green: calc. concentration of the intermediate Cu-O_2 adduct **b**, red: calc. and measured concentration of the O-core species **c**)

As k_{-1}, k_{-2} and k_{-3} were calculated to be zero, all three reactions are irreversible. A summary of the calculated kinetical data is given in Table 5.3. The small values for the activation enthalpies and the large negative activation entropies fall in line with values reported by Karlin et al.[145] All these reactions are entropy-driven because one molecule is generated from two precursors. The activation enthalpy for reaction **3** is smaller than for **2** which results in a preference for reaction pathway **2** at higher temperatures. Interestingly, the differences between the two solvents are not really significant, although an influence of the solvent was expected.[85]

In conclusion, it has to be recorded that dinuclear and mononuclear Cu(I) complexes behave with respect to their kinetics totally different in the Cu-O_2 adduct formation which is in accordance with the literature.[85, 86] The dinuclear precursors, possessing a predefined reaction site for the oxygen-uptake, react in a first-order reaction whereas the mononuclear precursors react via a more complex pathway.

Table 5.3: Kinetic data for the reaction of [Cu(btmgp)I] with O_2, k at 193 K

Solvent	CH_2Cl_2	THF
$k_1[s^{-1}]$	50(1)	53(1)
$\Delta H_1^{\ddagger}$[kJ mol^{-1}]	7(1)	2(1)
$\Delta S_1^{\ddagger}$[J mol^{-1}K^{-1})]	-170(7)	-210(8)
$k_2[M^{-1}s^{-1}]$	6.4(1)*10^4	8.3(1)*10^3
$\Delta H_2^{\ddagger}$[kJ mol^{-1}]	5(1)	11(1)
$\Delta S_2^{\ddagger}$[J mol^{-1}K^{-1})]	-240(8)	-140(5)
$k_3[M^{-1}s^{-1}]$	7.6(1)*10^4	5.6(1)*10^4
$\Delta H_3^{\ddagger}$[kJ mol^{-1}]	2(1)	1(1)
$\Delta S_3^{\ddagger}$[J mol^{-1}K^{-1})]	-130(6)	-180(7)

5.5 Conclusion of the O_2 Activation with Copper(I) Bisguanidine Complexes

Due to their ability to delocalise the positive charge over the guanidine moiety, these ligands are able to stabilise high metal oxidation states which are established in a variety of copper complexes containing the $Cu_2O_2^{2+}$ core portion. The analysis of the bonding situation comprising this site attached to a bisguanidine residue reveals that the coordination properties of the imine nitrogen donor atoms depend on the substitution pattern within the guanidine moieties. Thus, it is possible to influence directly the reactivity of the copper(I) bisguanidine complexes towards molecular oxygen by introducing properly designed substituents. Sterically demanding alkyl groups raise the energy of the LUMO which has the appropriate symmetry to accept electrons from the $Cu_2O_2^{2+}$ core portion and thus destabilise the P-core state within these complexes. On the other hand, integrating both amine groups of a guanidine residue into a five- or six-membered ring favours the P-core over the O-core state by strengthening the π-conjugation within the ligand and thus lowering the energy of the LUMO. Based on these interrelations between steric features of the ligands and the electron distribution within the $Cu_2O_2^{2+}$ core portions of dinuclear Cu_2O_2 complexes, new insights into the mechanism of dioxygen activation are provided and strategies towards ligand modification can be developed which are directed towards tailored reaction systems capable to hydroxylate substrates in pre-defined positions.

6 Products of hydroxylation reactions

6.1 Hydroxylation of copper btmgp complexes

6.1.1 Crystal structures of btmgp containing hydroxylation products

The reaction of both precursor complexes [Cu(btmgp)I] and $[Cu_2(btmgp)_2][PF_6]_2$ (**C3**) with dioxygen (Scheme 6.1) was investigated by low temperature UV/Vis monitoring (section 5.1).

The primarily formed species are bis-μ-oxodicopper(III) complexes containing the Cu_2O_2 core with fully reduced oxygen and copper in the oxidation state +3 in both cases. Crystals obtained from these reactions in form of red needles were not suited for X-ray diffraction. Upon reaction of [Cu(btmgp)I] and **C3** with O_2, intensive LMCT absorption bands at 300 and 400 nm are observed which are characteristic for the O-core complexes known so far. These species are unstable even at -80 °C in dichloromethane. The initial red solutions change their colours to bluish-green upon warming up to room temperature within 1 - 2 h. This behaviour was described by Schneider for the first time for bisguanidine copper complexes.[112] From these solutions, two different complex types could be isolated in equal amounts (vide infra): the reaction of precursor [Cu(btmgp)I] with oxygen yields the novel bis(μ-alkoxo)(μ-iodo)-bridged dinuclear copper complex $[Cu_2(btmmO)_2I]^+$ containing an iodide ion in a novel bridging situation as well as the hydroxo-bridged dinuclear copper complex $[Cu_2(btmgp)_2(\mu\text{-}OH)_2]^{2+}$. In a similar manner, precursor **C3** reacts to the bis(μ-alkoxo)-bridged dinuclear copper complex $[Cu_2(btmmO)_2]^{2+}$ (**C15**) and the hydroxo-bridged dinuclear copper complex $[Cu_2(btmgp)_2(\mu\text{-}OH)_2]^{2+}$.[113]

The complex cation $[Cu_2(btmmO)_2I]^+$ which occurs in crystals of $[Cu_2(btmmO)_2I]I\cdot\frac{1}{2}EtOH$ is formed in the reaction of [Cu(btmgp)I] with oxygen; its unexpected properties derive from the coordination by two N donor functions, two bridging oxygen atoms from the hydroxylated ligands and the presence of an iodide ion as a third bridge (Figure 6.2). Selected distances and angles of $[Cu_2(btmmO)_2I]^+$ are listed in Table 6.1.[112]

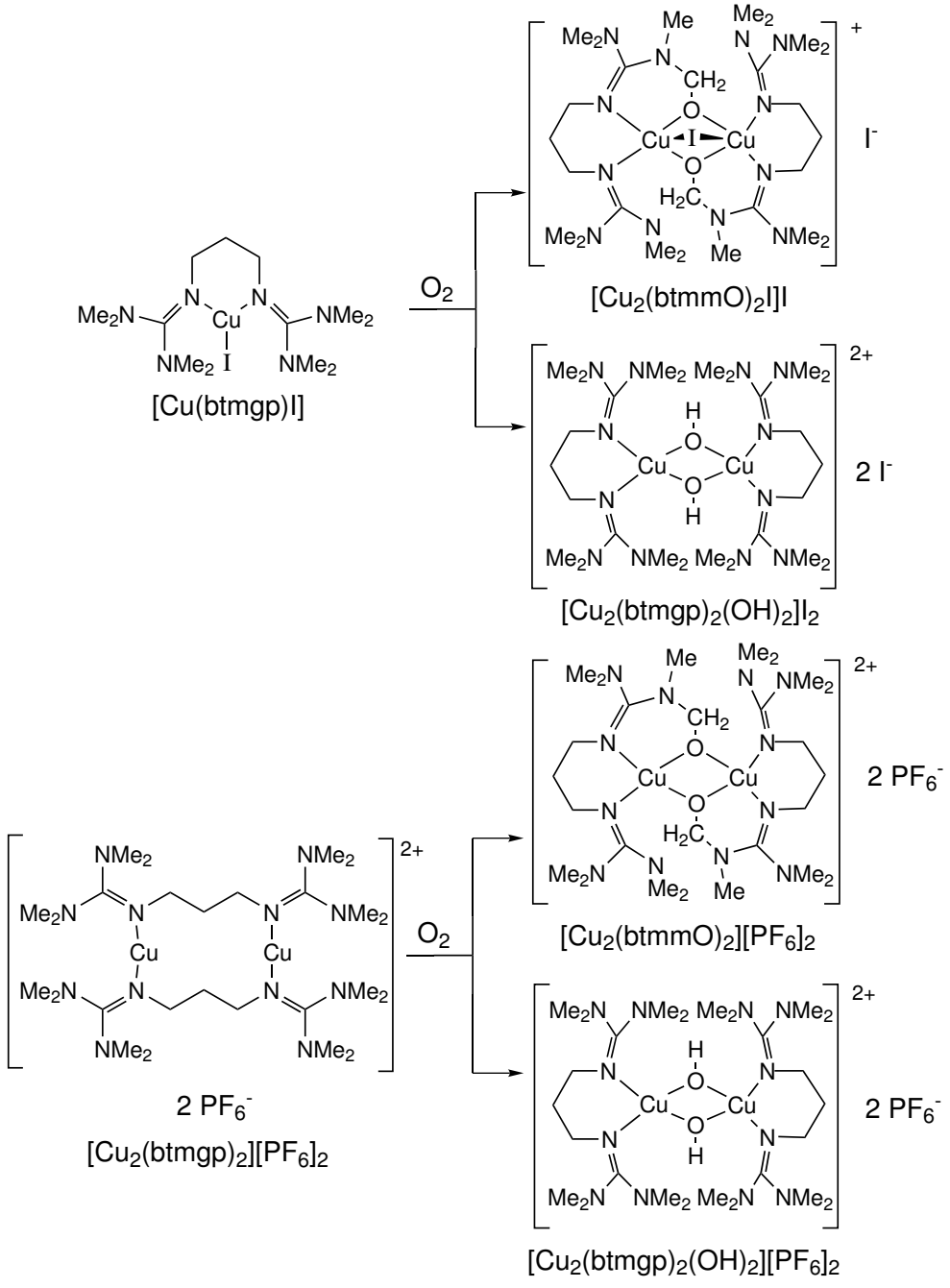

Figure 6.1: Activation of oxygen with [Cu(btmgp)I] and $[Cu_2(btmgp)_2][PF_6]_2$

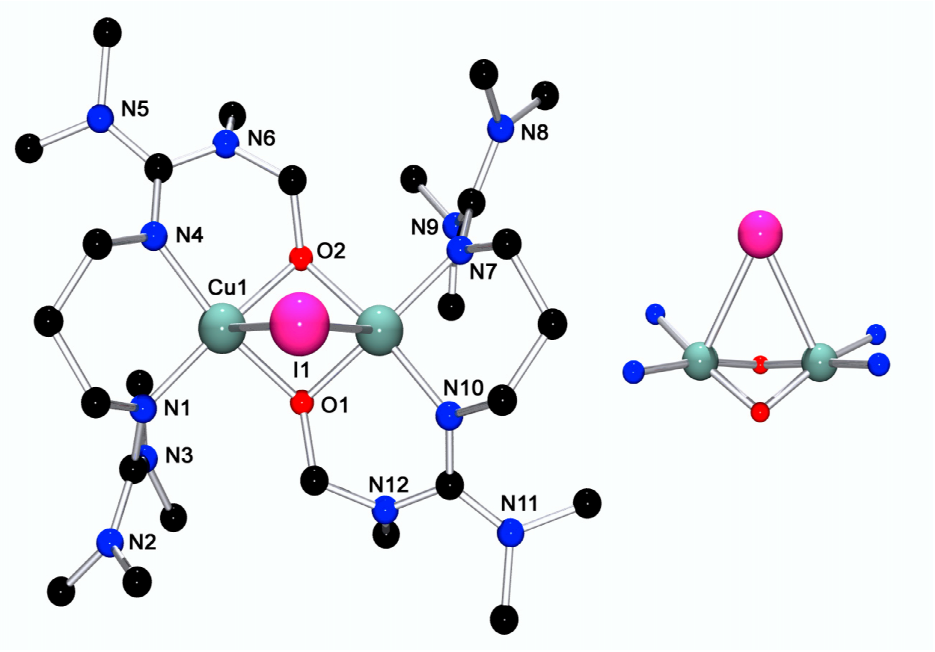

Figure 6.2: Molecular structure of $[Cu_2(btmmO)_2I]^+$ in crystals of $[Cu_2(btmmO)_2I]I\cdot\frac{1}{2}EtOH$ (left), magnification of the μ-iodo bridged Cu_2O_2 unit [112]

The other component has been shown by X-ray diffraction and vibrational spectroscopy to represent the bis(μ-hydroxo)-dicopper(II) species $[Cu_2(btmgp)_2(OH)_2]^{2+}$ (see Fig. 6.4) which occurs in crystals of $[Cu_2(btmgp)_2(OH)_2]I_2$ (**C15**).

The bis(μ-hydroxo)-dicopper(II) species is also formed if **C3** is used as the precursor complex instead of [Cu(btmgp)I]. In this case, however, the complex salt $[Cu_2(btmgp)_2(OH)_2][PF_6]_2$ has been isolated. Moreover, as a non-coordinating counteranion has been used, the bis(μ-alkoxo)-dicopper(II) species $[Cu_2(btmmO)_2]^{2+}$ obtained as the other reaction product and identified in crystals of $[Cu_2(btmmO)_2][PF_6]_2\cdot 2MeCN$ (**C15**) lacks the iodide bridge present in $[Cu_2(btmmO)_2I]^+$ (Fig. 6.3).

The reaction of [Cu(btmgp)I] and $[Cu_2(btmgp)_2][PF_6]_2$ (**C3**) with molecular oxygen transforms one half of the coordinated bis(tetramethyl)guanidinopropane molecules into bis(trimethylmethoxy)guanidino-propane ligands which have been identified as the alkoxo components within the bis(μ-alkoxo)dicopper(II) complexes $[Cu_2(btmmO)_2I]I\cdot\frac{1}{2}EtOH$ and $[Cu_2(btmmO)_2][PF_6]_2\cdot 2MeCN$ (**C15**) (Figures 6.2 and 6.3). This oxidation reaction deserves attention due to the fact that no other tool capable to introduce one single -CH_2OH functionality into bis(tetramethyl)guanidinopropane is known so far.

Selected distances and angles of the crystal structure of **C15** are listed in Table 6.2, and parameters relating to the data collection and refinement are listed in Table A11. Both complex cations $[Cu_2(btmmO)_2I]^+$ and $[Cu_2(btmmO)_2]^{2+}$ shown in Figs. 6.2 and 6.3, respectively, contain the $Cu_2(btmmO)_2$ entity; they differ, however, with respect to their bridging states.

Table 6.1: Selected distances and angles of $[Cu_2(btmmO)_2I]^+$ [112]

Distances (Å)		**Angles (°)**	
Cu(1)...Cu(2)	2.8026(7)	O(1)-Cu(1)-O(2)	77.67(9)
Cu(1)-O(1)	1.972(2)	O(1)-Cu(2)-O(2)	76.99(9)
Cu(1)-O(2)	1.944(2)	Cu(1)-O(1)-Cu(2)	91.10(9)
Cu(2)-O(1)	1.953(2)	Cu(1)-O(2)-Cu(2)	90.78(9)
Cu(2)-O(2)	1.992(2)	N(1)-Cu(1)-N(4)	91.3(1)
Cu(1)-N(1)	1.973(3)	N(7)-Cu(2)-N(10)	93.2(1)
Cu(1)-N(4)	1.968(3)		
Cu(2)-N(7)	1.961(3)		
Cu(2)-N(10)	2.002(2)		

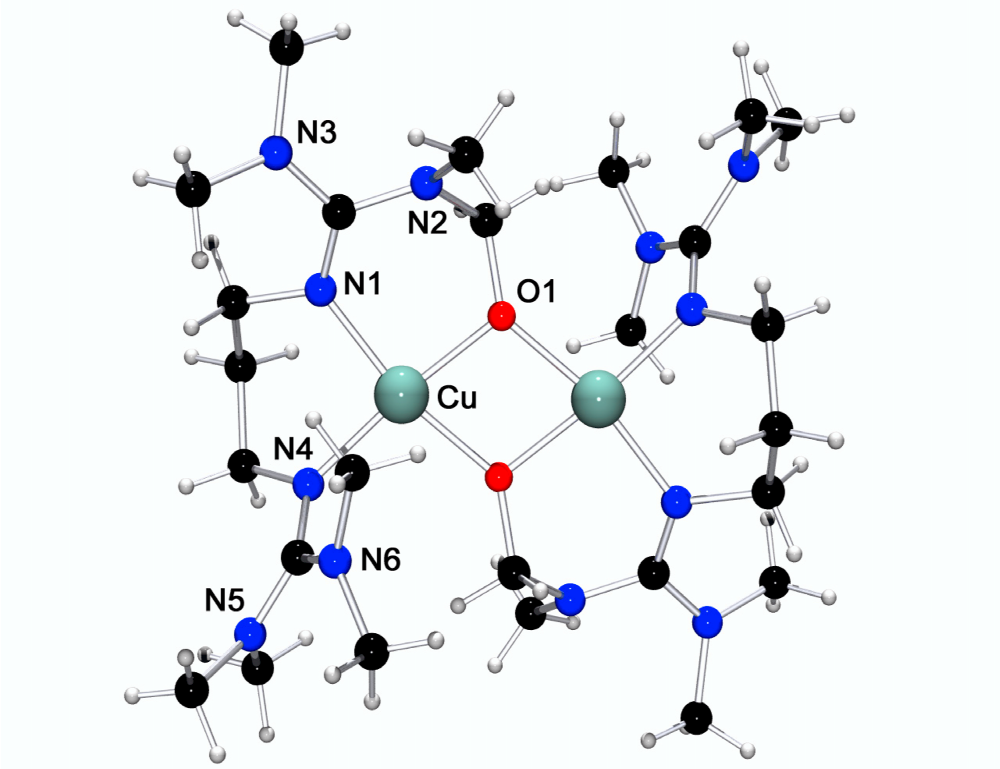

Figure 6.3: Molecular structure of $[Cu_2(btmmO)_2]^{2+}$ in crystals of **C15**

The complex cation $[Cu_2(btmmO)_2I]^+$ is an extension of the complex cation in **C15** and can be derived thereof by introducing an iodide ligand as a third bridge. This modification results into a fold of the Cu_2O_2 heterocyclic unit along the O...O vector allowing the Cu atoms to approach the iodide ligand at distances of 3.237 Å (Fig. 6.2, right). The resulting Cu...Cu distance is as short as 2.803(1) Å, and the dihedral angle within the butterfly-shaped Cu_2O_2 core portion is 131.8(1)°.

In crystals of $[Cu_2(btmmO)_2I]I{\cdot}\frac{1}{2}EtOH$, each copper atom is surrounded by its ligands in

Table 6.2: Selected distances and angles of $[Cu_2(btmmO)_2]_2^{2+}$ in crystals of **C15** (The primed atoms are derived from the unprimed ones by inversion.)

Distances (Å)		**Angles (°)**	
Cu...Cu	3.035(1)	O(1)-Cu(1)-O(1')	75.65(8)
Cu(1)-O(1)	1.910(2)	Cu(1)-O(1)-Cu(1')	104.35(8)
Cu1-O(1')	1.932(2)	N(1)-Cu(1)-N(4)	93.34(9)
Cu(1)-N(1)	1.961(2)		
Cu(1)-N(4)	1.961(2)		

a square-pyramidal manner resulting in the blue colour of the compound. The apical position of the N_2O_2I pyramid is occupied by iodine. Crystals of **C15** contain the complex cation $[Cu_2(btmmO)_2]^{2+}$ which lacks the iodide bridge. Each copper atom is surrounded by a cisoid N_2O_2 donor set in a square-planar manner. The resulting colour of the compound is red. Due to completely planar CuN_2O_2 fragments - the complex cations are situated on inversion centers -, the Cu...Cu distance amounts to 3.035(1) Å and thus is much longer than in $[Cu_2(btmmO)_2I]^+$. Due to the reduced number of ligand donor functions, the averaged Cu-N and Cu-O bond distances within **C15** (1.949(2) and 1.921(2) Å, respectively) are shorter than the corresponding bond distances within $[Cu_2(btmmO)_2I]^+$ (1.976(2) and 1.965(2) Å, respectively). The introduction of the iodide bridge and the resulting fold of the Cu_2O_2 core portion in $[Cu_2(btmmO)_2I]^+$ is accompanied by a change in the conformation of the six-membered chelate heterocycle formed by the propylene-bridged N donor functions. Thus, on going from $[Cu_2(btmmO)_2]^{2+}$ to $[Cu_2(btmmO)_2I]^+$, the chair conformation is switched to the boat-like structure. The other chelate rings which involve the oxygen donor functions are twisted. It is interesting to note that the iodide bridge of the complex cation $[Cu_2(btmmO)_2I]^+$ as well as the isolated iodide counterion has survived the O-core state of the reaction intermediate $[Cu_2O_2(btmgp)_2]^{2+}$ which contains copper in the oxidation state +3.

Both the dicationic bis(μ-hydroxo)-dicopper(II) species $[Cu_2(btmgp)_2(\mu\text{-}OH)_2]^{2+}$ (Fig. 6.4) in crystals of $[Cu_2(btmgp)_2(OH)_2][I]_2$ and $[Cu_2(btmgp)_2(OH)_2][PF_6]_2$ are isostructural demonstrating that the counterions have only limited influence on the overall structure.[112, 113] This influence, however, can be detected if the Cu...Cu distances (3.008(2) vs. 3.032(1) Å) are compared, but is virtually undetectable regarding the average Cu-O and Cu-N distances and the corresponding valence angles which are almost identical. Due to crystallo-

graphic site symmetries (i) the Cu_2O_2 cores in both dications are strictly planar. The chelate heterocycles adopt in both complexes the chair conformation. Selected distances and angles of the crystal structure of $[Cu_2(btmgp)_2(\mu\text{-}OH)_2]^{2+}$ are listed in Table 6.3.

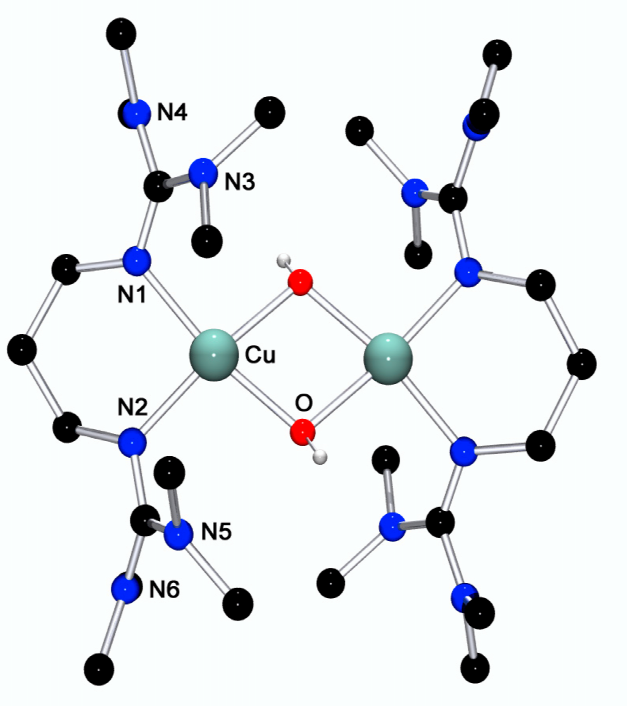

Figure 6.4: Molecular structure of $[Cu_2(btmgp)_2(\mu\text{-}OH)_2]^{2+}$ [113]

Table 6.3: Selected distances and angles of $[Cu_2(btmgp)_2(\mu\text{-}OH)_2]^{2+}$ (The primed atoms are derived from the unprimed ones by inversion.) [112, 113]

Distances (Å)		**Angles (°)**	
Cu...Cu'	3.008(2)	O-Cu-O'	78.6(2)
Cu-O	1.953(5)	Cu-O-Cu'	101.4(2)
Cu-O'	1.934(5)	N(1)-Cu-N(2)	94.0(2)
Cu-N(1)	1.999(5)		
Cu-N(2)	1.975(5)		

6.1.2 Discussion of the reaction mechanism

The formation of equal amounts of $[Cu_2(btmmO)_2I]I\cdot\frac{1}{2}EtOH$ and $[Cu_2(btmgp)_2(OH)_2][I]_2$ and of $[Cu_2(btmgp)_2(OH)_2][PF_6]_2$ and $[Cu_2(btmmO)_2][PF_6]_2\cdot 2MeCN$, respectively, is in accordance with the idea that both the bis(μ-alkoxo)- and the bis(μ-hydroxo)dicopper(II) species may originate from a common precursor complex, the hitherto non-identified

species $[Cu_2(btmmO)(OH)(btmgp)]^{2+}$. Possible mechanisms for the formation of the (hypothetical) (μ-alkoxo)(μ-hydroxo)dicopper(II) complex have been discussed by Itoh et al.,[86, 149, 52, 150] and a recent quantum mechanical calculation arrives at the same suggestion.[151] However, the fact that no such complexes have ever been observed so far raises the question whether this assumption reflects the chemical reality or not. Our results clearly show that the Cu(III) species $[Cu_2(\mu\text{-}O)_2(btmgp)_2]^{2+}$ formed as an intermediate is not reduced by iodide ions and thus might be indicative for a mechanism different from the ones cited above which are based either on the abstraction of an H atom followed by a rearrangement step or on a concerted insertion of O into a C-H bond.[48] An alternative reaction pathway which might also result in the formation of the (hypothetical) (μ-alkoxo)(μ-hydroxo)dicopper(II) intermediate could be initiated by the nucleophilic attack of an oxygen atom of the $Cu_2(\mu\text{-}O)_2$ core directed towards a methyl group followed by interception of the released hydride ion as a third ligand bridge and subsequent rearrangement. Though this hypothesis is speculative in nature, the formation of a hydride bridge seems chemically possible in the light of the observation that iodide ions do not reduce Cu(III) in the O-core stage. Moreover, if the interception of the hydride ion is slow compared to a competing electrophilic attack of the $Cu_2(\mu\text{-}O)_2$ core activated in such a manner towards a methyl group of the second ligand, then the formation of the (μ-alkoxo)(μ-hydroxo)dicopper(II) intermediate is avoided and the bis(μ-alkoxo)dicopper(II) complex is directly formed under proton release. The hydride ion which is now accessible to the system is suited to attack a protonated O-core of another reaction intermediate in a nucleophilic manner resulting in the formation of the bis(μ-hydroxo)dicopper(II) complex $[Cu_2(btmgp)_2(\mu\text{-}OH)_2]^{2+}$. The proton required to initiate this reaction step might originate from ubiquitous catalytic proton sources. Once started, the reaction is driven by protons released during the formation of $[Cu_2(btmmO)_2]_2^{2+}$.

6.1.3 Electrochemistry of $[Cu_2(btmmO)_2][PF_6]_2 \cdot 2MeCN$ C15

The cyclovoltammogram of **15** (0.1 mol/L $[NBu_4][PF_6]$; 50 mV/s; Au/Pt/Ag-AgCl) shows a single reversible electron transfer at 1.27 V/NHE (Figure 6.5) which assigns the Cu(II)/Cu(I) redox pair of complex **C15**. The form of the cyclovoltammogramm indicates that at approximately 1.9 V/Ag-AgCl, the ligand begins to get oxidised.

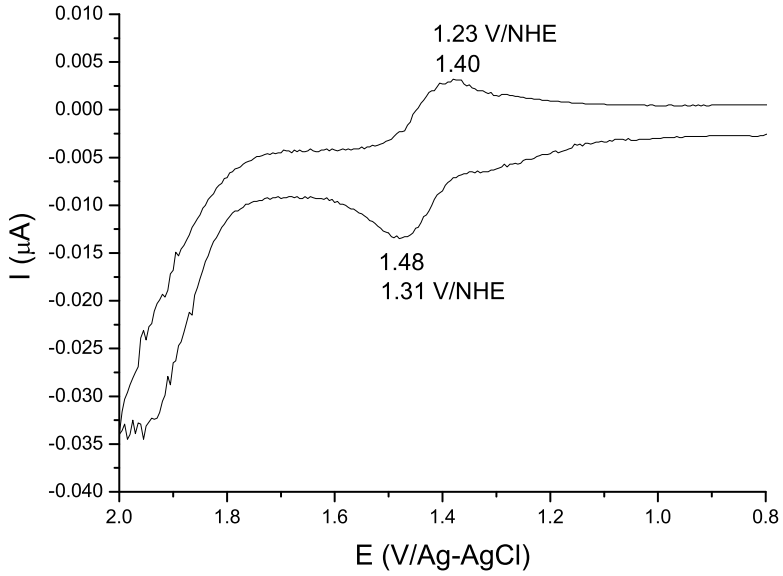

Figure 6.5: Cyclovoltammogram of **C15** in CH_2Cl_2

6.2 Hydroxylation of copper TMG_2MePA complexes

6.2.1 Crystal structures of TMG_2MePA containing hydroxylation products

The reaction of several TMG_2MePA containing precursor complexes $[Cu(TMG_2MePA)][X]$ (X = PF_6^-, ClO_4^-, BF_4^- and I^-) with dioxygen (Scheme 6.6) was investigated by low temperature UV/Vis monitoring (section 5.1).

Similar to the reaction of bmtgp supported complexes, the primarily formed species are bis-μ-oxodicopper(III) complexes containing the Cu_2O_2 core with fully reduced oxygen and copper in the oxidation state +3 in both cases. Unfortunately, no crystals suitable for X-ray diffraction could be obtained from these reactions. From these solutions, two different complex types could be isolated in equal amounts: the bis(μ-alkoxo)-bridged dinuclear copper complexes $[Cu_2(TMMoG_2MePA)_2]^{2+}$ and the hydroxo-bridged dinuclear copper complexes $[Cu_2(TMG_2MePA)_2(\mu\text{-}OH)_2]^{2+}$.

Crystals of $[Cu_2(TMMoG_2MePA)_2][PF_6]_2$ (**C16**), $[Cu_2(TMMoG_2MePA)_2][ClO_4]_2$ (**C17**) and $[Cu_2(TMMoG_2MePA)_2][BF_4]_2$ (**C18**) could be isolated by vapour diffusion of diisopropylether into acetonitrilic solutions as green needles. The corresponding bis(μ-hydroxo) dicopper species could only be crystallised in form of $[Cu_2(TMG_2MePA)_2(\mu\text{-}OH)_2][Cu_2I_4]$ (**C19**) (dark green needles) and $[Cu_2(TMG_2MePA)_2(\mu\text{-}OH)_2][I_3^-]_2$ (**C20**) (bright yellow needles) after the reaction of $[Cu(TMG_2MePA)]I$ with dioxygen. A reaction mechanism for the concomitant formation of both species is assumed which ressembles the mechanism described

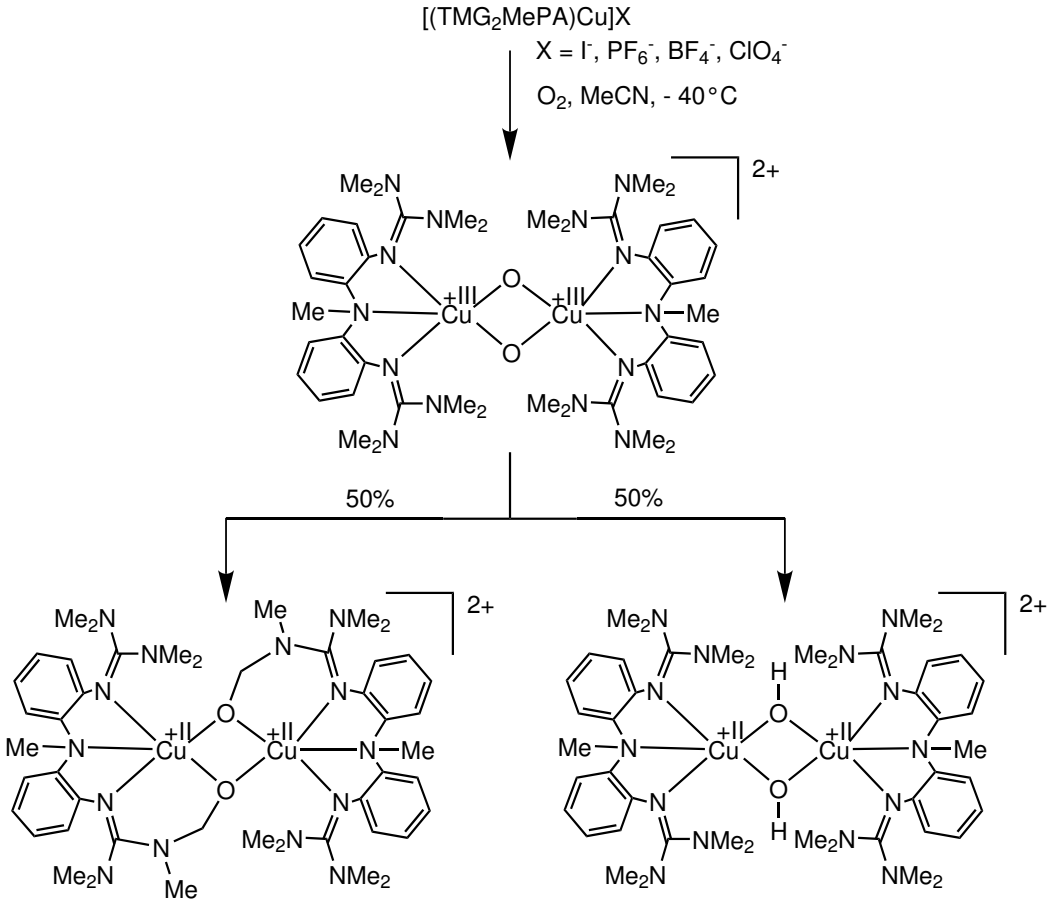

Figure 6.6: Activation of oxygen with [Cu(TMG$_2$MePA)][X] (X = PF_6^-, ClO_4^-, BF_4^- and I^-)

above for btmgp supported complexes. The reaction starting from the bis-μ-oxodicopper(III) complex will proceed either via a very unstable (μ-alkoxo)(μ-hydroxo)dicopper(II) complex state or via a hydride transition state (vide supra) to the two coupled product species.

All five complex salts crystallise in the triclinic space group $P\bar{1}$. Crystals of **C16**, **C17**, **C18** and **C19** contain one molecule per unit cell. Crystals of **C20** contain two molecules per unit cell, in crystals of **C16** 1.8 molecules of MeCN are also present. The results of the structure analyses are shown in Figures 6.7 - 6.9, while selected bond lengths and angles are collected in Table 6.4, and parameters relating to the data collection and refinement are listed in the Tables A11 - A13. As the bis(μ-hydroxo) dicopper complexes **C16** and **C17** are isostructural, only the structure of **C16** is denoted in the Figures. Similarily, the bis(μ-hydroxo) dicopper complexes **C19** and **C20** are isostructural, therefore, only complex **C19** has been depicted in Figure 6.9.

Reaction of [Cu(TMG$_2$MePA)][X] (X = PF_6^-, ClO_4^-, BF_4^- and I^-) with molecular oxygen transforms one half of the coordinated *N*-methyl-bis(tetramethyl)guanidinodiphenyleneamine molecules into *N*-methyl-

Table 6.4: Selected distances and angles of the bis(μ-alkoxo) and bis(μ-hydroxo) dicopper(II) complex cations containing the tripodal ligand TMG_2MePA

Distances (Å)	**C16**	**C17**	**C18**	**C19**	**C20**
Cu...Cu	3.068(1)	3.058(1)	2.991(1)	3.051(1)	3.044(1)
Cu-N$_{imine}$	1.988	1.990	2.036	2.007	1.998
Cu-N$_{amine}$	2.349	2.348	2.147	2.344	2.398
Cu-O	1.934	1.931	1.914	1.936	1.940
N=C(av)	1.333	1.325	1.331	1.318	1.319
Angles (°)					
N$_{imine}$**-Cu-N**$_{imine}$	97.5	97.5	109.5	99.4	97.4
N$_{imine}$**-Cu-N**$_{amine}$	77.2	77.6	79.9	77.4	76.9
O-Cu-O	75.1	75.3	77.2	76.0	76.6
N$_{amine}$**-C-N**$_{amine}$**(av)**	118.1	118.2	118.6	116.3	116.7
ρ	0.986	0.981	0.991	0.969	0.975

bis(trimethylmethoxy)guanidino-diphenyleneamine ligands which have been identified as the alkoxo components within the bis(μ-alkoxo)dicopper(II) complexes **C16**, **C17** and **C18** (Figs. 6.7 and 6.8). Both complex cations **C16** and **C18** shown in Figs. 6.7 and 6.8, respectively, contain the $Cu_2(TMMoG_2MePA)_2$ entity but they differ from the coordination mode of their copper centres. In crystals of **C16** and **C17**, each copper atom is surrounded by its ligands in a square-pyramidal manner. The apical position of the N_2O_2N pyramid is occupied by the amine function of TMG_2MePA. This coordination comes clear by regarding the Cu-N$_{imine}$ distances which measure 1.989 Å in average and the Cu-N$_{amine}$ distances of 2.349 Å defining the apical position. The N_2O_2 donor set provides a good square-planar environment with Cu-O distances of 1.933 Å. However, the N$_{imine}$-Cu-N$_{imine}$ angles are slightly widened up to 97.5° and the O-Cu-O angles are diminuished to 75.2° due to conformational and geometrical restrictions of the ligand which offers the apical N donor function with the amine group. In crystals of **C18**, the situation is totally different although the counterion only has been changed from the non-coordinating sphere-symmetrical hexafluorophosphate or perchlorate to the similar tetrafluoroborate. The Cu-N$_{imine}$ distances are elongated to 2.036 Å whereas the Cu-N$_{amine}$ distance is drastically shortened to 2.147 Å. Thus, the coordination of the copper centre can be described as distorted trigonal bipyramidal with the N2 and O1 atoms as apices and the N$_{imine}$ atoms and the O1A atom as equatorial donors. The deviation of the copper atom of this plain (N1N3O1A) amounts up to 0.065(1)

Å. As a measure for the degree of trigonality, the structural index parameter $\tau = (\beta - \alpha)/60°$ [152] was established by Addison and Reedijk.[153] For **C16** and **C17**, τ is almost zero (0.06 for **C16**, 0.05 for **C17**) indicating a perfectly planar square-pyramidal coordination. For **C18**, τ is calculated to be 0.55 which denotes the high degree of trigonalisation clearly. The angle between the apical positions is 170.3(1)° which shows the deviation from an ideal trigonal pyramid with 180°. However, although the coordination has changed seriously, the equivalency of the two N_{imine} donor functions has been kept. These findings illustrate that the equilibrium between the two coordinational modes is very fragile and that the energy of the transition state is so small that packing forces can switch the equilibrium to the other side. The values of the structural parameter ρ lie between 0.97 and 0.99 indicating a good delocalisation of the positive charge within the guanidine moiety in the stabilisation of the Cu(II) complexes **C16** - **C20**.

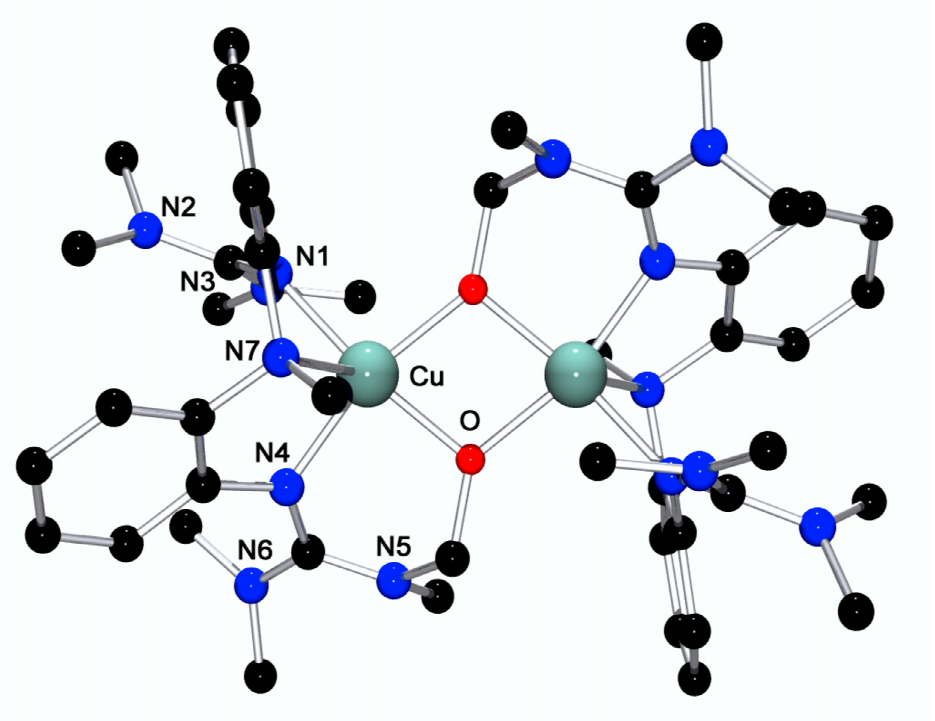

Figure 6.7: Molecular structure of $[Cu_2(TMMoG_2MePA)_2]^{2+}$ in crystals of **C16** and **C17**

In crystals of **C19** and **C20** (Figure 6.9), the geometric centre of the cation lies on a crystallographic inversion centre and the resulting Cu_2O_2 core is thus strictly planar. The Cu atom is coordinated in a square-pyramidal manner by two guanidine N atoms, one amine N atom and the two bridging O atoms like in **C16** and **C17**. The structural index parameter τ is calculated to be 0.12 for **C19** and 0.05 for **C20** indicating an almost ideal square-pyramidal coordination. The Cu-N_{imine}, Cu-N_{amine} and Cu-O distances and the corresponding angles are according with those of **C16** and **C17**. The N_{amine}-C-N_{amine} angles are slightly

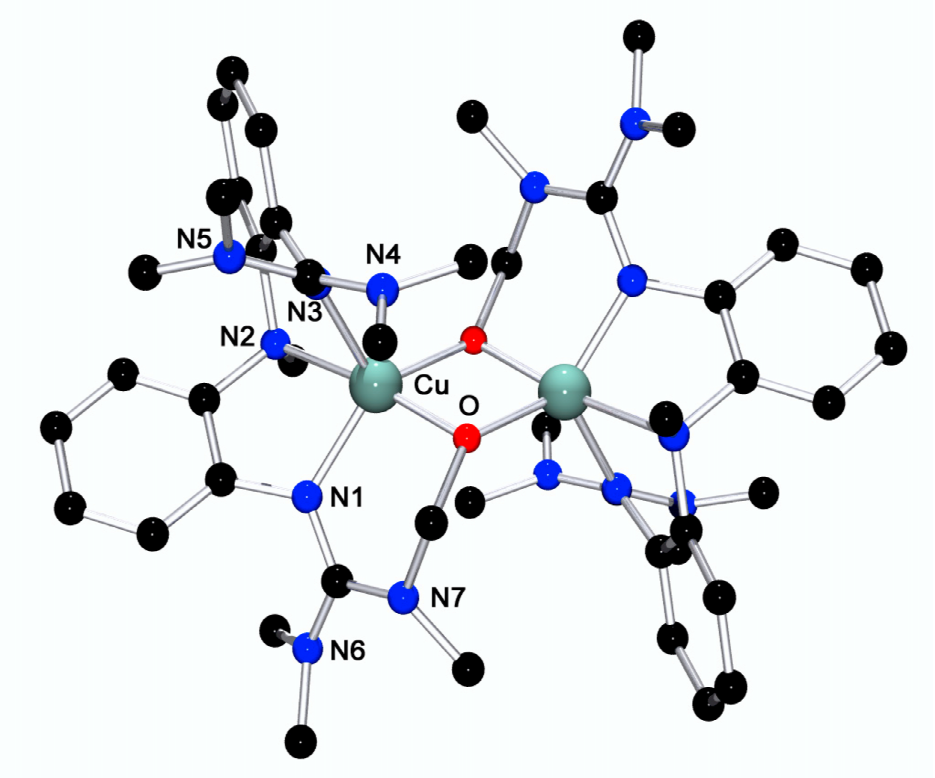

Figure 6.8: Molecular structure of $[Cu_2(TMMoG_2MePA)_2]^{2+}$ in crystals of **C18**

diminuished to 116.5° because the NMe_2 is not forced to spread like in the hydroxylated ligands in **C16**, **C17** and **C18**.

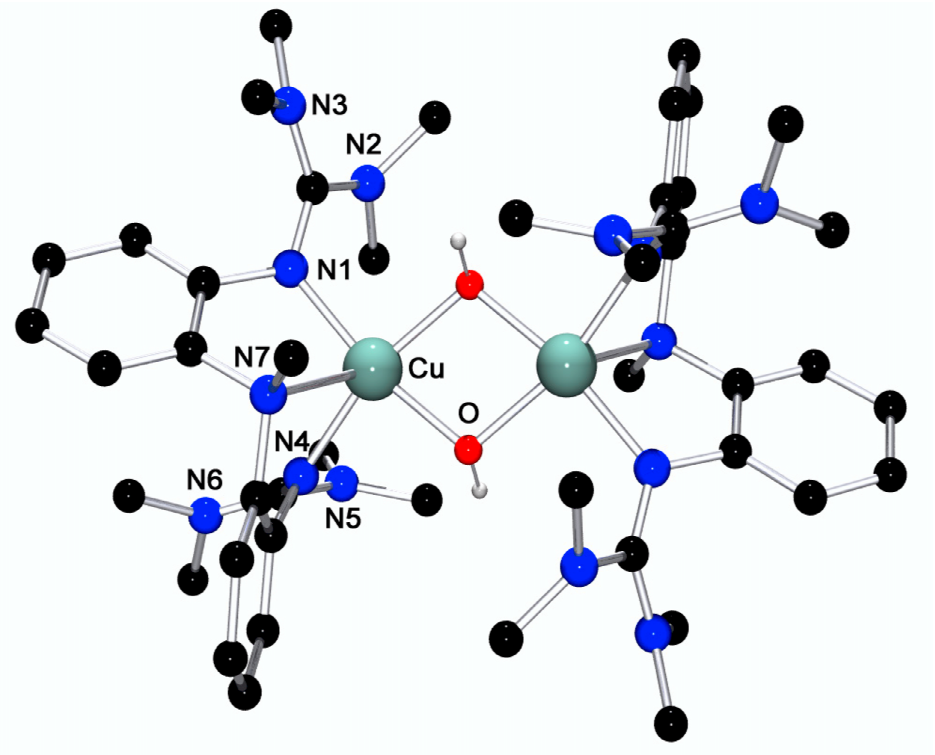

Figure 6.9: Molecular structure of $[Cu_2(TMG_2MePA)_2(\mu\text{-}OH)_2]^{2+}$ in crystals of **C19** and **C20**

6.2.2 Electrochemistry of $[Cu_2(TMMoG_2MePA)_2][PF_6]_2$ C16

The cyclovoltammogram of **16** (0.1 mol/L $[NBu_4][PF_6]$; 50 mV/s; Au/Pt/Ag-AgCl) shows an irreversible electron transfer at 1.065 V/NHE (Figure 6.10). This oxidation wave is caused by the oxidation of the ligand (see section 3.4). The form of the cyclovoltammogramm indicates that several redox processes occur which can not be attributed to single electron transfers. This behaviour might be due to the aromatic spacer of the ligand.

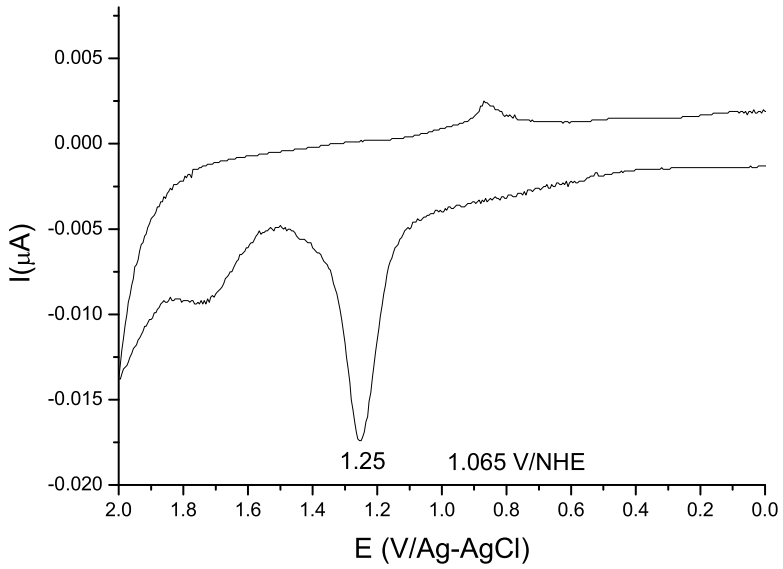

Figure 6.10: Cyclovoltammogram of **C16** in CH_2Cl_2

6.3 Hydroxylation of copper $DMEG_2p$ complexes

The reaction of the $DMEG_2p$ containing precursor complex $[Cu_2(DMEG_2p)_2][PF_6]_2$ (**C5**) with dioxygen (Scheme 6.11) was investigated by low temperature UV/Vis monitoring (section 5.1). Although at low temperatures a $\mu-\eta^2:\eta^2$-peroxo complex is formed, the alkoxylated product complex $[Cu_2(MMoEG_2p)_2][PF_6]_2$ (**C21**) can be isolated analogously to the reaction of btmgp and TMG_2MePA supported complexes via bis-μ-oxodicopper(III) complexes. Thus, the P-core complex converts at higher temperatures to the O-core which hydroxylates the $DMEG_2p$ ligand at one of its N-CH_3 functions to form the $MMoEG_2p$ ligand. The accompanying bis(μ-hydroxo) dicopper(II) complex which forms equimolarily could not be crystallised. From the reaction solution in MeCN, red crystals of the bis(μ-alkoxo) dicopper(II) complex $[Cu_2(MMoEG_2p)_2][PF_6]_2$ (**C21**) could be obtained by vapour diffusion of diisopropylether. The complex salt **C21** crystallises in the monoclinic space group $P2_1/c$. Crystals of **C21** contain two crystallographically independent but otherwise

identical molecules and a total of eight molecules per unit cell. A view of the structure of $[Cu_2(MMoEG_2p)_2]^{2+}$ in crystals of **C21** is shown in Figure 6.12, while selected bond lengths and angles are collected in Table 6.5, and parameters relating to the data collection and refinement are listed in Table A14.

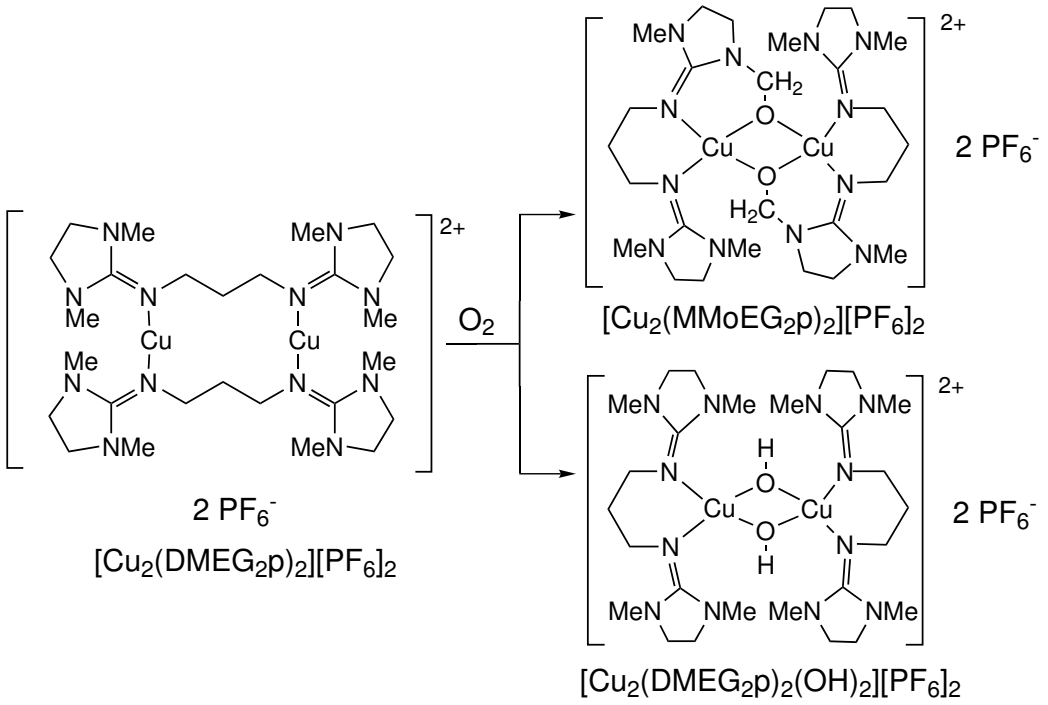

Figure 6.11: Activation of oxygen with $[Cu_2(DMEG_2p)]_2[PF_6]_2$ (**C5**)

Table 6.5: Selected distances and angles of the bis(μ-alkoxo) dicopper(II) complex cation in crystals of **C21** in comparison with btmgp and TMG_2MePA containing complexes

Distances (Å)	**C21**	**C15**	**C16**
Cu...Cu'	3.032(1)	3.035(1)	3.068(1)
Cu-N$_{imine}$	1.939	1.961	1.988
Cu-N$_{amine}$			2.349
Cu-O	1.921	1.921	1.934
N=C(av)	1.308	1.313	1.333
Angles (°)			
N$_{imine}$**-Cu-N**$_{imine}$	95.1	93.3	97.5
O-Cu-O	74.4	75.7	75.1
Cu-O-Cu'	105.6	104.4	-
N$_{amine}$**-C-N**$_{amine}$**(av)**	109.9	116.3	118.1

The centroid of the cation lies on a crystallographic inversion centre and the resulting Cu_2O_2

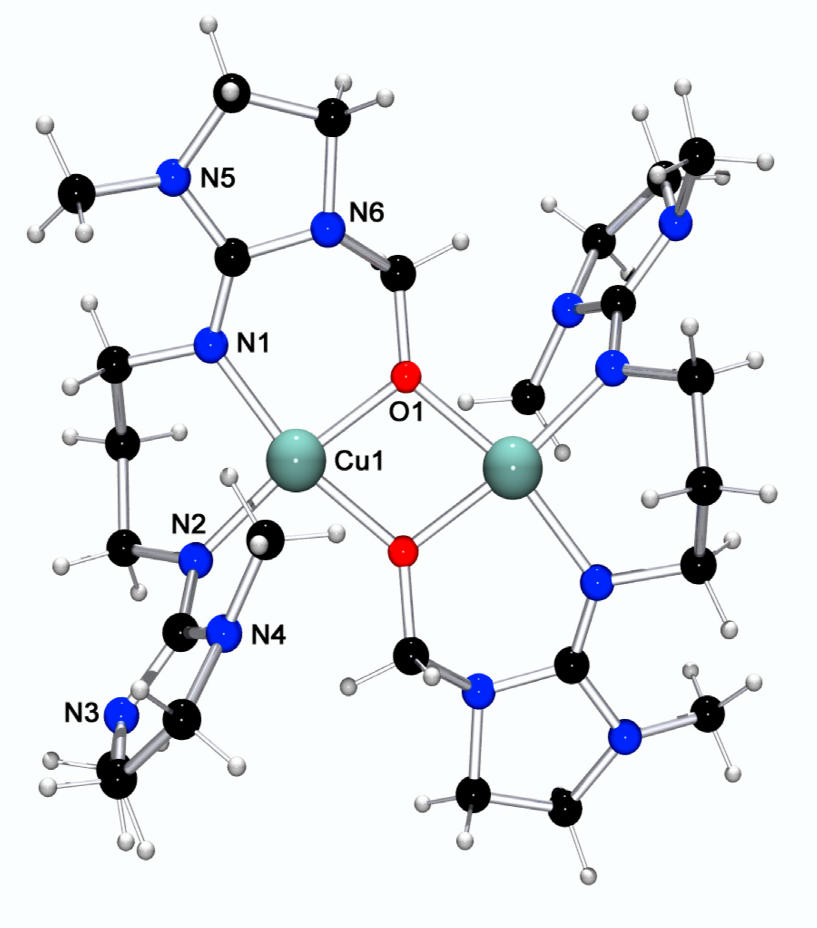

Figure 6.12: Molecular structure of $[Cu_2(MMoEG_2p)_2]^{2+}$ in crystals of **C21**

core is thus strictly planar. The Cu atom is coordinated in a planar quadratic manner by two guanidine N atoms and the two bridging O atoms. The deviation of the Cu atom from the N_2O_2 plane (averaged deviation: 0.022 Å) is 0.002(1) Å, and the chelate heterocycle adopts a chair conformation. The Cu-N distances are slightly shortened in comparison with the other bis(μ-alkoxo) dicopper(II) complex cations, whereas the geometric parameters as Cu-O distances and O-Cu-O and Cu-O-Cu angles of the Cu_2O_2 core are almost identical. The bite angle N_{imine}-Cu-N_{imine} of 95.1° is comparable with those of the already described bis(μ-alkoxo) dicopper(II) complexes. The N_{amine}-C-N_{amine} angles are diminuished towards the tetramethyl guanidine systems as the ethylene linker in the ligand $DMEG_2p$ tights the N_{amine} atoms together. The structural parameter ρ is calculated to be 0.949, a value which is rather small regarding the values of around 0.98 for TMG_2MePA containing complexes. This may be due to the aliphatic spacer in **C21** which does not support the delocalisation within the guanidine moiety.

6.4 Hydroxylation of copper DPipG$_2$p complexes

The reaction of the DPipG$_2$p containing precursor complex $[Cu_2(DPipG_2p)_2][PF_6]_2$ (**C9**) with dioxygen (Scheme 6.6) was investigated by low temperature UV/Vis monitoring (section 5.1). Analogously to the reaction of btmgp and TMG$_2$MePA supported complexes, the bis-μ-oxodicopper(III) complex reacts presumably to two products, a bis(μ-alkoxo) and a bis(μ-hydroxo) dicopper(II) complex. From the reaction solution in MeCN, only blue crystals of the bis(μ-hydroxo) dicopper(II) complex $[Cu_2(DPipG_2p)_2(\mu\text{-}OH)_2][PF_6]_2$ (**C22**) could be obtained by vapour diffusion of diisopropylether. The complex salt **C22** crystallises in the monoclinic space group P2$_1$/n. Crystals of **C22** contain two molecules per unit cell. The projection of $[Cu_2(DPipG_2p)_2(\mu\text{-}OH)_2]_2^{2+}$ as the result of the structure analysis is shown in Figure 6.14, while selected bond lengths and angles are collected in Table 6.6, and parameters relating to the data collection and refinement are listed in Table A14.

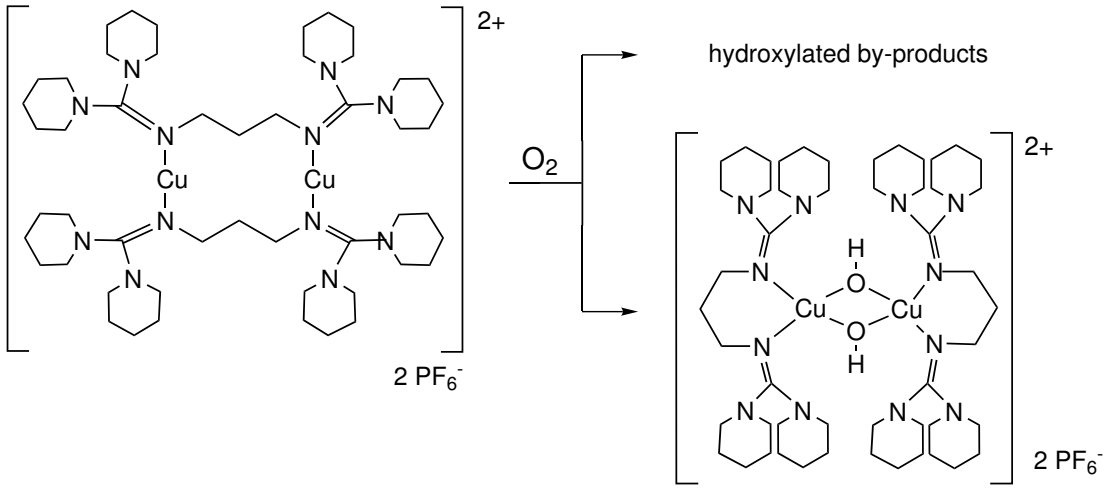

Figure 6.13: Activation of oxygen with $[Cu_2(DPipG_2p)_2][PF_6]_2$ (**C9**)

The centroid of the cation lies on a crystallographic inversion centre and the resulting Cu_2O_2 core is thus strictly planar. The Cu atom is coordinated in a planar quadratic manner by two guanidine N atoms and the two bridging O atoms. The deviation of the Cu atom from the N_2O_2 plane is 0.036 (1) Å, and the chelate heterocycle adopts a chair conformation. The presence of the hydroxo H atom was confirmed from Fourier maps. The Cu...Cu and mean Cu-O distances (3.0740 (6) and 1.935 (2) Å) are clearly elongated compared with those of di-μ-oxo-bridged Cu_2O_2 moieties, which are in the ranges 2.743 (1) - 2.906 (1) and 1.796 (6) - 1.865 (3) Å, respectively. Similar observations hold for related Fe complexes.[48] As pointed out by Que and Tolman,[48] the significant differences between the short (in $M_2(\mu\text{-}O)_2$) and long (in $M_2(\mu\text{-}OH)_2$) M-O distances are obviously a suitable measure for distinguishing

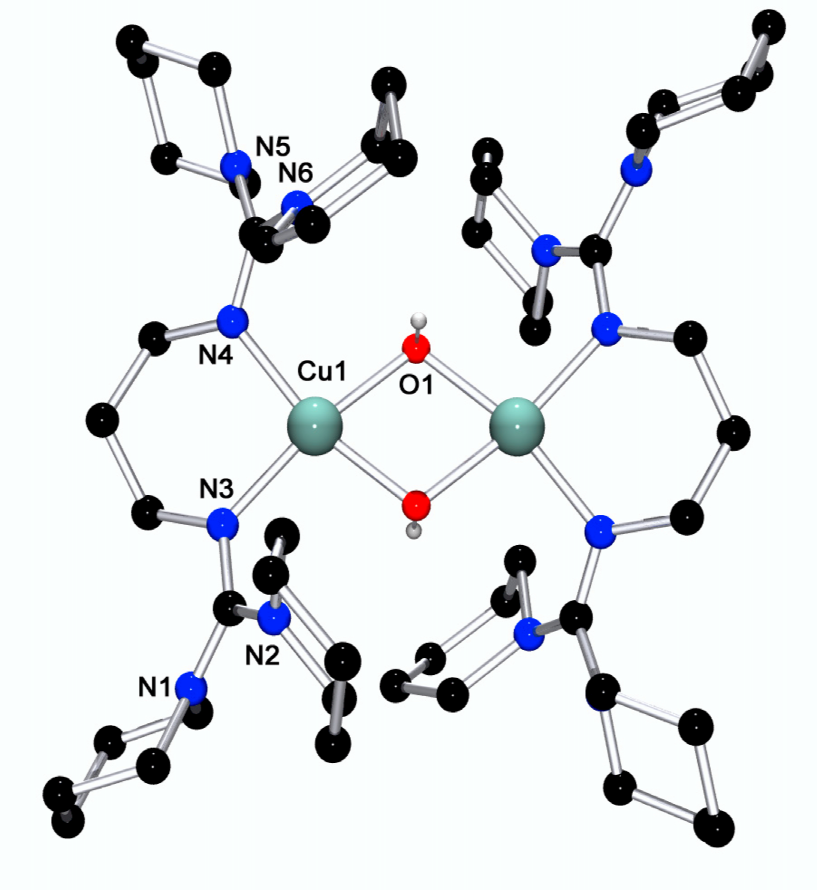

Figure 6.14: Molecular structure of $[Cu_2(DPipG_2p)_2(\mu\text{-}OH)_2]_2^{2+}$ in crystals of **C22**

Table 6.6: Selected distances and angles of the bis(μ-hydroxo) dicopper(II) complex cation $[Cu_2(DPipG_2p)_2(\mu\text{-}OH)_2]^{2+}$ in crystals of **C22** in comparison with btmgp and TMG_2MePA containing complexes

Distances (Å)	**C22**	**$[Cu_2(btmgp)_2(\mu\text{-}OH)_2]^{2+}$**	**C20**
Cu...Cu'	3.0740(6)	3.008(2)	3.051(3)
Cu-N_{imine}	1.975	1.987	2.007
Cu-N_{amine}			2.344
Cu-O	1.935	1.944	1.936
N=C(av)	1.314	1.317	1.318
Angles (°)			
N_{imine}-Cu-N_{imine}	96.0	94.0	99.4
O-Cu-O	74.8	78.6	76.0
Cu-O-Cu'	105.2	101.4	104.0
N_{amine}-C-N_{amine}(av)	116.8	116.4	116.3

between these two species. The bite angle N_{imine}-Cu-N_{imine} of 96.0° is comparable with those of the already described bis(μ-hydroxo) dicopper(II) complexes. The structural parameter ρ is calculated to be 0.964, a value which is only slightly smaller than those calculated for TMG_2MePA containing complexes.

6.5 Hydroxylation of copper TMG_2ch complexes

The reaction of the TMG_2ch containing precursor complexes $[Cu_2(TMG_2ch)_2][X]_2$ (X = I^-, PF_6^- and ClO_4^-) with dioxygen (Scheme 6.7) was investigated by low temperature UV/Vis monitoring (section 5.1). Analogously to the reaction of btmgp and TMG_2MePA supported complexes, the bis-μ-oxodicopper(III) complex reacts presumably to two products, a bis(μ-alkoxo) and a bis(μ-hydroxo) dicopper(II) complex. The O-core hydroxylates the TMG_2ch ligand at one of its N-CH_3 functions in order to form the novel $TMMoG_2ch$ ligand providing a N_2O donor set. From the reaction solution in MeCN, only red crystals of the bis(μ-alkoxo) dicopper(II) complexes $[Cu_2(TMMoG_2ch)_2][X]_2$ (X = I^-, PF_6^- and ClO_4^-) could be obtained by vapour diffusion of diisopropylether. The corresponding bis(μ-hydroxo) dicopper(II) compound does not crystallise but is formed as blue amorphous product. The complex salts **C23**, **C24** and **C25** crystallise in the monoclinic space group $P2_1/n$. Crystals of **C23**, **C24** and **C25** contain two molecules per unit cell. The results of the structure analysis is shown in Figure 6.16, while selected bond lengths and angles are collected in Table 6.7, and parameters relating to the data collection and refinement are listed in Table A15 and A16.

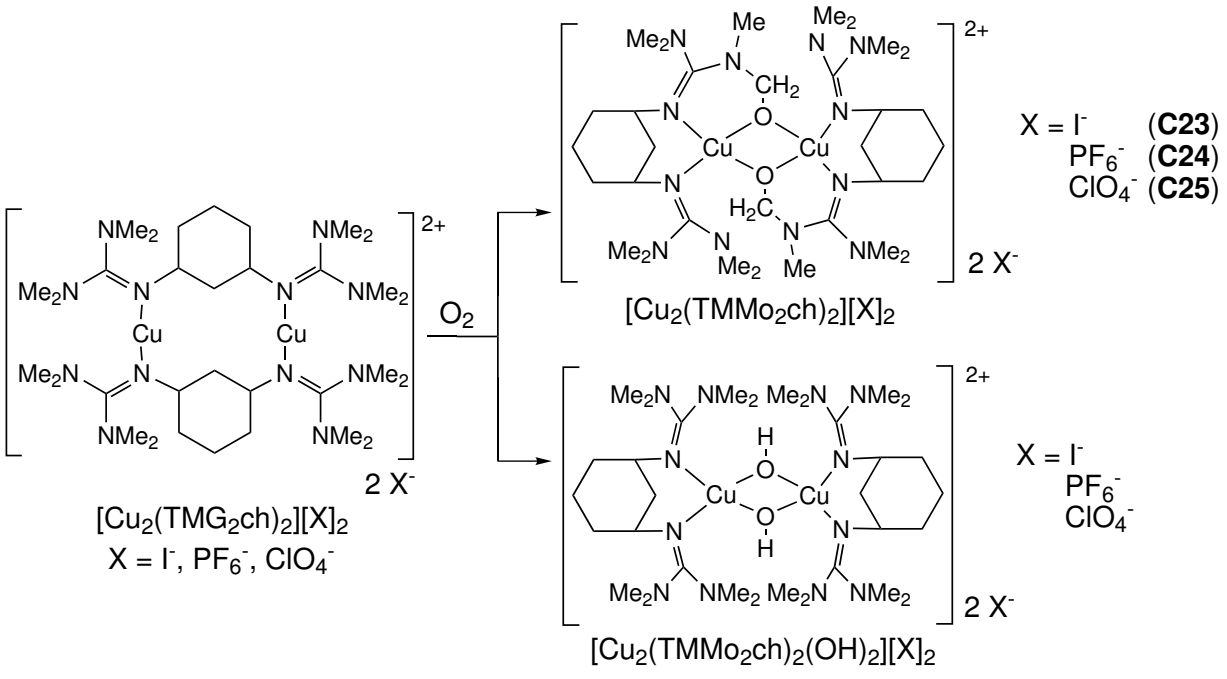

Figure 6.15: Activation of dioxygen with $[Cu_2(TMG_2ch)_2][X]_2$ (X = I^-, PF_6^- and ClO_4^-)

The precursor complexes $[Cu_2(TMG_2ch)_2][X]_2$ (X = I^-, PF_6^- and ClO_4^-) contain the cis isomer of the TMG_2ch ligand in its bis-equatorial conformation coordinating in a bridging mode. Interestingly, after the reaction with oxygen, the $TMMoG_2ch$ ligand coordinates the Cu_2O_2 core in a chelating mode under conformational change to the bis-axial conformation.

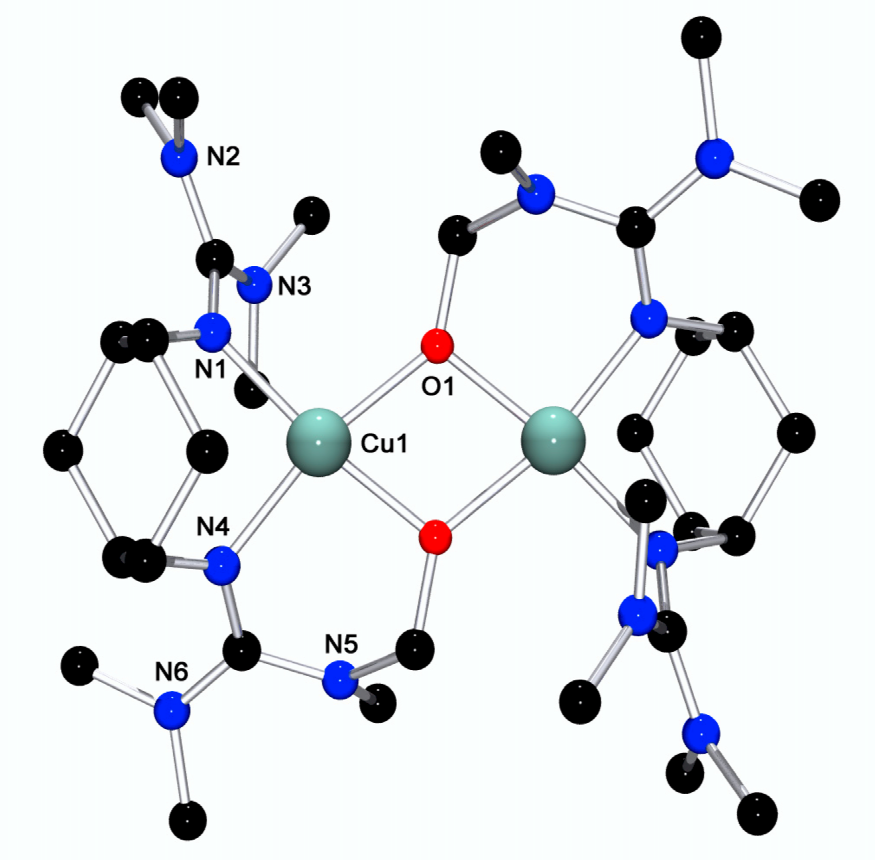

Figure 6.16: Molecular structure of $[Cu_2(TMMoG_2ch)_2]^{2+}$ in crystals of **C23**, **C24** and **C25**

Table 6.7: Selected distances and angles of the bis(μ-alkoxo) dicopper(II) complex cation $[Cu_2(TMMoG_2ch)_2]^{2+}$ in crystals of **C23**, **C24** and **C25** in comparison with $[Cu_2(btmmO)_2]^{2+}$ in **C15**

Distances (Å)	**C23**	**C24**	**C25**	**C15**
Cu...Cu'	3.0581(8)	3.0525(6)	3.045(1)	3.035(1)
Cu-N$_{imine}$	1.945	1.945	1.945	1.961(2)
Cu-O	1.929	1.923	1.919	1.921
N=C(av)	1.311	1.319	1.311	1.313
Angles (°)				
N$_{imine}$**-Cu-N**$_{imine}$	94.3	94.3	94.7	93.3
O-Cu-O	75.1	75.0	75.0	75.7
Cu-O-Cu'	104.9	105.0	105.0	104.4
N$_{amine}$**-C-N**$_{amine}$**(av)**	116.6	116.6	117.7	116.3
ρ	0.972	0.966	0.976	0.965

This result shows that the energetic barrier between the bridging and the chelating mode as well as between the bis-equatorial and the bis-axial conformation is small. The centroid of

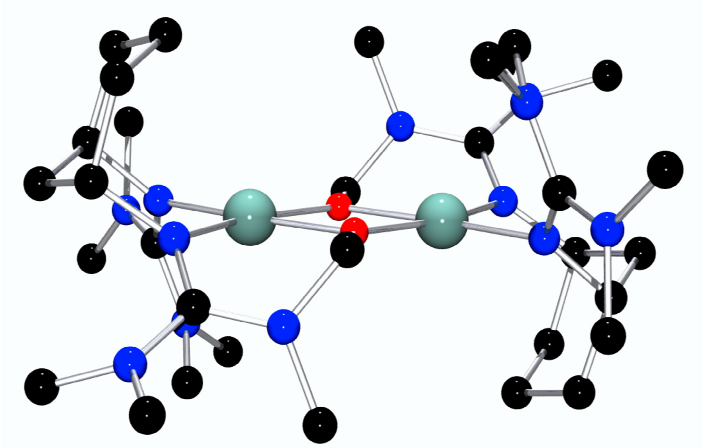

Figure 6.17: Perspective showing the double-chair conformation of $[Cu_2(TMMoG_2ch)_2]^{2+}$ in crystals of **C23**, **C24** and **C25**

the cations lies on a crystallographic inversion centre and the resulting Cu_2O_2 core is thus strictly planar. The Cu atom is coordinated in a planar quadratic manner by two guanidine N atoms and the two bridging O atoms. The deviation of the Cu atom from the N_2O_2 plane is 0.017(1), 0.019(1) and 0.014(1) Å (for **C23**, **C24** and **C25** with averaged plane deviations of 0.022, 0.022 and 0.029 Å), respectively, and the chelate heterocycle adopts a chair conformation. The cyclohexyl ring exhibits the chair conformation as well. Due to the inversion centre, the two cyclohexyl rings of each side of the complex cation are oriented to opposite directions and thus do not disturb each other sterically. The Cu-N distances are significantly shortened in comparison with the other bis(μ-alkoxo) dicopper(II) complex cations, whereas the geometric parameters as Cu-O distances and O-Cu-O and Cu-O-Cu angles of the Cu_2O_2 core are almost identical. The bite angles N_{imine}-Cu-N_{imine} are comparable with those of the already described bis(μ-alkoxo) dicopper(II) complexes. The N_{amine}-C-N_{amine} angles are according to those of the other tetramethyl guanidine systems. The structural parameters ρ for **C23**, **C24** and **C25** are calculated to be around 0.97, a value which is slightly smaller than those calculated for TMG_2MePA containing complexes. This might be due to the aliphatic spacer.

6.6 Hydroxylation of a copper MorphDMG$_2$p complex and subsequent reaction

The reaction of the MorphDMG$_2$p containing precursor complex $[Cu_2(MorphDMG_2p)_2][PF_6]_2$ with dioxygen (Scheme 6.6) gives the bis(μ-fluoro) dicopper(II) complex $[Cu_2(MorphDMG_2p)_2(\mu\text{-}F)_2][PF_6]_2$ (**C26**). Analogously to the reaction

of other bisguanidine supported complexes, the reaction leads via a bis-μ-oxodicopper(III) complex presumably to two products, a bis(μ-alkoxo) and a bis(μ-hydroxo) dicopper(II) complex. The bis(μ-hydroxo) dicopper(II) complex reacts in the following step with the present hexafluorophosphate ions abstracting fluorine ions and crystallising from the reaction solution in MeCN as blue crystals of the bis(μ-fluoro) dicopper(II) complex $[Cu_2(MorphDMG_2p)_2(\mu\text{-}F)_2][PF_6]_2$ (**C26**) by vapour diffusion of diisopropylether. Cu(II) complexes are known to be able to abstract fluorine from hexafluorophosphate as has been discussed by Holm et al.[154] The complex salt **C26** crystallises in the monoclinic space group $P2_1/n$. Crystals of **C26** contain two molecules per unit cell. The structure as the result of the structure analysis is shown in Figure 6.19, while selected bond lengths and angles are collected in Table 6.8, and parameters relating to the data collection and refinement are listed in Table A16.

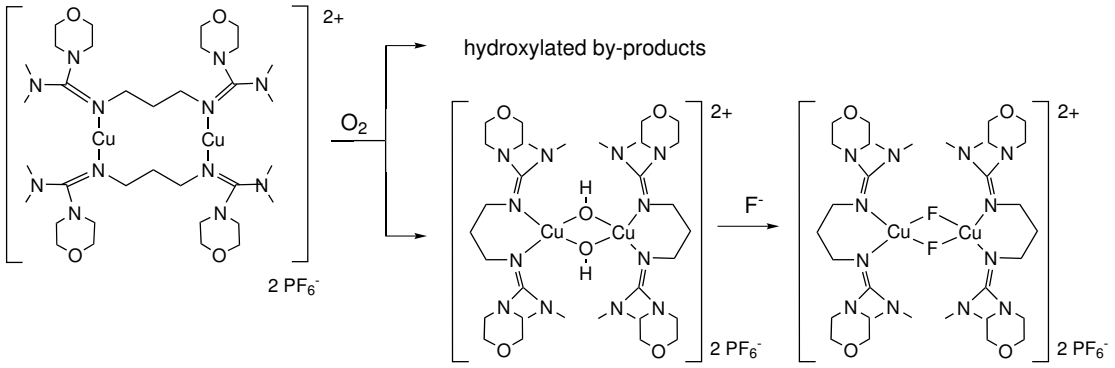

Figure 6.18: Activation of oxygen with $[Cu_2(MorphDMG_2p)_2][PF_6]_2$

Table 6.8: Selected distances and angles of the complex cation $[Cu_2(MorphDMG_2p)_2(\mu\text{-}F)_2]^{2+}$ in crystals of **C26** in comparison with $[Cu_2(DPipG_2p)_2(\mu\text{-}OH)_2]^{2+}$ **C22** (X = F^- or OH^-, resp.)

Distances (Å)	**C26**	**C22**
Cu...Cu'	3.0376(8)	3.0740(6)
Cu-N$_{imine}$	1.960	1.975
Cu-X	1.948(2)	1.935
N=C(av)	1.308	1.314
Angles (°)		
N$_{imine}$**-Cu-N**$_{imine}$	96.5(1)	96.0
X-Cu-X	77.0(1)	74.8
Cu-X-Cu'	103.0(1)	105.2
N$_{amine}$**-C-N**$_{amine}$**(av)**	115.5	116.8

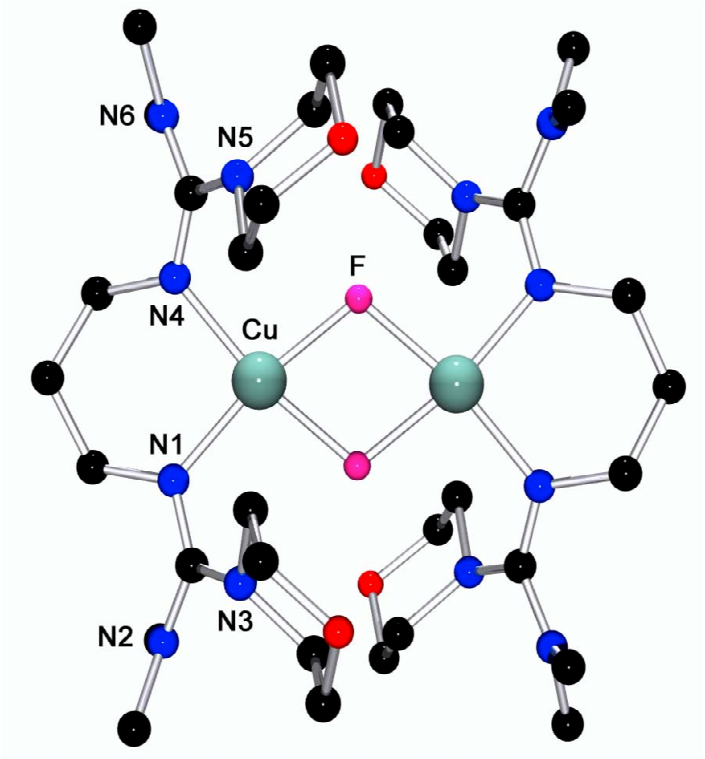

Figure 6.19: Molecular structure of $[Cu_2(MorphDMG_2p)_2(\mu\text{-}F)_2]_2^{2+}$ in crystals of **C26**

The geometric centre of the cation lies on a crystallographic inversion centre and the resulting Cu_2F_2 core is thus strictly planar. The Cu atom is coordinated in a square-planar manner by two guanidine N atoms and the two bridging F atoms. The deviation of the Cu atom from the N_2F_2 plane is 0.059(1) Å, and the chelate heterocycle adopts a chair conformation. The Cu...Cu and Cu-F distances (3.0376(8) and 1.960 Å) are slightly shortened compared with those of di-μ-hydroxo-bridged Cu_2O_2 moieties due to the higher electronegativity of fluorine. The bite angle N_{imine}-Cu-N_{imine} of 96.5° and all the other characteristics (see Table 6.8) are comparable with those of the already described bis(μ-hydroxo) dicopper(II) complexes. Interestingly, no significant difference between the two halfs of the guanidine moieties (dimethylamino and morpholino) can be made; the corresponding N=C bonds and the N_{amine}-C-N_{amine} are equal to another. The morpholine rings in chair conformation are oriented to each other which appears to help the packing of the complex cation (Figure 6.19). The structural parameter ρ is calculated to be 0.962, a typical value for a Cu(II) guanidine complex.[108]

6.7 Conclusion of the Hydroxylation Properties of Copper bisguanidine complexes

The reaction products have been identified as alkoxo-bridged dinuclear copper complexes demonstrating that the bidentate permethylated guanidine ligands have been hydroxylated in an unprecedented manner.[86, 149, 52, 150] An insertion of an oxygen atom into a C-H-bond of an N-methyl-group a-standing to an amino-group by a rearrangement of a bis(μ-oxo)dicopper(III) species is the first time to the best of our knowledge, although it has been previously reported that the carbon adjacent to an amino or phenyl group was hydroxylated by bis(μ-oxo)dicopper(III) species [86, 149] and that the β-carbon was hydroxylated via different intermediates,[148, 150] even when this position was unactivated.[155]

7 Catalytic activity of copper bisguanidine systems

7.1 General remarks

An important topic of the present work is the determination of the tyrosinase and catecholase activity of several of the oxygenated copper bisguanidine complexes described in Chapter 6. Generally, phenolic substrates should be *ortho*-hydroxylated in a tyrosinase-like reaction (Figure 7.1, reaction 1). For this reaction, 2,4-di^{tert}butylphenol was selected as a substrate because the sterically demanding ^{tert}butyl groups prevent undesired side reactions, e.g. the ring opening reaction known from iron-containing catechol-dioxygenases in nature and in model systems.[3] In addition, reactions with the differently substituted substrate 2,6-di^{tert}butylphenol were carried out in order to test the *para*-hydroxylation activity of the oxygenated copper bisguanidine complexes (Figure 7.1, reaction 2). Since in 2,6-di^{tert}butylphenol the *ortho*-position is occupied, only a *para*-hydroxylation reaction can occur. This hydroxylation can be followed by an oxidation to the *para*-quinone. A reason for the test of this reaction type is the interest in the *para*-hydroxylation of 2,3,5-trimethylphenol to 2,3,5-trimethyl-*p*-hydroquinone and subsequent oxidation to 2,3,5-trimethyl-*p*-quinone, an important educt compound in the synthesis of vitamin E. Its derivatives possess as antioxidants strong antimutagene activity.[156]

In order to test the catecholase reactivity, 3,5-di^{tert}butylcatechol was used as a substrate because due to its small redox potential of -1.19 V, this catechol can be easily oxidised to 3,5-di^{tert}butylquinone (Figure 7.1, reaction 3). Again, the sterically demanding ^{tert}butyl groups prevent side reactions like a C-C bond breaking between the two C=O bonds.

For the investigation of these different reactivities, the above-mentioned copper bisguanidine complexes were oxygenated at low temperatures and at room temperature followed by addition of the substrates. The results of theses experiments are presented in the following sections.

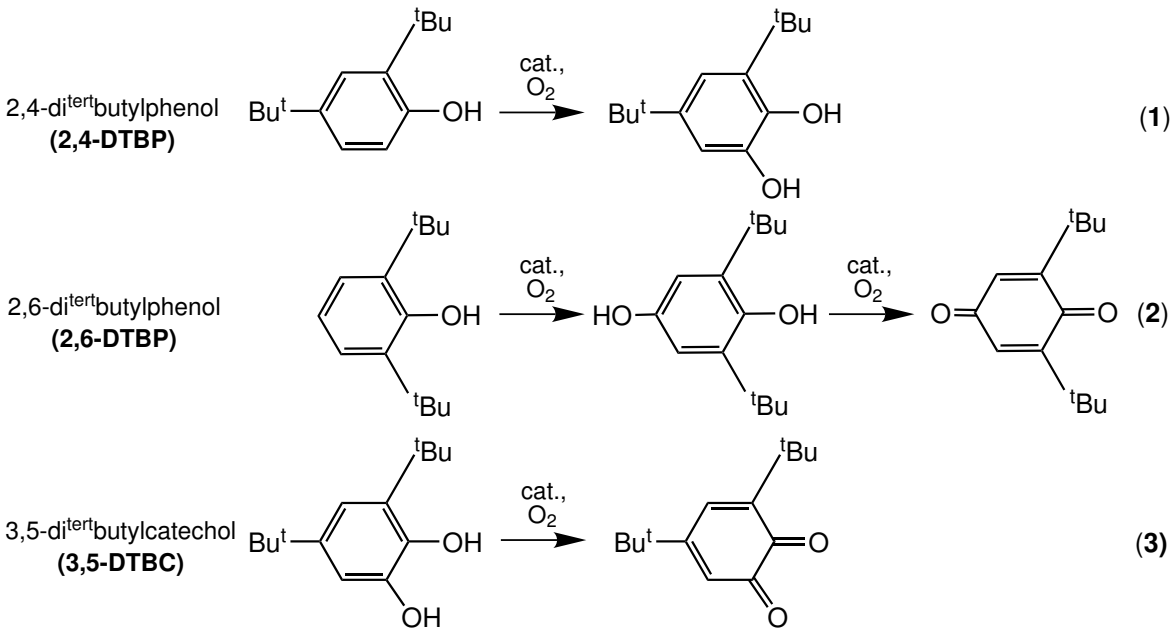

Figure 7.1: Oxygenation and oxidation reactions

7.2 Reactions with 2,4-di^{tert}butylphenol and 2,6-di^{tert}butylphenol

All attempts to react 2,4-di^{tert}butylphenol and 2,6-di^{tert}butylphenol at low temperatures (-40° - -80°C) failed. After detecting the formation of the oxygenated copper species by UV/vis spectroscopy, the addition of 2,4-di^{tert}butylphenol and 2,6-di^{tert}butylphenol did not lead to any reaction. Thus, these experiments were carried out at room temperature after the following procedure: 0.033 mmol of the Cu(I)bisguanidine complex in 10 mL of dichloromethane was oxygenated by stirring for 2 min in the presence of air. Afterwards, 100 mg (0.5 mmol) of substrate was added to the stirred solution. This reaction mixture typically changed its colour from blue-green to yellow, red or brown (depending from the selected complex). After 16 h of stirring at room temperature, the reaction was quenched by the addition of 10 mL of 5% perchloric acid.[157] After 5 min of stirring, the phases were separated and the aqueous phase was extracted with dichloromethane. The organic phases were combined and dried with Na_2SO_4. These solutions were analysed by means of gaschromatographic separation and mass spectrometric analysis in order to determine the conversion and the selectivity of the reactions.

In fact, by carrying out these experiments at room temperature it remains unclear if the oxidising species is a specific state (like O- or P-core) or a product of the decay of these species.

It turned out that the substrates 2,4-di^{tert}butylphenol and 2,6-di^{tert}butylphenol were not hydroxylated but coupled. In all of the obtained GC/MS data for the reaction of 2,4-DTBP, the 410 m/z peak with a retention time of 20:16 min is present (Figure 7.2), whereas for the reaction of 2,6-DTBP, the 410 m/z peak with a retention time of 22:53 min is found (Figure 7.3). Since both substrates possess a molecular mass of 206 g/mol, the peak at 410 m/z appears to be indicative for their dimer. The most probable reaction pathway is the C-O coupling reaction in the *ortho*- or *para*-position, respectively. Figure 7.4 shows possible coupling products. The reaction in the *ortho*- or *para*-position to the hydroxyl group is favourised over the reaction in the *ortho*- or *para*-position to the ^{tert}butyl groups.[116] Furthermore, the constitution of the reaction products was confirmed by ^{1}H-NMR analysis.

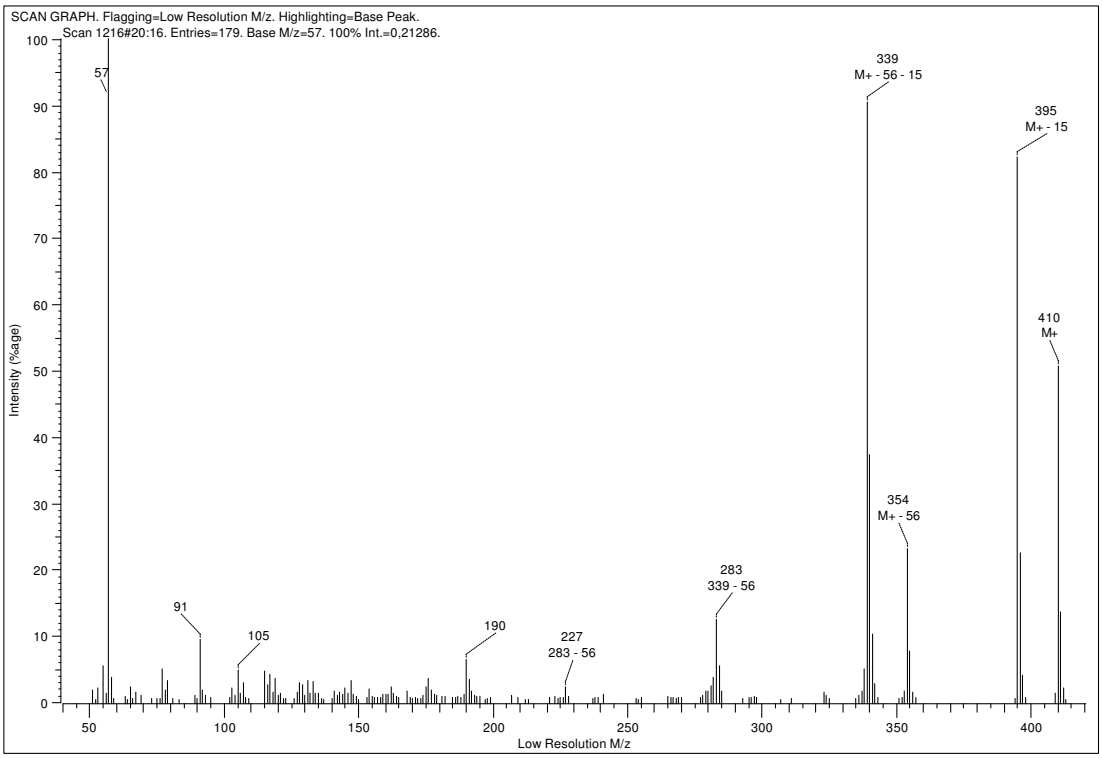

Figure 7.2: Reaction product of 2,4-di^{tert}butylphenol with the retention time of 20:16 min

Similar observations have been described by Ackermann [158] and Reedijk.[159] The mechanism of this reaction has been subject of much discussion during the last decades, and several mechanistic proposals have been made accordingly.[160] These proposals include the coupling of dialkylphenols by a radical pathway or by an ionic mechanism, both for C-O and C-C coupling. For this discussion, only the C-O coupling is taken into account and depicted in the Figures 7.5 and 7.6. There are three possible reaction pathways: a) an attack of a phenol radical occurs at the para-position of another phenol, b) a phenoxonium species attacks electrophilically another phenol in para-position and c) a phenol attacks nucleophili-

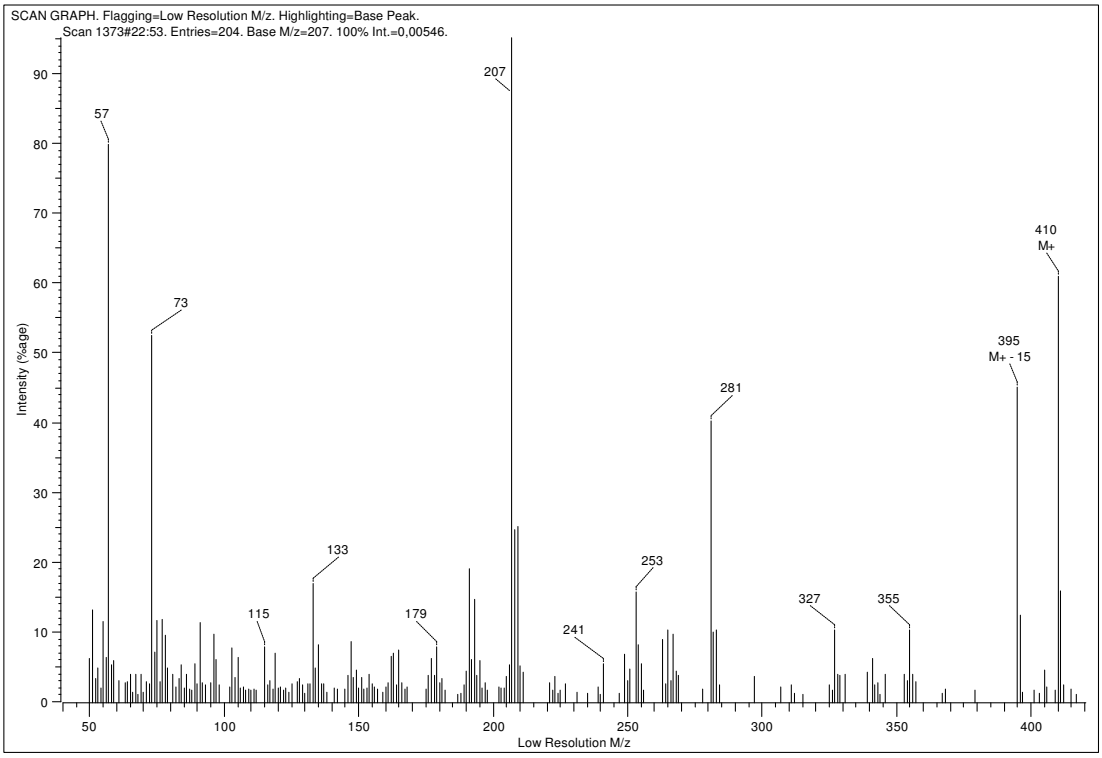

Figure 7.3: Reaction product of 2,6-di^{tert}butylphenol with the retention time 22:53 min

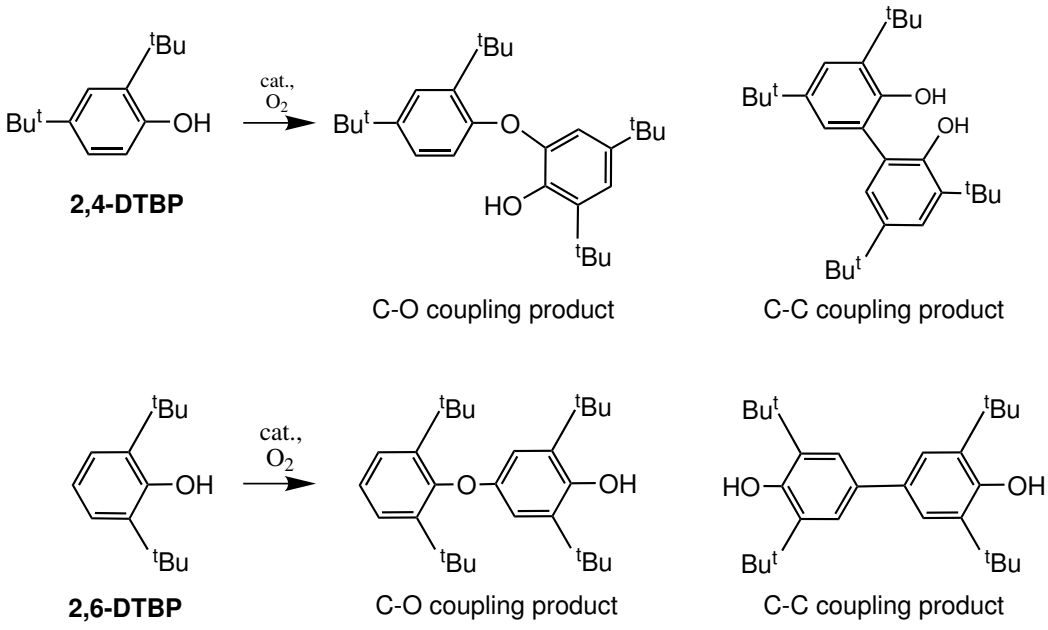

Figure 7.4: Possible coupling products of 2,4-di^{tert}butylphenol and 2,6-di^{tert}butylphenol

cally the para-position of a coordinated phenoxonium species which has been generated by a two-electron-transfer within a (μ-phenoxo)(μ-hydroxo)dicopper species (Figure 7.6).
Several theoretical works came to the consideration that, regarding the calculated atomic charges of the monomeric species, the electrophilic pathway (b) is not a viable option, since

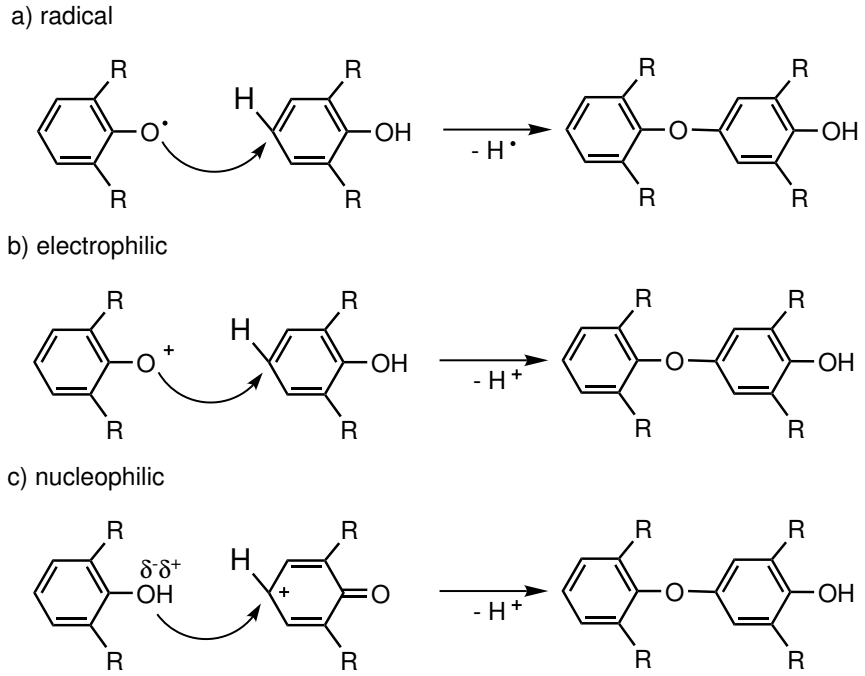

Figure 7.5: Mechanistic pathways proposed for the oxidative coupling of dialkylphenols [160]

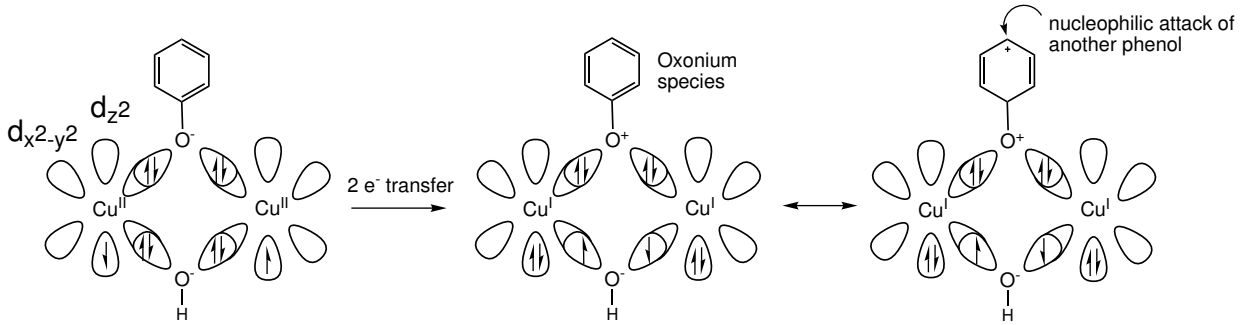

Figure 7.6: Simplified orbital representation of the two-elctron phenol oxidation within a (μ-phenoxo)(μ-hydroxo)dicopper species (adapted from [160])

it would require the attack of a cation with a positively charged oxygen atom on the para carbon of the phenol.[161] The radical pathway is regarded to be unlikely as well because it is known that a radical initiator mainly yields the C-C coupling product. Furthermore, the results of calculations favour a phenoxonium cation over a phenoxy radical as the key intermediate species. This strongly supports a mechanism, which involves the formation of a phenolate-bridged dinuclear copper(II) species as the catalytically intermediate. This bridging phenolate may experience a two-electron oxidation, resultung in a phenoxinium cation that is possibly still coordinated to the dinuclear copper(I) species, as its oxygen still bears a partial negative charge. The cation can then be attacked by a phenol (as shown in Figure 7.6) or by a phenolate to give the coupled phenylether. The calculated data clearly show that the singlet cation is a likely subject for nucleophilic attack on its para carbon.[160]

The triplet cation on the other hand is definitely not a target, since the para carbon bears a partial negative charge. It is not immediately obvious which one of the cationic species will be formed after the two-electron oxidation of a phenolate anion. It can be argued, however, that in the case of a dinuclear (μ-phenoxo)(μ-hydroxo)bridged copper(II) catalytic intermediate, the copper ions are almost certain to be strongly antiferromagnetically coupled.[162] This means that the unpaired electrons of the copper ions will have opposite spins. It stands to reason that after the double one-electron oxidation of the phenolate, the transferred electrons will form electron pairs with the unpaired electrons of the copper ions, as shown schematically in Figure 7.6. To make this possible, these transferred electrons must have opposite spins. Therefore, the overall spin state of the bridging phenolate (S = 0) will not change upon being oxidised to the cation. So, it can be concluded that the phenoxonium cation formed in this reaction will be in the singlet state.[160]

7.3 Reactions with 3,5-di^{tert}butylcatechol

The reaction of 3,5-di^{tert}butylcatechol with oxygenated copper bisguanidine species containg aliphatic or aromatic ligands proceeded even at low temperatures very fast. The formation of the oxidised product, 3,5-di^{tert}butyl-*o*-quinone, could be observed by means of UV/vis spectroscopy. 3,5-di^{tert}butyl-*o*-quinone shows a diagnostic absorption band at 400 nm. The development of this absorption band is a good probe to investigate the kinetics of the oxidation reaction. As example for this type of reactions, the time-dependent UV/Vis absorption spectra of the reaction of $[(DMPG_2mX)_2Cu_2O_2]^{2+}$ at -80°C in CH_2Cl_2 with 3,5-DTBC is presented in Figure 7.7. Very often, the oxidation reaction proceeds too fast even at -80°C to be followed by UV/vis spectroscopy. This was the case with all bisguanidine ligands incorporating an aliphatic spacer. Generally, these ligands show higher oxidation activitites (see Table 7.1. Appearently, copper dioxygen species supported by bisguanidine ligands with aromatic spacers are milder oxidants. The observation of the absorption band at 400 nm was only possible when there was not already another absorption band present like it is in O-core species the case which exhibit at 300 and 400 nm very strong absorption bands. Hence, the observation of the 3,5-di^{tert}butyl-*o*-quinone absorption band is only possible by using aromatic bisguanidine ligands which stabilise a P-core upon reaction with dioxygen. The absorption at 400 nm can be plotted directly versus the time for a kinetic analysis as it is depicted in Figure 7.8. Oxygen was present in excess, the solution had a concentration of 6.6 mM of substrate which is an excess, too. In the first 70 minutes, the reaction remains

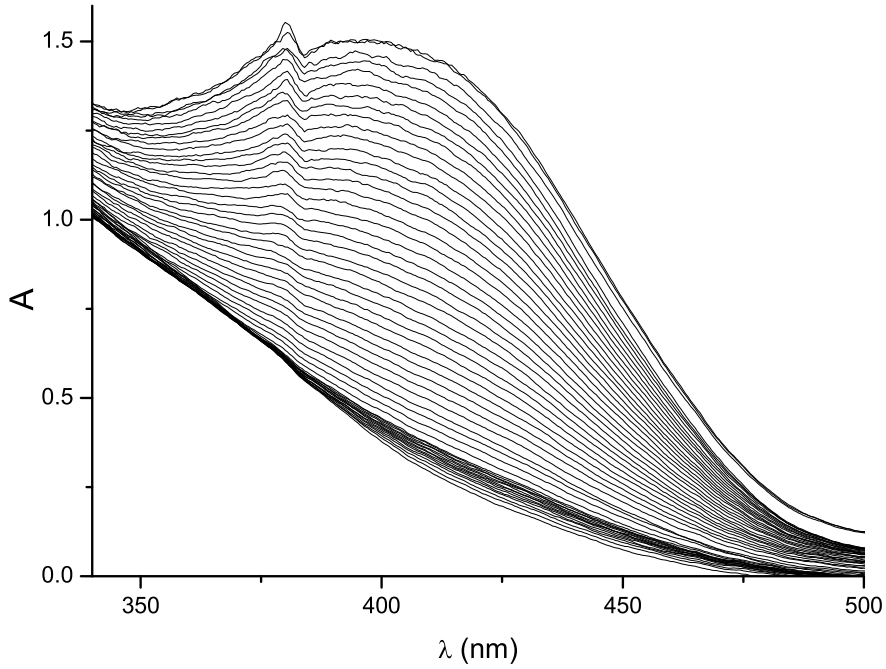

Figure 7.7: UV/vis absorption spectrum observed upon addition of 50 mg 3,5-di^{tert}butylcatechol into a solution of $[(DMPG_2mX)_2Cu_2O_2]^{2+}$ in CH_2Cl_2 (0.5 mM, -80°C) (first section: every 5 min, second section: every 10 min)

relatively slowly. The kinetic constant k_{obs} can be fitted by a zeroth order plot directly from the absorption vs. time plot to be 0.0009 M/min. In the second part of the plot, the reaction proceeds faster with a zeroth order constant of 0.0031 M/min. Possibly, the protons released in the oxidation reactions in the first 100 min facilitate further oxidation reactions resulting in a three times higher reaction rate. The kinetic results can be explained by a nearer look at the kinetic equations: mostly, the reaction is depending in first order from the catalyst, in first order from the substrate and in first order from the oxygen.[53] If the catalyst complex already contains two copper molecules, the prerequisite for the two-electron oxidation from catechol to quinone are given. If a dinuclear catalyst complex has to be formed before the catalytic reaction, the kinetics are more complicated.[53] Hence, in the present case, the observed kinetic constant k_{obs} is described by the following equations:

$$-\frac{dc}{dt} = v_r = k^* c_{cat} c_{subs} c_{O_2}$$

$$k_{obs} = k^* c_{cat} c_{subs} c_{O_2}$$

Oxygen is present in excess; during the reaction, the concentration of the catalyst complex c_{cat} remains constant, unless there are side reactions. The substrate concentration c_{subs} is also comparably high and remains constant as well. Under these conditions, the plot has to be of zeroth order, otherwise, the reaction does not proceed catalytically.

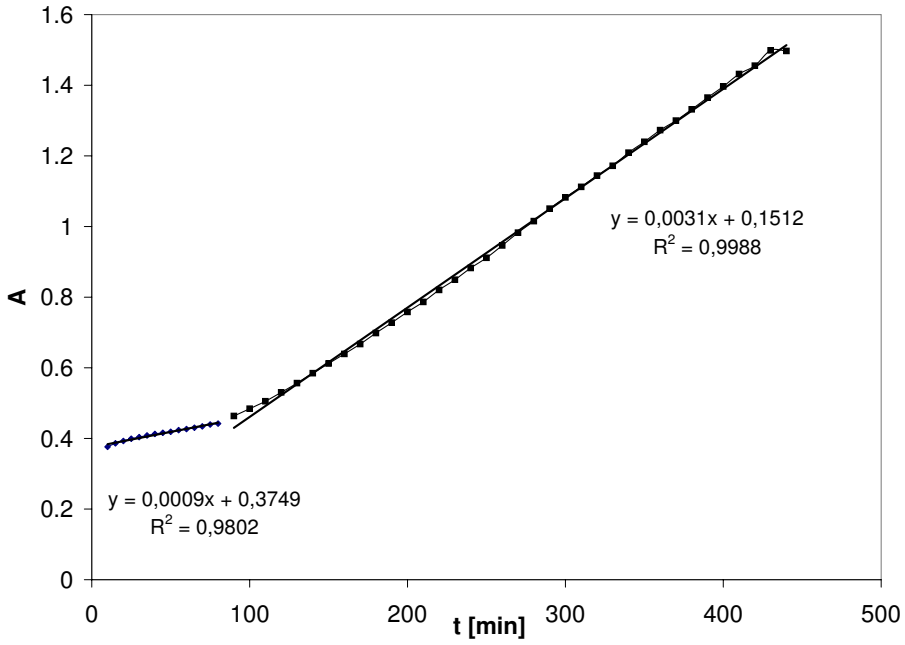

Figure 7.8: Plot of the absorption at 400 nm (3,5-DTBQ) vs. the time for the reaction of $[(DMPG_2mX)_2Cu_2O_2]^{2+}$ in CH_2Cl_2 (0.5 mM, -80°C) with 3,5-DTBC (6.6 mM)

Attempts to vary the concentration of the catalyst complex were not successful because the concentration range for these low temperature UV/Vis measurements is very narrow. The same reason restricted the variation of the substrate concentration. Figure 7.9 shows the absorption vs. time plot at -80°C for a substrate concentration of 13.2 mM. The reaction proceeds faster as the reaction constant of 0.0041 M/min assigns. This observation is in accordance with data reported in the literature [158] referring to Michaelis-Menten kinetics often found in catalytic systems.

Finally, to determine the conversion and the selectivity of the catecholase reaction, the experiments were carried out at room temperature after the following procedure, analogously to that described above for the reaction of 2,4- and 2,6-DTBP. 0.033 mmol of the Cu(I) bisguanidine complex in 10 mL of dichloromethane were oxygenated by stirring for 2 min in the presence of air. Afterwards, 100 mg (0.45 mmol) of 3,5-DTBC were added to the stirred solution. This reaction mixture usually changed its colour from blue-green to dark brown. After 16 h of stirring at room temperature, the reaction was quenched by the addition of 10 mL of 5% perchloric acid. After 5 min of stirring, the phases were separated and the aqueous phase was extracted with dichloromethane. The combined organic phases were dried with Na_2SO_4. These solutions were analysed by means of gaschromatographic separation and mass spectrometric analysis in order to determine the conversion and the selectivity of the reactions.

Since the reaction product 3,5-DTBQ is highly reactive, the presence of 3,5-DTBQ could not

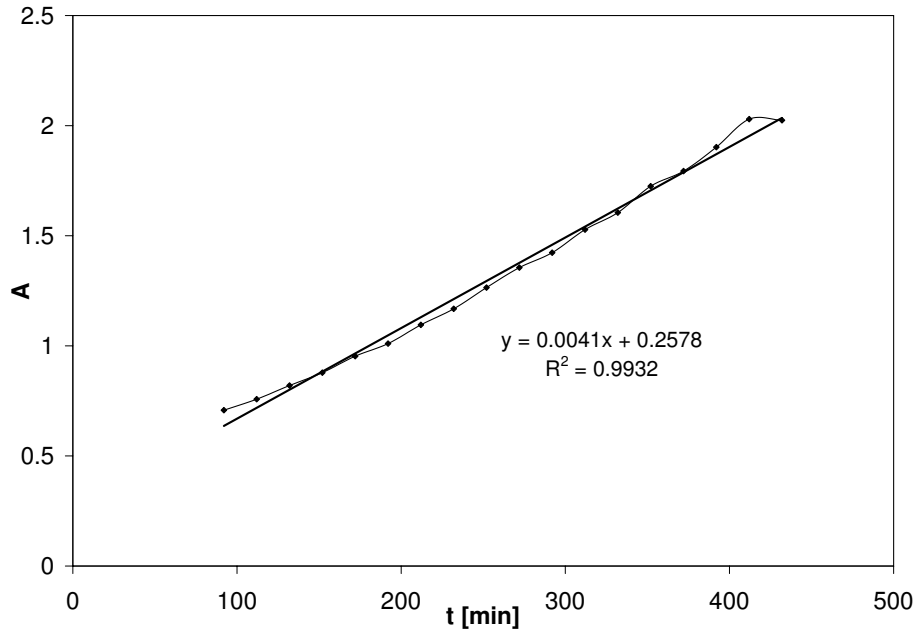

Figure 7.9: Plot of the absorption at 400 nm (3,5-DTBQ) vs. the time for the reaction of $[(DMPG_2mX)_2Cu_2O_2]^{2+}$ in CH_2Cl_2 (0.5 mM, -80°C) with 3,5-DTBC (13.2 mM)

be proved in the GC/MS analysis, but a succeeding product with m/z of 278 and a retention time of 13:02 min instead. The formation of this subsequent product can be understood by regarding the following mechanism (see Figure 7.11).

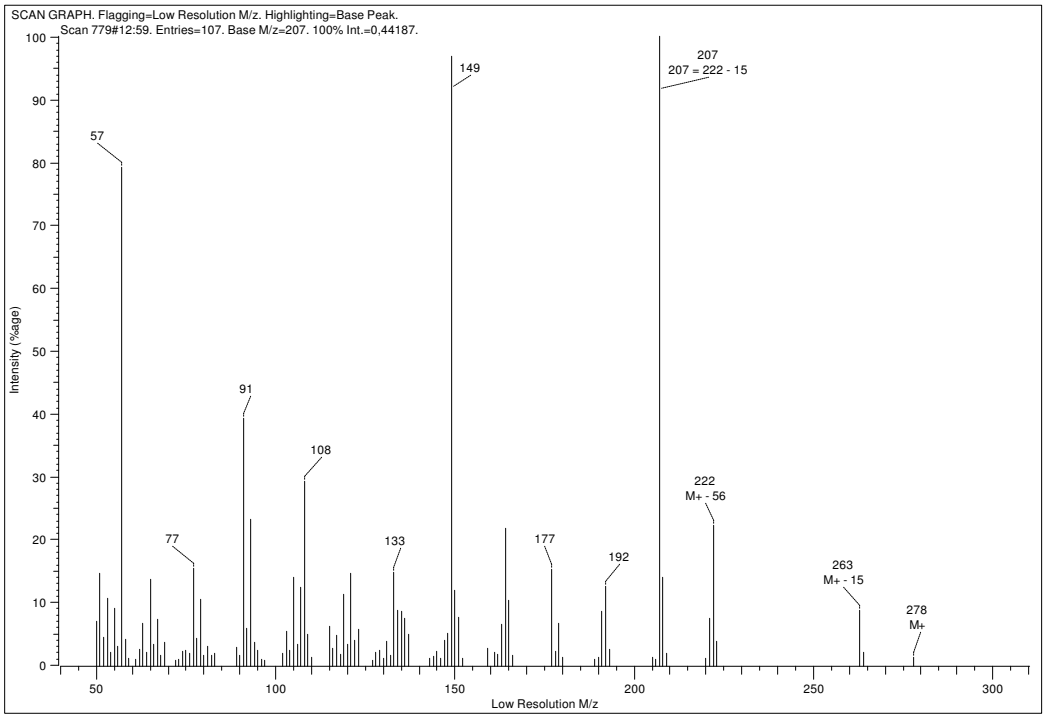

Figure 7.10: Reaction product of 3,5-di^{tert}butylcatechol with the retention time of 13:02 min

3,5-DTBC is known to abstract isobutene in a retro-Friedel-Crafts reaction with Cu(II) as Lewis acid.[163] The isobutene can react with the quinone in a Diels-Alder reaction to the

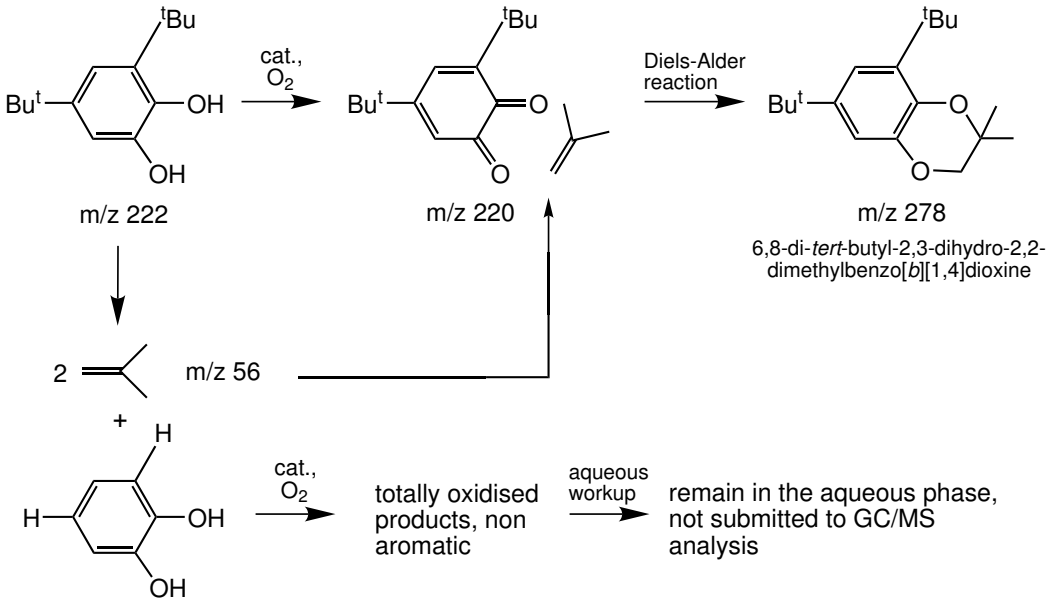

Figure 7.11: Hypothetical mechanism of the reaction of 3,5-DTBC via 3,5-DTBQ to 6,8-di-^{tert}-butyl-2,3-dihydro-2,2-dimethylbenzo[b][1,4]dioxine

aromatic compound 6,8-di-^{tert}-butyl-2,3-dihydro-2,2-dimethylbenzo[b][1,4]dioxine.[164] The driving force of this reaction is the fact that after the Diels-Alder reaction, the aromaticity is restored. However, in the GC/MS data, very often no educt is found and 100 % of the product are present. Thus, all the 3,5-DTBC should have reacted to quinone, but the GC/MS analysis only refers to the organic phase. Comparative studies with unsubstituted catechol show that under these conditions the catechol is oxidised to the point that the C-C bond between the hydroxy functions is broken.[165] Finally, these non-aromatic, totally oxidised residues end up in the aqueous phase and are not submitted to GC/MS analysis. Hence, referring only to the organic phase, the GC/MS data reflect at maximum 66 % yield corrected to the educt compound. The data reported in Table 7.1 are strictly related to the results in the organic phase.

7.4 Screening of the library of bisguanidine ligands regarding the oxidation activity

Based on the results described above, the catalytic oxidation activity of all copper bisguanidine complexes has to be investigated. Therefore, the library of bisguanidine ligands has to be screened regarding the conversion and the selectivity in the oxidation reactions with 2,4-DTBP, 2,6-DTBP and 3,5-DTBC. Table 7.1 summarises the results of the screening of a representative part of the bisguanidine ligand library.

Table 7.1: Screening of representative copper bisguanidine complexes towards their catalytic abilities in % conversion (% selectivity) (*: related to GC/MS data, absolute maximum yield 66 %)

No.	**Catalyst**	**2,4-DTBP**	**2,6-DTBP**	**3,5-DTBC***
1	[Cu(btmgp)I]	100%(60%)	100%(80%)	100%(95%)
2	$[Cu_2(btmgp)_2][PF_6]_2$	90%(95%)	80%(100%)	100%(100%)
3	$[Cu_2(TMG_2ch)_2]I_2$	100%(80%)	100%(100%)	95%(90%)
4	$[Cu_2(TMG_2ch)_2][PF_6]_2$	95%(95%)	90%(100%)	100%(90%)
5	$[Cu(DMEG_2p)I]$	100%(100%)	100%(100%)	100%(95%)
6	$[Cu_2(DMEG_2p)_2][PF_6]_2$	80%(95%)	100%(100%)	100%(95%)
7	$[Cu(DMEG_2ch)I]$	100%(80%)	95%(100%)	95%(95%)
8	$[Cu_2(DMEG_2ch)_2][PF_6]_2$	20%(100%)	10%(100%)	100%(100%)
9	$[Cu_2(DMPG_2p)_2][PF_6]_2$	100%(95%)	40%(95%)	100%(80%)
10	$[Cu(DPPG_2p)]_n[CuI_2]_n$	90%(80%)	50%(100%)	80%(90%)
11	$[Cu(TiPG_2p)I]$	40%(100%)	50%(20%)	100%(100%)
12	$[Cu_2(DPipG_2p)_2][PF_6]_2$	100%(50%)	100%(100%)	100%(20%)
13	$[Cu(B(DMPip)G_2p)I]$	100%(95%)	70%(100%)	60%(95%)
14	$[Cu(B(TMPip)G_2p)I]$	20%(95%)	15%(100%)	20%(95%)
15	$[Cu(DMorphG_2p)I]$	50%(100%)	70%(90%)	100%(100%)
16	$[Cu(TMG_2MePA)I]$	90%(90%)	95%(90%)	90%(20%)
17	$[Cu(TMG_2mX)I]$	70%(80%)	20%(95%)	85%(95%)
18	$[Cu(DMEG_2mX)I]$	80%(90%)	30%(95%)	95%(95%)
19	$[Cu(DMPG_2mX)I]$	95%(70%)	100%(95%)	100%(90%)
20	$[Cu(TMG_2py)I]$	0%(-)	0%(-)	60%(95%)
21	$[Cu(TEG_2py)I]$	30%(100%)	0%(-)	20%(95%)
22	$[Cu(MorphDMG_2p)I]$	40%(100%)	70%(95%)	10%(100%)
23	$[Cu((DMPip)DMG_2p)I]$	40%(100%)	30%(60%)	100%(100%)
24	$[Cu(B^FPPG_2p)I]$	70%(95%)	80%(100%)	90%(95%)

Special attention has been paid to the role of the counterion (coordinating or non-coordinating) and the type of the spacer (aromatic or aliphatic). Conversion and selectivity are based on the gaschromatographic data. The mass spectrometric analysis assured that the product could be identified (vide supra). All catalytic experiments were carried out after

the procedure already described in the sections 7.2 and 7.3.

Comparing the activity of copper iodine and copper hexafluorophosphate containing complexes, complexes based on CuI reach better conversions (entries No. 1, 3, 5, and 7). Possibly, the iodine acts as co-catalyst in the electron transfer. Incorporating the same guanidine moiety, complexes with aliphatic bisguanidine ligands (Nos. 1 - 10) seem to be better catalysts than those with aromatic bisguanidine ligands (Nos. 15 - 20). When the guanidine groups get highly sterically demanding, the conversion is decreasing (Nos. 11, 13, 14, 15) as the access to the active centre is made more difficult. Perhaps, by using a substrate with smaller subsituents, the conversion can be enhanced. The optimisation of the catalyst-substrate-relationship is object to further investigations. However, the selectivity in exactly these systems is relatively high. The non-symmetric systems (Nos. 22 and 23) do not show sufficient conversion bot relatively good selectivities. The perfluorinated system of No. 24 exhibits average conversions and very good selectivities. This can be explained by the extraordinary stability of the oxygenated species (see section 5.2) which is too stable to be a strong oxidant. The properties of a mild oxidant are accompanied by higher selectivities as potential side reactions are supressed.

Figure 7.12 denotes the reaction yields of selected catalyst complexes. Catalyst no. 5 incorporating an aliphatic ligand is an effective catalyst for all three reactions as the reactions yields are at their maximum values. Catalyst no. 9 contains a similar ligand with slightly bigger guanidine moieties, but the yield of the coupling reaction of 2,6-DTBP decreases drastically. This trend is confirmed by catalyst no. 11, a highly sterically hindered system with tetra-iso-propylguanidine groups, which generally shows lower conversions (Table 7.1). Catalyst no. 15 also shows lower yields for 2,4- and 2,6-DTBP, but with reversed relation: now, the reaction with 2,6-DTBP is favourised over the reaction with 2,4-DTBP. Probably, the dimorpholinoguanidino unit can fold up better than the other systems. Until this point of discussion, the yields for the reaction with 3,5-DTBC were very good. In the case of no. 16, the aromatic TMG_2MePA system supports such a strong oxidant that the reaction products are destroyed oxidatively resulting in only 20% yield for the product with 3,5-DTBC and almost 90% yield for the phenolic substrates. Contrarily, the pyridine-based systems of nos. 20 and 21 are such weak catalysts that they only oxidise 3,5-DTBC sufficiently. The small difference of tetramethylguanidino (No. 20) to tetraethylguanidino (No. 21) units results in 30% more yield for the 2,4-DTBP dimerisation for No. 21 but 40 % less yield for the oxidation of 3,5-DTBC. Catalyst no. 22, a non-symmetric system, is the single catalyst which exhibits clearly better yields for both of the phenolic substrates than for the catechol.

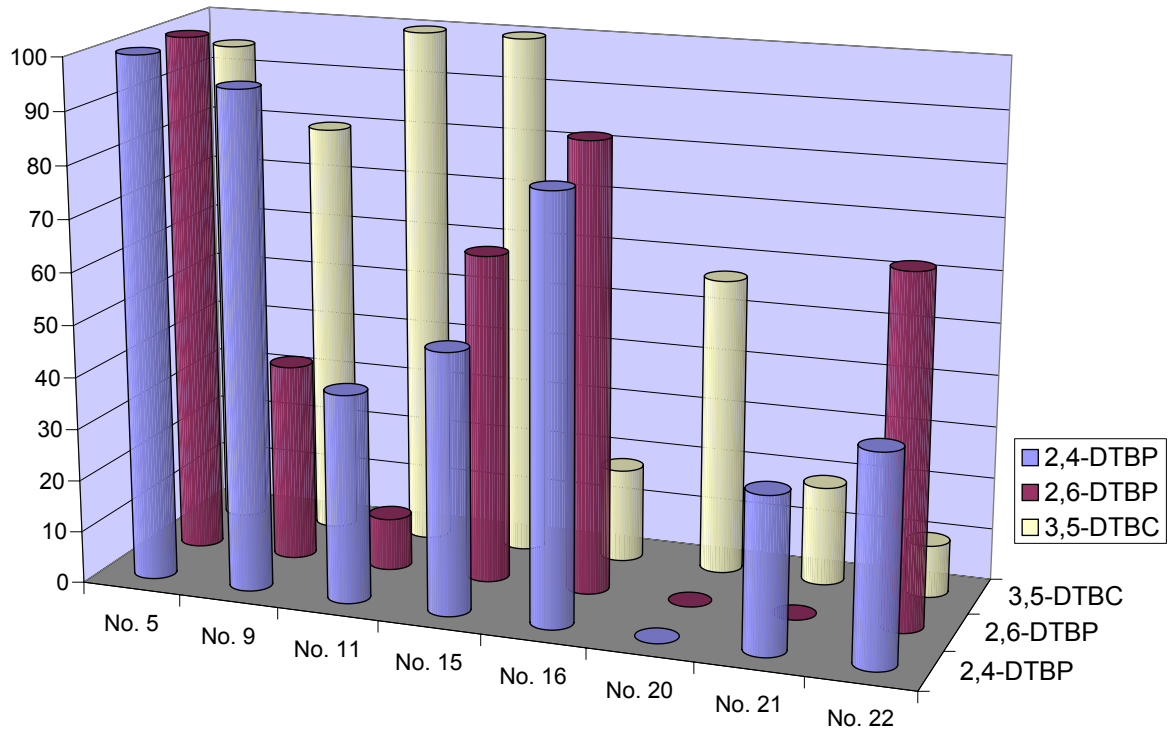

Figure 7.12: Overview of the reaction yields (conversion x selectivity) selected complexes

7.5 Conclusion of the catalytic results

In summary, bisguanidine copper complexes represent a new class of oxidation catalysts. The ability of oxidation is depending from the accessibility of the reaction centre: "small" ligands result in better oxidation catalysts whereas sterically demanding systems show with substrates like 2,4-DTBP and 2,6-DTBP reduced conversions by high selectivity. The results show that the reactivity of the catalysts can be controlled by the steric impact of the guanidine substituents. Ligands with high steric demands are supposingly better suited for the oxidation of substrates with smaller substituents like 2,6-dimethylphenol. The polymerisation of 2,6-dimethylphenol is an important research field [38] as the polymerisation product PPO is a high melting, very resistant plastic. Examples like no. 20 and 21, where the difference between methyl and ethyl groups changes the catalytic situation totally, reveal that there are numerous effects imposed on the reaction centre which can not be predicted. For each substrate can be designed a suited catalytic system by comparing the electronic features of the ligand spacer, the steric demand of the substituents and the role of the counterion. The present screening of the library of bisguanidine ligands provides with some clues in tailored ligand design for copper-catalysed reactions.

8 Experimental Section

8.1 Material and Methods

8.1.1 General Remarks

All manipulations were performed under pure dinitrogen (99,996%) dried with P_4O_{10} granulate using Schlenk techniques or a glovebox and with abs. solvents. Solvents were purified according to literature procedures and also kept under nitrogen. Triethylamine and 1,3-diaminopropane were used as purchased from Fluka.

8.1.2 Physical measurements

NMR spectroscopy: The ^{1}H, ^{13}C and ^{19}F spectra were recorded with the spectrometers Bruker AMX 300 (^{1}H: 300.13 MHz, ^{13}C: 75.47 MHz, ^{19}F: 282.38 MHz) and WMX 500 (^{1}H: 500.13 MHz, ^{13}C: 125.77 MHz), respectively. The solvents and temperatures are noted for every substance.
EXSY ^{1}H NMR measurements: Temperature variable EXSY spectra of compounds **L1-1**, **L1-2** and **L1-4** were recorded with the pulse program noesygpph from Bruker's pulse program library. The mixing time tm was optimised according to the literature [166] and amounted to 200 ms. As the observed exchange process of the methyl groups is a simple two-side case with equal populations and uncoupled spins the exchange rate constant is calculated [166] from the integrals of diagonal- and cross-peaks: $k = \tau - m^{-1}\ \ln[(r+1)/(r-1)]$ with $r = (I_{D1}+I_{D2})/(I_{C1}+I_{C2})$ and I_{D1}, I_{D2} = Integrals of the diagonal peaks; I_{C1}, I_{C2} = Integrals of the cross-peaks.
IR spectroscopy: The infrared spectra were recorded with the FT-IR spectrometer Nicolet P510.
UV/Vis spectroscopy: The UV/Vis spectra were recorded with a Perkin-Elmer Lambda 45 spectrometer in combination with the Hellma UV/Vis-low temperature-interface (1cm path length cell), excess O_2.
Crystal Structure Analyses: Crystal data for all compounds are presented in the Appendix. X-ray diffraction data were collected with a Bruker-AXS SMART APEX CCD diffractometer using MoK_α radiation ($\lambda = 0.71073$ Å). Data reduction and absorption correction were performed with SAINT and SADABS.[167] The structures were solved by direct and conventional Fourier methods and all non-hydrogen atoms refined anisotropically with full-matrix least-squares procedures based on F^2 (SHELXTL [167]). Hydrogen atoms were derived from difference Fourier maps and placed at idealized positions, riding on their parent C atoms, with isotropic displacement parameters $U_{iso}(H) = 1.2U_{eq}(C)$ and $1.5U_{eq}$(C methyl).

All methyl groups were allowed to rotate but not to tip.

Mass spectrometry: The EI mass spectra were recorded at a Finnigan MAT 40 mass spectrometer with 70 eV and 200°C source temperature; the CI mass spectra at the same spectrometer with isobutane as reactand gas and 130°C source temperature. The GC-MS unit contains a F-S capillar DB5 30m (0.25mm, 0.2 μm, 1 μL split 1:150, He: 0.4 bar). The temperature program was 80°C, 1 min; 10°/min; 300°C.

Elemental analyses: The elemental analyses were performed with a Perkin-Elmer 2400 analysator. Microanalyses for hexafluorophosphate containing compounds were performed at the Mikroanalytisches Labor, Ilse Beetz, Kronach, Germany.

Cyclic voltammetry: Cyclovoltammetric measurements were performed with the electrochemical device Metrohm E 505 equipped with a potentiostat Model VersaStat by EG&G in combination with the PC-program Electrochemical Analysis Software 3.0 Model 250 by EG&G. The electrochemical cell was operated under argon, with glassyC/glassyC/Ag/AgCl or Au/Pt/saturated Ag/AgCl serving as working, counter and reference electrodes, respectively. CV curves were obtained at scan rates of 100mV/s working at 25°C in MeCN/0.1 m nBu$_4$NPF$_6$. As the complexes are extremely air sensitive, the copper(I) solutions were transferred into the CV cell with a steel capillar under argon pressure.

8.2 Synthesis of educt compounds

Tetrakis(acetonitrile)copper(I)hexafluorophosphate [Cu(MeCN)$_4$][PF$_6$] *Caution! The following procedure should be carried out in a well-ventilated hood because of the toxicity of the HF fumes evolved from HPF$_6$.* To a mechanically stirred suspension of 4.0 g (28 mmol) of copper(I)oxide in 80 mL of MeCN in a 125 mL Erlenmeyer flask is added 10 mL of 60-65% HPF$_6$ (about 113 mmol of HPF$_6$) in 2 ml protions. The reaction is very exothermic and may cause the solution to boil. However, the reaction temperature is not critical and the warming is beneficial in that the product remains dissolved. After addition of the final portion of HPF$_6$, the solution is stirred for about 3 min and is then filtered hot through a medium-porosity frit to remove small amounts of undissolved black solid (some white [Cu(MeCN)$_4$][PF$_6$] may begin to crystallise before filtration; if so, it is washed with a minimum amount of MeCN). The pale-blue solution is cooled in a freezer to about -20°C for several hours (addition of an equal volume of diethyl ether and cooling to 0°C yields equivalent results), whereupon a blue-tinged white microcrystalline precipitate of [Cu(MeCN)$_4$][PF$_6$] forms. The solid is collected by filtration, washed with diethyl ether, and immediately redissolved in 100 mL of MeCN. A small amount of blue material, presumably a Cu^{2+} species, remains undissolved and is removed by filtration. To the filtrate (which may still retain a slight blue colour) is added 100 mL of diethyl ether, and the mixture is allowed to stand for several hours at -20°C. The precipitated complex may still retain a bluish cast, in which case a second recrystallisation may be necessary if high purity is desired. This second recrystallisation is carried out using 80 mL each of MeCN and diethyl ether. The product is pure white and is dried *in vacuo* for about 30 min immediately after being washed with diethyl ether. The yield is 12.5 g (60%) and is dependent on recrystallisation losses.

1,3-Bis(*N,N,N´,N´*-tetramethylguanidino)propane (btmgp):[105, 112]
1,3-Dibromopropane (14 mL, 0.14 mmol) was added to freshly distilled *N,N,N´,N´*-tetramethylguanidine (100 mL, 0.80 mol) and heated to 100°C for 12 h. During this time, the reaction mixture solidified. The excess of tetramethylguanidine was distilled off and a freshly prepared sodium ethoxide solution [6.6 g (0.28 mol) Na in 70 mL ethanol/70 mL THF] was added to the pale brown residue. The mixture was stirred for 5 h. The resulting NaBr was filtered off and the solvents, together with any remaining tetramethylguanidine, were removed under reduced pressure at room temperature. The product was isolated by vacuum distillation (b.p. 110°C/0.05 mbar). Yield: 15.2 g (41 %)
^{1}H-NMR (300 MHz, $CDCl_3$, 25°C): δ = 1.56 (qi, 2H, CH_2, ^3J = 6.7 Hz), 2.44 (s, 12H, CH_3), 2.99 (t, 4H, CH_2, ^3J = 6.7 Hz) ppm. ^{13}C-NMR (75 MHz, $CDCl_3$, 25°C): δ = 35.2 (CH_2), 38.5 (CH_3), 39.3 (CH_3), 47.3 (CH_2), 159.6 (C_{gua}) ppm. IR (film between NaCl plates, $\tilde{\nu}$ [cm^{-1}]): 2994*m*, 2931*s*, 2913*s*, 2870*vs*, 2836*s*, 2799*m*, 1622*vs* ($\tilde{\nu}$(C=N)), 1494*m*, 1451*m*, 1363*vs*, 1310*w*, 1234*m*, 1184*w*, 1135*s*, 1108*w*, 1092*w*, 1062*m*, 1025*w*, 1011*m*, 984*w*, 957*w*, 913*m*, 881*w*, 810*w*, 746*m*, 725*w*, 648*w*, 577*m*, 501*w*, 436*vw*.

8.3 Synthesis of product compounds

8.3.1 Synthesis of substituted ureas

N,N,N´,N´-Dipropylpropyleneurea. Based on a literature procedure,[131] N,N´-trimethyleneurea (Fluka, 0.05 mol, 5 g) was treated in freshly destilled dioxane (200 mL) with NaH (0.11 mol, 2.64 g). The reaction mixture was heated to reflux for 16 h and then cooled to room temperature. After propyl iodide (0.2 mol, 34.0 g, 59.2 mL) was added, the reaction mixture was heated to reflux for further 16 h and filtered to remove precipitated NaI. After evaporation of the solvent, vacuum destillation of the residual oil yields the product as yellow oil yield ca. 60 %. ^{1}H-NMR (500 MHz, $CDCl_3$, 25°C): δ = 0.83 (t, 6H, CH_3), 1.50 (m, 4H, CH_2), 1.89 (m, 2H, CH_2), 3.23 (m, 8H, CH_2) ppm. ^{13}C-NMR (125 MHz, $CDCl_3$, 25°C): δ = 11.2 (CH_3), 21.0 (CH_2), 22.5 (CH_2), 45.7 (CH_2), 49.7(CH_2), 155.9 (C. quart) ppm.

N,N,N´,N´-Bis(heptafluoropropyl)propyleneurea. N,N´-trimethyleneurea (Fluka, 0.05 mol, 5 g) was treated in freshly destilled diethylether (200 mL) with NaH (0.11 mol, 2.64 g). The reaction mixture was heated to reflux for 36 h and then cooled with ice-water. After heptafluoropropyl iodide (0.1 mol, 29.2 g, 24 mL) was added, the reaction mixture was heated to reflux for further 36 h and filtered over chromatographic silica to remove precipitated NaI. Isolation is impossible due to the high volatility (b.p. $\approx$ 25°C)
^{19}F (282.38 MHz, C_6D_6, 25°C): δ = -83.3 (t, 6F, CF_3), -133.5 (t, 2F, CF_2), -139.3 (m, 2F, CF_2) ppm.

8.3.2 Synthesis of Vilsmeier salts

Caution! Phosgene is a severe toxic agent that can cause pulmonary embolism and in the case of heavy exposition may be lethal. Use only in a well-ventilated fume hood.

***N,N,N´,N´*-Tetramethylchloroformamidinium Chloride (V1):**

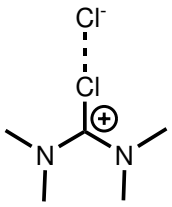

In a Schlenk flask fitted with a condensor cooled to -30°C, phosgene was passed at 0°C through a solution of tetramethylurea (Fluka, 48.4 g, 417 mmol, 50 mL) in dry toluene (300 mL) for 60 min. The reaction mixture was stirred 2 h at room temperature and for further 24 h at 30°C. After the mixture cooled to room temperature, the white solid was filtrated and washed with dry diethyl ether. The residual white powder was dried in vacuo, yield: 95 %.

***N,N,N´,N´*-Tetraethylchloroformamidinium Chloride (V2):**

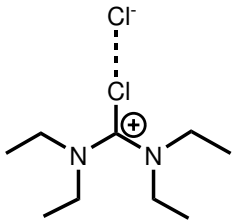

In a Schlenk flask fitted with a condensor cooled to -30°C, phosgene was passed at 0°C through a solution of tetraethylurea (Fluka, 263 mmol, 50 mL) in dry toluene (300 mL) for 60 min. The reaction mixture was stirred 2 h at room temperature and for further 24 h at 40°C. After the mixture cooled to room temperature, the toluene was decanted. The residual yellow oil was washed with dry diethylether and dried in vacuo, yield: 95 %.

^{1}H-NMR (500 MHz, $CDCl_3$, 25°C): d= 1.30 (t, 12H, CH_3), 3.71 (q, 8H, CH_3) ppm.

***N,N,N´,N´*-Tetraisopropylchloroformamidinium chloride (V3):**

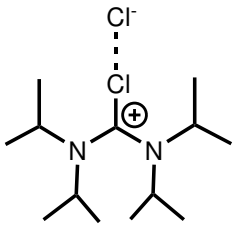

In a Schlenk flask fitted with a condensor cooled to -40°C, phosgene was passed through a solution of diisopropylamine (0.2 mol, 20.2 g, 14.5 mL) and NEt_3 (0.2 mol, 20.2 g, 27.9 mL) in dry MeCN (200 mL) at 0°C (attention: highly exothermic) for 15 min. The formation of the urea took place immediately, the solution was not stirrable due to its high viscosity. After 30 min, the reaction mixture was allowed to come to room temperature and it was stirred again. Then, the mixture was heated for 40 h to 40°C. After the mixture cooled to room temperature, the solvent was evaporated under reduced pressure in order to obtain the product with NEt_3HCl as by-product as colourless wax, yield ca. 80 % (22.6 g).

***N,N,N´,N´*-Dimethylethylenchloroformamidinium Chloride (V4):**

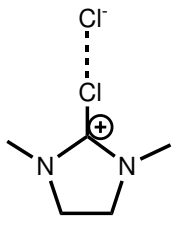

In a Schlenk flask fitted with a condensor cooled to -30°C, phosgene was passed at 0°C through a solution of 1,3-dimethyl-2-imidazolidinone (Fluka, 68.5 g, 600 mmol) in dry toluene (300 mL) for 50 min. The reaction mixture was stirred for 2 h at room temperature and for another 12 h at 40°C. After the mixture cooled down to room temperature, the white precipitate formed was collected by filtration, washed three times with dry diethyl ether, and dried in vacuo, yield: 95 %.

***N,N,N´,N´*-Dimethylpropylenchloroformamidinium Chloride (V5):**

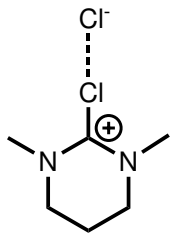

In a Schlenk flask fitted with a condensor cooled to -30°C, phosgene was passed at 0°C through a solution of N,N,N´,N´-Dimethylpropyleneurea (Fluka, 76.9 g, 600 mmol) in dry toluene (300 mL) for 50 min. The reaction mixture was stirred for 2 h at room temperature and for another 24 h at 40°C. After the mixture cooled down to room temperature, the white precipitate formed was collected by filtration, washed three times with dry diethyl ether, and dried in vacuo, yield: 95 %.

***N,N,N´,N´*-Dipropylpropylenchloroformamidinium Chloride (V6):**

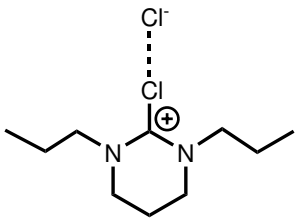

In a Schlenk flask fitted with a condensor cooled to -30°C, phosgene was passed at 0°C through a solution of N,N,N´,N´-Dipropylpropyleneurea (90 mmol, 16.6 g) in dry toluene (150 mL) for 20 min. The reaction mixture was stirred for 2 h at room temperature and for another 80 h at 40°C. After the mixture was cooled to room temperature, the toluene was decanted. The residual orange oil was washed with dry diethylether and dried in vacuo, yield: 80 %. ^{1}H-NMR (500 MHz, $CDCl_3$, 25°C): δ = 0.86 (t, 6H, CH_3), 1.65 (m, 4H, CH_2), 2.19 (m, 2H, CH_2), 3.62 (t, 4H, CH_2), 3.87 (t, 4H, CH_2) ppm. ^{13}C-NMR (125 MHz, $CDCl_3$, 25°C): δ = 10.8 (CH_3), 19.6 (CH_2), 20.7 (CH_2), 49.5 (CH_2), 57.7 (CH_2), 151.1 (C. quart) ppm.

***N,N,N´,N´*-Dipiperidylchloroformamidinium Chloride (V7):**

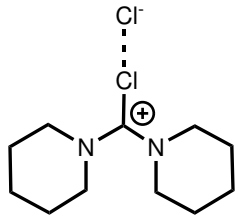

In a Schlenk flask fitted with a condensor cooled to -30°C, phosgene was passed at 0°C through a solution of 1,1´-carbodipiperidine (Aldrich, 12.5 g, 63.8 mmol) in dry MeCN (200 mL) for 30 min. The reaction mixture was stirred 6 h at room temperature and for another 36 h at 40°C. After the mixture cooled down to room temperature, the solvent was evaporated under reduced pressure in order to obtain the product as colourless oil, yield ca. 70 %.

***N,N,N´,N´*-Bis(dimethylpiperidyl)chloroformamidinium chloride (V8):**

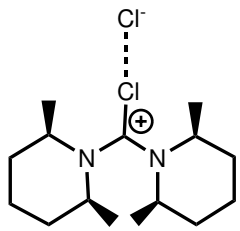

In a Schlenk flask fitted with a condensor cooled to -30°C, phosgene was passed through a solution of cis-2,6-dimethylpiperidine (0.1 mol, 11.3 g, 9.3 mL) and NEt_3 (0.1 mol, 10.1 g, 14.0 mL) in dry MeCN (200 mL) at 0°C for 15 min. After 30 min, the reaction mixture was allowed to come to room temperature and heated for 36 h to 40°C. After the mixture cooled to room temperature, the solvent was evaporated under reduced pressure in order to obtain the product as well as NEt_3HCl as colourless powder, yield ca. 65 %.

***N,N,N´,N´*-Bis(tetramethylpiperidyl)chloroformamidinium chloride (V9):**

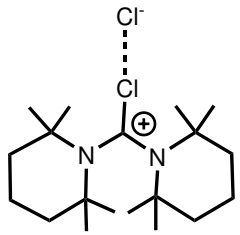

In a Schlenk flask fitted with a condensor cooled to -30°C, phosgene was passed through a solution of 2,2,6,6-tetramethylpiperidine (0.1 mol, 14.1 g, 11.7 mL) and NEt_3 (0.1 mol, 10.1 g, 14.0 mL) in dry MeCN (200 mL) at 0°C for 15 min. After 30 min, the reaction mixture was allowed to come to room temperature and heated for 50 h to 40°C. After the mixture cooled to room temperature, the solvent was evaporated under reduced pressure in order to obtain the product as well as NEt_3HCl as yellow powder, yield ca. 57 %.

N,N,N´,N´-Diimidazolylchloroformamidinium chloride (V10):

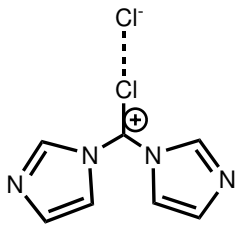

In a Schlenk flask fitted with a condensor cooled to -30°C, phosgene was passed at 0°C through a solution of 1,1´-carbonyl-diimidazole (Fluka, 154 mmol, 25 g) in dry MeCN (300 mL) for 15 min. The reaction mixture was stirred for 2 h at room temperature and for another 30 h at 40°C. After the mixture was cooled to room temperature, the excess of phosgene and the MeCN were evaporated under reduced pressure. The yellow residue was dried in vacuo, yield: 80 %.

N,N,N´,N´-Dimorpholinochloroformamidinium chloride (V11):

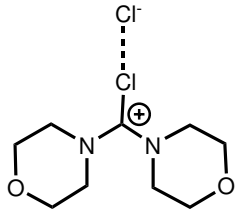

In a Schlenk flask fitted with a condensor cooled to -40°C, phosgene was passed through a solution of morpholine (0.2 mol, 17.4 g, 17.5 mL) and NEt_3 (0.2 mol, 20.2 g, 27.9 mL) in dry MeCN (250 mL) at 0°C (attention: highly exothermic) for 15 min. The formation of the urea took place immediately, the solution was not stirrable due to its high viscosity. After 30 min, the reaction mixture was allowed to come to room temperature and it was stirred again. Then, the mixture was heated for 50 h to 40°C. After the mixture cooled to room temperature, the solvent was evaporated under reduced pressure in order to obtain the product with NEt_3HCl as by-product as yellow oil, yield ca. 70 %.

N,N,N´,N´-Dithiomorpholinochloroformamidinium chloride (V12):

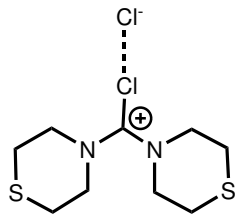

In a Schlenk flask fitted with a condensor cooled to -40°C, phosgene was passed through a solution of thiomorpholine (0.49 mol, 5 g) and NEt_3 (0.97 mol, 9.7 g, 13.4 mL) in dry MeCN (150 mL) at 0°C for 15 min. After 30 min, the reaction mixture was allowed to come to room temperature and heated for 50 h to 40°C. After the mixture cooled to room temperature, the solvent was evaporated under reduced pressure in order to obtain the product as well as NEt_3HCl as yellow powder, yield ca.45 %.

8.3.3 Synthesis of guanidine ligands

General synthesis of bisguanidine ligands with chloroformamidinium chlorides V1, V2, V4, V5, V6, V7 and V10:
A solution of the chloroformamidinium chloride (40 mmol) in dry MeCN (60 mL) was added dropwise under vigorous stirring to an ice-cooled solution of a bisamine (20 mmol) and triethylamine (5.57 mL, 4.04 g, 40 mmol) in dry MeCN (30 mL). After 3 h at reflux, a solution of NaOH (1.6 g, 40 mmol) in water was added. Under vacuum, solvents and NEt_3 were evaporated. In order to deprotonate the bis-hydrochloride, 50 wt % KOH (aq, 25 mL) was added and the free base was extracted into the MeCN phase (3x25 mL). The organic phase was dried with Na_2SO_4 over charcoal. After filtration over Celite, the solvent was evaporated under reduced pressure.

General synthesis of bisguanidine ligands with chloroformamidinium chlorides V3, V8, V9, V11, V12:
The reaction mixture containing the chloroformamidinium chloride (40 mmol) in dry MeCN (60 mL) was added dropwise under vigorous stirring to an ice-cooled solution of a bisamine (20 mmol) and triethylamine (5.57 mL, 4.04 g, 40 mmol) in dry MeCN (30 mL). After 3 h at reflux, a solution of NaOH (4.8 g, 120 mmol) in water was added. Under vacuum, solvents and NEt_3 were evaporated. In order to deprotonate the bis-hydrochloride, 50 wt % KOH (aq, 25 mL) was added and the free base was extracted into the MeCN phase (3x25 mL). The organic phase was dried with Na_2SO_4 over charcoal. After filtration over Celite, the solvent was evaporated under reduced pressure.

2-(2-(2-(tetramethylguanidino)ethoxy)ethoxy)-N-(tetramethylguanidino)ethaneamine, TMG_2doo (L1-2):

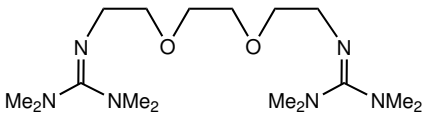

Colourless oil, yield: 96 %. ^{1}H-NMR (500 MHz, $CDCl_3$, 25°C): δ = 2.51 (s, 12H, CH_3), 2.60 (s, 12H, CH_3), 3.19 (t, 4H, CH_2, ^3J = 6.9 Hz), 3.44 (t, 4H, CH_2, ^3J = 6.9 Hz), 3.51 (s, 4H, CH_2) ppm. ^{13}C-NMR (125 MHz, $CDCl_3$, 25°C): δ = 38.6 (CH_3), 39.5 (CH_3), 49.4 (CH_2), 70.2 (CH_2), 73.3 (CH_2), 160.8 (C_{gua}) ppm. IR (film between NaCl plates, $\tilde{\nu}$ [cm^{-1}]): 2995*w*, 2868*vs*, 2800*w*, 1619*vs* ($\tilde{\nu}$ (C=N)), 1496*m* ($\tilde{\nu}$ (C=N)), 1452*m* ($\tilde{\nu}$ (C=N)), 1367*vs*, 1299*w*, 1236*m*, 1137*s* ($\tilde{\nu}$ (C-O-C)), 1064*m* ($\tilde{\nu}$ (C-O-C)), 991*w*. EI-MS (m/z, (%)): 344.4 (1) [M^+], 300 (5) [M^+ - NMe_2], 230 (2) [M^+- $(NMe_2)_2CN$], 186 (7) [M^+- $(NMe_2)_2CN(CH_2)_2O$], 173 (8) [M^+- NMe_2, $NC(NMe_2)_2$], 141 (71) [M^+- $(NMe_2)_2CN(CH_2)_2O$], 129 (44) [M^+- $(NMe_2NCH_3CN(CH_2)_2O(CH_2)_2$], 114 (6) [$M^+$- $(NMe_2)_2CN(CH_2)_2O(CH_2)_2$], 100 (17), 85 (100) [$M^+$- $(NMe_2)_2CN(CH_2)_2O(CH_2)_2N$, CH_3], 71 (17) [M^+- $(NMe_2)_2CN(CH_2)_2O(CH_2)_2$, NMe_2]. elemental analysis, calcd. for $C_{16}H_{36}N_6O_2$: C 55.77, H 10.54, N 24.40 ; found : C 55.54, H 10.89, N 24.15.

[H_2 TMG_2doo]I_2·Et_2O ([H_2L1-2]I_2·Et_2O):

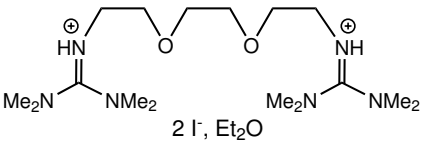

Compound **L1-2** (688 mg, 2 mmol) was dissolved in THF (10 mL) and added to a suspension of ammonium iodide (576 mg, 4 mmol) in THF (10 mL). The reaction mixture was refluxed for 2 h and the solvent removed under reduced pressure. The resulting precipitate was dissolved in acetonitrile (15 mL) and filtered. Diethylether was added to the colourless filtrate by vapor diffusion to form [H_2L1-2]I_2 as colourless needles. ^{1}H-NMR (500 MHz, CD_3CN, 25 °C): δ = 2.95 (s, 12H, CH_3), 3.09 (s, 12H, CH_3), 3.37 (t, 4H, CH_2, ^3J = 5.2 Hz), 3.61 (s, 4H, CH_2), 3.78 (t, 4H, CH_2, ^3J = 5.2 Hz), 8.8 (s, very broad, 2H) ppm. ^{13}C-NMR (125 MHz, $CDCl_3$, 25°C): δ = 40.0 (CH_3), 40.4 (CH_3), 45.3 (CH_2), 69.4 (CH_2), 70.4 (CH_2), 162.2 (C_{gua}) ppm. IR (KBr, $\tilde{\nu}$ [cm^{-1}]): 3456*m* ($\tilde{\nu}$ (N-H)), 3178*m* ($\tilde{\nu}$ (N-H)), 2943*w*, 2858*w*, 1620*vs* ($\tilde{\nu}$ (C=N)), 1584*vs* ($\tilde{\nu}$ (C=N)), 1462*m*, 1450*m*, 1404*s*, 1315*w*, 1173*w*, 1135*m*, 1115*m*, 1092*m*, 889*w*. elemental analysis (after drying *in vacuo*), calcd. for $C_{16}H_{38}N_6O_2I_2$: C 31.99, H 6.38, N 14.00 ; found : C 32.19, H 6.23, N 13.93.

***N*^{1},*N*^{3}-bis(1,1,3,3-tetramethyl-guanidine)-cyclohexane-1,3-diamine, TMG_2ch (L1-3):**

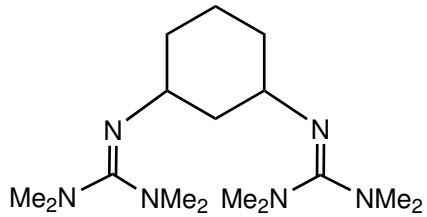

Colourless oil, yield: 95 %. ^{1}H-NMR (500 MHz, $CDCl_3$, 25 °C): δ = 1.0-1.6 (m, 8H, CH_2 from ring), 2.42 (s, 12H, CH_3), 2.49 (s, 12H, CH_3), 3.44 (m, 2H, CH) ppm. ^{13}C-NMR (125 MHz, $CDCl_3$, 25 °C): δ = 20.0 (CH_2), 32.6 (CH_2), 33.7 (CH_2), 39.1 (CH_3), 39.6 (CH_3), 50.7 (CH), 159.2 (C_{gua}) ppm. IR (film between NaCl plates, $\tilde{\nu}$ [cm^{-1}]): 2993*m*, 2925*m*, 2856*m*, 1618*vs*($\tilde{\nu}$ (C=N)), 1496*vs* ($\tilde{\nu}$ (C=N)), 1450*s*, 1402*m*, 1363*m*, 1236*m*, 1126*s*, 1056*w*, 1012*w*. EI-MS: m/z (%): 310.3 (49) [M^+], 267 (11) [M^+-NMe_2+H], 212 (5), 195 (50), 151 (75), 100 (52), 85 (55), 71 (100), 57 (22). elemental analysis calcd. for $C_{16}H_{34}N_6$: C 61.88, H 11.04, N 27.08 ; found : C 61.72, H 11.38, N 26.90.

2,2´-Bis[2*N*-(1,1´,3,3´-tetramethyl-guanidine)]-diphenyleneamine, TMG_2PA (L1-4):

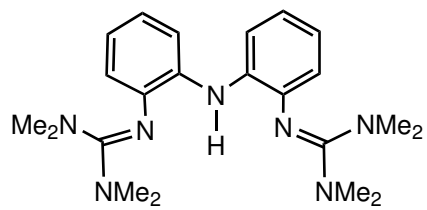

Off-white powder, after recrystallisation colourless needles, yield: 81 %, m.p. 128°C. ^{1}H-NMR (500 MHz, $CDCl_3$, 25 °C): δ = 2.68 (s, 24H, CH_3), 6.53 (dd, 2H, ^3J = 7.72 Hz, ^4J = 1.5 Hz), 6.71 (dt, 2H, ^3J = 7.60 Hz, ^4J = 1.5 Hz), 6.82 (dt, 2H, ^3J = 7.70 Hz, ^4J = 1.5 Hz), 6.95 (s, 1H, N-H), 7.37 (dd, 2H, ^3J = 7.70 Hz, ^{4}J = 1.6 Hz) ppm. ^{1}H-NMR (300 MHz, CD_3CN, 25°C): δ = 2.64 (s, 24H, CH_3), 6.44 (dd, 2H, ^3J = 7.6 Hz, ^4J = 1.3 Hz), 6.67 (dt, 2H, ^3J = 7.60 Hz, ^4J = 1.3 Hz), 6.77 (dt, 2H, ^3J = 7.60 Hz, ^4J = 1.3 Hz), 7.24 (s, 1H, N-H), 7.30 (dd, 2H, ^3J = 7.60 Hz, ^4J = 1.3 Hz) ppm. ^{13}C-NMR (75 MHz, CD_3CN, 25°C): δ = 38.6 (CH_3), 112.8,

116.9, 119.9, 120.0, 135.5, 140.4, 159.4 (C_{gua}) ppm. IR (KBr, $\tilde{\nu}$ [cm^{-1}]) : 3446*vw*, 3302*w* ($\tilde{\nu}$ (N-H)), 3062*w*, 3033*w* , 2993*w*, 2941*m*, 2916*m*, 2873*m*, 2841*m*, 2808*w*, 2789*w*, 1597*vs* ($\tilde{\nu}$ (C=N)), 1591*vs* ($\tilde{\nu}$(C=N)), 1570*vs* ($\tilde{\nu}$(C=N)), 1565*vs* ($\tilde{\nu}$(C=N)), 1512*vs*, 1508*vs* , 1483*s*, 1437*m*, 1419*s*, 1379*vs*, 1338*m*, 1265*m*, 1230*m*, 1215*m*, 1140*s*, 1111*m*, 1062*w*, 1051*w*, 1034*w*, 1020*s*, 922*w*, 911*w*, 852*w*, 777*m*, 731*s*, 710*w*, 654*w*, 619*w*, 552*w*. UV/Vis (CH_2Cl_2, λ_{max} [nm] (ϵ [$M^{-1}cm^{-1}$]): 242 (13900), 323 (10100). EI-MS (CH_2Cl_2, m/z (%)): 350 (100) [M^+ - 45], 305 (10) [M^+ - 90], 58 (18). elemental analysis calcd. for $C_{22}H_{33}N_7$: C 66.80, H, 8.41, N 24.79, found: C 66.45, H 8.74, N 24.40.

_N_-methyl-2,2´-bis[2N-(1,1´,3,3´-tetramethyl-guanidine)]-diphenylene-amine, TMG_2MePA (L1-5):

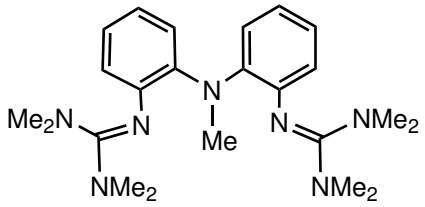

Dark red-violet powder, yield: 76 %, m.p. 95°C
^{1}H-NMR (300 MHz, $CDCl_3$, 25°C): δ = 2.58 (s, 24H, CH_3), 3.38 (s, 3H, N-CH_3), 6.45 (m, 2H), 6.75 - 6.85 (m, 6H). ^{13}C-NMR (75 MHz, CD_3CN, 25°C): δ = 39.9 (CH_3), 68.3 (CH_3), 115.6, 117.8, 120.7, 122.8, 130.6, 131.6, 159.2 (C_{gua}). IR (KBr, $\tilde{\nu}$ [cm^{-1}]): 3180*vw*, 2941*w*, 2870*w*, 2793*w*, 1626*vs* ($\tilde{\nu}$(C=N)), 1552*vs* ($\tilde{\nu}$(C=N)), 1504*m*, 1473*m*, 1458*m*, 1438*m*, 1414*m*, 1402*m*, 1308*m*, 1254*w*, 1227*w*, 1165*m*, 1127*vs*, 1065*m*, 1036*m*, 906*w*, 877*w*, 849*w*, 762*m*, 747*m*, 619*m*, 503*w*. UV/Vis (CH_2Cl_2, λ_{max} [nm] (ϵ [$M^{-1}cm^{-1}$]): 260 (12900), 322 (4300), 517 (450). EI-MS (CH_2Cl_2, m/z (%)): 409 (100) [M^+], 364 (70) [M^+ - 45], 319 (52) [M^+ - 90], 58 (75), 44 (33) [NMe_2^+]. elemental analysis calcd. for $C_{23}H_{35}N_7$: C 67.45, H 8.61, N 21.94, found: C 67.84, H 8.88, N 21.85.

_N,N´_-bis(1,1,3,3-tetramethyl-guanidine)-_m_-xylylene-a,a´-diamine, TMG_2mX (L1-6):

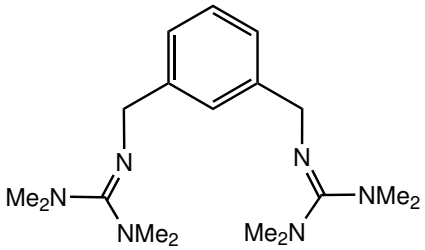

Colourless oil, yield: 96 %.
^{1}H-NMR (500 MHz, $CDCl_3$, 25°C): δ = 2.65 (s, 24H, CH_3), 4.40 (s, 4H, CH_2), 7.13 (m, 3H, CH), 7.28 (s, 1H, CH) ppm. ^{13}C-NMR (125 MHz, $CDCl_3$, 25°C): δ = 38.7 (CH_3), 52.9 (CH_2), 124.4 (CH), 125.7 (CH), 127.4 (CH), 143.0 (quart. C), 160.1 (C_{gua}) ppm. IR (film between NaCl plates, $\tilde{\nu}$ [cm^{-1}]): 2996*w*, 2925*m*, 2884*m*, 2796*w*, 1554*vs* ($\tilde{\nu}$(C=N)), 1457*m*, 1423*m*, 1390*s*, 1346*w*, 1238*w*, 1155*m*, 1108*w*, 1062*w*, 1031*w*. EI-MS (m/z (%)) = 332.4(42) [M^+], 279 (11), 234 (12) [M^+-C(NMe_2)$_2$ + 2H], 213 (28), 175 (18), 149 (42), 116 (31), 105 (68) [CH_2-Ph-CH_2^+ +1], 91 (13) [$C_7H_7^+$], 85 (82), 72(80), 57 (59). elemental analysis calcd. for $C_{18}H_{32}N_6$: C 65.01, H 9.71, N 25.29, found: C 64.92, H 10.06, N 25.02.

N^2,N^6-bis(1,1,3,3-tetramethyl-guanidine)pyridine-2,6-diamine, TMG_2py (L1-7):

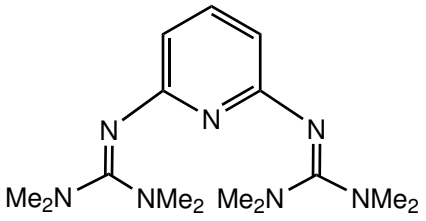

Colourless waxy solid, yield: 93 %.
^{1}H-NMR (500 MHz, $CDCl_3$): δ = 2.73 (s, 24H, CH_3), 6.30 (d, 2H, ^3J = 7.48 Hz), 7.37 (t, 1H, ^3J = 7.48 Hz) ppm. ^{13}C-NMR (125 MHz, $CDCl_3$): δ = 39.9 (CH_3), 107.7 (CH), 138.4 (CH), 158.0 (quart. C), 161.4 (C_{3gua}) ppm. IR (KBr, $\tilde{\nu}$ [cm^{-1}]): 3062*m*, 2993*m*, 2937*s*, 2871*s*, 1604*s*, 1552*vs* ($\tilde{\nu}$(C=N)), 1539*vs* ($\tilde{\nu}$(C=N)), 1411*vs*, 1389*vs*, 1225*s*, 1213*s*, 1132*vs*, 1058*m*, 1022*s*, 1003*m*, 912*m*, 812*s*, 739*m*, 614*w*, 555*w*, 514*w*, 441*w*. EI-MS (m/z (%)) = 305.3(81) [M$^+$], 290(9) [M$^+$-CH_3], 261 (11) [M$^+$-NMe_2], 245 (15), 202 (48), 189 (22), 161 (12), 132 (31), 116 (49) [$H_2N{=}CN_2Me_4^+$], 85 (50), 72(100). elemental analysis calcd. for $C_{15}H_{27}N_7$: C 58.97, H 8.91, N 32.11, found: C 58.72, H 9.16, N 32.02.

N^1,N^3-bis(1,1,3,3-tetraethyl-guanidine)-propane-1,3-diamine, TEG_2p (L2-1):

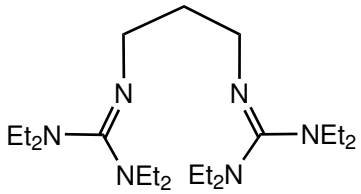

Colourless oil, yield: 97 %.
^{1}H-NMR (500 MHz, $CDCl_3$, 25°C): δ = 1.00 (s, 24H, CH_3), 1.78 (m, 2H, CH_2), 3.00 (q, 8H, CH_2), 3.12 (q, 8H, CH_2), 3.14 (t, 4H, CH_2) ppm. ^{13}C-NMR (125 MHz, $CDCl_3$, 25°C): δ = 12.9 (CH_3), 13.6 (CH_3), 35.9 (CH_2), 41.3 ($\underline{CH_2}CH_3$), 42.5 ($CH_2\underline{CH_3}$), 48.7 (CH_2), 158.0 (C_{gua}) ppm. IR (film between NaCl plates, $\tilde{\nu}$ [cm^{-1}]): 2966*m*, 2929*m*, 2870*m*, 1610*vs* ($\tilde{\nu}$(C=N)), 1454*w*, 1400*m*, 1375*m*, 1336*w*, 1300*w*, 1261*s*, 1219*w*, 1134*w*. EI-MS (m/z (%)): 382.4(73) [M$^+$], 353(19) [M$^+$-Et]310 (5) [M$^+$-NEt_2], 228 (12) [M$^+$-C(NEt_2)$_2$], 205(62), 198(57), 142 (51), 113 (100) [$CH_2N{=}C(NEt_2)_2^+$], 85 (42), 72(41) [NEt_2]. elemental analysis calcd. for $C_{21}H_{46}N_6$: C 65.90, H 12.12, N 21.97, found: C 65.61, H 12.37, N 22.02.

N^1,N^3-bis(1,1,3,3-tetraethyl-guanidine)-*m*-xylylene-a,a´-diamine, TEG_2mX (L2-6):

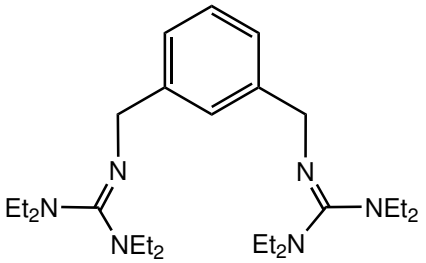

Colourless oil, yield: 95 %.
^{1}H-NMR (500 MHz, $CDCl_3$, 25°C): δ = 1.07 (s, 24H, CH_3), 3.10 (q, 8H, CH_2), 3.22 (q, 8H, CH_2), 4.36 (s, 4H, CH_2), 7.22 (m, 3H, CH), 7.29 (s, 1H, CH) ppm. ^{13}C-NMR (125 MHz, $CDCl_3$, 25°C): δ = 13.4 (CH_3), 41.4 (benzyl-CH_2), 42.7 (CH_2), 124.9 (CH), 126.5 (CH), 127.6 (CH), 143.3 (quart. C), 159.1 (C_{gua}) ppm. IR (film between NaCl plates, $\tilde{\nu}$ [cm^{-1}]): 2968*m*, 2929*m*, 2870*m*, 1604*vs* ($\tilde{\nu}$(C=N)), 1450*m*, 1403*m*, 1375*m*, 1338*w*, 1302*w*, 1261*s*, 1203*w*, 1132*w*, 1068*w*. EI-MS (m/z (%)): 444.4(70) [M$^+$], 372 (22) [M$^+$-NEt_2], 275 (75) [M$^+$-HN=C(NEt_2)$_2$], 172 (39) [$H_2N{=}C(NEt_2)_2^+$], 119(31), 105(75) [CH_2-Ph-CH_2^+ +1], 91 (11) [$C_7H_7^+$], 72(100) [NEt_2]. elemental analysis calcd. for $C_{26}H_{48}N_6$: C 70.21, H 10.89, N 18.91, found: C 70.06, H 11.20, N 18.74.

N^2,N^6-bis(1,1,3,3-tetraethyl-guanidine)-pyridine-2,6-diamine, TEG_2py (L2-7):

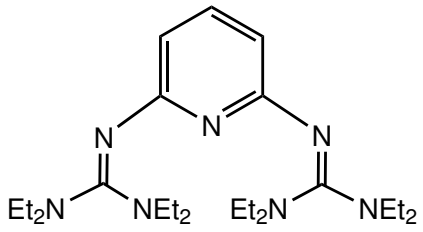

Colourless oil, yield: 95 %. ^{1}H-NMR (500 MHz, $CDCl_3$, 25°C): δ = 1.06 (m, 24 H, CH_3), 3.07 (m, 16 H, CH_2), 6.22 (d, 2 H, ^3J = 7,8 Hz), 7.22 (t, 1 H, ^3J = 7,8 Hz). ^{13}C-NMR (125 MHz, $CDCl_3$, 25°C): δ = 12.82 (CH_3), 42.66 (CH_2), 104.99 (CH), 138.48 (CH), 157.90 (C_{quat}), 159.37 (C_{gua}). IR (film between NaCl plates, $\tilde{\nu}$ [cm^{-1}]): 3064*vw*, 2970*s*, 2931*m*, 2871*m*, 1556*vs* ($\tilde{\nu}$(C=N)$_{Gua}$), 1531*vs* ($\tilde{\nu}$(C=N)$_{Gua}$), 1483*m*, 1446*vs*, 1417*vs* ($\tilde{\nu}$(C=N)$_{py}$), 1377*s*, 1356 *m*, 1269*vs*, 1198*m*, 1136*vs*, 1057*m*. EI-MS (m/z (%)): 417 (8) [M^+], 388 (2) [M^+ - Et], 345 (1) [M^+ - NEt_2], 274 (3) [M^+ - 2 NEt_2 + H], 263 (52) [M^+ - $C(NEt_2)_2$ + 2 H], 191 (49) [M^+ - $C(NEt_2)_2$ - NEt_2 + 2 H], 172 (58) [$H_2N{=}C(NEt_2)_2^+$], 163 (52) [M^+ - $C(NEt_2)_2$ - NEt_2 - Et + 3 H], 100 (70) [$H_2N{=}C(NEt_2)_2^+$ - NEt_2], 72 (100) [NEt_2], 29 (61) [Et]. elemental analysis calcd. for $C_{23}H_{43}N_7$: C 66.13, H 10.38, N 23.49, found: C 65.81, H 10.55, N 23.64.

N^1,N^3-bis(1,1,3,3-tetraisopropyl-guanidine)-propane-1,3-diamine, $TiPG_2p$ (L3-1):

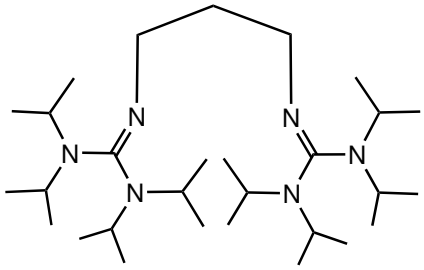

Off-white powder, yield: 81 %.
^{1}H-NMR (500 MHz, $CDCl_3$, 25°C): δ = 1.23 (d, 24H, CH_3), 1.46 (d, 24H, CH_3), 1.59 (m, 2H, CH_2), 3.31 (t, 4H, CH_2), 3.40 (m, 4H, CH), 3.82 (m, 4H, CH) ppm. ^{13}C-NMR (125 MHz, $CDCl_3$, 25°C): δ = 19.2 (CH_3), 21.4 (CH_3), 31.6 (CH_2), 36.7 (CH_2), 45.2 (CH), 47.4 (CH), 157.7 (C_{gua}) ppm. IR (KBr, $\tilde{\nu}$ [cm^{-1}]): 2972*s*, 2845*m*, 2774*m*, 2721*m*, 1699*s*, 1622*vs* ($\tilde{\nu}$(C=N)), 1525*vs*, 1473*s*, 1451*m*, 1405*m*, 1309*m*, 1153*m*, 765*w*. EI-MS (m/z (%)): 494.4(0.1) [M^+], 459 (1) [M^+-Me], 429 (5), 401 (1), 355(8), 314(13), 281(5), 230(90) [$(^iPr_2N)_2C{=}NH_2^+$+2H], 215(19), 175(9), 149(11), 114(20) [$(^iPr_2N)_2CH_2^+$], 112(18) [$(^iPr_2N)_2C^+$], 86(100) [^{i}Pr-N-CH-CH_3^++H], 56(81) [^{i}PrNH$^+$], 41 (76). elemental analysis calcd. for $C_{29}H_{62}N_6$: C 70.37, H 12.64, N 16.99, found: C 70.16, H 12.90, N 16.95.

N^1,N^3-bis-(1,3-dimethyl-imidazolidin-2-ylidene)-propane-1,3-diamine, $DMEG_2p$ (L4-1):

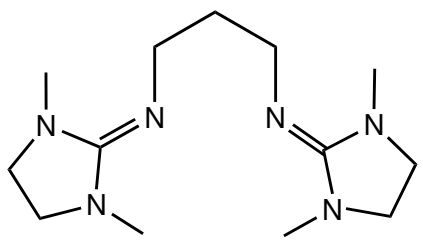

Colourless oil which slowly crystalises, yield: 95 %.
^{1}H-NMR (500 MHz, $CDCl_3$, 25°C): δ =1.57 (m, 2H, CH_2), 2.60 (s, 12H, CH_3), 2.95 (b, 8H, CH_2), 3.26 (t, 4H, CH_2) ppm. ^{13}C-NMR (125 MHz, $CDCl_3$, 25°C): δ = 32.1 (CH_2), 36.3 (CH_3), 45.0 (CH_2), 49.3 (CH_2), 157.3 (C_{gua}) ppm. IR (film between NaCl plates, $\tilde{\nu}$ [cm^{-1}]): 2931*s*, 2831*s*, 1660*vs* ($\tilde{\nu}$(C=N)), 1651*vs* ($\tilde{\nu}$(C=N)), 1485*s*, 1435*m*, 1422*m*, 1384*m*, 1336*w*, 1263*m*, 1241*w*,

1113*w*. EI-MS: m/z (%) 266.3 (39) [M^+], 249 (4) [M^+-Me], 205 (5), 152 (10), 140 (60) [$CH_2CH_2N{=}CN_2C_4H_{10}^+$], 126 (80) [$CH_2N{=}CN_2C_4H_{10}^+$], 114 (100) [$H_2N{=}CN_2C_4H_{10}^+$], 98 (32), 84 (25), 70 (24). elemental analysis, calcd. for $C_{13}H_{26}N_6$: C 58.61, H 9.84, N 31.55 ; found: C 58.93, H 9.58, N 31.49.

2-(2-(2-(1,3-dimethylimidazolidin-2-ylideneamino)ethoxy)ethoxy)-N-(1,3-di-methylimidazolidin-2-ylideneamino)-ethanamine, $DMEG_2$doo (L4-2):

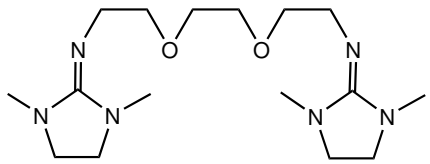

Colourless oil, yield: 98 %.
^{1}H-NMR (500 MHz, $CDCl_3$, 25°C): δ = 2.77 (s, 6H, CH_3), 2.79 (s, 6H, CH_3), 3.15 (s, 8H, CH_2), 3.59 (b, 8H, CH_2), 3.66 (s, 4H, CH_2). ^{13}C-NMR (125 MHz, $CDCl_3$, 25°C): δ = 31.5 (CH_3), 36.3 (CH_3), 47.4 (CH_2), 49.4 (CH_2), 70.5 (CH_2), 73.7 (CH_2), 157.9 (C_{gua}). IR (film between NaCl plates, $\tilde{\nu}$ [cm^{-1}]): 2915*w*, 2858*m*, 1666*vs* ($\tilde{\nu}$(C=N)), 1617*vs* ($\tilde{\nu}$(C=N)), 1483*m*, 1441*m*, 1383*m*, 1302*w*, 1122*s* ($\tilde{\nu}$(C-O-C)), 1023*m*. EI-MS (m/z, (%)): 340.2 (1) [M^+], 325 (1) [M^+-Me], 184 (4), 140 (9) [$CH_2CH_2N{=}CN_2Me_2C_2H_4^+$], 126 (100) [$CH_2N{=}CN_2Me_2C_2H_4^+$], 112 (8), 85 (3). elemental analysis calcd. for $C_{16}H_{32}N_6O_2$: C 56.43, H 9.48, N 24.69, found: C 56.21, H 9.76, N 24.81.

N^1,N^3-bis(1,3-dimethylimidazolidin-2-ylidene)cyclohexane-1,3-diamine, $DMEG_2$ch (L4-3):

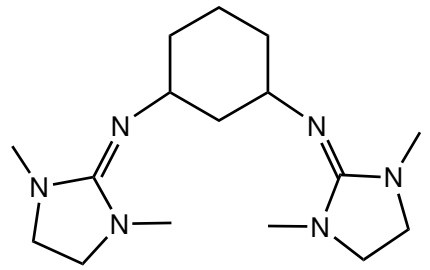

Colourless powder, yield: 93 %.
^{1}H-NMR (500 MHz, $CDCl_3$, 25°C): δ = 1.16-1.72 (m, 8H, CH_2 from ring), 2.71 (s, 12H, CH_3), 3.05 (m, 8H, CH_2), 4.05 (m, 2H, CH) ppm. ^{13}C-NMR (125 MHz, $CDCl_3$, 25°C): δ = 20.0 (CH_2), 25.6 (CH_2), 35.7 (CH_2), 45.1 (CH_2), 49.0 (CH_3), 53.2 (CH), 155.8 (C_{gua}) ppm. IR (KBr, $\tilde{\nu}$ [cm^{-1}]): 2933*s*, 2852*s*, 1660*vs*($\tilde{\nu}$(C=N)), 1637*vs* ($\tilde{\nu}$(C=N)), 1477*m*, 1442*m*, 1410*m*, 1379*s*, 1259*s*, 1226*s*, 1142*w*, 1119*w*, 1095*w*, 1065*w*, 1032*s*, 991*m*, 953*s*, 908*m*, 877*m*, 877*m*, 850*m*, 766*w*, 719*m*, 669*w*, 642*m*, 580*m*, 538*w*, 503*w*. EI-MS (m/z (%)): 306.2 (11) [M^+], 263 (19), 193 (100) [M^+- $N{=}CN_2(C_2H_4)Me_2$-H], 152 (35), 114 (32) [$H_2N{=}CN_2(C_2H_4)Me_2^+$], 98 (29), 70 (23), 55 (15). elemental analysis calcd. for $C_{16}H_{30}N_6$: C 62.69, H 9.87, N 27.43, found: C 62.41, H 10.03, N 27.56.

N^1,N^3-bis(1,3-dimethylimidazolidin-2-ylidene)-xylylene-a,a´-diamine, $DMEG_2mX$ (L4-6):

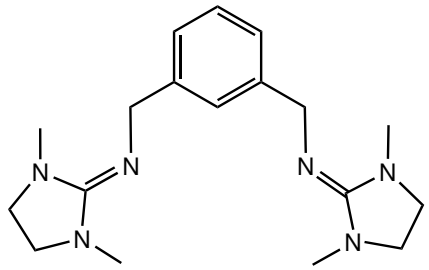

Colourless oil, yield: 96 %.
^{1}H-NMR (500 MHz, $CDCl_3$, 25°C): δ = 2.78 (s, 12H, CH_3), 3.18 (t, 8H, CH_2), 4.67 (s, 4H, CH_2), 7.24 (m, 3H, CH), 7.39 (s, 1H, CH) ppm. ^{13}C-NMR (125 MHz, $CDCl_3$, 25°C): δ = 31.5 (CH_3), 45.06 (CH_2), 49.54 (CH_2), 50.89 (CH_2), 124.4 (CH), 125.4 (CH), 127.7 (CH), 143.2 (C_{quat}), 157.7 (C_{gua}) ppm. IR (film between NaCl plates, $\tilde{\nu}$ [cm^{-1}]): 2935m, 2843m, 1655vs ($\tilde{\nu}$(C=N)),1483m, 1437m, 1384m, 1350w, 1269s, 1230w, 1199w, 1065w. EI-MS (m/z (%)): 328.3(19) [M^+], 313.2(8) [M^+-Me], 232.2(78), 215(26), 126(56) [$CH_2N{=}CMe_2C_2H_4^+$], 114(100) [$H_2N{=}CMe_2C_2H_4^+$], 112(60) [$N_3C_5H_{10}^+$], 106(81), 91.1(40) [$C_7H_7^+$]. elemental analysis calcd. for $C_{18}H_{28}N_6$: C 65.81, H 8.60, N 25.60, found: C 65.61, H 8.97, N 25.42.

N^2,N^6-bis(1,3-dimethylimidazolidin-2-ylidene)pyridine-2,6-diamine, $DMEG_2py$ (L4-7):

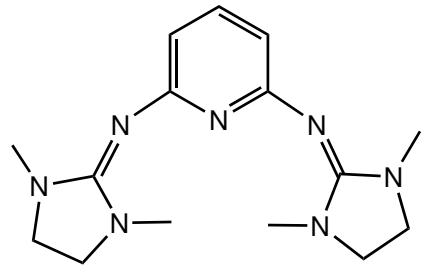

Colourless waxy solid, yield: 92 %.
^{1}H-NMR (500 MHz, $CDCl_3$, 25°C): δ = 2.65 (s, 12H, CH_3), 3.30 (s, 8H, CH_2), 6.23 (d, 2H, ^{3}J = 7.7 Hz), 7.23 (t, 1H, ^{3}J = 7.7 Hz) ppm. ^{13}C-NMR (125 MHz, $CDCl_3$, 25°C): δ = 34.9 (CH_3), 48.2 (CH_2), 108.2 (CH), 138.6 (CH), 157.8 (C_{quat}), 160.9 (C_{gua}) ppm. IR (KBr, $\tilde{\nu}$ [cm^{-1}]): 3161w, 3064w, 2919m, 2852m, 1616vs ($\tilde{\nu}$(C=N)), 1569s ($\tilde{\nu}$(C=N)), 1541vs, 1429s, 1281s, 1236m, 1193w, 1144w, 1038m, 955m, 808m, 702w, 669w, 582w. EI-MS (m/z (%)) = 301.2 (89) [M^+], 300 (100) [M^+-H], 245 (9), 205 (39) [M^+- $CN_2Me_2C_2H_4^+$ +2H], 204 (58) [M^+-$CN_2Me_2C_2H_4^+$+H], 189 (9), 132 (7), 114 (11), 98 (8) [$N{=}CN_2Me_2C_2H_4^+$], 70 (29). elemental analysis calcd. for $C_{15}H_{23}N_7$: C 59.76, H 7.70, N 32.54, found: C 59.49, H 7.91, N 32.60.

N^1,N^3-bis(tetrahydro-1,3-dimethylpyrimidin-2(1H)-ylidene)-propane-1,3-diamine, $DMPG_2p$ (L5-1):

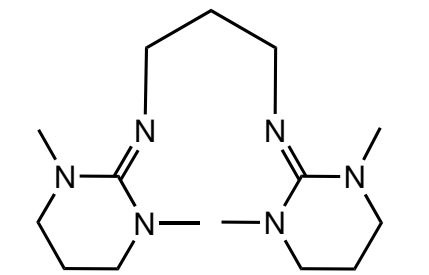

Colourless oil which slowly crystallises, yield: 94 %.
^{1}H-NMR (500 MHz, $CDCl_3$, 25°C): δ = 1.50 (m, 2H, CH_2), 1.68 (m, 4H, CH_2), 2.70 (s, 12H, CH_3), 2.95 (m, 8H, CH_2), 3.02 (t, 4H, CH_2); ^{13}C-NMR (125 MHz, $CDCl_3$, 25°C): δ = 20.9 (CH_2), 32.3 (C_a), 39.3 (CH_3), 45.8 (C_b), 48.4 (CH_2), 157.5 (C_{gua}) IR (KBr, $\tilde{\nu}$ [cm^{-1}]): 2921s, 2858s, 1621vs ($\tilde{\nu}$(C=N)), 1576s ($\tilde{\nu}$(C=N)), 1541s, 1458m, 1419m, 1375m, 1321m, 1271w, 1236w, 1113w, 1047w, 1016w, 708w, 669w, 607w, 557w, 522w. CI-MS: m/z 294.25 (M^+). elemental analysis calcd. for $C_{15}H_{30}N_6$: C 61.17, H 10.28, N 28.55, found: C 61.53, H 10.01, N 28.42.

2-(2-(2-(tetrahydro-1,3-dimethylpyrimidin-2(1H)-ylideneamino)ethoxy)ethoxy)-N-(tetrahydro-1,3-dimethylpyrimidin-2(1H)-ylideneamino)-ethanamine, $DMPG_2$doo (L5-2):

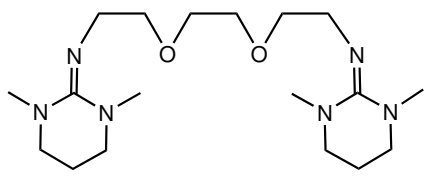

Colourless oil, yield: 93 %.
^{1}H-NMR (300 MHz, $CDCl_3$, 25°C): δ = 1.58 (m, 4H, CH_2), 1.88 (m, 8H, CH_2), 2.85 (s, 12H, CH_3), 3.20 (t, 4H, CH_2), 3.54 (b, 8H, CH_2). ^{13}C-NMR (125 MHz, $CDCl_3$, 25°C): δ = 21.6 (CH_2), 38.4 (CH_3), 39.1 (CH_3), 48.1 (CH_2), 49.6 (CH_2), 70.5 (CH_2), 73.9 (CH_2), 160.1 (C_{gua}). IR (film between NaCl plates, $\tilde{\nu}$ [cm^{-1}]): 2925*w* , 2865*m* , 1635*vs* ($\tilde{\nu}$(C=N)), 1620*vs* ($\tilde{\nu}$(C=N)), 1558*m*, 1541*s*, 1458*m* , 1386*m* , 1309*w*, 1261*m*, 1101*s* ($\tilde{\nu}$(C-O-C)), 1045*m*, 850*w*, 742*w*, 627*s*. EI-MS (m/z, (%)): 368.4 (1) [M^+], 266 (21), 205 (8), 152 (9), 173 (8) [M^+- NMe_2, $NC(NMe_2)_2$], 141 (65) [M^+- $(NMe_2)_2CN(CH_2)_2O$], 128 (100) [$H_2N{=}CN_2Me_2C_3H_6^+$], 98 (34), 70 (48). elemental analysis calcd. for $C_{18}H_{36}N_6O_2$: C 58.65, H 9.85, N 22.81, found: C 58.42, H 10.16, N 22.73.

***N*-methyl-2,2´-bis[tetrahydro-1,3-dimethylpyrimidin-2(1H)-ylidene]-diphenyleneamine, $DMPG_2$MePA (L5-5):**

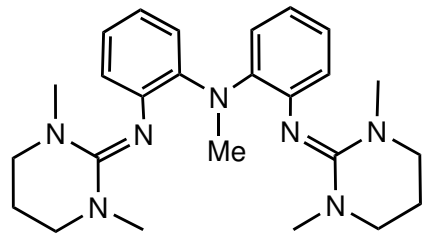

Dark red-violet oil, yield: 68 %.
^{1}H-NMR (300 MHz, $CDCl_3$, 25°C): δ = 1.65 (m, 4H, CH_2) ppm, 1.9 (m, 8H, CH_3), 2.9 (s, 15H, CH_3), 6.7 (m, 4H, CH), 6.95 (m, 4H, CH). ^{13}C-NMR (125 MHz, CD_3CN, 25°C): δ = 21.1 (CH_2), 38.0 (CH_3), 48.6 (CH_2), 69.1 (N-CH_3), 115.2, 117.6, 122.1, 124.6, 136.5 (C_{quat}), 142.1(C_{quat}), 153.3 (C_{gua}) ppm. IR (KBr, $\tilde{\nu}$ [cm^{-1}]): 3065*w* , 3025*w* , 2940*m* , 2869*m* , 2345*w* , 1621*vs* ($\tilde{\nu}$(C=N)), 1563*vs* ($\tilde{\nu}$(C=N)), 1546*vs* ($\tilde{\nu}$(C=N)), 1452*s* , 1417*s*, 1317*s*, 1120*m*, 1052*m*, 746*s*. EI-MS (CH_2Cl_2, m/z (%)): 433.6 (1) [M^+], 419 (2) [M^+- 14], 323 (5), 285 (3), 252 (100), 213 (98), 181 (33), 128 (30) [$H_2N{=}CN_2Me_2C_3H_6^+$], 112 (29), 69 (48), 58 (69). elemental analysis calcd. for $C_{25}H_{35}N_7$: C 69.24, H 8.14, N 22.62, found: C 69.02, H 8.49, N 22.49.

N^1,N^3-bis(tetrahydro-1,3-dimethylpyrimidin-2(1H)-ylidene)- xylylene-a,a´-diamine, $DMPG_2$mX (L5-6):

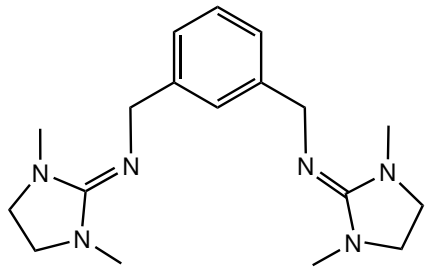

Colourless oil, yield: 95 %.
^{1}H-NMR (500 MHz, $CDCl_3$, 25°C): δ = 1.83 (q, 4H, CH_2), 2.86 (s, 12H, CH_3), 3.07 (t, 8H, CH_2), 4.36 (s, 4H, CH_2), 7.21 (m, 3H, CH), 7.33 (s, 1H, CH) ppm. ^{13}C-NMR (125 MHz, $CDCl_3$, 25°C): δ = 20.5 (CH_2), 39.0 (CH_3), 48.3 (CH_2), 51.57 (CH_2), 124.9 (CH), 126.5 (CH), 127.9 (CH), 142.6 (C_{quat}), 157.6 (C_{gua}) ppm. IR (film between NaCl plates, $\tilde{\nu}$ [cm^{-1}]): 2635*m*, 2843*m*, 1655*vs* ($\tilde{\nu}$(C=N)), 1483*m*, 1437*m*, 1402*w*, 1385*m*, 1350*w*, 1269*s*, 1231*w*, 1199*w*, 1065*w*.

EI-MS: m/z (%) = 356.3 20) [M^+], 229(15), 178 (5), 149 (7), 128(100) [$H_2N{=}CN_2Me_2C_3H_6^+$], 99 (22), 57 (23). elemental analysis calcd. for $C_{20}H_{32}N_6$: C 67.36, H 9.05, N 23.58, found: C 67.12, H 9.41, N 23.47.

N^2,N^6-bis(tetrahydro-1,3-dimethylpyrimidin-2(1H)-ylidene)pyridine-2,6-diamine, $DMPG_2py$ (L5-7):

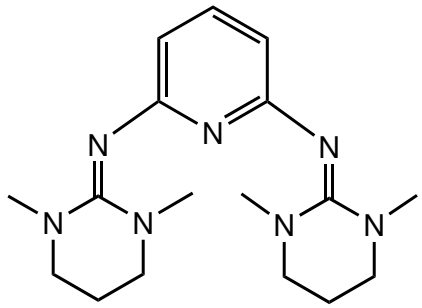

Colourless waxy solid, yield: 94 %.
^{1}H-NMR (500 MHz, $CDCl_3$, 25°C): δ = 1.90 (m, 4H, CH_2), 2.78 (s, 6H, CH_3), 2.84 (s, 6H, CH_3), 3.17 (m, 8H, CH_2), 5.74 (d, 1H, ^3J = 7.7 Hz), 5.89 (d, 1H, ^3J = 7.7 Hz), 7.10 (t, 1H, ^3J = 7.7 Hz) ppm. ^{13}C-NMR (125 MHz, $CDCl_3$, 25°C): δ = 22.2 (CH_2), 35.6 (CH_3), 39.2 (CH_3), 47.8 (CH_2), 104.7 (CH), 138.5 (CH), 157.8 (C_{quat}), 161.9 (C_{gua}) ppm. IR (KBr, $\tilde{\nu}$ [cm^{-1}]): 3010w, 2902w, 2856w, 1624vs ($\tilde{\nu}$(C=N)), 1529vs, 1448s, 1413s, 1317s, 1252m, 1221m, 1157w, 1109w, 1059m, 802w, 756w, 709w, 474w. EI-MS (m/z (%)) = 329.2 (62) [M^+], 314 (4) [M^+-Me], 245 (33), 219 (100) [M^+- $CN_2Me_2C_3H_6^+$ +2H], 218 (48) [M^+- $CN_2Me_2C_3H_6^+$ +H], 191 (9), 148 (28), 112 (25) [$N_2Me_2C_3H_6^+$], 109 (19), 70 (11). elemental analysis calcd. for $C_{17}H_{27}N_7$: C 61.96, H 8.27, N 29.77, found: C 61.65, H 8.42, N 29.93.

N^1,N^3-bis(tetrahydro-1,3-dipropylpyrimidin-2(1H)-ylidene)propane-1,3-diamine, $DPPG_2p$ (L6-1):

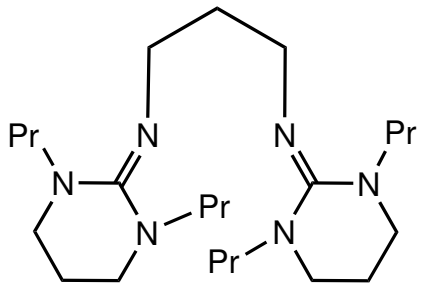

Yellowish oil, yield: 89 %.
^{1}H-NMR (500 MHz, $CDCl_3$, 25°C): δ = 0.83 (t, 12H, CH_3), 1.44 (q, 2H, CH_2), 1.56 (m, 8H, CH_2), 1.91 (m, 4H, CH_2), 3.19 (m, 20H, CH_2) ppm. ^{13}C-NMR (125 MHz, $CDCl_3$, 25°C): δ = 11.6 (CH_3), 21.3 (CH_2), 22.7 (CH_2), 46.1 (CH_2), 49.9 (CH_2), 53.7 (CH_2), 158.0 (C_{gua}) ppm. IR (film between NaCl plates, $\tilde{\nu}$ [cm^{-1}]): 2960s, 2931m, 2871m, 1633vs ($\tilde{\nu}$(C=N)), 1604vs ($\tilde{\nu}$(C=N)), 1500m, 1456m, 1363m, 1325w, 1296m, 1263w, 1207s, 1099m. EI-MS (m/z (%)): 406.4 (9) [M^+], 391 (1) [M^+-Me], 363 (1) [M^+-Pr], 240 (10), 211 (15), 184 (28) [$H_2N{=}CN_2Pr_2C_3H_6^+$], 155 (100), 113 (38), 70 (32), 98 (29), 70 (23), 55 (15). elemental analysis calcd. for $C_{23}H_{46}N_6$: C 67.92, H 11.41, N 20.67, found: C 67.61, H 11.67, N 20.72.

N^1,N^3-bis(piperidin-1-yl)methylene)propane-1,3-diamine, DPipG$_2$p (L7-1):

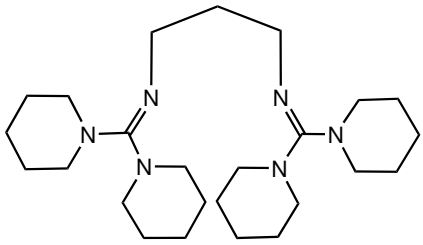

Colourless crystals, yield: 84 %. ^{1}H-NMR (500 MHz, $CDCl_3$, δ = 1.48-1.61 (m, 24H, Pip-CH_2), 1.80 (q, 2H, CH_2), 3.02 (t, 16H, Pip-CH_2), 3.18 (t, 4H, CH_2). ^{13}C-NMR (125 MHz, $CDCl_3$, 25°C): δ = 24.8 (Pip), 25.9 (Pip), 34.5 (C_a), 46.7 (C_b), 49.1 (Pip), 160.0 (Cquart.). IR (KBr, $\tilde{\nu}$ [cm^{-1}]): 2978*m*, 2962*m*, 2927*vs*, 2877*m*, 2846*m*, 2835*m*, 2808*m*, 1626*vs* ($\tilde{\nu}$(C=N)), 1608*s* ($\tilde{\nu}$(C=N)), 1442*m*, 1398*s*, 1367*s*, 1346*m*, 1327*m*, 1246*s*, 1209*s*, 1199*m*, 1168*w*, 1159*w*, 1134*m*, 1124*m*, 1089*w*, 1032*m*, 1012*w*, 981*w*, 956*m*, 926*w*, 910*m*, 879*m*, 850*m*, 725*w*, 636*vw*. EI-MS: m/z (%) 430 (42) [M$^+$], 346 (10) [M$^+$-Pip], 237 (13), 222 (81), 196 (12), 154 (41), 126 (43), 85 (51) [HPip$^+$], 84 (100) [Pip$^+$], 69 (22). elemental analysis calcd. for $C_{25}H_{46}N_6$: C 69.71, H 10.77, N 19.52, found: C 69.47, H 10.95, N 19.52.

N^1,N^3-bis(bis(2,6-dimethylpiperidin-1-yl)methylene)propane-1,3-diamine, B(DMPip)G$_2$p (L8-1):

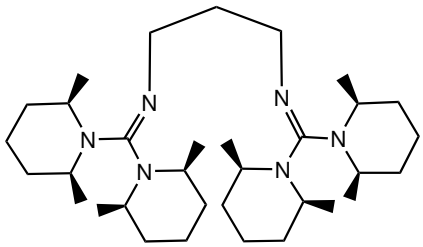

Yellowish oil, yield: 76 %.
^{1}H-NMR (500 MHz, $CDCl_3$, 25°C): δ = 1.01 (d, 24H, CH_3), 1.53 (m, 16H, CH_2), 1.61 (m, 2H, CH_2), 1.68 (m, 8H, CH_2), 2.58 (m, 8H, CH), 2.70 (t, 4H, CH_2) ppm. ^{13}C-NMR (125 MHz, $CDCl_3$, 25°C): δ = 21.5 (CH_2), 23.0 (CH_3), 24.9 (CH_2-Pip), 33.9 (CH_2-Pip), 39.8 (CH_2), 52.4 (CH), 157.0 (C_{gua}) ppm. IR (film between NaCl plates, $\tilde{\nu}$ [cm^{-1}]): 2958*s*, 2931*s*, 2871*m*, 1693*vs* ($\tilde{\nu}$(C=N)), 1651*vs* ($\tilde{\nu}$(C=N)), 1643*vs* ($\tilde{\nu}$(C=N)), 1537*s*, 1479*m*, 1415*m*, 1373*w*, 1311*m*, 1275*w*, 1236*w*, 1159*m*. EI-MS (m/z (%)): 542 (0.01) [M$^+$], 430 (1) [M$^+$-Me_2Pip], 292 (13) [M$^+$-N=C(Me_2Pip)$_2$], 279 (14) [M$^+$-CH_2N=C(Me_2Pip)$_2$ +H], 237 (9) [(Me_2Pip)$_2$CH$_+$], 183 (22), 149 (48), 112 (43) [Me_2Pip$^+$], 98 (100) [CH_3CH(CH_2)$_3$CHCH_3], 56 (39). elemental analysis calcd. for $C_{33}H_{62}N_6$: C 72.99, H 11.52, N 15.49, found: C 72.64, H 11.75, N 15.61.

N^1,N^3-bis(bis(2,2,6,6-tetramethylpiperidin-1-yl)methylene)propane-1,3-diamine, B(TMPip)G$_2$p (L9-1):

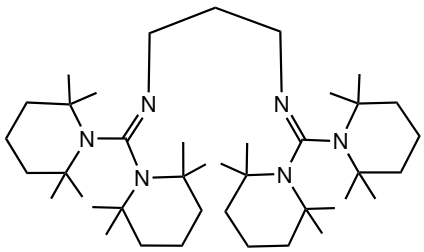

Yellow oil, yield: 72 %.
^{1}H-NMR (500 MHz, $CDCl_3$, 25°C): δ = 1.05 (s, 48H, CH_3), 1.18 (m, 2H, CH_2), 1.50 (m, 8H, CH_2), 3.17 (t, 16H, CH_2), 3.29 (t, 4H, CH_2) ppm. ^{13}C-NMR (125 MHz, $CDCl_3$, 25°C): δ = 13.2 (CH_3), 13.9 (CH_3), 16.3 (CH_2), 35.0 (CH_2), 40.4 (CH_2), 41.1 (CH_2), 42.2 (CH_2), 56.7 (C_{quat}), 156.4 (C_{gua}) ppm. IR (film between NaCl plates, $\tilde{\nu}$ [cm^{-1}]): 2970*s*, 2935*m*, 2733*w*, 1645*vs* ($\tilde{\nu}$(C=N)), 1531*vs*, 1454*m*, 1379*s*, 1351*m*, 1271*s*, 1223*m*, 1182*w*. EI-MS (m/z (%)): 654 (0.01) [M$^+$], 408 (2), 340 (4), 308 (8) [(Me_4Pip)$_2$C=NH_2^+], 268 (6), 240 (13), 184(21), 157 (28), 140 (11)

[Me_4Pip], 126 (35) [Me_4Pip-N], 109 (58), 84 (22) [($Me_2C(CH_2)_3$], 69 (37) [$MeC(CH_2)_3$], 58 (100). elemental analysis calcd. for $C_{41}H_{78}N_6$: C 75.16, H 12.01, N 12.83, found: C 74.91, H 12.37, N 12.72.

N^1,N^3-bis(di(imidazol-1-yl)methylene)propane-1,3-diamine, DImG_2p (L10-1):

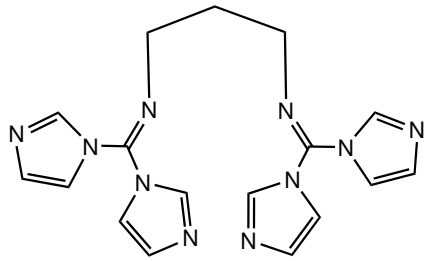

Yellow powder, yield: 58 %.

^{1}H-NMR (500 MHz, $CDCl_3$, 25°C): δ = 1.92 (m, 2H, CH_2), 3.3 (m, 4H, =N-CH_2-), 7.12 (s, 8H, =N-CH=CH-N-), 7.71 (s, 4H, -N-CH=N-) ppm. ^{13}C-NMR (125 MHz, $CDCl_3$, 25°C): δ = 21.3 (CH_2), 40.0 (CH_2), 121.9 (CH=CH), 135.1 (CH), 155.2 (C_{gua}) ppm. IR (KBr, $\tilde{\nu}$ [cm^{-1}]): 3122*m*, 3035*m*, 2935*m*, 2843*m*, 2698*m*, 2607*m*, 1791*m*, 1689*s*, 1652*vs*, 1533*vs*, 1482*s*, 1442*vs*, 1373*m*, 1324*s*, 1257*s*, 1222*w*, 1197*w*, 1141*m*, 1095*s*, 1064*s*, 1035*m*. EI-MS (m/z (%)): 362,3(0,1) [M^+], 212(10), 179(21), 151 (22), 123(35), 116(24), 68(100) [$C_3H_4N_2^+$]. elemental analysis calcd. for $C_{17}H_{18}N_{10}$: C 56.33, H 5.01, N 38.66, found: C 56.43, H 5.16, N 38.41.

N^1,N^3-bis(dimorpholinomethylene)propane-1,3-diamine, DMorphG_2p (L11-1):

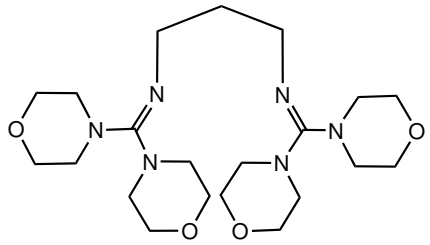

White powder, after recrystallisation colourless needles, yield: 71 %.

^{1}H-NMR (500 MHz, $CDCl_3$, 25°C): δ = 1.75 (q, 2 H, CH_2), 3.02-3.38 (broad, 18 H, CH_2), 3.64-6.76 (m, 14 H, CH_2) ppm. ^{13}C-NMR (125 MHz, $CDCl_3$, 25°C): δ = 25.58, 44.0, 47.2, 48.5, 157.3 (C_{gua}) ppm. IR (KBr, $\tilde{\nu}$ [cm^{-1}]): 2967*m*, 2898*m*, 2844*m*, 1633*vs* ($\tilde{\nu}$(C=N)), 1600*vs* ($\tilde{\nu}$(C=N)), 1436*s*, 1386*m*, 1357*m*, 1268*vs*, 1228*m*, 1114*vs* ($\tilde{\nu}$(C-O)), 1027*m*, 883*s*, 601*m*. EI-MS (m/z (%)): 438.3(6) [M^+], 408 (11) [M^+-CH_2O], 393 (12) [M^+-CH_3CH_2O], 363 (21) [M^+-2(CH_2O)-(CH_3CH_2O)], 283 (13) [M^+-C_3H_6NC(Morph)], 254 (6) [M^+-C_6H_6NC(Morph)-(CH_2O), 226 (14) [M^+-CH_2NC(Morph)$_2$], 196 (42) [M^+-C_3H_6NC(Morph)$_2$], 171 (17) [M^+-CNC_3H_6NC(Morph)$_2$], 127 (61) [M^+-CNC_3H_6NC(Morph)$_2$-C_3H_6], 86 (37) [Morph]. elemental analysis calcd. for $C_{21}H_{38}N_6O_4$: C 57.50, H 8.74, N 19.17, found: C 57.31, H 8.97, N 18.87.

2-(2-(2-(dimorpholinomethyleneamino)ethoxy)ethoxy)-N-(dimorpholino-methylene)ethanamine, DMorphG_2doo (L11-2):

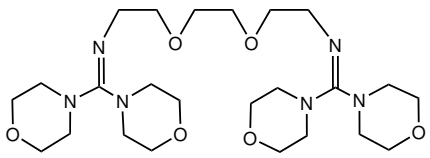

White powder, after recrystallisation colourless needles, yield: 65 %.

^{1}H-NMR (500 MHz, $CDCl_3$, 25°C): δ = 3.1-3.3 (broad, 16 H, Morph-CH_2), 3.41 (t, 4 H, CH_2), 3.61 (t, 4 H, CH_2), 3.66 (s, 4H, CH_2), 3.69 (m, 16 H, Morph-CH_2) ppm. ^{13}C-NMR (125 MHz, $CDCl_3$, 25°C): δ = 47.2 (Morph-CH_2), 48.3, 66.8 (Morph-CH_2), 67.1, 70.5, 163.8 (C_{gua}) ppm. IR (KBr, $\tilde{\nu}$ [cm^{-1}]):

2972*m* , 2893*s*, 2856*s*, 1647*m* ($\tilde{\nu}$(C=N)), 1621*vs* ($\tilde{\nu}$(C=N)), 1458*m*, 1413*s*, 1390*s*, 1360*m*, 1300*m*, 1265*vs*, 1228*m*, 1115*vs* ($\tilde{\nu}$(C-O)), 1070*m*, 1032*s*, 991*w*, 966*w*, 881*s*, 833*w*, 611*w*. EI-MS (m/z (%)): 512.6(0.1) [M^+], 426 (4) [M^+-Morph], 314 (5) [M^+-NC(Morph)$_2$], 270 (19) [M^+-NC(Morph)$_2$-$(CH_2)_2$O)], 226 (18) [M^+- NC(Morph)$_2$-2$(CH_2)_2$O)], 200 (22) [(Morph)$_2$CNH-2^+], 169 (52), 127 (100), 114 (69), 86 (37)[Morph], 70 (69) [Morph-O]. elemental analysis calcd. for $C_{24}H_{44}N_6O_6$: C 56.21, H 8.66, N 16.40, found: C 56.10, H 8.87, N 16.64.

N^1,N^3-bis(dithiomorpholinomethylene)propane-1,3-diamine, DSMorphG_2p (L12-1):

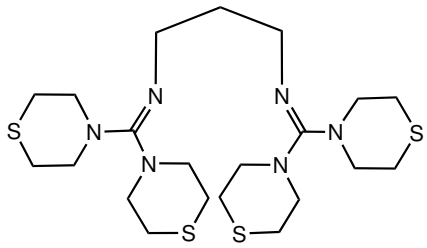

Yellowish powder, yield: 66 %.
^{1}H-NMR (500 MHz, $CDCl_3$, 25°C): δ = 1.25 (q, 2H, CH_2), 2.65 (m, 16, CH_2), 3.2 (m, 16H, CH_2), 3.4 (t, 4H, CH_2) ppm. ^{13}C-NMR (125 MHz, $CDCl_3$, 25°C): δ = 13.5 (CH_2), 27.0 (SMorph-CH_2), 42.3 (SMorph-CH_2), 46.6 (CH_2), 158.0 (C_{gua}) ppm. IR (KBr, $\tilde{\nu}$ [cm^{-1}]): 2969*m*, 2911*m*, 1733*m*, 1621*vs* ($\tilde{\nu}$(C=N)), 1533*s*, 1405*s*, 1374*m*, 1292*m*, 1251*m*, 1205*m*, 1170*m*. EI-MS (m/z (%)): 502.1(23) [M^+], 487(76), 469 (98) [M^+-S], 443(45) [M^+-SEt], 400(33) [M^+-SMorph], 384 (34), 298 (9) [M^+-2SMorph], 196 (23) [M^+-3SMorph], 143 (100) [HN=C-SMorph$^+$], 102(44) [SMorph$^+$], 87 (38), 69 (30). elemental analysis calcd. for $C_{21}H_{38}N_6S_4$: C 50.18, H 7.63, N 16.73, found: C 50.02, H 7.41, N 16.45.

bis(N^1, N^1-(morpholino)-N^3, N^3-dimethyl-methylene)propane-1,3-diamine, (Morph)DMG_2p (L13-1):

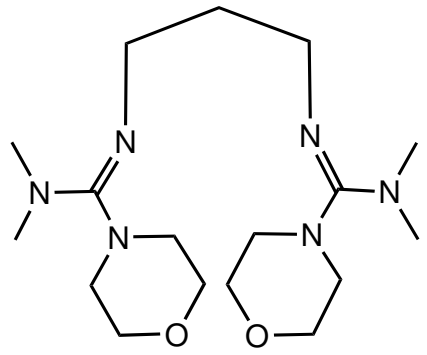

Yellowish oil, yield: 78 %.
^{1}H-NMR (500 MHz, $CDCl_3$, 25°C): δ = 1.77 (q, 2 H, CH_2), 2.57 (s, 12H, CH_3), 2.78-2.98 (broad,18 H, CH_2), 3.06-3.37 (m, 14 H, CH_2) ppm. ^{13}C-NMR (125 MHz, $CDCl_3$, 25°C): δ = 36.1 (CH_2), 39.1 (CH_3), 47.1 (Morph-CH_2), 48.7, 49.6, 159.3 (C_{gua}) ppm. IR (film between NaCl plates, $\tilde{\nu}$ [cm^{-1}]): 2975*m* , 2891*m*, 2852*m*, 1633*s* ($\tilde{\nu}$(C=N)), 1623*vs* ($\tilde{\nu}$(C=N)), 1457*m*, 1423*s*, 1397*s*, 1355*m*, 1304*m*, 1255*s*, 1225*m*, 1112*vs* ($\tilde{\nu}$(C-O)), 1075*m*, 1037*s*, 969*w*, 866*m*, 754*w*, 619*w*. EI-MS (m/z (%)): 354.3 (25) [M^+], 309 (9)[M^+-NMe_2], 279 (12), 241 (33), 198 (12), 184 (69), 154 (23), 127 (48), 86 (100) [Morph$^+$], 72 (84). elemental analysis calcd. for $C_{17}H_{34}N_6O_2$: C 57.58, H 9.67, N 23.72, found: C 57.78, H 10.02, N 23.39.

bis(N^1, N^1-(2,6-dimethylpiperidin-1-yl)-N^3, N^3-dimethyl-methylene)propane-1,3-diamine, (DMPip)DMG_2p (L14-1):

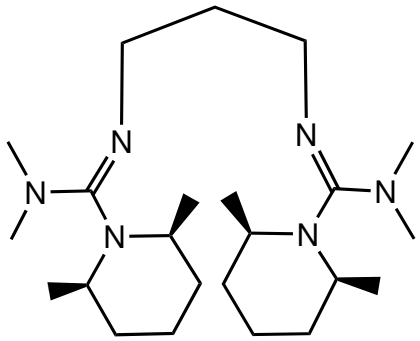

Yellowish oil, yield: 71 %.
^{1}H-NMR (500 MHz, $CDCl_3$, 25°C): δ = 1.03-1.54 (m, 14H, CH_2), 2.79 (s, 12H, CH_3), 2.91 (d, 12H, Pip-CH_3), 3.18-3.49 (m, 8H, CH_2) ppm. ^{13}C-NMR (125 MHz, $CDCl_3$, 25°C): δ = 20.4 (CH_2), 23.0 (CH_2), 30.3 (Pip-CH_3), 31.2 (Pip-CH_3), 36.2 (CH_2-Pip), 36.4 (CH_3), 38.5 (CH_2), 53.8 (CH), 159.1 (C_{gua}) ppm. IR (film between NaCl plates, $\tilde{\nu}$ [cm^{-1}]): 2953*s*, 2935*s*, 2873*m*, 1683*s* ($\tilde{\nu}$(C=N)), 1655*vs* ($\tilde{\nu}$(C=N)), 1647*vs* ($\tilde{\nu}$(C=N)), 1526*m*, 1475*m*, 1418*m*, 1372*w*, 1314*m*, 1272*m*, 1231*w*, 1153*m*. EI-MS (m/z (%)): 406.3 (0.01) [M^+], 362 (0.5) [M^+-NMe_2], 294 (1) [M^+-Me_2Pip], 237 (33) [$(Me_2Pip)_2CH_+$], 183 (45), 149 (51), 124 (100), 112 (43) [Me_2Pip^+], 98 (71) [$CH_3CH(CH_2)_3CHCH_3$], 56 (68). elemental analysis calcd. for $C_{23}H_{46}N_6$: C 67.92, H 11.41, N 20.67, found: C 67.71, H 11.75, N 20.34.

N^1,N^3-bis(tetrahydro-1,3-bis(heptafluoropropyl)pyrimidin-2(1H)-ylidene)propane-1,3-diamine, B^FPPG_2p:

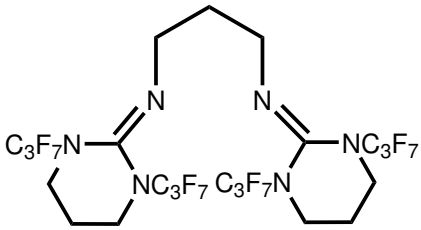

In a Schlenk flask fitted with a condensor cooled to -40°C, phosgene was passed through the etheric solution of N,N,N´,N´-Bis(heptafluoropropyl)propyleneurea (0.05 mmol) at 0°C for 15 min. After 15 min, the reaction mixture was allowed to come to room temperature. The reaction with 1,3-diaminopropane had to be carried out immediately due to the thermal instability of the intermediately formed Vilsmeier salt. The general procedure described above was changed regarding time and temperature of reaction: room temperature and 36 h. The product was obtained as yellow oil, yield: 8 %.
^{1}H-NMR (500 MHz, $CDCl_3$, 25°C): δ = 1.66 (m, 4H, CH_2), 1.81 (m, 2H, CH_2), 3.15 (m, 4H, CH_2), 3.36 (m, 8H, CH_2) ppm. ^{13}C-NMR (125 MHz, $CDCl_3$, 25°C): δ = 21.5 (CH_2), 22.6 (CH_2), 30.5 (CH_2), 40.8 (CH_2), 157.1 (C_{gua}) ppm. IR (film between NaCl plates, $\tilde{\nu}$ [cm^{-1}]): 2944*s*, 2864*m*, 1577*vs* ($\tilde{\nu}$(C=N)), 1525*m*, 1328*m*, 1130*m*, 1064*m*, 956*w*, 833*w*.

8.3.4 Synthesis of copper(I)bisguanidine complexes

General synthesis of bisguanidine copper(I) complexes:
1 mmol of a copper(I) salt was added to a stirred solution of the ligand (1.05 mmol) in MeCN (15 mL). After 30 min of stirring, diethylether (20 mL) was added to obtain the colourless product.

[Cu(TMG$_2$PA*)I] (C1):

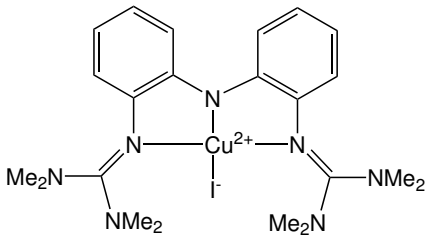

To a suspension of CuI (190 mg, 1 mmol) in 10 mL of THF a solution of TMG$_2$PA (435 mg, 1.1 mmol) in 10 mL of THF was added dropwise. After 30 min of stirring, the red suspension turned dark green. After evaporation of the solvent under reduced pressure, 15 mL of MeCN were added. Dark green crystals suitable for X-ray diffraction were obtained by slow diffusion of diethylether, yield: 77 % (450 mg).

m.p. 189°C. IR (KBr, $\tilde{\nu}$ [cm^{-1}]): 3045w ($\tilde{\nu}$(CH$_{arom}$)), 2925m ($\tilde{\nu}$(CH$_{aliph}$)), 2881w, 2792w, 1612m ($\tilde{\nu}$(C=N)), 1570s ($\tilde{\nu}$(C=N)), 1557vs ($\tilde{\nu}$(C=N)), 1518vs ($\tilde{\nu}$(C=N)), 1475vs, 1466vs, 1439m, 1417s, 1396vs, 1352m, 1329m, 1284m, 1263m, 1230w, 1211m, 1180w, 1159m, 1142m, 1109w, 1061w, 1034m, 920w, 911w, 862w, 843w, 804w, 739m, 733m, 559w. UV/Vis (CH_2Cl_2, λ_{max} [nm] (ϵ [M^{-1}cm^{-1}]): 290 (14000), 345 (10500), 645 (1700). EI-MS (CH_2Cl_2, m/z (rel. intensity)): 584 (5) [M$^+$], 457 (5) [M$^+$ - I], 395 (6) [M$^+$ - CuI], 350 (100) [M$^+$ - CuI -NMe$_2^+$], 306 (42) [M$^+$ - CuI -2 NMe$_2^+$], 263 (38), 234 (51), 205 (44), 161 (82), 118 (22), 85 (57), 58 (37) [CH$_2$NMe$_2^+$], 44 (70) [NMe$_2^+$]. elemental analysis calcd. for $C_{22}H_{32}N_7Cu_I$: C 45.17, H 5.51, N 16.76, found: C 45.65, H 5.24, N 16.17.

[Cu(DMorphG$_2$p)I] (C2):

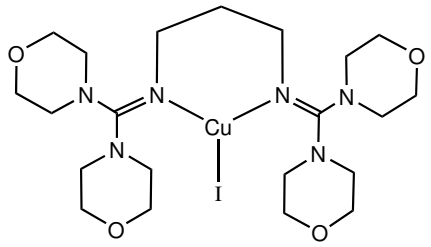

To a suspension of CuI (190 mg, 1 mmol) in 10 mL of THF a solution of DMorphG$_2$p (481 mg, 1.1 mmol) in 10 mL of THF was added dropwise. After 30 min of stirring, diethylether (20 mL) was added to obtain the colourless product, yield: 90 % (565 mg). Crystals suitable for X-ray diffraction were grown by slow diffusion of diethylether into MeCN.

IR (KBr, $\tilde{\nu}$ [cm^{-1}]): 2964m ($\tilde{\nu}$(CH$_{aliph}$)), 2902m, 2852w, 1560vs ($\tilde{\nu}$(C=N)), 1427s, 1382m, 1357m, 1330s, 1263m, 1236m, 1114s ($\tilde{\nu}$(C-O)), 1066s, 1031w, 887w. elemental analysis calcd. for $C_{21}H_{38}N_6O_4CuI$: C 40.12, H 6.10, N 13.38, found: C 40.35, H 6.44, N 12.97.

[Cu$_2$(btmgp)$_2$][PF$_6$]$_2$ (C3):

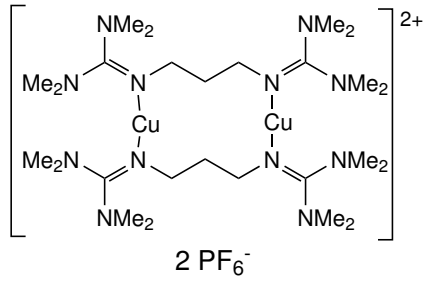

[Cu(MeCN)$_4$][PF$_6$] (372 mg, 1 mmol) was added to a stirred solution of btmgp (284mg, 1.05 mmol) in MeCN (15 mL). After 30 min of stirring, diethylether (20 mL) was added to obtain the colourless product, yield: 90 % (430 mg). Crystals suitable for X-ray diffraction were grown by slow diffusion of diethylether into MeCN.

^{1}H-NMR (300 MHz, $CDCl_3$, 25 °C): δ = 2.28 (m, 2H, H$_b$), 2.89 (s, 12H, CH$_3$), 2.91 (s, 12H, CH$_3$), 3.32 (m, 4H, H$_a$) ppm. IR (KBr, $\tilde{\nu}$ [cm^{-1}]): 3435w, 2953m ($\tilde{\nu}$(CH$_{aliph}$)), 2931m ($\tilde{\nu}$(CH$_{aliph}$)), 2881m, 2853w, 1564s ($\tilde{\nu}$(C=N)), 1558s ($\tilde{\nu}$(C=N)), 1539s ($\tilde{\nu}$(C=N)), 1477m, 1464m, 1456m, 1427m,

1416*m*, 1408*m*, 1398*s* ($\tilde{\nu}$(C=N)), 1362*m* ($\tilde{\nu}$(C=N)), 1337*vw*, 1240*w*, 1169*m* ($\tilde{\nu}$(C=N)), 1161*w*, 1123*w*, 1070*m* ($\tilde{\nu}$(C=N)), 1024*w*, 1011*w*, 899*w*, 876*m*, 839*vs* ($\tilde{\nu}$(P-F)), 779*w*, 557*m*. UV/Vis (CH_2Cl_2, λ_{max} [nm] (ϵ [$M^{-1}cm^{-1}$]): no bands, shoulder at 360 (233). elemental analysis, calcd. for $C_{26}H_{60}N_{12}Cu_2P_2F_{12}$: C 32.60, H 6.31, N 17.55 ; found : C 32.66, H 6.39, N 17.52.

[Cu_2(TMG$_2$ch)$_2$][I]$_2$ (C4):

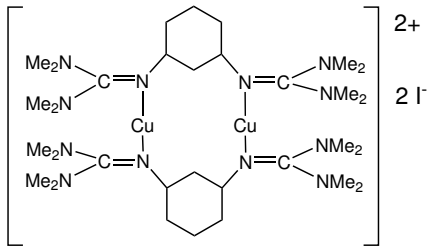

CuI (190 mg, 1 mmol) was added to a stirred solution of TMG$_2$ch (326 mg, 1.05 mmol) in MeCN (15 mL). After 30 min of stirring, diethylether (20 mL) was added to obtain the colourless product, yield: 45 % (225 mg). Crystals suitable for X-ray diffraction were grown by slow diffusion of diethylether into MeCN.

IR (KBr, $\tilde{\nu}$ [cm^{-1}]): 2929*m* ($\tilde{\nu}$(CH_{aliph})), 1616*vs* ($\tilde{\nu}$(C=N)), 1572*vs* ($\tilde{\nu}$(C=N)), 1560*vs* ($\tilde{\nu}$(C=N)), 1458*m*, 1403 *m*, 1232*m*, 1171*w*, 1142*m*, 1036*m*, 899*w*, 808*w*, 545*w*. elemental analysis calcd. for $C_{32}H_{68}N_{12}Cu_2I_2$: C 38.36, H 6.84, N 16.78, found: C 38.02, H 7.21, N 16.47.

[Cu_2(DMEG$_2$p)$_2$][PF_6]$_2$ (C5):.

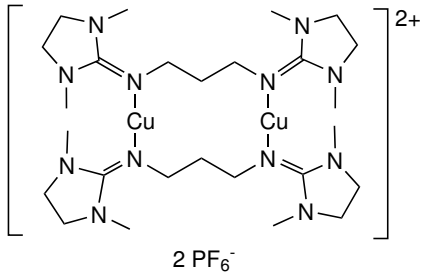

[Cu(MeCN)$_4$][PF_6] (372 mg, 1 mmol) was added to a stirred solution of DMEG$_2$p (279 mg, 1.05 mmol) in MeCN (15 mL). After 30 min of stirring, diethylether (20 mL) was added to obtain the colourless product, yield: 82 % (389 mg). Crystals suitable for X-ray diffraction were grown by slow diffusion of diisopropylether into MeCN.

^{1}H-NMR (500 MHz, CD_3CN, 25 °C): δ = 1.82 (m, 2H, CH_2), 3.00 (s, 12H, CH_3), 3.46 (b, 8H, CH_2), 3.65 (t, 4H, CH_2) ppm. ^{13}C-NMR (125 MHz, CD_3CN, 25 °C): δ = 35.0 (C_a), 35.6 (CH_3), 45.2 (C_b), 49.2 (CH_2), 162.4 (C_{gua}) ppm. IR ($\tilde{\nu}$ [cm^{-1}]): 2929*s*, 2894*s*, 1631*s* ($\tilde{\nu}$(C=N)), 1601*vs* ($\tilde{\nu}$(C=N)), 1512*m* ($\tilde{\nu}$(C=N)), 1490*m*, 1459*m*, 1419*m*, 1400*m*, 1345*w*, 1300*s*, 1232*w*, 1208*w*, 1121*w*, 1076*w*, 1034*w*, 970*vw*, 839*vs* ($\tilde{\nu}$(P-F)), 723*w*, 646*w*, 557*vs*, 484*w*. elemental analysis (after drying in vacuo), calcd. for $C_{26}H_{52}N_{12}Cu_2P_2F_{12}$: C 32.88, H 5.52, N 17.70 ; found : C 33.19, H 5.28, N 17.93.

$[Cu_2(DMEG_2ch)_2][Cu_2I_4]$ (C6) and $[Cu_2(DMEG_2ch)_2][Cu_4I_6]$ (C7):

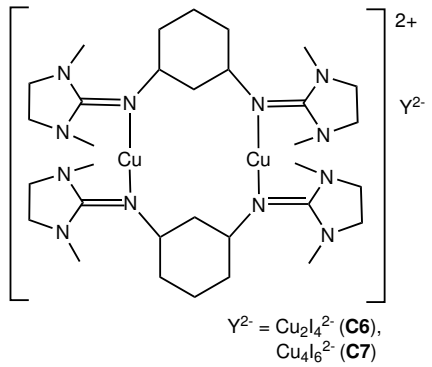

CuI (190 mg, 1 mmol) was added to a stirred solution of $DMEG_2ch$ (321 mg, 1.05 mmol) in MeCN (15 mL). After 30 min of stirring, diethylether (20 mL) was added slowly. The next day, colourless crystals of **C6** and yellow crystals of **C7** were grown. In a repetition of this experiment, only colourless crystals of **C6** were obtained, yield: 42 % (208 mg).

IR (KBr, $\tilde{\nu}$ [cm^{-1}]): 2931*m* ($\tilde{\nu}(CH_{aliph})$), 1623*vs* ($\tilde{\nu}$(C=N)), 1583*vs* ($\tilde{\nu}$(C=N)), 1560*vs* ($\tilde{\nu}$(C=N)), 1508*m*, 1457 *m*, 1419*m*, 1374*m*, 1295*m*, 1122*w*, 1035*m*, 964*w*, 879*w*, 806*w*, 528*w*. elemental analysis calcd. for $C_{32}H_{60}N_{12}Cu_4I_4$ (**C6**): C 27.96, H 4.40, N 12.23, found: C 28.61, H 4.44, N 12.36.

$[Cu_2(DMPG_2p)_2][PF_6]_2$ (C8):

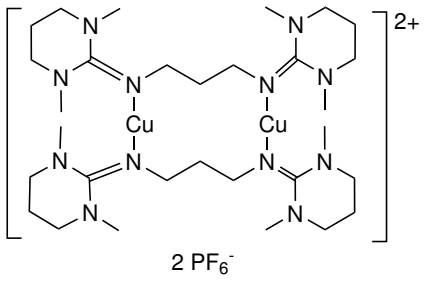

$[Cu(MeCN)_4][PF_6]$ (372 mg, 1 mmol) was added to a stirred solution of $DMPG_2p$ (308.7 mg, 1.05 mmol) in MeCN (15 mL). After 30 min of stirring, diethylether (20 mL) was added to obtain the colourless product, yield: 86 % (433 mg). Crystals suitable for X-ray diffraction were grown by slow diffusion of diisopropylether into MeCN.

^{1}H-NMR (500 MHz, CD_3CN, 25 °C): δ = 1.62 (m, 2H, CH_2), 1.71 (m, 4H, CH_2), 2.95 (s, 12H, CH_3), 3.15 (m, 8H, CH_2) ppm. 13C-NMR (125 MHz, CD_3CN, 25 °C): δ = 22.3 (CH_2), 34.8 (C_a), 40.1 (CH_3), 46.3 (C_b), 49.7 (CH_2), 160.6 (C_{gua}) ppm. IR (KBr, $\tilde{\nu}$ [cm^{-1}]): 2953*s*, 2919*s*, 2864*s*, 2831*m*, 1564*vs* ($\tilde{\nu}$(C=N)), 1552*vs* ($\tilde{\nu}$(C=N)), 1537*vs* ($\tilde{\nu}$(C=N)), 1473*s*, 1453*s*, 1419*s*, 1403*vs* ($\tilde{\nu}$(C=N)), 1376*s*, 1354*s*, 1325*s*, 1313*s*, 1272*w*, 1236*s*, 1206*w*, 1162*w*, 1113*w*, 1084*m*, 1050*m*, 1014*m*, 837*vs* ($\tilde{\nu}$(P-F)), 769*s*, 557*s*, 511*m*. elemental analysis, calcd. for $C_{30}H_{60}N_{12}Cu_2P_2F_{12}$: C 35.82, H 6.01, N 16.71 ; found : C 35.64, H 6.07, N 16.58.

$[Cu_2(DPipG_2p)_2][PF_6]_2$ (C9):.

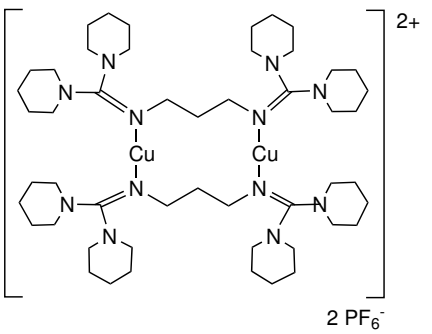

$[Cu(MeCN)_4][PF_6]$ (372 mg, 1 mmol) was added to a stirred solution of $DPipG_2p$ (452 mg, 1.05 mmol) in MeCN (15 mL). After 30 min of stirring, diethylether (20 mL) was added to obtain the colourless product, yield: 82 % (524 mg). Crystals suitable for X-ray diffraction were grown by slow diffusion of diisopropylether into MeCN.

^{1}H-NMR (500 MHz, CD_3CN, 25 °C): δ = 1.48-1.58 (m, 24H, Pip-CH_2), 1.71 (q, 2H, CH_2), 3.05 (t, 16H, Pip-CH_2), 3.55 (t, 4H, CH_2) ppm. ^{13}C-NMR (125 MHz, CD_3CN, 25 °C): δ = 24.0 (Pip),

25.2 (Pip), 25.6 (Pip) 33.8 (C_a), 47.6 (C_b), 49.3 (Pip), 160.2 (C_{gua}) ppm; IR (KBr, $\tilde{\nu}$ [cm^{-1}]): 2934m ($\tilde{\nu}(CH_{aliph})$), 2852m ($\tilde{\nu}(CH_{aliph})$), 1626s ($\tilde{\nu}$(C=N)), 1554s ($\tilde{\nu}$(C=N)), 1548s ($\tilde{\nu}$(C=N)), 1491m ($\tilde{\nu}$(C=N)), 1440m, 1372m, 1341w, 1261w, 1253m, 1236w, 1211w, 1203w, 1163m, 1114w, 1078m, 1023m, 1016w, 985w, 907w, 839vs ($\tilde{\nu}$(P-F)), 787m, 705w, 581w, 555m. elemental analysis, calcd. for $C_{50}H_{92}N_{12}Cu_2P_2F_{12}$: C 46.98, H 7.25, N 13.15 ; found : C 46.99, H 7.22, N 13.19.

$[Cu(DMEG_2p)]_n[PF_6]_n$ (C10):

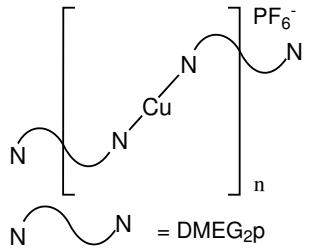

$[Cu(MeCN)_4][PF_6]$ (372 mg, 1 mmol) was added to a stirred solution of $DMEG_2p$ (279 mg, 1.05 mmol) in THF (15 mL). After 30 min of stirring, diethylether (20 mL) was added to obtain the colourless product, yield: 86 % (433 mg). Crystals suitable for X-ray diffraction were grown by slow diffusion of diethylether into THF.
IR (KBr, $\tilde{\nu}$ [cm^{-1}]): 2933w ($\tilde{\nu}(CH_{aliph})$), 1634vs ($\tilde{\nu}$(C=N)), 1595vs ($\tilde{\nu}$(C=N)), 1487w, 1372m, 1298m, 1139w, 1037w, 962w, 838vs ($\tilde{\nu}$(P-F)), 803w, 692w, 637w. elemental analysis calcd. for $C_{26}H_{52}N_{12}Cu_2P_2F_{12}$: C 32.88, H 5.52, N 17.70 ; found : C 33.27, H 5.23, N 18.05.

$[Cu(DMEG_2p)]_n[I]_n$ (C11):

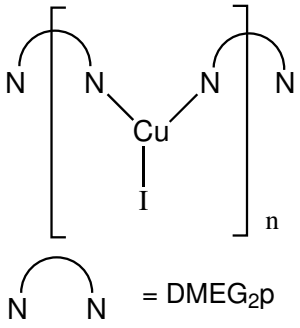

CuI (190 mg, 1 mmol) was added to a stirred solution of $DMEG_2p$ (279 mg, 1.05 mmol) in MeCN (15 mL). After 30 min of stirring, diethylether (20 mL) was added to obtain the colourless product, yield: 86 % (433 mg). Crystals suitable for X-ray diffraction were grown by slow diffusion of diethylether into MeCN.
IR (KBr, $\tilde{\nu}$ [cm^{-1}]): 2931w ($\tilde{\nu}(CH_{aliph})$), 1635vs ($\tilde{\nu}$(C=N)), 1595vs ($\tilde{\nu}$(C=N)), 1488w, 1371m, 1299m, 1139w, 1037m, 962w, 800w, 694w, 640w. elemental analysis calcd. for $C_{26}H_{52}N_{12}Cu_2I_2$: C 34.21, H 5.75, N 18.42 ; found : C 33.97, H 5.49, N 18.02.

$[Cu(TMG_2mX)]_n[I]_n$ (C12):

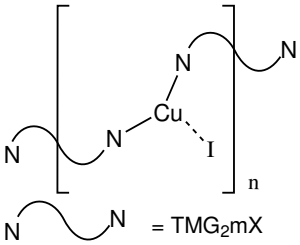

CuI (190 mg, 1 mmol) was added to a stirred solution of TMG_2mX (349 mg, 1.05 mmol) in MeCN (15 mL). After 30 min of stirring, diethylether (20 mL) was added to obtain the colourless product, yield: 90 % (470 mg). Crystals suitable for X-ray diffraction were grown by slow diffusion of diethylether into MeCN.
IR (KBr, $\tilde{\nu}$ [cm^{-1}]): 3053w ($\tilde{\nu}(CH_{arom})$), 2999m ($\tilde{\nu}(CH_{aliph})$), 2932s, 2891s, 2842s, 2792m, 1558vs ($\tilde{\nu}$(C=N)), 1525vs ($\tilde{\nu}$(C=N)), 1473vs ($\tilde{\nu}$(C=N)), 1425s, 1385vs, 1350vs, 1225s, 1145s, 1069s, 1036s, 993m, 910m, 881s, 796s, 735w,

703*s*, 630*w*, 595*m*, 541*w*, 506*w*. elemental analysis calcd. for $C_{36}H_{64}N_{12}Cu_2I_2$: C 41.37, H 6.18, N 16.09 ; found : C 41.02, H 6.43, N 16.37.

$[Cu(DPPG_2p)]_n[CuI_2]_n$ (C13):

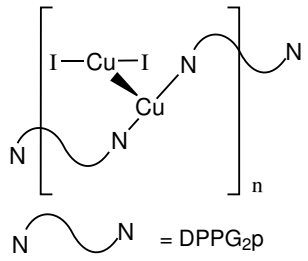

CuI (190 mg, 1 mmol) was added to a stirred solution of $DPPG_2p$ (426 mg, 1.05 mmol) in MeCN (15 mL). After 30 min of stirring, the solvent was removed under reduced pressure. From the residual oil crystals suitable for X-ray diffraction were grown after 3 months.
IR (KBr, $\tilde{\nu}$ [cm^{-1}]): 2962*m* ($\tilde{\nu}(CH_{aliph})$), 2873*w*, 1604*vs* ($\tilde{\nu}$(C=N)), 1508*s* ($\tilde{\nu}$(C=N)), 1457*m*, 1374*m*, 1324*w*, 1211*m*, 1101*w*, 943*w*, 892*w*, 752*w*, 640*w*.

$[Cu_2(TMGbenzPA)_2][PF_6]_2$ (C14):

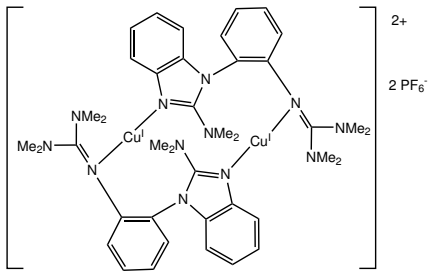

To a solution of 375 mg (1 mmol) $[Cu(MeCN)_4][PF_6]$ in 10 ml of MeCN a solution of 366 mg (1,05 mmol) TMG_2PA in 10 mL of MeCN was added dropwise. The reaction mixture was refluxed for 2 h. An colourless solution formed. Crystals suitable for X-ray diffraction were grown by slow diffusion of diisopropylether into MeCN, yield: 58 % (648 mg). IR (KBr, $\tilde{\nu}$ [cm^{-1}]): 3070*vw* ($\tilde{\nu}(CH_{arom})$), 2939*w* ($\tilde{\nu}(CH_{aliph})$), 1622*vs*(C=N), 1579*vs* ($\tilde{\nu}$(C=N)), 1567*vs* ($\tilde{\nu}$(C=N)), 1522*vs*, 1491*s*, 1471*vs*, 1454*m*, 1423*vs*, 1414*vs*, 1405*vs*, 1396*vs*, 1317*m*, 1294*w*, 1280*w*, 1255*vw*, 1147*w*, 837*vs* ($\tilde{\nu}$(P-F)), 742*m*, 557*s*.

8.3.5 Synthesis of copper(II)complexes

$[Cu_2(btmmO)_2][PF_6]_2 \cdot 2CH_3CN$ (C15):

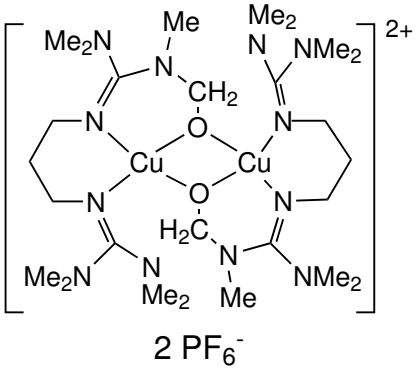

A solution of 287 mg (0.3 mmol) of $[Cu_2(btmgp)_2][PF_6]_2$ (**C3**) in 50 mL of MeCN was treated at -40°C with pure oxygen. The formerly colourless solution turns to red and upon warming to dark blue. Single crystals were obtained by vapour diffusion of pentane into this solution in red needles. Yield: 46 % (151 mg).
^{1}H-NMR (300 MHz, $CDCl_3$, δ = 1.26 (s, 18H, CH_3), 1.62 (s, 18H, CH_3), 2.93 (m, 12H), 3.04 (s, 6H, CH_2), 3.42 (s, 4H, -CH_2O-) ppm. IR (KBr, $\tilde{\nu}$ [cm^{-1}]): 2931*m* ($\tilde{\nu}(CH_{aliph})$), 2907*m* ($\tilde{\nu}(CH_{aliph})$), 2811*w*, 1621*s* ($\tilde{\nu}$(C=N)), 1574*s* ($\tilde{\nu}$(C=N)), 1556*s* ($\tilde{\nu}$(C=N)), 1520*m* ($\tilde{\nu}$(C=N)), 1473*m*, 1456*m*, 1446*m*, 1428*m*, 1417*m*, 1400*s* ($\tilde{\nu}$(C=N)), 1371*m*, 1348*w*, 1336*w*, 1272*w*, 1238*w*, 1214*w*, 1203*w*, 1169*m*, 1145*w*, 1115*w*, 1088*m*, 1068*m*, 1043*m* ($\tilde{\nu}$(C-O)), 999*w*, 931*m*, 904*m*, 837*vs* ($\tilde{\nu}$(P-F)), 793*m*, 785*w*,

$702w$, $586w$, $557s$, $431w$.
UV/vis (CH_2Cl_2, λ_{max} [nm] (ϵ [$M^{-1}cm^{-1}$]): 252 (12700), 296 (3300), 393 (1200), 550 (470); elemental analysis (after drying in vacuo), calcd. for $C_{26}H_{58}O_2N_{12}Cu_2P_2F_{12}$: C 31.61, H 5.92, N 17.02 ; found: C 31.09, H 5.76, N 17.03.

$[Cu_2(TMMoG_2MePA)_2][PF_6]_2$ (C16):

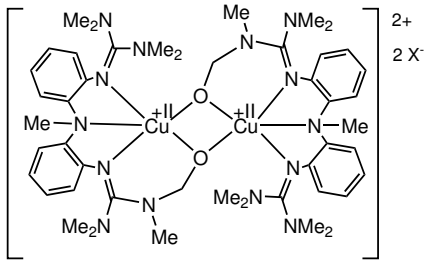

A solution of 309 mg (0.5 mmol) of [Cu(TMG$_2$MePA)][PF_6] in 50 mL of MeCN was treated at room temperature with dioxygen. After standing for one week, dark green crystals suitable for X-ray diffraction were obtained, yield: 41 % (133 mg).
IR (KBr, $\tilde{\nu}$ [cm^{-1}]): $3066w$ ($\tilde{\nu}(CH_{arom})$), $2937m$ ($\tilde{\nu}(CH_{aliph})$), $2889m$, $1549vs$ ($\tilde{\nu}$(C=N)), $1487vs$, $1425vs$, $1338m$, $1269m$, $1161m$, $1030s$ ($\tilde{\nu}$(C-O)), $840vs$ ($\tilde{\nu}$(P-F)), $756m$, $630w$, $557vs$, $475w$.

$[Cu_2(TMMoG_2MePA)_2][ClO_4]_2$ (C17): A solution of 286 mg (0.5 mmol) of [Cu(TMG$_2$MePA)][ClO_4] in 50 mL of MeCN was treated at room temperature with dioxygen. After standing for three weeks, dark green crystals suitable for X-ray diffraction were obtained, yield: 47 % (142 mg).
IR (KBr, $\tilde{\nu}$ [cm^{-1}]): $3063w$ ($\tilde{\nu}(CH_{arom})$), $2964w$ ($\tilde{\nu}(CH_{aliph})$), $2935w$ ($\tilde{\nu}(CH_{aliph})$), $1635s$ ($\tilde{\nu}$(C=N)), $1616s$ ($\tilde{\nu}$(C=N)), $1585s$ ($\tilde{\nu}$(C=N)), $1558vs$ ($\tilde{\nu}$(C=N)), $1521vs$, $1488s$, $1457s$, $1398vs$, $1338m$, $1261s$, $1094vs$ ($\tilde{\nu}$(Cl-O)), $1035s$ ($\tilde{\nu}$(C-O)), $916w$, $802m$, $752m$, $702m$, $669m$, $622s$, $594m$, $526m$, $458w$.

$[Cu_2(TMMoG_2MePA)_2][BF_4]_2$ (C18): A solution of 280 mg (0.5 mmol) of [Cu(TMG$_2$MePA)][BF_4] in 50 mL of MeCN was treated at room temperature with dioxygen. By vapour diffusion of diisopropylether, dark green crystals suitable for X-ray diffraction were obtained, yield: 39 % (115 mg).
IR (KBr, $\tilde{\nu}$ [cm^{-1}]): $3069w$ ($\tilde{\nu}(CH_{arom})$), $2971w$ ($\tilde{\nu}(CH_{aliph})$), $2936w$ ($\tilde{\nu}(CH_{aliph})$), $1638s$ ($\tilde{\nu}$(C=N)), $1619s$ ($\tilde{\nu}$(C=N)), $1581vs$ ($\tilde{\nu}$(C=N)), $1555vs$ ($\tilde{\nu}$(C=N)), $1523vs$, $1487s$, $1395s$, $1338m$, $1265s$, $1036s$ ($\tilde{\nu}$(C-O)), $919w$, $805w$, $754m$, $706m$, $673m$, $623m$, $597w$, $528w$.

$[Cu_2(TMG_2MePA)_2(\mu\text{-}OH)_2][Cu_2I_4]$ (C19) and $[Cu_2(TMG_2MePA)_2(\mu\text{-}OH)_2][I_3]_2$ (C20):

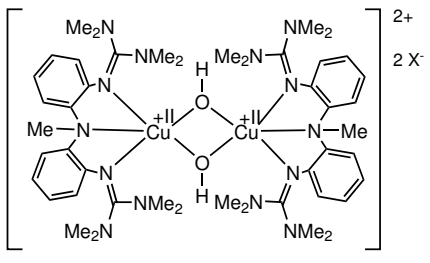

A solution of 300 mg (0.5 mmol) of [Cu(TMG$_2$MePA)]I in 50 mL of MeCN was treated at room temperature with dioxygen. By vapour diffusion of diisopropylether, dark green crystals of **C19** suitable for X-ray diffraction were obtained, yield: 34 % (107 mg). Additionally, after further vapour diffusion of diisopropylether, bright yellow crystals of **C20** suitable for X-ray

diffraction were obtained, yield: 8 % (46 mg). IR (KBr, $\tilde{\nu}$ [cm^{-1}]): 3466w ($\tilde{\nu}$(O-H)), 3062w ($\tilde{\nu}$(CH$_{arom}$)), 2974w ($\tilde{\nu}$(CH$_{aliph}$)), 1622s ($\tilde{\nu}$(C=N)), 1585vs ($\tilde{\nu}$(C=N)), 1552s ($\tilde{\nu}$(C=N)), 1525s, 1485s, 1396m, 1339w, 1262m, 914w, 807w, 757w, 707m, 675w, 625w, 522vw.

[Cu$_2$(MMoEG$_2$p)$_2$][PF$_6$]$_2$ (C21):

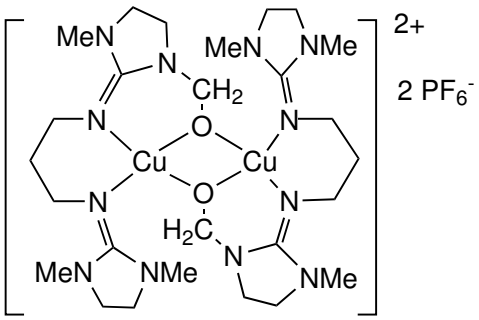

A solution of 475 mg (0.5 mmol) of [Cu$_2$(DMEG$_2$p)$_2$][PF$_6$]$_2$ in 50 mL of MeCN was treated at room temperature with dioxygen. By vapour diffusion of diisopropylether, dark red crystals of **C21** suitable for X-ray diffraction were obtained, yield: 42 % (206 mg).
IR (KBr, $\tilde{\nu}$ [cm^{-1}]): 2933s, 2892s, 1625s ($\tilde{\nu}$(C=N)), 1606vs ($\tilde{\nu}$(C=N)), 1504m, 1495s, 1461m, 1416s, 1402m, 1343m, 1303s, 1127m, 1078w, 1034w ($\tilde{\nu}$(C-O)), 838vs ($\tilde{\nu}$(P-F)), 726w, 641w, 558vs, 482vw.

[Cu$_2$(DPipG$_2$p)$_2$(μ-OH)$_2$][PF$_6$]$_2$ (C22):

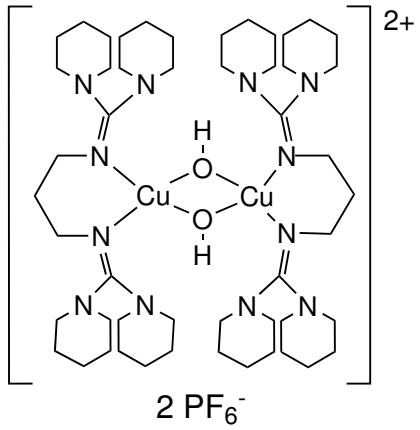

A solution of 262 mg (0.2 mmol) of [Cu$_2$(DPipG$_2$p)$_2$][PF$_6$]$_2$ (**C9**) in 50 mL of MeCN was treated at room temperature with dioxygen. After standing for one week, dark blue crystals suitable for X-ray diffraction were obtained, yield: 45 % (121 mg).
IR (KBr, $\tilde{\nu}$ [cm^{-1}]): 3446vw ($\tilde{\nu}$(O-H)), 2937s ($\tilde{\nu}$(CH$_{aliph}$)), 2852s, 1533vs ($\tilde{\nu}$(C=N)), 1495s ($\tilde{\nu}$(C=N)), 1446vs, 1371s, 1335m, 1253m, 1226m, 1205m, 1164w, 1141m, 1110m, 1070w, 1020m, 948m, 917w, 839vs ($\tilde{\nu}$(P-F)), 744m, 622w, 597w, 557m, 487w.

[Cu$_2$(TMMoG$_2$ch)$_2$][I]$_2$ (C23):

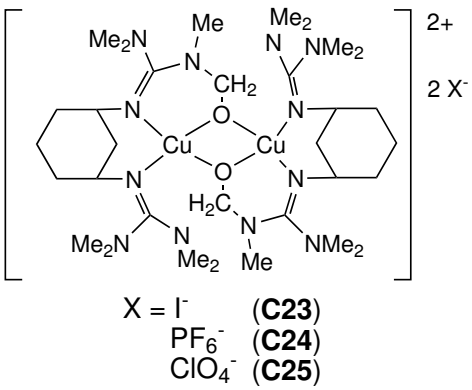

A solution of 500 mg (0.5 mmol) of [Cu$_2$(TMG$_2$ch)$_2$][I]$_2$ (**C4**) in 50 mL of MeCN was treated at room temperature with dioxygen. By vapour diffusion of diisopropylether, dark red crystals of **C23** suitable for X-ray diffraction were obtained, yield: 41 % (212 mg).
IR (KBr, $\tilde{\nu}$ [cm^{-1}]): 2941m ($\tilde{\nu}$(CH$_{aliph}$)), 1616vs ($\tilde{\nu}$(C=N)), 1576vs ($\tilde{\nu}$(C=N)), 1458m, 1396s, 1313w, 1224w, 1164w, 1060w, 1033m ($\tilde{\nu}$(C-O)), 885w, 723w.

[Cu$_2$(TMMoG$_2$ch)$_2$][PF$_6$]$_2$ (C24): A solution

of 519 mg (0.5 mmol) of $[Cu_2(TMG_2ch)_2][PF_6]_2$ in 50 mL of MeCN was treated at room temperature with dioxygen. By vapour diffusion of diisopropylether, red crystals of **C24** suitable for X-ray diffraction were obtained, yield: 44 % (235 mg).
IR (KBr, $\tilde{\nu}$ [cm^{-1}]): 2941*w* ($\tilde{\nu}$ (CH_{aliph})), 1613*s* ($\tilde{\nu}$(C=N)), 1544*vs* ($\tilde{\nu}$(C=N)), 1475*s*, 1393*s*, 1236*m*, 1168*m*, 1033*m* ($\tilde{\nu}$(C-O)), 903*m*, 845*w*, 837*vs* ($\tilde{\nu}$ (P-F)), 783*w*, 622*m*, 563*w*.
$[Cu_2(TMMoG_2ch)_2][ClO_4]_2$ (C25): A solution of 473 mg (0.5 mmol) of $[Cu_2(TMG_2ch)_2][ClO_4]_2$ in 50 mL of MeCN was treated at room temperature with dioxygen. By vapour diffusion of diisopropylether, dark red crystals of **C25** suitable for X-ray diffraction were obtained, yield: 39 % (191 mg).
IR (KBr, $\tilde{\nu}$ [cm^{-1}]): 2943*w* ($\tilde{\nu}$ (CH_{aliph})), 1618*s* ($\tilde{\nu}$(C=N)), 1541*vs* ($\tilde{\nu}$(C=N)), 1473*m*, 1396*s*, 1234*w*, 1166*w*, 1093*vs* ($\tilde{\nu}$ (Cl-O)), 1034*m* ($\tilde{\nu}$(C-O)), 908*w*, 848*w*, 786*w*, 678*w*, 624*m*, 568*w*.

$[Cu_2(MorphDMG_2p)_2(\mu\text{-}F)_2][PF_6]_2$ (C26):

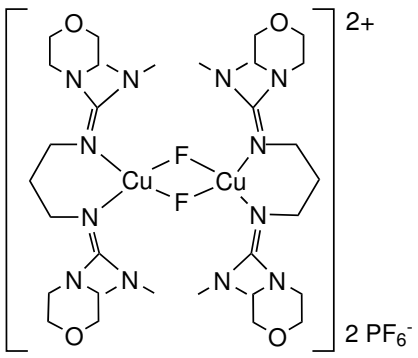

A solution of 563 mg (0.5 mmol) of $[Cu_2(MorphDMG_2p)_2][PF_6]_2$ in 20 mL of MeCN was treated at room temperature with dioxygen. Dark blue crystals suitable for X-ray diffraction were grown by slow diffusion of diisopropylether into MeCN, yield: 48 % (278 mg). IR (KBr, $\tilde{\nu}$ [cm^{-1}]): 2924*m* ($\tilde{\nu}$(CH_{aliph})), 2856*m* ($\tilde{\nu}$(CH_{aliph})), 1616*s* ($\tilde{\nu}$(C=N)), 1558*vs* ($\tilde{\nu}$(C=N)), 1468*s*, 1398*s*, 1267*m*, 1111*s*, 1066*m*, 887*w*, 840*vs* ($\tilde{\nu}$(P-F)), 759*w*, 617*w*, 555*w*.

8.3.6 Catalytic reactions with 2,4-di^{tert}butylphenol, 2,6-di^{tert}butylphenol and 3,5-di^{tert}butylcatechol

In order to have exactly the same conditions for the catalytical screening, 0.1 mmol of Cu(I) bisguanidine complex was freshly prepared in 30 mL of CH_2Cl_2 (see section 8.3.4. for preparation). This stem solution was divided in three parts of 10 mL each which were oxygenated by stirring for 2 min in the presence of air. Afterwards, to each part, 100 mg (0.48 mmol) of 2,4-di^{tert}butylphenol or of 2,6-di^{tert}butylphenol or 100 mg (0.45 mmol) of 3,5-DTBC were added to the stirred solution, respectively. After 16 h of stirring at room temperature, the reaction was quenched by the addition of 10 mL of 5% perchloric acid. After 5 min of stirring, the phases were separated and the aqueous phase was extracted with CH_2Cl_2. The combined organic phases were dried with Na_2SO_4. These solutions were analysed by means of gaschromatographic separation and mass spectrometric analysis in order to determine the conversion and the selectivity of the reactions.
As comparative experiment, this procedure was carried out with pure CH_2Cl_2 instead of the Cu(I) complex solutions. The GC/MS analyses revealed that the educts remained unchanged.

9 Conclusion and Perspective

The assembly of bisguanidine molecules starting from secondary amines and phosgene for use in biomimetic coordination chemistry, especially in the field of copper-controlled oxygen activation, has provided a set of bifunctional N-donor ligands. Each member of this set adjusts the redox capabilities of its corresponding Cu(I) complexes towards molecular oxygen in a specific fashion depending on the spatial demands of the guanidine functionalities as well as on the conformational freedom possible within the steric limits allowed by the spacer fragments connecting these units. In contrast to established literature procedures, this method to arrive at bisguanidine molecules is not dependent from predefined peralkylated urea precursors as we start from secondary amines as simple building blocks and thus define the urea intermediates by simply choosing suitably substituted educts. The synthetic protocol has been optimised to obtain overall yields in the range from 65 to 95 %. The modular approach allows the universal modification of the aliphatic guanidine substitution as well as of the spacers with respect to rigidity, extension of the backbone and additional donor functions. In general, such a matrix of bisguanidine ligands can also be screened regarding their ability to stabilise complexes of other transition metals in unusually high oxidation states.

By applying this modular approach, 30 new bisguanidine ligands have been synthesised and characterised which are depicted on Figure 9.1. Furthermore, the crystal structures of **L1-4**, **L5-1**, **L7-1**, **L11-1** and $[H_2$**L1-2**$]I_2 \cdot Et_2O$ are discussed regarding their characteristics as these ligands are the first unprotonated guanidine ligands to be crystallised. Furthermore, the multi-step synthesis of the first fluorinated bisguanidine ligand B^FPPG_2p was successfully accomplished. Starting with this library of bisguanidine ligands, several copper(I) bisguanidine complexes could be crystallised which are summarised in Figure 9.2: the mononuclear compounds **C1** and **C2** are examples for the chelating coordination mode of these ligands. In fact, in the course of the synthesis of **C1**, the Cu(I) is oxidised to Cu(II) under deprotonation of the ligand and reduction of the released proton. **C1** exhibits a distorted butterfly-like coordination geometry whereas **C2** is coordinated trigonal-planar like its predecessor [Cu(btmgp)I]. The dinuclear complexes **C3** - **C9** contain twelve-membered heterocyclic structures with linear coordinated Cu(I) atoms. The folding of their propylene chains and their corresponding interligand H...H separations can be correlated with the Cu...Cu distances which vary between 4.121 and 5.054 Å. **C10** - **C13** exhibit molecular chain structures with great differences in the Cu coordination: in crystals of **C10**, the copper is

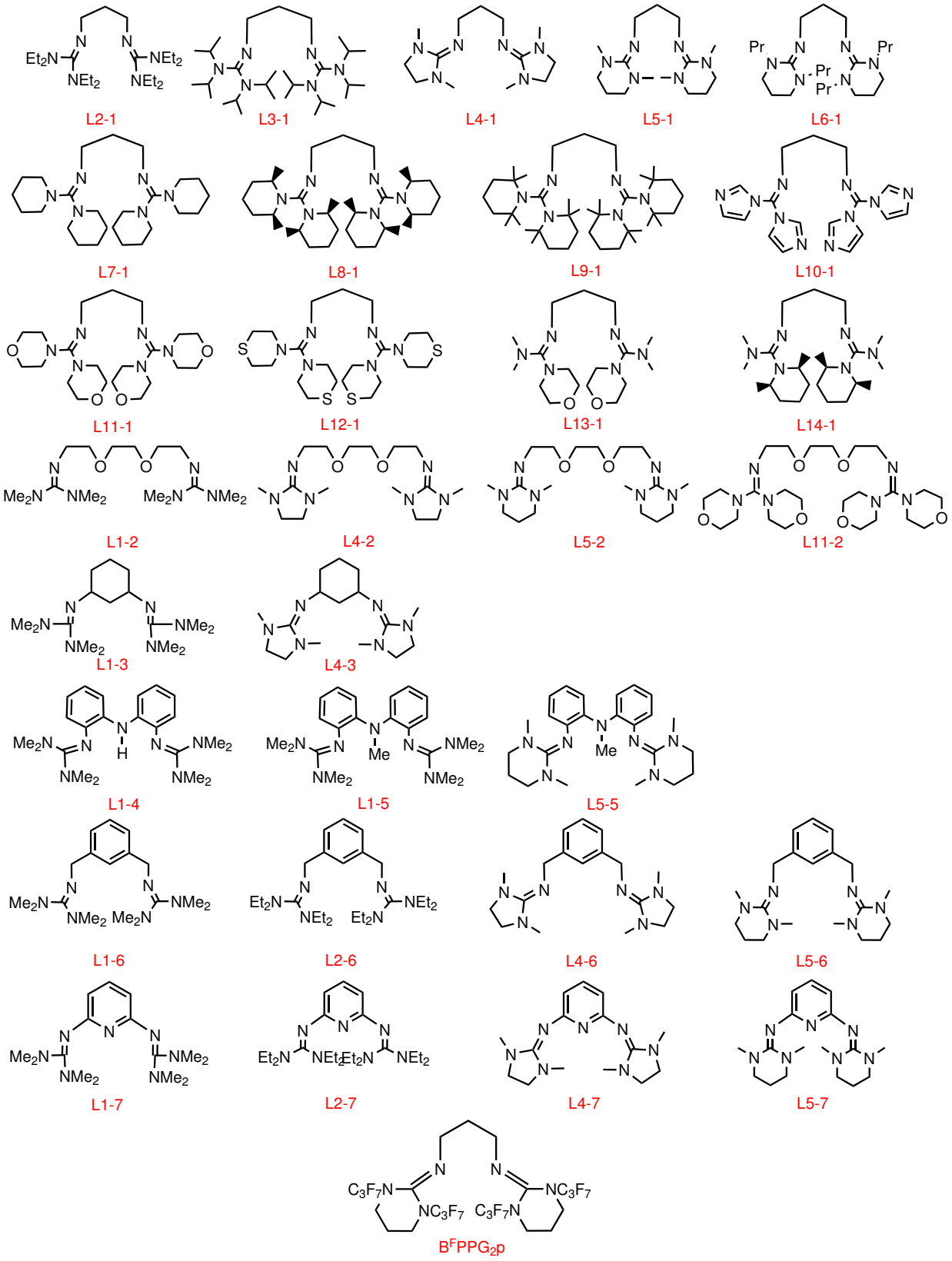

Figure 9.1: Schematic summary of the synthesised bisguanidine ligands

coordinated linearly, whereas in **C11** (by using the same ligand **L4-1**), the Cu1 atom is coordinated distorted trigonal and the Cu2 atom trigonal-planar. In **C12**, a coordination mode in between these two is realized. **C13** exhibits a twisted double T-shaped structure

motif with a $N_2Cu..CuI_2$ unit. The Cu...Cu interaction of 2.6732(6) Å is quite short. The dinuclear complex **C14** was obtained after a cyclisation reaction of ligand **L1-4** and the subsequent coordination of Cu(I). In summary, it could be shown that the novel bidentate guanidine ligands are capable of stabilising μ-η^2:η^2-peroxo dicopper(II) cores as well as bis(μ-oxo) dicopper(III) cores. It turned out that the decision between these two cores is made by the inherent torsion of the guanidine system. Twisted systems like **C2**, **C3**, **C4** and **C9** with angles around 35° favour the stabilisation of an O-core complex, whereas "flat" systems with angles around 16° incorporated in **C5** and **C6** support P-core complexes. **C8** and **C13** have angles which are in the middle of this range with 24.8 and 28.5°, respectively. Hence, it can be understood why **C8** shows solvent-depending behaviour. The sensitive P/O-core equilibrium can be shifted at this point only by a change from a coordinating solvent to a non-coordinating one. In an attempt to elucidate the principal factors that control the P-core/O-core equilibrium, the degree of conjugation within the guanidine moiety has been successfully correlated with the reaction behaviour of the corresponding copper(I) complex towards oxygen. Additionally, the ligands determine not only whether a P-core or an O-core is formed, but they also tune the stability by shielding effects of highly sterically demanding groups. By using these effects, two rare examples of room-temperature stable O-cores and one room-temperature stable P-core could be observed.

The combination of the modular approach with this correlation allows the prediction of the properties of a desired bisguanidine ligand.

Some of the observed bis(μ-oxo) dicopper(III) cores insert oxygen in a non-activated C-H-bond of the ligands. The formation of the novel ligands bis(trimethylmethoxyguanidino)propane (btmmO), bis(trimethylmethoxyguanidino)-*N*-methyl-diphenyleneamine ($TMMoG_2MePA$), bis(methylmethoxyethyleneguanidino)propane ($MMoEG_2p$) and bis(trimethylmethoxyguanidino)cyclohexane ($TMMoG_2ch$) represent the first hydroxylations of an N-methyl group. These ligands could be obtained complex-stabilised in the bis(μ-alkoxo)-bridged dinuclear copper complexes **C15** (btmmo), **C16** - **C18** ($TMMoG_2MePA$), **C21** (($MMoEG_2p$) and **C23** - **C25** ($TMMoG_2ch$). On the other hand, the corresponding bis(μ-hydroxo)-bridged dinuclear copper complexes **C19**, **C20** and **C22** were obtained as well. In **C15**, **C21** - **C25**, the copper(II) atoms are coordinated in a square-planar manner, in **C16**, **C17**, **C19** and **C20** square-pyramidal and in **C18** trigonal-bipyramidal. **C26** was crystallised after the reaction of a bis(μ-hydroxo)-bridged dinuclear copper complex with the hexafluorophosphate anion to give the corresponding bis(μ-fluoro)-bridged dinuclear copper complex with square-planar coordination.

Finally, the generated Cu_2O_2 species were screened regarding their suitability as oxidation catalysts in the reactions with 2,4-di^{tert}butylphenol, 2,6-di^{tert}butylphenol and 3,5-di^{tert}butylcatechol. In fact, the investigated systems did not show tyrosinase activity but very efficient catechol oxidase activity. 2,4-di^{tert}butylphenol and 2,6-di^{tert}butylphenol have been oxidatively coupled to phenylethers. 3,5-di^{tert}butylcatechol has been successfully

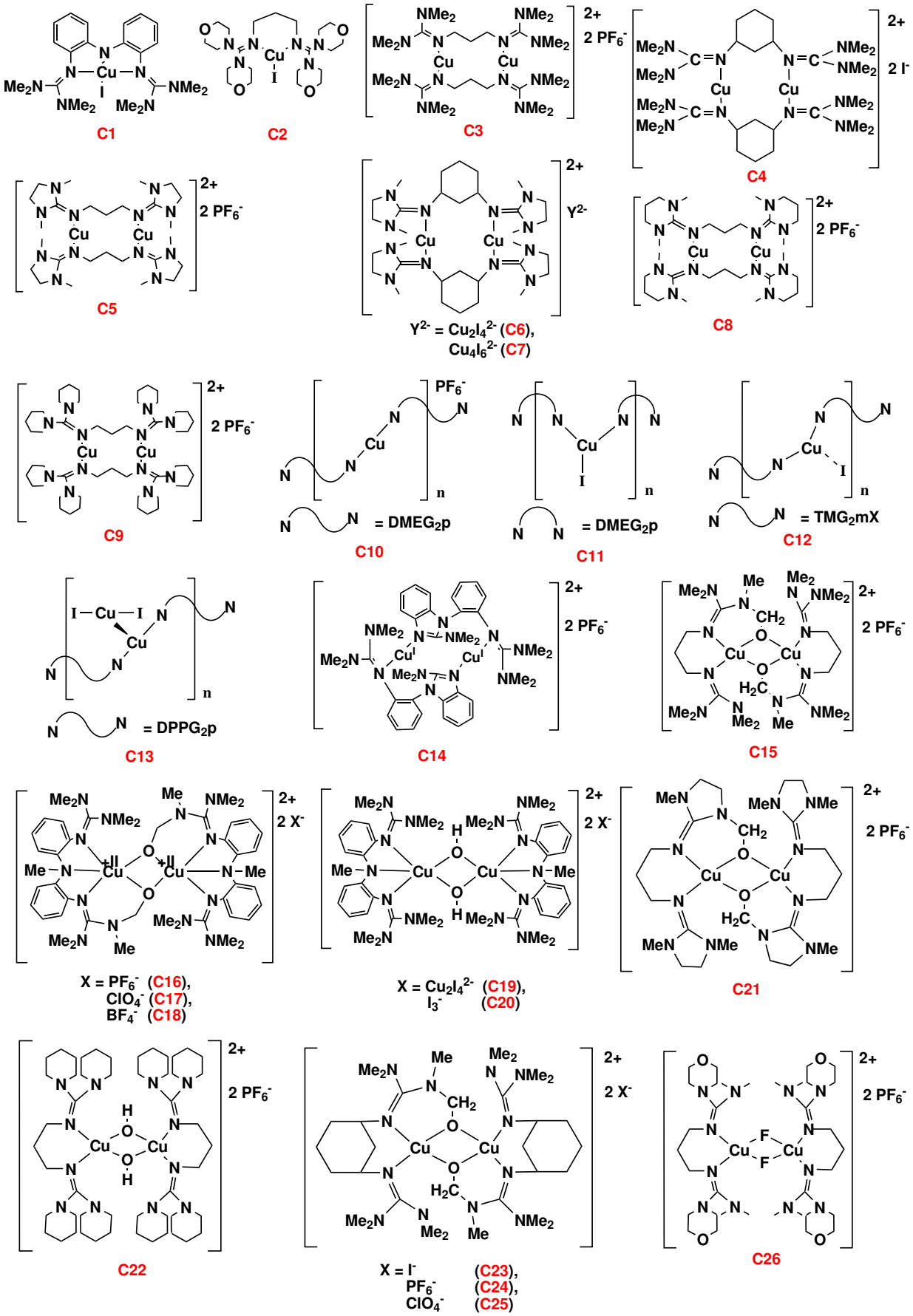

Figure 9.2: Schematic summary of the synthesised bisguanidine copper complexes

oxidised to 3,5-di^{tert}butyl-o-quinone at low temperatures, this product reacts at room temperature to a substituted benzodioxine as subsequent product. The ability of oxidation is depending from the accessibility of the reaction centre: "small" ligands stabilise stronger oxidation catalysts whereas sterically demanding systems show with substrates like 2,4-DTBP and 2,6-DTBP reduced conversions by high selectivity.

A perspective for further investigations would be the screening of this library of bisguanidine ligands and their copper(I) complexes for catalytic reactions like the coupling of benzyl-halogenids and the selective mono-dealkylation of substituted anilines. The possibility of controlling the oxidation selectivity by peripheric modifications is a particularly attractive feature of this ligand design. In general, such a matrix of bisguanidine ligands can also be screened regarding their ability to stabilise complexes of other transition metals in unusually high oxidation states, concerning that these ligands have proven to be stable against fragmentation reactions.

Bibliography

[1] D.F. Shriver, P.W. Atkins, C.H. Langford, *Anorganische Chemie*, VCH, Weinheim, **1992**

[2] W. Kaim, B. Schwederski, *Bioanorganische Chemie*, Teubner Studienbücher, Stuttgart, **1995**

[3] S.J. Lippard, J.M. Berg, *Bioanorganische Chemie*, Spektrum Akademischer Verlag, **1995**

[4] K. Wieghardt, *Nachr. Chem. Techn. Lab.* **1985**, *33*, 961

[5] J.A. Ibers, R.H. Holm, *Science* **1980**, *209*, 223

[6] J.M. Zuo, M. Kim, M. O´Keefe, J.C.H. Spence, *Nature* **1999**, *401*, 49

[7] K.M. Merz, R. Hoffmann, *Inorg. Chem.* **1988**, *27*, 2120

[8] W. Kaim, J. Rall, *Angew. Chem.* **1996**, *108*, 47

[9] A. Volbeda, G.W. Hol, *J. Mol. Biol.* **1989**, *209*, 249

[10] E.I. Solomon, U.M. Sundaram, T.E. Machonkin, *Chem. Rev.* **1996**, *96*, 2563

[11] J.P. Klinman, *Chem. Rev.* **1996**, *96*, 2541

[12] M. Fontecave, J.-L. Pierre, *Coord. Chem. Rev.* **1998**, *170*, 125

[13] R.H. Holm, P. Kennepohl, E.I. Solomon, *Chem. Rev.* **1996**, *96*, 2239

[14] F. Fujisetti, K.H. Schröter, R.A. Steiner, P.I. van Noort, T. Pijning, H.J. Rulebook, K.H. Kalk, M.R. Egmond, B.W. Dijkstra, *Structure* **2002**, *10*, 259

[15] A. Sánchez-Ferrer, J.N. Rodriguez-Lopez, F. Garcia-Cánovas, F. Garcia-Carmona, *Biochim. Biophys. Acta* **1995**, *1247*, 1

[16] E.I. Solomon, P. Chen, M. Metz, S.-K. Lee, A.E. Palmer, *Angew. Chem.* **2001**, *113*, 4702

[17] C. Gerdemann, C. Eicken, B. Krebs, *Acc. Chem. Res.* **2002**, *35*, 183

[18] A. Rompel, H. Fischer, D. Meiwes, K. Buldt-Karentzopoulos, R. Dillinger, F. Tuczek, H. Witzel, B. Krebs, *J. Biol. Inorg. Chem.* **1999**, *4*, 56

[19] H. Decker, F. Tuczek, *Trends Biochem. Sci.* **2000**, *25*, 392

[20] H. Decker, R. Dillinger, F. Tuczek, *Angew. Chem.* **2000**, *112*, 1656

[21] J.R. Walker, P.H. Ferrar, *Biotechnol. Genet. Eng. Rev.* **1998**, *15*, 457

[22] T. Klabunde, C. Eicken, J.C. Sacchettini, B. Krebs, *Nat. Struct. Biol.* **1998**, *5*, 1084

[23] W.P.J. Gaykema, W.G.J. Hol, J.M. Vereijken, N.M. Soeter, H.J. Bak, J.J. Beintema, *Nature* **1984**, *309*, 23

[24] B. Hazes, K.A. Magnus, C. Bonaventura, J. Bonaventura, Z. Dauter, K.H. Kalk, W.G.L. Hol, *Proteins Sci.* **1993**, *2*, 597

[25] K.A. Magnus, B. Hazes, H. Ton-That, C. Bonaventura, J. Bonaventura, W.G.L. Hol, *Proteins - Structure, Function and Genetics* **1994**, *19*, 302

[26] K.A. Magnus, H. Ton-That, J.E. Carpenter, *Chem. Rev.* **1994**, *94*, 727

[27] M.E. Cuff, K.I. Miller, K.E. van Holde, W.A. Hendrickson, *J. Mol. Biol.* **1998**, *278*, 855

[28] K.E. van Holde, E.F.J. van Bruggen, *Biol. Macromol., Part A* **1971**, 1

[29] K.E. van Holde, K.I. Miller, *Adv. Proteins Chem.* **1995**, *47*, 1

[30] A.L. Hughes, *Immunogenetics* **1999**, *49*, 106

[31] C. Eicken, B. Krebs, J.C. Sacchettini, *Curr. Opin. Struc. Biol.* **1999**, *9*, 677

[32] M.A. Halcrow, *Angew. Chem.* **2001**, *113*, 358

[33] K.D. Karlin, S. Kaderli, A.D. Zuberbühler, *Acc. Chem. Res.* **1997**, *30*, 139

[34] N. Kitajima, Y. Moro-oka, *Chem. Rev.* **1994**, *94*, 737

[35] P.L. Holland, W.B. Tolman, *Coord. Chem. Rev.* **1999**, *192*, 855

[36] L.M. Mirica, M. Vance, D.J. Rudd, B. Hedman, K.O. Hodgson, E.I. Solomon, T.D.P. Stack, *Science* **2005**, *308*, 1890

[37] G.W. Parshall, D.D. Ittel, *Homogeneous Catalysis, The Applications and Chemistry of Catalysis by Soluble Transition Metal Complexes*, 2nd ed., John Wiley & Sons, INC, New York, **1992**

[38] A.S. Hay, H.S. Stafford, G.F. Endres, J.W. Eustance, *J. Am. Chem. Soc.* **1959**, *81*, 6335

[39] US Patent 2 893 541 and 2 831 895, **1955** to Dow Chemical Co.

[40] a) Ger. Offen. 2 221 624, **1972** to Hoffmann-La Roche AG; b) EP 475 272 A2, **1992** to BASF AG

[41] EP Patent 0 127 888, **1984**, EP 0 167 153, **1985**, US Patent 4 828 762, **1986** to Mitsubishi Gas Chemical Corp.

[42] R. Jira, In *Applied Homogeneous Catalysis with Organometallic Compounds*, B. Cornils, W.A. Herrmann (Eds.), VCH, Weinheim, **1996**, 405

[43] C. Elschenbroich, A. Salzer, *Organometallchemie*, 4th ed., Teubner Studienbücher, Stuttgart, **2004**

[44] H. Gampp, A.D. Zuberbühler, *Metal Ions Biol. Syst.* **1981**, *12*, 133

[45] L.M. Mirica, X. Ottenwaelder, T.D.P. Stack, *Chem. Rev.* **2004**, *104*, 1013

[46] T.D.P. Stack, *J. Chem. Soc., Dalton Trans.* **2003**, 1881

[47] A.G. Blackman, W.B. Tolman, *Struct. Bonding* (Berlin) **2000**, *97*, 179

[48] L. Que, Jr., W.B. Tolman, *Angew. Chem.* **2002**, *114*, 1160

[49] E.A. Lewis, W.B. Tolman, *Chem. Rev.* **2004**, *104*, 1047

[50] S. Schindler, *Eur. J. Inorg. Chem.* **2000**, 2311

[51] C.X. Zhang, H.-C. Liang, K.J. Humphreys, K.D. Karlin, In *Advances in Catalytic Activation of Dioxygen by Metal Complexes*, L.I. Simandi, Ed., Kluwer, Dorddrecht, Boston, London, **2003**, Vol. 26

[52] I. Blain, P. Slama, M. Giorgi, T. Tron, M. Réglier, *Rev. in Mol. Biotech.* **2002**, *90*, 95

[53] A. Granata, E. Monzani, L. Casella, *J. Biol. Inorg. Chem.* **2004**, *9*, 903

[54] C. Zhang, S. Kaderli, M. Costas, E. Kim, Y. Neuhold, K.D. Karlin, A.D. Zuberbühler, *Inorg. Chem.* **2003**, *42*, 1807

[54] P. Chen, J. Bell, B.A. Eipper, E.I. Solomon, *Biochemistry* **2004**, *43*, 5735

[55] D.J.E. Spencer, N.W. Aboelella, A.M. Reynolds, P.L. Holland, W.B. Tolman, *J. Am. Chem. Soc.* **2002**, *124*, 2108

[56] N.W. Aboelella, E.A. Lewis, A.M. Reynolds, W.W. Brennessel, C.J. Cramer, W.B. Tolman, *J. Am. Chem. Soc.* **2002**, *124*, 10660

[57] Z. Tyeklár, R.R. Jacobsen, N. Wei, N.N. Murthy, J. Zubieta, K.D. Karlin, *J. Am. Chem. Soc.* **1993**, *115*, 2677

[58] R.R. Jacobsen, Z. Tyeklár, A. Farooq, K.D. Karlin, S. Liu, J. Zubieta, *J. Am. Chem. Soc.* **1988**, *110*, 3690

[59] K. Komiyama, H. Furutachi, S. Nagatomo, A. Hashimoto, H. Hayashi, S. Fujinami, A. Suzuki, T. Kitagawa, *Bull. Chem. Soc. Jpn.* **2004**, *77*, 59

[60] N. Kitajima, K. Fujisawa, Y. Moro-oka, K. Toriumi, *J. Am. Chem. Soc.* **1989**, *111*, 8975

[61] N. Kitajima, K. Fujisawa, C. Fujimoto, Y. Moro-oka, S. Hashimoto, T. Kitagawa, K. Toriumi, K. Tatsumi, A. Nakamura, *J. Am. Chem. Soc.* **1992**, *114*, 1277

[62] M. Kodera, K. Katayama, Y. Tachi, K. Kano, S. Hirota, S. Fujinami, S. Suzuki, *J. Am. Chem. Soc.* **1999**, *121*, 11006

[63] J.A. Halfen, S. Mahapatra, E.C. Wilkinson, S. Kaderli, V.G. Young, Jr., L. Que, Jr., A.D. Zuberbühler, W.B. Tolman, *Science* **1996**, *271*, 1397

[64] T. Osako, S. Nagatomo, Y. Tachi, T. Kitagawa, S. Itoh, *Angew. Chem.* **2002**, *114*, 4501

[65] A.P. Cole, D.E. Root, P. Mukherjee, E.I. Solomon, T.D.P. Stack, *Science* **1996**, *273*, 1848

[66] J. Reim, B. Krebs, *Angew. Chem.* **1994**, *106*, 2040

[67] K.D. Karlin, R.W. Cruse, Y. Gultneh, J.C. Hayes, J. Zubieta, *J. Am. Chem. Soc.* **1984**, *106*, 3372

[68] K. Fujisawa, M. Tanaka, Y. Moro-oka, N. Kitajima, *J. Am. Chem. Soc.* **1994**, *116*, 12079

[69] V. Mahadevan, Z. Hou, A.P. Cole, D.E. Root, T.P. Lal, E.I. Solomon, T.D.P. Stack, *J. Am. Chem. Soc.* **1997**, *119*, 11996

[70] L.M. Mirica, M. Vance, D. Jackson-Rudd, B. Hedman, K.O. Hodgson, E.I. Solomon, T.D.P. Stack, *J. Am. Chem. Soc.* **2002**, *124*, 9332

[71] B.F. Straub, F. Rominger, P. Hofmann, *J. Chem. Soc., Chem. Commun.* **2000**, 1611

[72] N.W. Aboelella, S.V. Kryatov, B.F. Gherman, W.W. Brennessel, V.G. Young, Jr., R. Sarangi, E.V. Rybak-Akimova, K.O. Hodgson, B. Hedman, E.I. Solomon, C.J. Cramer, W.B. Tolman, *J. Am. Chem. Soc.* **2004**, *126*, 16896

[73] P.L. Holland, K.R. Rodgers, W.B. Tolman, *Angew. Chem.* **1999**, *111* 1210

[74] M. Taki, S. Teramae, S. Nagatomo, Y. Tachi, T. Kitagawa, S. Itoh, S. Fukuzumi, *J. Am. Chem. Soc.* **2002**, *124*, 6367

[75] P. Chaudhuri, H. Hess, T. Weyhermüller, K. Wieghardt, *Angew. Chem.* **1999**, *111*, 1165

[76] K.D. Karlin, M.S. Haka, R.W. Cruse, Y. Gultneh, *J. Am. Chem. Soc.* **1985**, *107*, 5828

[77] K.D. Karlin, M.S. Nasir, B.I. Cohen, R.W. Cruse, S. Kaderli, A.D. Zuberbühler, *J. Am. Chem. Soc.* **1994**, *116*, 1324

[78] B.M.T. Lam, J.A. Halfen, V.G. Young, Jr., J.R. Hagadorn, P.L. Holland, A. Lledos, L. Cucurull Sanchez, J.J. Novoa, S. Alvarez, W.B. Tolman, *Inorg. Chem.* **2000**, *39*, 4059

[79] F. Meyer, H. Pritzkow, *Angew. Chem.* **2000**, *112*, 2199

[80] M.J. Henson, M.A. Vance, C.X. Zhang, H.C. Liang, K.D. Karlin, E.I. Solomon, *J. Am. Chem. Soc.* **2003**, *125*, 5186

[81] L. Santagostini, M. Gullotti, E. Monzani, L. Casella, R. Dillinger, F. Tuczek, *Chem. Eur. J.* **2000**, *6*, 519

[82] M. Becker, F.W. Heinemann, S. Schindler, *Chem. Eur. J.* **1999**, *5*, 3124

[83] H. Börzel, P. Comba, K.S. Hagen, M. Kerscher, H. Pritzkow, M. Schatz, S. Schindler, O. Walter, *Inorg. Chem.* **2002**, *41*, 5540

[84] K.D. Karlin, Y. Gultneh, *Prog. Inorg. Chem.* **1987**, *35*, 219

[85] K.D. Karlin, S. Kaderli, A.D. Zuberbühler, *Acc. Chem. Res.* **1997**, *30*, 139

[86] S. Itoh, H. Nakao, L.M. Berreau, T. Kondo, M. Komatsu, S. Fukuzumi, *J. Am. Chem. Soc.* **1998**, *120*, 2890

[87] Z. Hu, R.D. Williams, D. Tran, T.G. Spiro, S.M. Gorun, *J. Am. Chem. Soc.* **2000**, *122*, 3556

[88] S. Patai, *The Chemistry of amidines and imidates*, Wiley **1991**, *Vol. 2*, 485

[89] R. Schwesinger, *Nachr. Chem. Techn. Lab.* **1990**, *38*, 1214

[90] W. Kantlehner, J.J. Kapassakalidis, P. Speh, H.-J. Bräuner, *Liebigs Ann.* **1980**, *1*, 389

[91] Y. Gao, S.W. Arrit, B. Twamley, J.M. Shreeve, *Inorg. Chem.* **2005**, *44*, 1704

[92] R. Longhi, R.S. Drago, *Inorg. Chem.* **1965**, *4*, 11

[93] R. Snaith, K. Wade, B.K. Wyatt, *J. Chem. Soc. A* **1970**, 380

[94] P. Pruszynski, K.T. Leffek, B. Borecka, T.S. Cameron, *Acta Crystallogr., Sect. C* **1992**, *48*, 1638

[95] P.J. Bailey, S. Pace, *Coord. Chem. Rev.* **2001**, *214*, 91

[96] S.H. Oakley, D.B. Soria, M.P. Coles, P.B. Hitchcock, *J. Chem. Soc., Dalton Trans.* **2004**, 537

[97] S.H. Oakley, M.P. Coles, P.B. Hitchcock, *Inorg. Chem.* **2004**, *43*, 5168

[98] S.H. Oakley, M.P. Coles, P.B. Hitchcock, *Inorg. Chem.* **2003**, *42*, 3154

[99] I. Georgieva, N. Mintcheva, N. Trendafilova, M. Mitewa, *Vibr. Spectr.* **2001**, *27*, 153

[100] C.N. Morimoto, E.C. Lingafelter, *Acta Crystallogr., Sect. B* **1970**, *26*, 335

[101] T. Kolev, T. Todorov, R. Petrova, *Acta Crystallogr., Sect. E* **2002**, *58*, o111

[102] P.J. Bailey, K.J. Grant, S. Pace, S. Parsons, L.J. Stewart, *J. Chem. Soc., Dalton Trans.* **1997**, 4263

[103] J. Münchenberg, A.K. Fischer, H. Thönnesen, P.G. Jones, R. Schmutzler, *J. Organomet. Chem.* **1997**, *529 (1-2)*, 361

[104] S.H. Oakley, M.P. Coles, P.B. Hitchcock, *J. Chem. Soc., Dalton Trans.* **2004**, 1113

[105] S. Pohl, M. Harmjanz, J. Schneider, W. Saak, G. Henkel, *J. Chem. Soc., Dalton Trans.* **2000**, 3473

[106] S. Pohl, M. Harmjanz, J. Schneider, W. Saak, G. Henkel, *Inorg. Chim. Acta* **2000**, *311*, 106

[107] H. Wittmann, V. Raab, A. Schorm, J. Plackmeyer, J. Sundermeyer, *Eur. J. Inorg. Chem.* **2001**, 1937

[108] V. Raab, J. Kipke, O. Burghaus, J. Sundermeyer, *Inorg. Chem.* **2001**, *40*, 6964

[109] V. Raab, J. Kipke, R.M. Gschwind, J. Sundermeyer, *Chem. Eur. J.* **2002**, *8*, 1682

[110] H. Wittmann, A. Schorm, J. Sundermeyer, *Z. Anorg. Allg. Chem.* **2000**, *626*, 1583

[111] N. Kuhn, M. Grathwohl, M. Steinmann, G. Henkel, *Z. Naturforsch.* **1998**, *53b*, 997

[112] J. Schneider, Ph.D. Thesis, University of Duisburg **2000**

[113] S. Herres, A.J. Heuwing, U. Flörke, J. Schneider, G. Henkel, *Inorg. Chim. Acta* **2005**, *358*, 1089

[114] H. Bredereck, K. Bredereck, *Chem. Ber.* **1961**, *94*, 2278

[115] G. Wieland, G. Simchen, *Liebigs Ann. Chem.* **1985**, 2178

[116] H. Beyer, W. Walter, *Lehrbuch der organischen Chemie*, Hirzel Verlag, Stuttgart, **1998**

[117] W. Kantlehner, E. Haug, W.W. Mergen, P. Speh, T. Maier, J.J. Kapassakalidis, H.-J. Bräuner, H. Hagen, *Liebigs Ann. Chem.* **1984**, *1*, 108

[118] D. Bourissou, O. Guerret, F.P. Gabbai, G. Bertrand, *Chem. Rev.* **2000**, *100*, 39

[119] W.A. Herrmann, *Angew. Chem.* **2002**, *114*, 1342

[120] N. Kuhn, A. Abu-Rayyan, M. Göbner, M. Steimann, *Z. Anorg. Allg. Chem.* **2002**, *628*, 1721

[121] A.J. Arduengo, F. Davidson, H.V.R. Dias, J.R. Goerlich, D. Khasnis, W.J. Marshall, T.K. Prakasha, *J. Am. Chem. Soc.* **1997**, *119*, 12742

[122] R.W. Alder, P.R. Allen, M. Murray, A.G. Orpen, *Angew. Chem.* **1996**, *108*, 1211

[123] M. Otto, S. Conejero, Y. Canac, V.D. Romanenko, V. Rudzevitch, G. Bertrand, *J. Am. Chem. Soc.* **2004**, *126*, 1016

[124] N. Kuhn, A. Abu-Rayyan, M. Ströbele, *Z. Anorg. Allg. Chem.* **2002**, *628*, 2251

[125] N. Kuhn, H. Bohnen, D. Bläser, R. Boese, A.H. Maulitz, *J. Chem. Soc., Chem. Commun.* **1994**, 2283

[126] E.B. Chuklanova, A.I. Gusev, A.S. Zhdanov, Z.V. Belyakova, V.M. Shevchenko, V.D. Sheludyakov, *Koor. Khim.* **1987**, *13*, 1109

[127] F.L. Hirshfeld, H. Hope, *Acta Crystallogr. Sect. B*, **1980**, *36*, 406

[128] R. Shiba, M. Takahashi, H. Shinozaki, T. Ebisuno, M. Takimoto, *Bull. Chem. Soc. Jpn.* **1993**, *66*, 2665

[129] H.Kessler, D. Leibfritz, *Tetrahedron* **1970**, *26*, 1805

[130] A.V. Santoro, G. Mickevicius, *J. Org. Chem.* **1979**, *44*, 117

[131] C.-d. Li, S.L. Mella, A.C. Sartorelli, *J. Med. Chem.* **1981**, *24*, 1089

[132] B. Neumann, U. Siemeling, H.-G. Stammler, U. Vorfeld, J.G.P. Delis, P.W.N.M. van Leeuwen, K. Vrieze, J. Fraanje, K. Goubitz, F. Fabrizi de Biani, P. Zanello, *J. Chem. Soc., Dalton Trans.* **1997**, 4705

[133] R.D. Köhn, G. Seifert, Z. Pan, M.F. Mahon, G. Kociok-Köhn, *Angew. Chem.* **2003**, *115*, 818

[134] R.D. Köhn, Z. Pan, M. Haufe, G. Kociok-Köhn, *J. Chem. Soc., Dalton Trans.* **2005**, 2793

[135] J. Strähle and J. Beck, *Angew. Chem.* **1985**, *97*, 419

[136] P. Pyykkö, *Chem. Rev.* **1997**, *97*, 597

[137] H. Schmidbaur, *Gold. Bull.* **1990**, *23*,11

[138] P. Pyykkö, J. Li, N. Runeberg, *Chem. Phys. Lett.* **1994**, *218*, 133

[139] K.M. Merz, Jr., R. Hoffmann, *Inorg. Chem.* **1988**, *27*, 2120

[140] C. Kölmel, R. Ahlrichs, *J. Phys. Chem.* **1990**, *118*, 2679

[141] A. Martin, A.G. Orpen, *J. Am. Chem. Soc.* **1996**, *118*, 1464

[142] Resonance-Raman spectra are severely affected by fluorescence emission and thus not suited to contribute to the P-core/O-core question.

[143] A. Neuba, Diploma thesis, University of Paderborn, **2005**

[144] M.J. Baldwin, D.E. Root, J.E. Pate, K. Fujisawa, N. Kitajima, E.I. Solomon, *J. Am. Chem. Soc.* **1992**, *114*, 10421

[145] H.-C. Liang, K.D. Karlin, R. Dyson, S. Kaderli, B. Jung, A.D. Zuberbühler, *Inorg. Chem.* **2000**, *39*, 5884

[146] K.A. Connors, *Chemical kinetics*, Wiley-VCH, New York, **1990**

[147] S. Itoh, T. Kondo, M. Komatsu, Y. Oshiro, C. Li, N. Kanehisa, Y. Kai, S. Fukuzumi, *J. Am. Chem. Soc.* **1995**, *117*, 4714

[148] I. Blain, M. Giorgi, I. de Riggi, M. Reglier, *Eur. J. Inorg. Chem.* **2001**, 205

[149] S. Itoh, M. Taki, H. Nakao, P.L. Holland, W.B. Tolman, L. Que, Jr., S. Fukuzumi, *Angew. Chem.* **2000**, *112*, 409

[150] H. Arii, Y. Saito, S. Nagatomo, T. Kitagawa, Y. Funahashi, K. Jitsukawa, H. Masuda, *Chem. Lett.* **2003**, *32*, 156

[151] P. Spuhler, M.C. Holthausen, *Angew. Chem.* **2003**, *115*, 6143

[152] β and α are defined as the largest and the second largest metal centered angles between two donors A and B in a pentacoordinated molecule ($\beta \geq \alpha$).

[153] A. W. Addison, T.N. Rao, J. Reedijk, J. van Rijn, G.C. Verschoor, *J. Chem. Soc., Dalton Trans.* **1984**, 1349

[154] S.C. Lee, R.H. Holm, *Inorg. Chem.* **1993**, *32*, 4745

[155] J.A. Halfen, V.G. Young, Jr., W.B. Tolman, *Inorg. Chem.* **1998**, *37*, 2102

[156] M. Hirose, S. Iwata, E. Ito, Y. Nihro, S. Takahashi, Y. Mizoguchi, Y. Miki, T. Satoh, N. Ito, T. Shirai, *Carcinogenesis* **1995**, *16*, 2227

[157] S. Itoh, H. Kumei, M. Taki, S. Nagatomo, T. Kitagawa, S. Fukuzumi, *J. Am. Chem. Soc.* **2001**, *123*, 6708

[158] J. Ackermann, Ph.D. Thesis, University of Göttingen **2001**

[159] I.A. Koval, M. Huisman, A.F. Stassen, P. Gamez, O. Roubeau, C. Belle, J.-L. Pierre, E. Saint-Aman, M. Lüken, B. Krebs, M. Lutz, A.L. Spek, J. Reedijk, *Eur. J. Inorg. Chem.* **2004**, 4036

[160] P.J. Baesjou, W.L. Driessen, G. Challa, J. Reedijk, *J. Am. Chem. Soc.* **1997**, *119*, 12590

[161] G. Challa, W. Chen, J. Reedijk, *J. Makromol. Chem., Macromol. Symp.* **1992**, *59*, 59

[162] A. Benzekri, P. Dubourdeaux, J.-M. Latour, J. Laugier, P. Rey, *Inorg. Chem.* **1988**, *27*, 3710

[163] M. Hesse, H. Meier, B. Zeeh, *Spektroskopische Methoden in der organischen Chemie*, 3rd ed., Thieme Verlag, Stuttgart, **1987**

[164] V. Nair, S. Kumar, *J. Chem. Soc., Chem. Commun.* **1994**, 1341

[165] S. Herres-Pawlis, G. Henkel, unpublished results

[166] C.L. Perrin, T.J. Dwyer, *Chem. Rev.* **1990**, *90*, 935

[167] Bruker AXS Inc., Madison, Wisconsin, USA (2002). SAINT (Version 6.02), SHELXTL (Version 6.10), SADABS (Version 2.03)

10 Appendix

Table A1: Crystal data and structure refinement for **V2** and **L5-1**

	V2	**L5-1**
Identification code	h1257	h1036
Empirical formula	$C_9H_{20}Cl_2N_2$	$C_{15}H_{30}N_6$
Formula weight	227.17	294.45
Temperature	120(2) K	120(2) K
Wavelength	0.71073 Å	0.71073 Å
Crystal system	Triclinic	Triclinic
Space group	$P\bar{1}$	$P\bar{1}$
Unit cell dimensions	a = 7.9140(11) Å	a = 6.9057(7) Å
	b = 8.5959(12) Å	b = 7.6661(7) Å
	c = 9.5177(14) Å	c = 16.3568(16) Å
	α = 112.389(2)°	α = 89.307(3)°
	β = 94.883(3)°	β = 82.355(2)°
	γ = 98.166(2)°	γ = 73.152(2)°
Volume	585.70(14) $Å^3$	821.07(14)$Å^3$
Z	2	2
Density (calculated)	1.288 Mg/m^3	1.191 Mg/m^3
Absorption coefficient	0.516 mm^{-1}	0.075 mm^{-1}
F(000)	244	324
Crystal size	0.45 x 0.30 x 0.28 mm^3	0.20 x 0.15 x 0.10 mm^3
Theta range for data collection	2.34 to 27.48°	1.26 to 28.31°
Index ranges	-10≤ h≤10, -11≤k≤11, -12≤l≤12	-8≤h≤9, -9≤k≤10, -21≤l≤21
Reflections collected	5402	7147
Independent reflections	2637 [R(int) = 0.0187]	4053 [R(int) = 0.0465]
Completeness to theta	= 27.48°: 98.2 %	= 28.31°: 99.0 %
Absorption correction	Semi-empirical from equivalents	Semi-empirical from equivalents
Max. and min. transmission	0.8690 and 0.8010	0.916 and 0.833
Refinement method	Full-matrix least-squares on F^2	Full-matrix least-squares on F^2
Data / restraints / parameters	2637 / 0 / 122	4053 / 0 / 194
Goodness-of-fit on F^2	1.076	0.836
Final R indices [I¿2sigma(I)]	R1 = 0.0308, wR2 = 0.0795	R1 = 0.0540, wR2 = 0.0820
R indices (all data)	R1 = 0.0360, wR2 = 0.0876	R1 = 0.1233, wR2 = 0.1130
Largest diff. peak and hole	0.350 and -0.186 e·$Å^3$	0.232 and -0.165 e·$Å^3$

Table A2: Crystal data and structure refinement for **L7-1** and **L1-4**

	L7-1	**L1-4**
Identification code	h1085	h920
Empirical formula	$C_{25}H_{46}N_6$	$C_{22}H_{33}N_7$
Formula weight	430.68	395.55
Temperature	120(2) K	153(2) K
Wavelength	0.71073 Å	0.71073 Å
Crystal system	Monoclinic	Monoclinic
Space group	$P2_1/n$	$P2_1/n$
Unit cell dimensions	a = 10.0619(7) Å	a = 18.577(4) Å
	b = 19.8127(13) Å	b = 13.218(3) Å
	c = 12.7511(8) Å	c = 20.144(4) Å
	$\alpha = 90°$	$\alpha = 90°$
	$\beta = 99.594(2)°$	$\beta = 113.24(3)°$
	$\gamma = 90°$	$\gamma = 90°$
Volume	2506.4(3) $Å^3$	4545.0(16)$Å^3$
Z	4	8
Density (calculated)	1.141 Mg/m^3	1.156 Mg/m^3
Absorption coefficient	0.069 mm^{-1}	0.072 mm^{-1}
F(000)	952	1712
Crystal size	0.40 x 0.35 x 0.20 mm^3	0.30 x 0.15 x 0.12 mm^3
Theta range for data collection	1.92 to 28.34°	1.26 to 28.31°
Index ranges	-13≤h≤13, -22≤k≤26, -12≤l≤17	-23≤h≤23, -17≤k≤17, -20≤l≤26
Reflections collected	19511	24735
Independent reflections	6205 [R(int) = 0.0437]	10255 [R(int) = 0.1887]
Completeness to theta	= 28.34°: 99.2 %	= 28.31°: 90.5 %
Absorption correction	Semi-empirical from equivalents	Semi-empirical from equivalents
Max. and min. transmission	0.989 and 0.751	0.991 and 0.978
Refinement method	Full-matrix least-squares on F^2	Full-matrix least-squares on F^2
Data / restraints / parameters	6205 / 0 / 280	10255 / 0 / 539
Goodness-of-fit on F^2	0.863	0.587
Final R indices [I¿2sigma(I)]	R1 = 0.0420, wR2 = 0.0838	R1 = 0.0550, wR2 = 0.0764
R indices (all data)	R1 = 0.0682, wR2 = 0.0899	R1 = 0.2976, wR2 = 0.1195
Largest diff. peak and hole	0.217 and -0.154 e·$Å^3$	0.171 and -0.196 e·$Å^3$

Table A3: Crystal data and structure refinement for **L11-1** and $[H_2L\mathbf{1\text{-}2}]I_2 \bullet Et_2O$

	L11-1	$[H_2L\mathbf{1\text{-}2}]I_2 \bullet Et_2O$
Identification code	s1157	h1063
Empirical formula	$C_{21}H_{38}N_6O_4$	$C_{20}H_{48}I_2N_6O_3$
Formula weight	438.57	674.44
Temperature	120(2) K	120(2) K
Wavelength	0.71073 Å	0.71073 Å
Crystal system	Monoclinic	Monoclinic
Space group	C2/c	$P2_1/n$
Unit cell dimensions	a = 16.4003(11) Å	a = 8.1966(4) Å
	b = 8.2314(4) Å	b = 14.0360(7) Å
	c = 16.6413(9) Å	c = 12.3715(6) Å
	$\alpha = 90°$	$\alpha = 90°$
	$\beta = 92.310(2)°$	$\beta = 93.983(1)°$
	$\gamma = 90°$	$\gamma = 90°$
Volume	2244.7(2) $Å^3$	1419.87(12)$Å^3$
Z	4	2
Density (calculated)	1.298 Mg/m^3	1.578 Mg/m^3
Absorption coefficient	0.091 mm^{-1}	2.245 mm^{-1}
F(000)	952	680
Crystal size	0.40 x 0.38 x 0.28 mm^3	0.30 x 0.28 x 0.06 mm^3
Theta range for data collection	2.45 to 28.24°	2.20 to 28.29°
Index ranges	-21≤h≤21, -10≤k≤10, -22≤l≤22	-10≤h≤10, -18≤k≤16, -16≤l≤16
Reflections collected	13601	12043
Independent reflections	2771 [R(int) = 0.0347]	3515 [R(int) = 0.0204]
Completeness to theta	= 28.24°: 100.0 %	= 28.29°: 99.7 %
Absorption correction	Semi-empirical from equivalents	Semi-empirical from equivalents
Max. and min. transmission	0.908 and 0.797	0.984 and 0.677
Refinement method	Full-matrix least-squares on F^2	Full-matrix least-squares on F^2
Data / restraints / parameters	2771 / 1 / 145	3515 / 0 / 153
Goodness-of-fit on F^2	1.030	1.048
Final R indices [I¿2sigma(I)]	R1 = 0.0385, wR2 = 0.1043	R1 = 0.0266, wR2 = 0.0718
R indices (all data)	R1 = 0.0475, wR2 = 0.1076	R1 = 0.0304, wR2 = 0.0743
Largest diff. peak and hole	0.344 and -0.182 e·$Å^3$	1.194 (near I1 position)
		and -0.402 e·$Å^3$

Table A4: Crystal data and structure refinement for **C1** and **C2**

	C1	**C2**
Identification code	h878	s1144
Empirical formula	$C_{22}H_{32}CuIN_7$	$C_{21}H_{38}CuIN_6O_4$
Formula weight	584.99	629.01
Temperature	133(2) K	120(2) K
Wavelength	0.71073 Å	0.71073 Å
Crystal system	Orthorhombic	Orthorhombic
Space group	Pbca	Pnma
Unit cell dimensions	a = 18.1280(13) Å	a = 12.2998(6) Å
	b = 14.7193(10) Å	b = 26.4227(13) Å
	c = 18.2744(13) Å	c = 7.7061(4) Å
	$\alpha = 90°$	$\alpha = 90°$
	$\beta = 90°$	$\beta = 90°$
	$\gamma = 90°$	$\gamma = 90°$
Volume	4876.2(6) $Å^3$	2504.4(2)$Å^3$
Z	8	4
Density (calculated)	1.594 Mg/m^3	1.668 Mg/m^3
Absorption coefficient	2.185 mm^{-1}	2.144 mm^{-1}
F(000)	2360	1280
Crystal size	0.08 x 0.06 x 0.05 mm^3	0.30 x 0.14 x 0.10 mm^3
Theta range for data collection	2.10 to 28.28°	1.54 to 28.24°
Index ranges	-22≤h≤23, -19≤k≤18, -16≤l≤24	-16≤h≤16, -35≤k≤35, -10≤l≤10
Reflections collected	29665	29926
Independent reflections	5897 [R(int) = 0.0759]	3164 [R(int) = 0.0353]
Completeness to theta	= 28.28°: 97.3 %	= 28.24°: 100.0 %
Absorption correction	Semi-empirical from equivalents	Semi-empirical from equivalents
Max. and min. transmission	0.845 and 0.899	0.992 and 0.829
Refinement method	Full-matrix least-squares on F^2	Full-matrix least-squares on F^2
Data / restraints / parameters	5897 / 0 / 280	3164 / 0 / 154
Goodness-of-fit on F^2	0.538	1.058
Final R indices [I¿2sigma(I)]	R1 = 0.0421, wR2 = 0.0521	R1 = 0.0237, wR2 = 0.0569
R indices (all data)	R1 = 0.1633, wR2 = 0.0722	R1 = 0.0282, wR2 = 0.0581
Largest diff. peak and hole	0.533 and -0.457 e·$Å^3$	0.684 and -0.293 e·$Å^3$

Table A5: Crystal data and structure refinement for **C3** and **C4**

	C3	**C4**
Identification code	h910	h1251
Empirical formula	$C_{26}H_{60}Cu_2F_{12}N_{12}P_2$	$C_{32.74}H_{69.11}Cu_2I_2N_{12.37}$
Formula weight	957.88	1017.05
Temperature	153(2) K	120(2) K
Wavelength	0.71073 Å	0.71073 Å
Crystal system	Monoclinic	Monoclinic
Space group	$P2_1/n$	$P2_1/c$
Unit cell dimensions	a = 8.1774(13) Å	a = 11.9909(18) Å
	b = 15.574(3) Å	b = 14.999(2) Å
	c = 16.218(3) Å	c = 12.707(2) Å
	$\alpha = 90°$	$\alpha = 90°$
	$\beta = 96.473(3)°$	$\beta = 104.348(4)°$
	$\gamma = 90°$	$\gamma = 90°$
Volume	2052.3(6) $Å^3$	2214.1(6) $Å^3$
Z	2	2
Density (calculated)	1.550 Mg/m^3	1.526 Mg/m^3
Absorption coefficient	1.205 mm^{-1}	2.392 mm^{-1}
F(000)	992	1032
Crystal size	0.25 x 0.20 x 0.18 mm^3	0.20 x 0.15 x 0.10 mm^3
Theta range for data collection	1.82 to 28.28°	1.75 to 28.34°
Index ranges	-10≤h≤9, -19≤k≤20, -21≤l≤20	-15≤h≤16, -17≤k≤20, -16≤l≤16
Reflections collected	12491	22633
Independent reflections	4731 [R(int) = 0.0471]	5509 [R(int) = 0.0665]
Completeness to theta	= 28.28°: 93.1 %	= 28.34°: 99.9 %
Absorption correction	Semi-empirical from equivalents	Semi-empirical from equivalents
Max. and min. transmission	0.812 and 0.752	0.7959 and 0.6462
Refinement method	Full-matrix least-squares on F^2	Full-matrix least-squares on F^2
Data / restraints / parameters	4731 / 0 / 252	5509 / 0 / 231
Goodness-of-fit on F^2	1.033	0.984
Final R indices [I¿2sigma(I)]	R1 = 0.0457, wR2 = 0.1077	R1 = 0.0527, wR2 = 0.0675
R indices (all data)	R1 = 0.0589, wR2 = 0.1153	R1 = 0.1657, wR2 = 0.0880
Largest diff. peak and hole	0.912 and -0.423 e·$Å^3$	0.784 and -0.934 e·$Å^3$

Table A6: Crystal data and structure refinement for **C5** and **C6**

	C5	**C6**
Identification code	h1142	h1160
Empirical formula	$C_{30}H_{58}Cu_2F_{12}N_{14}P_2$	$C_{32}H_{60}Cu_4I_4N_{12}$
Formula weight	1031.92	1374.68
Temperature	293(2) K	120(2) K
Wavelength	0.71073 Å	0.71073 Å
Crystal system	Triclinic	Triclinic
Space group	$P\bar{1}$	$P\bar{1}$
Unit cell dimensions	a = 7.8306(4) Å	a = 9.0784(4) Å
	b = 11.6499(6) Å	b = 10.4432(5) Å
	c = 12.4737(7) Å	c = 12.7231(6) Å
	α = 78.019(1)°	α = 72.778(1)°
	β = 81.700(1)°	β = 74.856(1)°
	γ = 81.184(1)°	γ = 87.240(1)°
Volume	1092.5(1) $Å^3$	1111.59(9) $Å^3$
Z	1	1
Density (calculated)	1.568 Mg/m^3	2.054 Mg/m^3
Absorption coefficient	1.140 mm^{-1}	4.703 mm^{-1}
F(000)	532	664
Crystal size	0.20 x 0.12 x 0.1 mm^3	0.35 x 0.25 x 0.20 mm^3
Theta range for data collection	1.68 to 28.24°	1.73 to 28.20°
Index ranges	-10≤h≤10, -14≤k≤15, -16≤l≤16	-12≤h≤12, -13≤k≤13, -16≤l≤16
Reflections collected	14028	14059
Independent reflections	5385 [R(int) = 0.0398]	5429 [R(int) = 0.0140]
Completeness to theta	= 28.24°: 99.6 %	= 28.20°: 99.6 %
Absorption correction	Semi-empirical from equivalents	Semi-empirical from equivalents
Max. and min. transmission	0.968 and 0.813	0.990 and 0.726
Refinement method	Full-matrix least-squares on F^2	Full-matrix least-squares on F^2
Data / restraints / parameters	5385 / 0 / 276	5429 / 0 / 239
Goodness-of-fit on F^2	0.936	1.082
Final R indices [I¿2sigma(I)]	R1 = 0.0439, wR2 = 0.0905	R1 = 0.0186, wR2 = 0.0496
R indices (all data)	R1 = 0.0607, wR2 = 0.0952	R1 = 0.0201, wR2 = 0.0503
Largest diff. peak and hole	0.747 and -0.572 e·$Å^3$	0.608 and -0.551 e·$Å^3$

Table A7: Crystal data and structure refinement for **C7** and **C8**

	C7	**C8**
Identification code	h1162	h1015
Empirical formula	$C_{16}H_{30}Cu_3I_3N_6$	$C_{30}H_{60}Cu_2F_{12}N_{12}P_2$
Formula weight	877.78	1005.92
Temperature	120(2) K	150(2) K
Wavelength	0.71073 Å	0.71073 Å
Crystal system	Triclinic	Triclinic
Space group	$P\bar{1}$	$P\bar{1}$
Unit cell dimensions	a = 10.3549(5) Å	a = 9.5773(4) Å
	b = 11.0573(5) Å	b = 10.4201(5) Å
	c = 11.4562(5) Å	c = 10.7034(5) Å
	α = 77.379(1)°	α = 103.290(1)°
	β = 73.050(1)°	β = 96.936(1)°
	γ = 83.821(1)°	γ = 90.605(1)°
Volume	1223.05(10) $Å^3$	1031.13(8) $Å^3$
Z	2	1
Density (calculated)	2.384 Mg/m^3	1.620 Mg/m^3
Absorption coefficient	6.386 mm^{-1}	1.204 mm^{-1}
F(000)	828	520
Crystal size	0.22 x 0.15 x 0.12 mm^3	0.40 x 0.40 x 0.18 mm^3
Theta range for data collection	1.89 to 28.20°	1.97 to 26.37°
Index ranges	-12≤h≤13, -14≤k≤14, -13≤l≤15	-11≤h≤11, -13≤k≤13, -13≤l≤13
Reflections collected	15537	11105
Independent reflections	6003 [R(int) = 0.0342]	4181 [R(int) = 0.0182]
Completeness to theta	= 28.20°: 99.5 %	= 26.37°: 99.5 %
Absorption correction	Semi-empirical from equivalents	Semi-empirical from equivalents
Max. and min. transmission	0.906 and 0.711	0.986 and 0.899
Refinement method	Full-matrix least-squares on F^2	Full-matrix least-squares on F^2
Data / restraints / parameters	6003 / 0 / 275	4181 / 0 / 266
Goodness-of-fit on F^2	0.957	1.074
Final R indices [I¿2sigma(I)]	R1 = 0.0251, wR2 = 0.0511	R1 = 0.0262, wR2 = 0.0685
R indices (all data)	R1 = 0.0305, wR2 = 0.0524	R1 = 0.0274, wR2 = 0.0692
Largest diff. peak and hole	0.920 and -0.607 e·$Å^3$	0.338 and -0.182 e·$Å^3$

Table A8: Crystal data and structure refinement for **C9** and **C10**

	C9	**C10**
Identification code	h1091	h1150
Empirical formula	$C_{50}H_{92}Cu_2F_{12}N_{12}P_2$	$C_{30}H_{58}Cu_2F_{12}N_{14}P_2$
Formula weight	1278.38	1031.92
Temperature	120(2) K	120(2) K
Wavelength	0.71073 Å	0.71073 Å
Crystal system	Monoclinic	Monoclinic
Space group	C2/c	$P2_1/n$
Unit cell dimensions	a = 30.457(6) Å	a = 12.4821(5) Å
	b = 9.1394(18) Å	b = 25.0668(9) Å
	c = 21.278(4) Å	c = 15.0517(6) Å
	$\alpha = 90°$	$\alpha = 90°$
	$\beta = 95.375(4)°$	$\beta = 109.987(1)°$
	$\gamma = 90°$	$\gamma = 90°$
Volume	5897(2) $Å^3$	4425.8(3) $Å^3$
Z	4	4
Density (calculated)	1.440 Mg/m^3	1.549 Mg/m^3
Absorption coefficient	0.859 mm^{-1}	1.126 mm^{-1}
F(000)	2688	2128
Crystal size	0.22 x 0.15 x 0.10 mm^3	0.45 x 0.25 x 0.20 mm^3
Theta range for data collection	1.34 to 28.52°	1.62 to 28.24°
Index ranges	-40≤h≤40, -11≤k≤12, -28≤l≤22	-16≤h≤16, -33≤k≤33, -20≤l≤20
Reflections collected	26613	55794
Independent reflections	7392 [R(int) = 0.0596]	10946 [R(int) = 0.0445]
Completeness to theta	= 28.52°: 98.5 %	= 28.24°: 100.0 %
Absorption correction	Semi-empirical from equivalents	Semi-empirical from equivalents
Max. and min. transmission	0.937 and 0.119	0.948 and 0.807
Refinement method	Full-matrix least-squares on F^2	Full-matrix least-squares on F^2
Data / restraints / parameters	7392 / 0 / 354	10946 / 30 / 551
Goodness-of-fit on F^2	0.584	1.081
Final R indices [I¿2sigma(I)]	R1 = 0.0456, wR2 = 0.0627	R1 = 0.0494, wR2 = 0.1469
R indices (all data)	R1 = 0.1760, wR2 = 0.0792	R1 = 0.0651, wR2 = 0.1540
Largest diff. peak and hole	0.397 and -0.453 e·$Å^3$	0.908 and -0.691 e·$Å^3$

Table A9: Crystal data and structure refinement for **C11** and **C12**

	C11	**C12**
Identification code	h1118	h1014
Empirical formula	$C_{26}H_{52}Cu_2I_2N_{12}$	$C_{18}H_{32}CuIN_6$
Formula weight	913.68	522.94
Temperature	120(2) K	150(2) K
Wavelength	0.71073 Å	0.71073 Å
Crystal system	Monoclinic	Monoclinic
Space group	$P2_1/n$	$P2_1/n$
Unit cell dimensions	a = 9.1809(4) Å	a = 16.4723(10) Å
	b = 29.8038(13) Å	b = 8.2834(5) Å
	c = 12.7247(6) Å	c = 17.4478(10) Å
	$\alpha = 90°$	$\alpha = 90°$
	$\beta = 90.251(1)°$	$\beta = 111.441(1)°$
	$\gamma = 90°$	$\gamma = 90°$
Volume	3481.8(3) $Å^3$	2215.9(2) $Å^3$
Z	4	4
Density (calculated)	1.743 Mg/m^3	1.567 Mg/m^3
Absorption coefficient	3.031 mm^{-1}	2.393 mm^{-1}
F(000)	1824	1056
Crystal size	0.40 x 0.35 x 0.20 mm^3	0.40 x 0.28 x 0.10 mm^3
Theta range for data collection	1.37 to 28.20°	1.46 to 26.37°
Index ranges	-12≤h≤12, -39≤k≤37, -16≤l≤16	-20≤h≤20, -9≤k≤10, -17≤l≤21
Reflections collected	43526	14325
Independent reflections	8565 [R(int) = 0.0364]	4529 [R(int) = 0.0401]
Completeness to theta	= 28.20°: 99.9 %	= 26.37°: 99.9 %
Absorption correction	Semi-empirical from equivalents	Semi-empirical from equivalents
Max. and min. transmission	0.947 and 0.766	0.906 and 0.230
Refinement method	Full-matrix least-squares on F^2	Full-matrix least-squares on F^2
Data / restraints / parameters	8565 / 0 / 387	4529 / 0 / 243
Goodness-of-fit on F^2	1.108	1.043
Final R indices [I¿2sigma(I)]	R1 = 0.0336, wR2 = 0.0843	R1 = 0.0364, wR2 = 0.0734
R indices (all data)	R1 = 0.0402, wR2 = 0.0865	R1 = 0.0456, wR2 = 0.0771
Largest diff. peak and hole	0.991 and -1.150 e·$Å^3$	1.006 and -0.804 e·$Å^3$

Table A10: Crystal data and structure refinement for **C13** and **C14**

	C13	**C14**
Identification code	h1152	h965
Empirical formula	$C_{23}H_{46}Cl_{0.31}Cu_2I_{1.69}N_6$	$C_{40}H_{52}Cu_2F_{12}N_{12}P_2$
Formula weight	759.19	1117.96
Temperature	120(2) K	153(2) K
Wavelength	0.71073 Å	0.71073 Å
Crystal system	Orthorhombic	Monoclinic
Space group	$P2_12_12_1$	$P2_1/n$
Unit cell dimensions	a = 11.6357(6) Å	a = 8.111(2) Å
	b = 13.1877(7) Å	b = 22.126(6) Å
	c = 19.4201(10) Å	c = 12.998(3) Å
	$\alpha = 90°$	$\alpha = 90°$
	$\beta = 90°$	$\beta = 92.739(4)°$
	$\gamma = 90°$	$\gamma = 90°$
Volume	2980.0(3) $Å^3$	2330.1(11) $Å^3$
Z	4	2
Density (calculated)	1.692 Mg/m^3	1.593 Mg/m^3
Absorption coefficient	3.227 mm^{-1}	1.075 mm^{-1}
F(000)	1515	1144
Crystal size	0.40 x 0.20 x 0.20 mm^3	0.20 x 0.06 x 0.02 mm^3
Theta range for data collection	1.87 to 28.24°	1.82 to 28.33°
Index ranges	-15≤h≤15, -17≤k≤17, -25≤l≤25	-10≤h≤10, -29≤k≤29, -17≤l≤17
Reflections collected	37639	26716
Independent reflections	7374 [R(int) = 0.0392]	5592 [R(int) = 0.3381]
Completeness to theta	= 28.24°: 100.0 %	= 28.33°: 96.4 %
Absorption correction	Semi-empirical from equivalents	Face-indexed
Max. and min. transmission	0.977 and 0.671	0.959 and 0.785
Refinement method	Full-matrix least-squares on F^2	Full-matrix least-squares on F^2
Data / restraints / parameters	7374 / 3 / 329	5592 / 318 / 314
Goodness-of-fit on F^2	1.072	0.542
Final R indices [I¿2sigma(I)]	R1 = 0.0282, wR2 = 0.0671	R1 = 0.0466, wR2 = 0.0675
R indices (all data)	R1 = 0.0322, wR2 = 0.0688	R1 = 0.3041, wR2 = 0.1227
Largest diff. peak and hole	0.980 and -0.274 e·$Å^3$	0.287 and -0.300 e·$Å^3$

Table A11: Crystal data and structure refinement for **C15** and **C16**

	C15	**C16**
Identification code	h918	h975
Empirical formula	$C_{30}H_{64}Cu_2F_{12}N_{14}O_2P_2$	$C_{24.80}H_{36.70}CuF_6N_{7.90}OP$
Formula weight	1069.97	670.03
Temperature	153(2) K	153(2) K
Wavelength	0.71073 Å	0.71073 Å
Crystal system	Monoclinic	Triclinic
Space group	$P2_1/c$	$P\bar{1}$
Unit cell dimensions	a = 9.2716(6) Å	a = 10.6797(6) Å
	b = 16.6780(11) Å	b = 11.0477(6) Å
	c = 15.4515(11) Å	c = 13.9297(8) Å
	$\alpha = 90°$	$\alpha = 100.877(1)°$
	$\beta = 100.309(1)°$	$\beta = 109.994(1)°$
	$\gamma = 90°$	$\gamma = 99.403(1)°$
Volume	2350.7(3) $Å^3$	1469.73(14) $Å^3$
Z	2	2
Density (calculated)	1.512 Mg/m^3	1.514 Mg/m^3
Absorption coefficient	1.065 mm^{-1}	0.870 mm^{-1}
F(000)	1108	694
Crystal size	0.34 x 0.20 x 0.16 mm^3	0.40 x 0.25 x 0.2 mm^3
Theta range for data collection	1.81 to 28.29°	1.61 to 28.26°
Index ranges	-11≤h≤12, -22≤k≤15, -20≤l≤20	-14≤h≤14, -14≤k≤14, -18≤l≤18
Reflections collected	14728	17061
Independent reflections	5422 [R(int) = 0.0391]	6822 [R(int) = 0.0220]
Completeness to theta	= 28.29°: 92.7 %	= 28.26°: 93.7 %
Absorption correction	Semi-empirical from equivalents	Semi-empirical from equivalents
Max. and min. transmission	0.116 and 0.082	0.503 and 0.428
Refinement method	Full-matrix least-squares on F^2	Full-matrix least-squares on F^2
Data / restraints / parameters	5422 / 15 / 288	6822 / 0 / 389
Goodness-of-fit on F^2	0.907	1.062
Final R indices [I¿2sigma(I)]	R1 = 0.0435, wR2 = 0.0925	R1 = 0.0379, wR2 = 0.0993
R indices (all data)	R1 = 0.0671, wR2 = 0.0992	R1 = 0.0428, wR2 = 0.1048
Largest diff. peak and hole	0.539 and -0.387 e·$Å^3$	0.641 and -0.336 e·$Å^3$

Table A12: Crystal data and structure refinement for **C17** and **C18**

	C17	**C18**
Identification code	h1097	h1070
Empirical formula	$C_{49.16}H_{72.74}Cl_2Cu_2N_{15.58}O_{10}$	$C_{46}H_{68}B_2Cu_2F_8N_{14}O_2$
Formula weight	1239.99	1149.84
Temperature	120(2) K	120(2) K
Wavelength	0.71073 Å	0.71073 Å
Crystal system	Triclinic	Triclinic
Space group	$P\bar{1}$	$P\bar{1}$
Unit cell dimensions	a = 10.5848(10) Å	a = 10.1726(10) Å
	b = 10.8801(10) Å	b = 12.8486(13) Å
	c = 13.7502(13) Å	c = 13.5829(13) Å
	α = 100.689(2)°	α = 109.395(2)°
	β = 110.562(2)°	β = 99.991(2)°
	γ = 98.145(2)°	γ = 108.506(2)°
Volume	1419.6(2) $Å^3$	1508.8(3) $Å^3$
Z	1	1
Density (calculated)	1.450 Mg/m^3	1.265 Mg/m^3
Absorption coefficient	0.913 mm^{-1}	0.775 mm^{-1}
F(000)	649	598
Crystal size	0.20 x 0.20 x 0.04 mm^3	0.45 x 0.12 x 0.07 mm^3
Theta range for data collection	1.64 to 28.33°	1.67 to 28.36°
Index ranges	-14≤h≤14, -14≤k≤12, -17≤l≤18	-13≤h≤13, -17≤k≤17, -14≤l≤18
Reflections collected	13715	13022
Independent reflections	6999 [R(int) = 0.0598]	7417 [R(int) = 0.0587]
Completeness to theta	= 28.33°: 98.8 %	= 28.36°: 98.3 %
Absorption correction	Semi-empirical from equivalents	Semi-empirical from equivalents
Max. and min. transmission	0.992 and 0.544	0.943 and 0.423
Refinement method	Full-matrix least-squares on F^2	Full-matrix least-squares on F^2
Data / restraints / parameters	6999 / 21 / 395	7417 / 563 / 342
Goodness-of-fit on F^2	0.804	0.824
Final R indices [I¿2sigma(I)]	R1 = 0.0507, wR2 = 0.0802	R1 = 0.0832, wR2 = 0.2001
R indices (all data)	R1 = 0.1011, wR2 = 0.0896	R1 = 0.1670, wR2 = 0.2258
Largest diff. peak and hole	0.477 and -0.520 e·$Å^3$	1.172 and -0.642 e·$Å^3$

Table A13: Crystal data and structure refinement for **C19** and **C20**

	C19	**C20**
Identification code	h1022	h1108
Empirical formula	$C_{46}H_{72}Cu_4I_4N_{14}O_2$	$C_{46}H_{72}Cu_2I_6N_{14}O_2$
Formula weight	1614.94	1741.66
Temperature	120(2) K	120(2) K
Wavelength	0.71073 Å	0.71073 Å
Crystal system	Triclinic	Triclinic
Space group	$P\bar{1}$	$P\bar{1}$
Unit cell dimensions	a = 10.365(3) Å	a = 12.8344(5) Å
	b = 12.062(4) Å	b = 13.2872(6) Å
	c = 13.206(4) Å	c = 20.8307(9) Å
	α = 112.398(5)°	α = 97.149(1)°
	β = 92.525(6)°	β = 103.345(1)°
	γ = 105.352(6)°	γ = 112.581(1)°
Volume	1452.5(7) $Å^3$	3100.4(2) $Å^3$
Z	1	2
Density (calculated)	1.846 Mg/m^3	1.866 Mg/m^3
Absorption coefficient	3.618 mm^{-1}	3.719 mm^{-1}
F(000)	790	1676
Crystal size	0.18 x 0.10 x 0.04 mm^3	0.35 x 0.18 x 0.02 mm^3
Theta range for data collection	1.69 to 27.88°	1.03 to 28.33°
Index ranges	-13≤h≤13, -15≤k≤15, -17≤l≤17	-17≤h≤17, -17≤k≤17, -27≤l≤27
Reflections collected	18866	39396
Independent reflections	6911 [R(int) = 0.1248]	15344 [R(int) = 0.0701]
Completeness to theta	= 27.88°: 99.7 %	= 28.33°: 99.3 %
Absorption correction	Semi-empirical from equivalents	Semi-empirical from equivalents
Max. and min. transmission	0.939 and 0.654	0.989 and 0.825
Refinement method	Full-matrix least-squares on F^2	Full-matrix least-squares on F^2
Data / restraints / parameters	6911 / 0 / 325	15344 / 0 / 649
Goodness-of-fit on F^2	0.933	0.886
Final R indices [I¿2sigma(I)]	R1 = 0.0746, wR2 = 0.1416	R1 = 0.0486, wR2 = 0.0870
R indices (all data)	R1 = 0.1548, wR2 = 0.1671	R1 = 0.0967, wR2 = 0.1075
Largest diff. peak and hole	1.012 and -0.952 e·$Å^3$	1.722 (0.95 Å from I22 position) and -0.936 e·$Å^3$

Table A14: Crystal data and structure refinement for **C21** and **C22**

	C21	**C22**
Identification code	h1154	h1125
Empirical formula	$C_{26}H_{50}Cu_2F_{12}N_{12}O_2P_2$	$C_{50}H_{94}Cu_2F_{12}N_{12}O_2P_2$
Formula weight	979.80	1312.39
Temperature	120(2) K	120(2) K
Wavelength	0.71073 Å	0.71073 Å
Crystal system	Monoclinic	Monoclinic
Space group	$P2_1/c$	$P2_1/n$
Unit cell dimensions	a = 15.4730(8) Å	a = 12.3581(9) Å
	b = 21.9757(11) Å	b = 16.7472(13) Å
	c = 13.1940(6) Å	c = 14.7430(11) Å
	$\alpha = 90°$	$\alpha = 90°$
	$\beta = 113.507(1)°$	$\beta = 93.156(2)°$
	$\gamma = 90°$	$\gamma = 90°$
Volume	4114.0(4) $Å^3$	3046.6(4) $Å^3$
Z	4	2
Density (calculated)	1.582 Mg/m^3	1.431 Mg/m^3
Absorption coefficient	1.208 mm^{-1}	0.836 mm^{-1}
F(000)	2008	1380
Crystal size	0.40 x 0.08 x 0.07 mm^3	0.40 x 0.35 x 0.25 mm^3
Theta range for data collection	1.44 to 28.24°	1.84 to 27.88°
Index ranges	-20≤h≤20, -29≤k≤28, -17≤l≤17	-14≤h≤16, -22≤k≤22, -19≤l≤17
Reflections collected	51075	35133
Independent reflections	10156 [R(int) = 0.0625]	7264 [R(int) = 0.0501]
Completeness to theta	= 28.24°: 99.9 %	= 27.88°: 100.0 %
Absorption correction	Semi-empirical from equivalents	Semi-empirical from equivalents
Max. and min. transmission	0.940 and 0.694	0.985 and 0.777
Refinement method	Full-matrix least-squares on F^2	Full-matrix least-squares on F^2
Data / restraints / parameters	10156 / 107 / 533	7264 / 16 / 402
Goodness-of-fit on F^2	0.966	1.035
Final R indices [I¿2sigma(I)]	R1 = 0.0490, wR2 = 0.0829	R1 = 0.0549, wR2 = 0.1378
R indices (all data)	R1 = 0.1323, wR2 = 0.0967	R1 = 0.0920, wR2 = 0.1618
Largest diff. peak and hole	0.542 and -0.448 e·$Å^3$	0.984 and -0.864 e·$Å^3$

Table A15: Crystal data and structure refinement for **C23** and **C24**

	C23	**C24**
Identification code	h1177	h1204
Empirical formula	$C_{32}H_{66}Cu_2F_{12}N_{12}O_2P_2$	$C_{32}H_{66}Cu_2I_2N_{12}O_2$
Formula weight	1067.99	1031.85
Temperature	123(2) K	123(2) K
Wavelength	0.71073 Å	0.71073 Å
Crystal system	Monoclinic	Monoclinic
Space group	$P2_1/n$	$P2_1/n$
Unit cell dimensions	a = 9.1841(10) Å	a = 8.8505(7) Å
	b = 20.907(2) Å	b = 20.7116(15) Å
	c = 12.1186(13) Å	c = 11.6387(8) Å
	$\alpha = 90°$	$\alpha = 90°$
	$\beta = 93.388(2)°$	$\beta = 90.962(2)°$
	$\gamma = 90°$	$\gamma = 90°$
Volume	2322.9(4) $Å^3$	2133.2(3) $Å^3$
Z	2	2
Density (calculated)	1.527 Mg/m^3	1.606 Mg/m^3
Absorption coefficient	1.077 mm^{-1}	2.487 mm^{-1}
F(000)	1108	1044
Crystal size	0.25 x 0.20 x 0.20 mm^3	0.25 x 0.20 x 0.13 mm^3
Theta range for data collection	1.94 to 28.22°	1.97 to 28.08°
Index ranges	-12≤h≤12, -27≤k≤27, -16≤l≤15	-11≤h≤11, -27≤k≤27, -15≤l≤13
Reflections collected	23325	20358
Independent reflections	5714 [R(int) = 0.0733]	5193 [R(int) = 0.0576]
Completeness to theta	= 28.22°: 99.8 %	= 28.08°: 99.9 %
Absorption correction	Semi-empirical from equivalents	Semi-empirical from equivalents
Max. and min. transmission	0.976 and 0.772	0.977 and 0.859
Refinement method	Full-matrix least-squares on F^2	Full-matrix least-squares on F^2
Data / restraints / parameters	5714 / 29 / 324	5193 / 0 / 233
Goodness-of-fit on F^2	1.006	0.892
Final R indices [I¿2sigma(I)]	R1 = 0.0449, wR2 = 0.1031	R1 = 0.0441, wR2 = 0.0821
R indices (all data)	R1 = 0.0657, wR2 = 0.1124	R1 = 0.0651, wR2 = 0.0877
Largest diff. peak and hole	0.854 and -0.389 e·$Å^3$	0.854 and -0.995 e·$Å^3$

Table A16: Crystal data and structure refinement for **C25** and **C26**

	C25	**C26**
Identification code	h1301	h1202
Empirical formula	$C_{32}H_{66}Cl_2Cu_2N_{12}O_{10}$	$C_{38}H_{74}Cu_2F_{14}N_{14}O_4P_2$
Formula weight	976.95	1246.13
Temperature	120(2) K	123(2) K
Wavelength	0.71073 Å	0.71073 Å
Crystal system	Monoclinic	Monoclinic
Space group	$P2_1/n$	$P2_1/n$
Unit cell dimensions	a = 8.780(2) Å	a = 11.1872(11) Å
	b = 21.045(5) Å	b = 19.1481(19) Å
	c = 11.837(3) Å	c = 12.2954(12) Å
	$\alpha = 90°$	$\alpha = 90°$
	$\beta = 93.070(4)°$	$\beta = 91.595(2)°$
	$\gamma = 90°$	$\gamma = 90°$
Volume	2184.1(9) $Å^3$	2632.8(4) $Å^3$
Z	2	2
Density (calculated)	1.485 Mg/m^3	1.572 Mg/m^3
Absorption coefficient	1.162 mm^{-1}	0.971 mm^{-1}
F(000)	1028	1292
Crystal size	0.42 x 0.22 x 0.18 mm^3	0.40 x 0.32 x 0.23 mm^3
Theta range for data collection	1.94 to 27.48°	1.97 to 28.46°
Index ranges	-11≤h≤11, -27≤k≤25, -15≤l≤15	-14≤h≤12, -25≤k≤25, -16≤l≤16
Reflections collected	18812	22595
Independent reflections	5011 [R(int) = 0.0682]	6619 [R(int) = 0.0598]
Completeness to theta	= 27.48°: 99.8 %	= 28.46°: 99.7 %
Absorption correction	Semi-empirical from equivalents	Semi-empirical from equivalents
Max. and min. transmission	0.8182 and 0.6411	0.933 and 0.623
Refinement method	Full-matrix least-squares on F^2	Full-matrix least-squares on F^2
Data / restraints / parameters	5011 / 0 / 264	6619 / 6 / 339
Goodness-of-fit on F^2	1.011	0.857
Final R indices [I¿2sigma(I)]	R1 = 0.0581, wR2 = 0.1345	R1 = 0.0498, wR2 = 0.0931
R indices (all data)	R1 = 0.1117, wR2 = 0.1483	R1 = 0.0962, wR2 = 0.1043
Largest diff. peak and hole	0.509 and -0.800 e·$Å^3$	0.855 and -0.558 e·$Å^3$

List of Publications:

S. Herres, P. Hesemann, J.J.E. Moreau; Polystyrene Resins Incorporating BINOL Units: New Materials For Asymmetric Catalysis, *Eur. J. Org. Chem.* **2003**, 99-105

S. Herres, U. Flörke, G. Henkel; N,N´-Bis(dipiperidin-1-ylmethylene)-propane-1,3-diamine and N,N´-bis-(1,3-dimethylperhydropyrimidin-2-ylidene)propane-1,3-diamine, *Acta Crystallogr. Sect. C*, **2004**, *60*, o358-o360

S. Herres, U. Flörke, G. Henkel; The first di-μ-hydroxo-bridged binuclear copper complex containing a bisguanidine ligand, *Acta Crystallogr. Sect. C* **2004**, *60*, m659-m660

S. Herres-Pawlis, U. Flörke, G. Henkel; Catena-Poly[[μ-cyano-[1,3-bis(tetramethylguanidino)propane]dicopper(I)]-μ-cyano], *Acta Crystallogr. Sect. E* **2005**, *61*, m79-m81

S. Herres, A.J. Heuwing, U. Flörke, J. Schneider, G. Henkel; Hydroxylation of a Methyl Group: Synthesis of $[Cu_2(btmmO)_2I]^+$ and of $[Cu_2(btmmO)_2]^{2+}$ Containing the Novel Ligand (bis(trimethylmethoxy)guanidino-propane (btmmO) by Copper-Assisted Oxygen Activation, *Inorg. Chim. Acta* **2005**, *358*, 1089-1095

S. Herres-Pawlis, U. Flörke, G. Henkel; Tuning of Copper(I)-Dioxygen Reactivity by Bisguanidine Ligands, *Eur. J. Inorg. Chem.* **2005**, 3815-3824

S. Herres-Pawlis, A. Neuba, O. Seewald, T. Seshadri, H. Egold, U. Flörke, G. Henkel; A library of peralkylated bisguanidine ligands for use in biomimetic coordination chemistry, *Eur. J. Org. Chem.* **2005**, pub. adv.

U. Flörke, S. Herres-Pawlis, A.J. Heuwing, A. Neuba, O. Seewald, G. Henkel; The di-protonated 1,3-bis(N,N,N´,N´-tetramethylguanidinium)propane cation: packing and conformational changes, *Acta Crystallogr. Sect. C* **2005**, submitted

Fellowships and awards:

05/03 - 04/05	Fonds Fellowship of the Fonds der Chemischen Industrie
03/04	Aventis [i]Lab Award
05/05 - 10/05	"Promotionsabschlußstipendium" of the University of Paderborn

Conference contributions:

10/03 GDCh-Jahrestagung 2003 Munich (Poster: "Neuartige Kupferkomplexe mit aliphatischen und aromatischen Bisguanidin-Liganden")

03/04 GDCh-JungChemikerForum-Frühjahrssymposium 2004 Heidelberg (Oral presentation: "Tuning of Copper(I)-Dioxygen Reactivity by bisguanidine ligands")

07/04 36th International Conference on Coordination Chemistry 2004 Merida, Mexico (Oral presentation "Introduction of peralkylated bisguanidine ligands into copper-dioxygen chemistry: a double variety in ligand modification" and Poster "A novel aromatic tridentate peralkylated bisguanidine ligand and its features in copper-dioxygen chemistry")

01/05 Workshop on Biomimetic Oxygen Activation, Schloß Rauischholzhausen (Oral presentation: "Oxygen Activation and Transfer Mediated By Copper(I) Complexes with Bisguanidine Ligands" and Poster: "A Modular Approach in Bisguanidine Ligand Synthesis and its Features in Oxygen Activation and Transfer")

04/05 6th Conference on Inorganic Chemistry 2005, Funchal, Madeira (Oral presentation: "A Library of Peralkylated Bisguanidine Ligands for Use in Copper-Dioxygen Chemistry")

07/05 Symposium on the Activation of Dioxygen and Homogeneous Organic Catalysis (ADHOC) 2005 Cologne (Poster: "A Library of Peralkylated Bisguanidine Ligands for Copper Containing Oxidation Catalysts")

09/05 GDCh-Jahrestagung 2005 Düsseldorf (Oral presentation: "Eine Bibliothek aus Bisguanidin-Liganden zur Synthese von kupferhaltigen Oxidationskatalysatoren", Poster: "Sauerstoffaktivierung und -transfer durch Kupfer-Bisguanidin-Komplexe" and "Mangankomplexe mit polyfunktionellen Bisguanidinliganden")